The University of Sussex

Polo-like kinase 1 (PLK1) promotes centromere protection against a PICH/BLM-mediated deformation pathway

Owen Addis

Genome Damage and Stability PhD

September 2019

Declaration

I hereby declare that this thesis has not been and will not be, submitted in whole or in part to another University for the award of any other degree.

Signature: ……

Acknowledgments

I would like to express my appreciation to Dr Kok-Lung Chan for his valuable and constructive advice throughout this research. I would also like to give special thanks to Dr Ankana Tiwari for her advice, academic assistance and personal support during the early years of this research. Additionally, I wish to acknowledge the valuable help and support provided by Dr Tomisin Olukoga. Furthermore, I would like to extend my gratitude to Dr Jo Murray and Dr Thomas Etheridge for their help and advice reviewing this thesis.

Finally, I wish to save my biggest thank you to Dr Hannah Addis Jones. I don't think I could have got this far without you.

Abstract

Faithful chromosome segregation cannot be achieved without correctly aligning each chromosome pair, a process referred to as chromosome biorientation. Disabling the key mitotic kinase Polo like kinase 1 (PLK1) is known to impair multiple aspects of mitosis, particularly chromosome alignment. This is believed primarily due to unstable bipolar spindle-kinetochore attachments. However, contrary to this belief, PLK1 inactivation does not necessarily abolish metaphase establishment. Instead, it is shown to interfere with its long-term maintenance. This study has demonstrated that the failure of chromosome biorientation maintenance is driven by a previously undescribed mechanism that relies on PLK1 activity. Without active PLK1 during mitosis, BLM helicase is illegitimately recruited to and unwinds a specific centromere domain underneath the kinetochores. This recruitment is dependent on PICH translocase and leads to the impairment of centromere configuration and rigidity. Concurrently, bipolar spindle pulling forces enhance this centromere destructive pathway. During an absence of PLK1 activity, but under active spindle pulling forces, the distorted centromeric chromatin is promptly converted into an ultra-fine DNA structure. This has been referred to as 'pre-anaphase DNA threads', in order to distinguish them from the previously identified ultra-fine DNA bridges (UFBs) that form during anaphase. These new fragile DNA thread structures subsequently fail to withstand spindle tension. This results in centromere deformation that displays as whole-chromosome arm splitting, which has been termed as 'centromere dislocation'. This severely damages centromere integrity, whilst also destroying normal metaphase maintenance. Therefore, PLK1 serves as a centromere guardian in order to protect centromeres against deformation, which is driven by a PICH/BLM-mediated chromatin unwinding activity.

Table of Contents

Declaration ..... *i*

Acknowledgments ..... *ii*

Abstract ..... *iii*

Table of Contents ..... *iv*

Abbreviations ..... *viii*

Figures: Introduction ..... *x*

Figures: Results ..... *xi*

Chapter 1: Introduction *1*

1.1 Overview of Introduction **1**

1.2 Chromosome organisation by the action of condensin complexes **6**

1.2.1 Condensin structure and how it dictates mitotic chromosome assembly 6

1.2.2 Activation and spatiotemporal regulation of condensin 7

1.2.3 Condensin ensures correct centromere/kinetochore structure 9

1.3 Sister-chromatid cohesion is mediated by cohesin **12**

1.3.1 Structural composition of the cohesin complex 12

1.3.2 Regulation of cohesin loading onto DNA and its activity 13

1.3.3 A two-step process of cohesin removal during mitosis 14

1.3.4 Dissociation of cohesin during the 'prophase pathway' 14

1.3.5 Centromeric cohesin is cleaved by separase 15

1.3.6 Centromere cohesin cleavage is linked to the mitotic checkpoint 16

1.4 Centromere assembly **19**

1.4.1 Centromere structure: monocentric (point & regional) 20

1.4.2 Centromere identification by CENP-A 22

1.4.3 Centromere inheritance & regulation of CENP-A deposition 23

1.5 Kinetochore assembly **25**

1.5.1 The CCAN forms the link between the centromere and kinetochore 25

1.5.2 CENP-C/T (inner kinetochore) links to the outer kinetochore (KMN) 26

1.5.3 The KMN network links to microtubules 26

1.6 Kinetochore-microtubule (KT-MT) error correction and SAC activation **28**

1.6.1 The mitotic checkpoint complex (MCC) 28

1.6.2 Spindle tension and MT-KT error correction by Aurora B 29

1.7 Sister chromatid disjunction and the formation of UFBs **31**

1.7.1 Classification of ultra-fine DNA bridges (UFBs) 31

1.7.2 Types of UFBs 32

1.7.3 PICH (Plk1-interacting checkpoint helicase) 34
1.7.4 BLM (Bloom's syndrome helicase) 36
1.8 The mitotic regulator polo-like kinase 1 (PLK1) **39**
1.8.1 PLKs a family of serine/threonine kinases 40
1.8.2 Regulation of PLK1 activity 41
1.8.3 PLK1 function during centrosome maturation 43
1.8.4 PLK1 function in kinetochore-microtubule attachment stability 45
1.9 Summary **49**
Chapter 2: Materials & Methods ***51***
2.1 DNA plasmid construction **51**
2.1.1 DNA plasmids 51
2.1.2 Oligonucleotides for cloning 51
2.1.3 Bacterial transformation 52
2.1.4 Plasmid preparation and purification 52
2.1.5 Restriction enzyme digestion 53
2.1.6 Thermocycling (Polymerase Chain Reaction) 53
2.2 Human Cellular assays **53**
2.2.1 Human cell culture 53
2.2.2 Cell lines (parental) 54
2.2.3 Drugs & Inhibitors 55
2.2.4 Transfection of human cells 55
2.2.5 Stable cell line generation 58
2.3 Flow cytometry and fluorescent activated cell sorting (FACS) **60**
2.3.1 Flow cytometry cell cycle analysis 60
2.3.2 Cell sorting (FACS) 61
2.4 Antibodies **61**
2.4.1 Primary Antibodies (Immunofluorescence & Western blot) 61
2.4.2 Secondary Antibodies (Immunofluorescence & Western blot) 63
2.5 Western blotting **64**
2.6 High resolution microscopy **65**
2.6.1 Immunofluorescent staining (including Pre-extraction protocol) 65
2.6.2 DNA bridge immunofluorescent staining 66
2.6.3 K-fibre immunofluorescent staining 66
2.6.4 5-Ethynyl-2'-deoxyuridine (EdU) Click-iT staining 66
2.6.5 Acquisition of immunofluorescent imaging 67
2.6.6 Widefield live cell microscopy 67
2.6.7 Deconvolution (Huygens professional) 67
2.7 Cytogenic analysis **68**

2.7.1 Chromosome spread preparation 68

2.7.2 Centromere & Telomere FiSH (ctFiSH) 68

Chapter 3: PLK1 activity promotes metaphase maintenance 69

3.1 Introduction 69

3.2 Results 72

3.2.1 Inhibition of PLK1 by a small-molecule inhibitor, BI2536, arrests cells in mitosis ... 72

3.2.2 Cells remain capable of metaphase establishment when PLK1 activity is inhibited 73

3.2.3 PLK1 inactivation leads to a DNA linkage during metaphase collapse 75

3.2.4 Pre-anaphase DNA threads are not a result of protein mis-localisation to cellular cytoskeleton structures 77

3.2.5 Pre-anaphase DNA thread formation is not cell type specific 78

3.2.6 PLK1 inhibition causes both centromere and kinetochore disassembly 79

3.2.7 A mitotic function of PLK1 suppresses centromere deformation 81

3.2.8 Bipolar spindle attachment promotes centromere deformation during PLK1 inhibition 83

3.3 Discussion 85

Chapter 4: PLK1 suppresses whole chromosome arm breakage 90

4.1 Introduction 90

4.2 Results 92

4.2.1 PLK1 kinase activity is required to suppress chromosome fragmentation 92

4.2.2 PLK1 suppresses centromere breakage - 'centromere dislocation' 93

4.2.3 Centromere deformation is specifically suppressed by the activity of PLK1 94

4.2.4 Artificial tethering of PLK1 to the centromere/kinetochore fails to rescue centromere deformation 97

4.3 Discussion 100

Chapter 5: Catalytic activity of BLM and PICH promote centromere deformation during PLK1 inactivation 104

5.1 Introduction 104

5.2 Results 108

5.2.1 PLK1 suppresses the aberrant formation of PICH, BLM and RPA at centromeres during metaphase 108

5.2.2 MT-spindle tension promotes aberrant RPA foci formation at the centromere during PLK1 inhibition 110

5.2.3 BLM promotes centromere deformation during PLK1 kinase inhibition 112

5.2.4 PICH acts upstream of BLM during centromere deformation 114

5.2.5 PLK1 activity protects against PICH/BLM-dependent metaphase collapse 114

5.2.6 BLM helicase activity actively unwinds centromeric DNA during PLK1 inhibition 116

5.2.7 BLM and Topoisomerase IIIα (TOP3A) may act together to promote centromere deformation during PLK1 inhibition 118

5.2.8 PICH activity promotes centromere deformation when PLK1 activity is absent ... 120

5.3 Discussion 124

Chapter 6: General discussion and future directions 126

6.1 Summary of key findings 126

6.2 General discussion 127

Bibliography 139

Appendix: Publications during PhD 158

Addis Jones, O., Tiwari, A., Olukoga, T., Herbert, A. & Chan, KL. PLK1 facilitates chromosome biorientation by suppressing centromere disintegration driven by BLM-mediated unwinding and spindle pulling. *Nature Communications (2019), 10:2861* 158

Tiwari, A., Addis Jones, O. & Chan, KL. *53BP1 can limit sister-chromatid rupture and rearrangement driven by a distinct ultrafine DNA bridging-breakage process. Nature Communications (2018), 9(1):677* 158

Abbreviations

APC/C	Anaphase promoting complex/cyclosome
APH	Aphidicolin
BLM	Bloom's syndrome helicase
BS	Bloom's syndrome
BTR (complex)	BLM/Topoisomerase IIIα/RMI1/RMI2 complex
BUB	Budding uninhibited by benzimidazole genes
BUB1	Mitotic checkpoint serine/threonine kinase BUB1
BUBR1	Mitotic checkpoint serine/threonine protein kinase BUB1 beta
CCAN	Constitutive centromere associated network
CENP-A	Histone H3-like centromeric protein A
CENP-B	Major centromere autoantigen B
CFS	Common fragile site
CIN	Chromosome instability
CDK1	Cyclin-dependent kinase 1
CDC20	Cell division cycle protein 20 homolog (APC/C^{CDC20})
CPC	Chromosomal passenger complex
	(INCENP, Borealin, Survivin & Aurora B kinase)
dHJ	Double Holliday junction
dsDNA	Double stranded DNA
ESCO1/2	N-acetyltransferase
FA	Fanconi anaemia
FANCD2	Fanconi anaemia complementation group D2 protein
FISH	Fluorescent *in situ* hybridisation
HJURP	Holliday junction recognition protein
HR	Homologous recombination
HU	Hydroxyurea
INCENP	Inner centromere protein
KT	Kinetochore
KMN	Kinetochore microtubule network
	(KNL1, MIS12, NDC80 complex)

KNL1 (complex)	Kinetochore scaffold 1
	(KNL complex includes KNL1 & ZWINT)
KNL2	MIS18 binding protein
LRI	Late replication intermediate
MAD	Mitotic-arrest deficient (MAD1-2/BUBR1)
MAU2	Mau2 chromatid cohesion factor (Scc4)
MCC	Mitotic checkpoint complex (MAD2, BUBR1, BUB3)
MIS12 (complex)	Centromere protein MIS12 homolog
	(MIS12 complex includes MIS12, NSL1, PMF1 & DSN1)
MPS1	Multipolar spindle kinase 1
MT	Microtubule
NDC80 (complex)	Kinetochore protein NDC80 homolog
	(NDC80-HEC1, NUF2, SPC24 & SPC25)
NEBD	Nuclear envelope breakdown
NIPBL	Nipped-B-like protein (Scc2)
PDS5	Sister chromatid cohesion protein PDS5 homolog
PICH	PLK1-intercating checkpoint helicase
PLK1	Polo-like kinase 1
PP1	Serine/threonine Protein phosphatase PP1-alpha
PP2A	Serine/threonine Protein phosphatase PP2-alpha
RAD21 (Scc1)	Double-strand break repair protein rad21 homolog
RIF1	Telomere-associated protein RIF1
RMI1/2	RecQ-mediated genome instability protein 1/2
RPA	Replication protein A
SAC	Spindle assembly checkpoint
SA1/2/3	Cohesin subunit SA1/2/3 (STAG1/2/3) (Scc3)
SGO1	Shugoshin 1
SCE	Sister chromatid exchange
SMC	Structural maintenance of chromosomes
ssDNA	Single stranded DNA
TOP2α	Topoisomerase IIα
TOP3α	Topoisomerase IIIα
UFB	Ultra-fine DNA bridge
WAPL	Wings apart-like protein homolog

Figures: Introduction

Figure 1.1. Typical progression of the cell cycle……2

Figure 1.2. Mitotic chromosome assembly by condensin complexes……7

Figure 1.3. Sister chromatid cohesion is established and maintained by cohesin….13

Figure 1.4. Cohesin release by WAPL and cleavage by seperase……16

Figure 1.5. The spindle assembly checkpoint (SAC) and the regulation of the anaphase promoting complex (APC)……17

Figure 1.6. Characteristics of monocentric centromeres, including both point and regional centromeres……21

Figure 1.7. The centromere is identified by CENP-A deposition during telophase /G1……24

Figure 1.8. Complex assembly of the centromere-kinetochore axis.……27

Figure 1.9. KT-MT attachment and Aurora B dependent KT-MT regulation……28

Figure 1.10. Resolution of DNA intertwinements by the UFB binding complex maintains faithful chromosome segregation……33

Figure 1.11. PICH an ATP-dependent DNA translocase……34

Figure 1.12. BLM helicase promotes double Holliday junction (dHJ) dissolution…..37

Figure 1.13. The structural domains of PLK1-5……40

Figure 1.14. The activation and degradation cycle of PLK1……42

Figures: Results

Figure 3.1. BI2536 arrests cells in G2/M……..72

Figure 3.2. Cells fail to maintain metaphase alignment during PLK1 inhibition…….74

Figure 3.3. Bipolar spindle attachment during PLK1 inhibition……74

Figure 3.4. PLK1 recruits to ultra-fine DNA bridges (UFBs) during anaphase……75

Figure 3.5. PLK1, PICH, RPA, BLM and TOP3A decorate centromere linkages during PLK1 inhibition……77

Figure 3.6. Centromere linkages are protein coated DNA structures……78

Figure 3.7. PLK1 suppresses pre-anaphase DNA threads in various different cell lines……78

Figure 3.8. Kinetochores disassemble after metaphase following PLK1 inhibition..80

Figure 3.9. PLK1 inhibition promotes centromere DNA damage during mitosis……80

Figure 3.10. Pre-anaphase DNA threads are not due to interference of S-phase functions of PLK1……82

Figure 3.11. PLK1 suppresses pre-anaphase DNA thread formation in established metaphase cells……82

Figure 3.12. Microtubule forces promote pre-anaphase DNA thread formation during PLK1 inhibition……..83

Figure 3.13. Bipolar spindle-attachment is required for pre-anaphase DNA thread formation……..83

Figure 4.1. PLK1 inhibition causes chromosome fragmentation……92

Figure 4.2. PLK1 inhibition causes 'centromere dislocation'……94

Figure 4.3. Centromere dislocation results in chromatin breakage specifically within centromeric DNA……94

Figure 4.4. An alternative approach at targeting PLK1 kinase activity using PLK1as cells……..95

Figure 4.5. PLK1 kinase activity suppresses pre-anaphase DNA thread formation…96

Figure 4.6. Centromere deformation is not caused by trapping inactive PLK1 to its substrates……96

Figure 4.7. Schematic of domain structure & localisation of centromere tethered PLK1as cell lines……..97

Figure 4.8. Centromere tethered PLK1 is insufficient to prevent centromere deformation……97

Figure 4.9. Tethering PLK1 to the centromere is insufficient to prevent centromere dislocations……98

Figure 4.10. Tethering PLK1 to chromatin partially rescues centromere dislocations……..98

Figure 5.1. PLK1 inhibition promotes recruitment of BLM & RPA at the centromeres during metaphase……108

Figure 5.2. PLK1 kinase suppresses aberrant recruitment of RPA at the centromere during metaphase……109

Figure 5.3. PLK1 kinase may limit the loading of PICH at the centromere during metaphase……109

Figure 5.4. The aberrant recruitment of RPA after PLK1 inhibition is dependent on spindle-pulling forces……111

Figure 5.5. The aberrant loading of PICH during PLK1 inhibition is independent on spindle-pulling forces……111

Figure 5.6. KT-MT attachment promotes the aberrant recruitment of RPA at the centromere during PLK1 inhibition……112

Figure 5.7. BLM helicase promotes centromere deformation during PLK1 inhibition……113

Figure 5.8. The aberrant loading of RPA at centromeres is dependent on BLM during PLK1 inhibition……113

Figure 5.9. PICH promotes centromere deformation during PLK1 inhibition…….114

Figure 5.10. PICH functions upstream of BLM during centromere deformation when PLK1 is absent……114

Figure 5.11. Both PICH & BLM promote metaphase collapse during PLK1 inhibition……115

Figure 5.12. BLM promotes centromere deformation during PLK1 inhibition……115

Figure 5.13. Creation of a BLM helicase inactive stable cell line……116

Figure 5.14. BLM helicase activity promotes centromere deformation during PLK1 inhibition……116

Figure 5.15. Low BLM expression is sufficient to promote centromere deformation during PLK1 inhibition……117

Figure 5.16. BLM helicase actively unwinds centromeric DNA during PLK1 inhibition……118

Figure 5.17. TOP3A promotes centromere deformation during PLK1 inhibition…119

Figure 5.18. BLM requires its partner protein TOP3A for centromere recruitment……120

Figure 5.19. Creating PICH-translocase inactive RNAi resistant stable cell lines…121

Figure 5.20. PICH translocase activity promotes centromere deformation during PLK1 inhibition……122

Figure 5.21. Both BLM and PICH are phosphorylation targets of PLK1……..122

Figure 5.22. BLM recruitment to mitotic chromatin may be regulated by phosphorylation……..123

Figure 6.1. A model to demonstrate how PLK1 suppresses PICH/BLM-mediated centromere deformation……..128

Chapter 1: Introduction

1.1 Overview of Introduction

Faithful transmission of the genome during cellular division relies on various processes for its attainment. Cells must accomplish accurate genome duplication during DNA replication, whilst also ensuring that the newly synthesised DNA molecules remain connected until mitosis. In addition, the duplicated DNA molecules must undergo distinct organisation and arrangement. An interference in the action of any one of these processes can lead to errors in chromosome transmission and drive the progression of numerical chromosome instability (CIN). This is often displayed as an inheritable loss or gain of chromosome number, otherwise referred to as aneuploidy. The unequal inheritance of chromosome number is typically observed in a number of different cancers and can be attributed to errors in chromosome segregation (Vargas-Rondón et al. 2018). Better understanding of how such erroneous segregation arises remains critical to the understanding of certain disease progression, including the development of cancer.

Error-free chromosome segregation relies on fully duplicated condensed chromosomes being closely aligned during metaphase. This follows a process known as chromosome biorientation, which is achieved through bipolar attachment of the mitotic spindle to each chromosome. The mitotic spindle emanates from opposite poles of the cell, capturing sister chromatids at distinct genomic regions known as centromeres (McKinley and Cheeseman 2016). This specialist attachment by the mitotic spindle requires the pre-assembly of a macromolecular protein complex termed as the kinetochore (KT). Each KT is arranged at opposite sides of every centromere, which results in the formation of sister KT structures. Subsequently, sister KTs are then able to provide a foundation for the bipolar connection between the centromere and mitotic microtubules (MT) (Hinshaw and Harrison 2018). Once each chromosome has

established bipolar orientation and attachment, sister-chromatid separation can ensue during anaphase. This results in the equal distribution of duplicated genetic material into two identical daughter cells **(Fig. 1.1)**.

This multifaceted process of protein assembly and chromosome capture is tightly regulated, whilst also being monitored by a sophisticated surveillance mechanism. This surveillance system is referred to as the spindle assembly checkpoint (SAC) and functions to survey the status of spindle attachment. The detection of MT-attachment errors results in prolonged SAC activation and subsequently, anaphase progression is inhibited (Foley and Kapoor 2013; Heald and Khodjakov 2015). This inhibition is achieved by suppression of the anaphase promoting complex/cyclosome (APC/C^{CDC20}) (Musacchio and Salmon 2007). Hence, cells with incorrectly aligned chromosomes can be prevented from progressing into anaphase. Only when stable bipolar attachment is achieved (chromosome biorientation) can the SAC become satisfied. Consequently, the APC/C^{CDC20} becomes active and processes involved in achieving faithful chromosome segregation can ensue (Peters and Nishiyama 2012).

However, maintaining faithful chromosome segregation is not attained by simply upholding stable MT-KT attachment and SAC regulation. As previously eluded to, the correct assembly and organisation of chromosome architecture is also critical. Cohesion of sister chromatids must be maintained throughout DNA replication and requires its timely release during mitosis. Cohesion of sister chromatids is achieved through the action of SMC-containing complexes known as cohesin, which function to grasp the duplicated DNA molecules in order to hold them together (Nasmyth 2011). In addition, mitotic chromosome compaction is facilitated by the action of a structurally related SMC complex, known as condensin (Hirano 2005). Therefore, both cohesin and condensin function to ensure the correct assembly and organisation of chromosome architecture and hence provide crucial support to achieve faithful chromosome segregation.

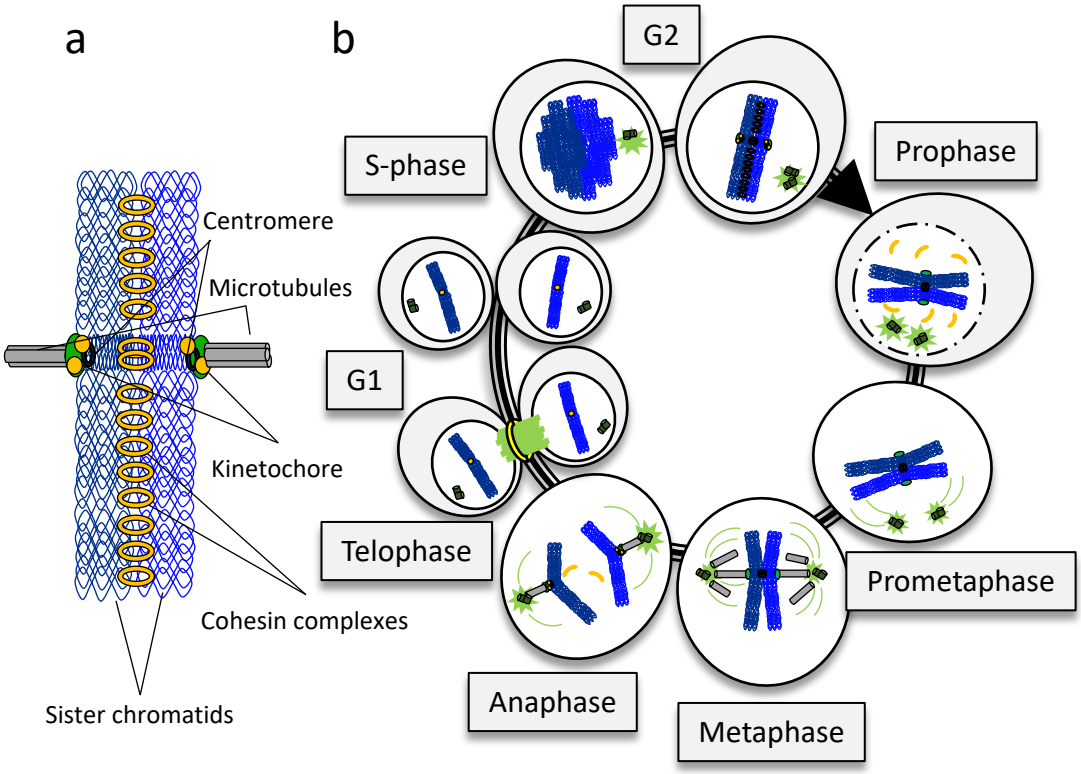

Figure 1.1. Typical progression of the cell cycle.
a) Representative image of a single chromosome, depicting the centromere, kinetochore and sister-chromatid cohesion by cohesin complexes. **b)** Diagram to depict each stage of the cell cycle. During DNA replication (S phase), sister chromatid cohesion is established. On entry into mitosis, the duplicated DNA is condensed by the action of condensin. This leads to the formation of distinct mitotic chromosomes during prophase. During prometaphase, microtubules begin to attach to sister kinetochores. At metaphase, chromosomes align at the centre of the cell due to bipolar spindle attachment (chromosome biorientation). This promotes sister-chromatid disjunction and supports equal chromosome transmission during anaphase.

In addition to the aforementioned features that ensure faithful chromosome segregation, cellular mechanisms functioning as late as anaphase have also been attributed to securing accurate transmission of the genome. It has been shown that separating sister chromatids are able to remain intertwined by DNA linkages, despite commitment to anaphase. These DNA linkages can take the form of bulky anaphase bridges, which are detectable through the use of conventional DNA staining methods such as DAPI; or alternatively, ultra-fine DNA bridges (UFBs). Unlike bulky anaphase bridges, UFBs are detectable by protein association rather than by conventional DNA staining methods (Baumann et al. 2007; Chan et al. 2007; Chan and Hickson 2009). UFBs can originate at various distinct chromosomal locations. These include centromeres, telomeres, ribosomal DNA (rDNA) regions and common fragile sites (CFS) (Fernández-Casañas and Chan 2018). UFBs are generally considered to be unresolved double-stranded DNA (dsDNA) catenanes, but it remains unclear whether dsDNA catenanes best describes the origin of all UFB formation(s). UFBs become observable through the detection of a distinct set of proteins, collectively referred to as the UFB-binding complex. The core of this complex consists of PICH (PLK-interacting checkpoint helicase), BLM (Bloom's syndrome helicase) and one of BLMs interacting partner proteins, Topoisomerase IIIα (TOP3) (Baumann et al. 2007; Chan et al. 2007). It is generally believed that the UFB-binding complex functions to resolve unprocessed DNA intertwinements, thereby functioning to promote faithful chromosome segregation (Fernández-Casañas and Chan 2018). However, the regulation and precise molecular mechanism of UFB resolution continues to be explored.

Many of the mechanistic processes involved in maintaining faithful chromosome segregation requires regulatory control by protein kinases. The activity of the mitotic kinase Polo-like kinase 1 (PLK1) has been attributed to several key events during mitosis (Barr et al. 2004; Zitouni et al. 2014). This includes a requirement for PLK1 activity during stable MT-KT attachment, an essential feature of chromosome biorientation (Barr et al. 2004; Lénárt et al. 2007; Sunkel and Glover 1988). Cells lacking PLK1 activity have been shown to display gross chromosomal mis-alignment patterns and this has been accredited to a failure of cells to correctly maintain stable MT-KT attachment (Lénárt et

al. 2007; Steegmaier et al. 2007). However, a precise molecular mechanism to fully explain this remains undescribed. Therefore, further investigation into the loss of function of PLK1 during mitosis may help to explain how PLK1 facilitates chromosome biorientation and promotes faithful chromosome segregation. In addition, PLK1 inactivation experiments may also help to reveal how UFB-binding proteins could be regulated.

PICH, one of the core UFB-binding proteins was originally identified through its interaction with PLK1 and both proteins display matching localisation patterns at kinetochores during mitosis (Baumann et al. 2007). Therefore, PLK1 may provide a regulatory role for PICH activity. However, a definitive explanation of PICH function and regulation remains uncertain. PICH has been shown to display evidence of DNA manipulation during *in vitro* studies and also displays a preference for recruiting to DNA molecules that are subject to increasing tension (Baumann et al. 2007; Biebricher et al. 2013). Consistent with this, PICH localises to centromeres, the principal site of tension during chromosome alignment. During chromosome biorientation, centromeric DNA encounters extensive pulling forces by the mitotic spindle and likely requires constant condensation activity to counteract this pulling. Therefore, the spatiotemporal localisation of PICH at kinetochores may support a functional role in maintaining centromeric DNA architecture, during chromosome biorientation. Thus, it is tempting to speculate that PLK1 may provide regulatory control for PICH activity and/or other UFB-binding proteins. Therefore, investigating the effects of PLK1 inactivation during chromosome biorientation will help to explore this hypothesis.

The following chapter will discuss and highlight some of the essential processes involved in ensuring faithful chromosome segregation. This will begin by discussing the importance of the structural organisation of chromosomes, which is generally achieved by the action of both condensin and cohesin complexes. In addition, it will highlight how cohesin maintenance is linked to the regulation of the mitotic checkpoint. An overview of centromere establishment and kinetochore assembly will also be discussed. This will include how errors in MT-KT attachment are believed to be corrected and thereby

safeguarding chromosome biorientation. Furthermore, the last steps of segregation will be considered, concentrating on the formation of UFB structures during anaphase, whilst also detailing the key proteins believed to be involved in their resolution. This will include PICH, BLM and the mitotic kinase PLK1. Finally, the results sections will discuss the experiments undertaken and provide data to support the findings that identify PLK1 as a critical component for the protection of centromeres during mitosis (Addis Jones et al. 2019).

1.2 Chromosome organisation by the action of condensin complexes

Chromosomes must be correctly assembled into three-dimensional chromatin structures in order for accurate sister chromatid separation to occur. Distinct chromosome assembly is largely accomplished by the action of condensin complexes (Hirano 2005). This is achieved during the initial stages of mitosis, although early chromosome assembly may also begin during interphase (Hirano 2016). The depletion of condensin complexes has been shown to lead to segregation defects, in particular chromatin bridges and cytokinesis failure (Hudson et al. 2003; Ono et al. 2003). Therefore, the establishment of condensed chromosomes during mitosis, via the action of condensin complexes, remains critical for ensuring faithful chromosome segregation.

1.2.1 Condensin structure and how it dictates mitotic chromosome assembly

Most eukaryotes contain two multi-subunit condensin complexes, condensin I and II. Structurally, each condensin complex shares the same core structural maintenance of chromosome (SMC) heterodimer. This consists of SMC2 and SMC4, which interact at the hinge domain such that together the coiled-coil arms (SMC2 and SMC4) adopt a V-like shape. A non-SMC subunit (Kleisin) forms a bridge between the SMC arms, completing the formation of a ring-like structure (Hirano 2016). This configuration is believed to enable SMC containing proteins to participate in DNA entrapment (Hirano and Hirano 2006; Nasmyth 2011). Condensin I and II can each be distinguished by structural differences in their non-SMC regulatory subunits. This includes a Kleisin subunit (CAP-H and H2) and a pair of HEAT subunits (CAP-D2/G and CAP-D3/G2) (Hirano 2016) **(Fig. 1.2a)**. However, despite a detailed understanding of condensin structure, it remains unclear how the ring-like condensin complex is able to organise chromatin correctly.

It is largely agreed that condensin activity directly contributes to achieving the rod-shaped chromosomes observed during mitosis (Hirano 2005, 2012, 2016). However, a precise molecular mechanism to explain how the mitotic chromosome is assembled

continues to be uncertain (Sakai et al. 2018). Despite this ambiguity, condensin promotes the formation of chromatin loops and the consecutive arrangement of such chromatin loops is the likely basis for chromosome assembly during mitosis (Gibcus et al. 2018; Sakai et al. 2018). However, explaining how such chromatin loops are organised remains a topic for debate in the field.

It is clear that mitotic chromosomes rely on condensin activity for their correct assembly. This has been demonstrated by depletion experiments. Following the depletion of condensin I, mitotic chromosomes become disorganised, being described as 'swollen' in appearance. In contrast, depletion of condensin II leads to a different chromosome disorganisation, described as 'curly' in shape (Ono et al. 2003). These observable architectural alterations highlight the importance of both condensin complexes to achieve the correct cylindrical shape of mitotic chromosomes. It has also been demonstrated with the use of Xenopus extracts that condensin I contributes to the lateral compaction (i.e. inward compaction) of chromosome architecture, along with another SMC containing complex cohesin (discussed in next section). In contrast, condensin II can provide axial shortening (i.e. top to bottom compaction) aiding in correct chromosome assembly (Shintomi and Hirano 2011) **(Fig. 1.2b)**. These findings provide a logical explanation of how condensin functions to achieve the rod-like shape of mitotic chromosomes.

1.2.2 Activation and spatiotemporal regulation of condensin

Condensin activity is regulated by different phosphorylation events (Bazile et al. 2010). Early *in vitro* studies inferred that cyclin dependent kinase 1 (CDK1) phosphorylation of condensin was able to promote its activity (Kimura et al. 1998). Recent reports have confirmed that CDK1-dependent phosphorylation was sufficient for condensin I activity (Shintomi et al. 2015). In addition, PLK1 has been reported to phosphorylate condensin II at a site on one of its non-SMC subunits, CAP-H2 (Kagami et al. 2017). This PLK1 dependent phosphorylation occurs after the initial CDK1 'priming' phosphorylation (St-

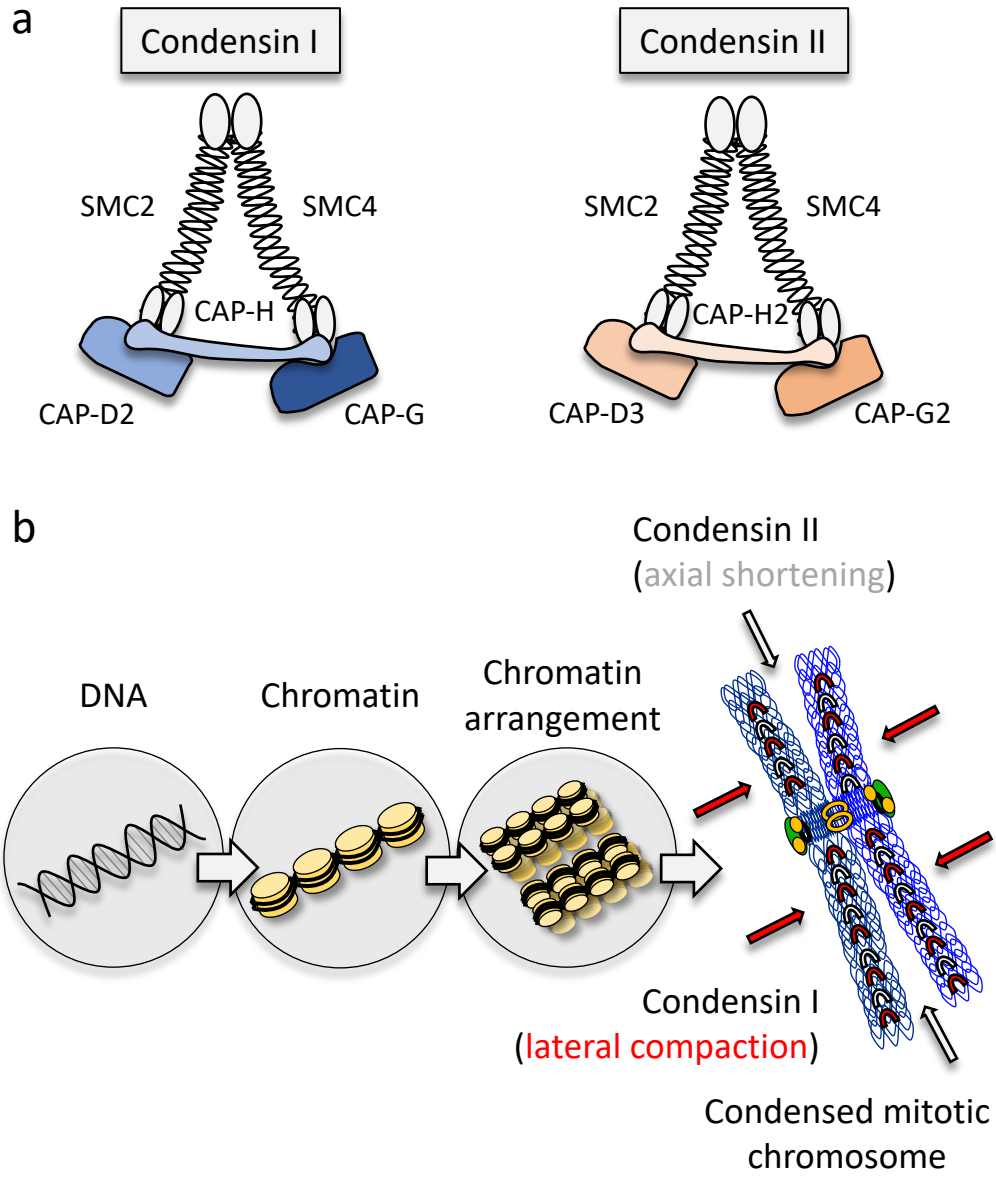

Figure 1.2. Mitotic chromosome assembly by condensin complexes.
a) Diagram to illustrate the structural features and components of Condensin I and Condensin II. **b)** Condensin plays vital roles in chromosome compaction and organisation, generating the distinctive mitotic chromosome architecture. DNA is organised around nucleosomes, which forms chromatin structures. Condensin supports the arrangement of chromatin loops, and influences how mitotic chromosomes are arranged. Condensin I is required for lateral compaction of chromatin loops (red lines), whilst condensin II may function to promote axial shortening (grey arrows) (diagrams adapted from Robellet, et al. 2017; Antonin & Heumann 2016; Hirano & Tatsuya 2012).

Pierre et al. 2009). Therefore, it has been suggested that CDK1-dependent phosphorylation promotes the initial stages of condensin activity, whilst PLK1 phosphorylation may ensure continual condensation as CDK1 levels begin to drop during late mitosis (Bazile et al. 2010). Therefore, PLK1 may ensure the continual compaction of chromosomes during later stages of mitosis. This highlights how essential processes involved in chromosome organisation and assembly require phosphorylation for their appropriate function.

The spatiotemporal regulation of each condensin complex is remarkably different. Condensin I can access nuclear chromatin following nuclear envelope breakdown (NEBD) and is exported out of the nucleus following mitotic exit (Ono et al. 2004). This would suggest that condensin I can only play a role in chromosome compaction during mitosis. In contrast, condensin II is present within the nucleus of interphase cells and has been reported to begin contributing to chromosome condensation as early as S phase (Ono et al. 2004, 2013). Inappropriate condensin activity during S phase is likely to have detrimental consequences. Therefore, condensin II interphase function(s) are probably tightly regulated. In support of this, a study using *Xenopus laevis* cell free extracts showed that mutations in the human MCPH1 protein resulted in an inhibitory function against condensin II activity during interphase. In humans, mutations in MCPH1 have been shown to result in primary microcephaly, highlighting the potential dangers of unregulated compaction of DNA before mitosis onset (Yamashita et al. 2011).

It remains uncertain whether condensin I and II have overlapping roles in chromosome organisation. Interestingly, both yeast species *Saccharomyces cerevisae and Schizosaccharomyces pombe* only contain condensin I. In contrast, vertebrates and plants contain both condensin I and II (Hirano 2005, 2012). Therefore, questions have arisen regarding the need for two condensins, unless they hold distinct functions. Depletion experiments across various different model systems have led to conflicting results regarding the activity of individual condensin complexes, something referred to as the 'condensin paradox' (Hirano 2016). However, depletion experiments in human HeLa cells demonstrated a need for both condensin I and II complexes in order for

correct mitotic chromosome assembly (Ono et al. 2003). Therefore, these experiments would imply that the activation and spatiotemporal control of condensin complexes remains critical to mitotic chromosome assembly.

1.2.3 Condensin ensures correct centromere/kinetochore structure

In addition to the critical role condensin plays in the assembly of chromosome architecture during mitosis, it has also been suggested that the function of condensin at the centromere/kinetochore is key to maintaining faithful chromosome segregation. Condensin I, and in particular condensin II, have been reported to concentrate at inner kinetochore regions (Ono et al. 2003, 2004). This could suggest that condensin plays a key role in correct centromere/kinetochore arrangement, especially as spindle pulling forces may disrupt chromosome centromere DNA compaction and organisation. The depletion of condensin in HeLa cells has been shown to result in kinetochore structure and function abnormalities, leading to chromosome misalignment and segregation defects (Ono et al. 2004; Samoshkin et al. 2009). Notably, the misalignment defects reported were due to errors in KT-MT attachment (Samoshkin et al. 2009). This was highlighted as merotelic attachments, which describes how a single kinetochore can bind microtubules from both spindle poles rather than one (Gregan et al. 2011). The segregation defects reported were due to an increase in chromosome bridge formation (Samoshkin et al. 2009). Therefore, condensin could function to correctly arrange chromatin composition, possibly at regions of the chromatin beneath kinetochores and thereby facilitating correct kinetochore assembly.

In support of this idea, the same study also showed that condensin is required for the deposition and maintenance of CENP-A, the centromere specific histone variant that is an essential component for kinetochore assembly (discussed in section 1.4). Condensin depletion led to a reduction in detectable newly synthesised CENP-A at the centromere (Samoshkin et al. 2009). The deposition of CENP-A at centromeres acts as the foundation for building the centromere-kinetochore axis (McKinley and Cheeseman 2016).

Therefore, a disruption to this assembly may well interfere with centromeric chromatin arrangement and consequently effect kinetochore assembly. This could suggest that condensin activity at the centromere is required for the establishment and possibly the maintenance of correct centromeric chromatin. In support of this idea, Samoshkin et al reported that the centromere architecture was altered, leading to the detection of centromere/kinetochore stretching. They showed a distortion of both outer kinetochore components BUB1 and HEC1, along with CENPA and core centromere region elongation, as displayed by CREST staining. The apparent stretching was dependent on microtubule tension, as co-treatment with nocodazole abolished the signs of kinetochore/centromere distortion (Samoshkin et al. 2009). These findings could support the idea that condensin activity may be required to counteract microtubule-spindle pulling forces. Therefore, condensin activity is probably required for correct centromere/kinetochore assembly and maintenance, perhaps by ensuring centromere rigidity.

In partial agreement with this idea, it has also been suggested that condensin is responsible for determining centromere chromatin stiffness. An absence of condensin in chicken DT40 cells has been shown to lead to mitotic delays, caused by a disruption in spindle checkpoint silencing. This was attributed to core centromeric chromatin deformation and weakening, rather than a disruption to chromatin near the kinetochore (Ribeiro et al. 2009). However, a later study described a lack of detectable kinetochore phenotypes after condensin depletion (Green et al. 2012). This highlights some of the conflicting reports that exist regarding condensin function at the centromere/kinetochore. However, the differences reported between core centromere distortion and kinetochore stretching could simply be due to disparities in the cellular systems examined (HeLa vs. DT40).

In summary, although disparities remain between experimental systems it is generally agreed that condensin plays a vital role in mitotic chromosome assembly. In particular, condensin ensures that centromeres are correctly arranged, which enables faithful

chromosome segregation. However, condensin is not the only factor to ensure structural integrity of chromosomes.

1.3 Sister-chromatid cohesion is mediated by cohesin

During DNA replication cells must generate identical copies of their genome in order for equal transmission into daughter cells. Chromatinisation of the duplicated DNA molecules establishes the formation of sister chromatids, which must remain together throughout S-phase and only begin separation during anaphase. This physical attachment is referred to as sister chromatid cohesion and is essential for chromosome biorientation. In particular, chromosome biorientation requires persistent centromeric sister chromatid cohesion to counteract the pulling forces generated by microtubules. This ensures the correct bipolar alignment of chromosomes during metaphase. Therefore, cohesion between sister chromatids can be considered to facilitate the symmetrical segregation that occurs during faithful chromosome separation (Peters 2012). Defects in chromosome cohesion can lead to the unequal distribution of genetic material and result in aneuploidy, a major cause of non-viable pregnancies (Munné et al. 2007). Therefore, understanding how sister chromatid cohesion is established and maintained, is key to explaining how cells prevent such erroneous outcomes. Although sister chromatid cohesion can be influenced by more than one factor, such as DNA entanglements generated during DNA replication (Holm 1994), the principal mediator of cohesion comes from the action of a multi-subunit protein complex called cohesin (Nasmyth 2001).

1.3.1 Structural composition of the cohesin complex

Cohesin is a member of the SMC complex family and has structural similarities to condensin (Nasmyth and Haering 2005). Much like condensin, cohesin forms a ring-like structure, which consists of two SMC coil-coiled arms and a non-SMC containing Kleisin subunit. Cohesin features two SMC proteins, SMC1 and SMC3. The Kleisin subunit (Scc1/RAD21) forms a bridge between these two SMC arms (Haering et al. 2002). In addition to this core structure, cohesin complexes also contain further subunits. These include the Scc3 subunit in yeast or stromal antigen SA/STAG in higher eukaryotes.

Further still, vertebrates contain at least two SA/STAG proteins, called SA1 and SA2 (Losada et al. 2000; Sumara et al. 2000). The Scc3/SA subunit binds directly to the Kleisin subunit (Scc1/RAD21), whilst several other factors also interact with the Scc1 and Scc3/SA subunits. These include PDS5, sororin and WAPL (Nasmyth and Haering 2005) **(Fig. 1.3a)**. These additional factors are believed to dictate the dynamic association of cohesin on the DNA.

1.3.2 Regulation of cohesin loading onto DNA and its activity

Cohesion of sister chromatids by cohesin ensures that duplicated sister chromatids are maintained together until anaphase, a pre-requisite for faithful chromosome segregation. Loading of cohesin complexes onto the DNA begins prior to S phase, whilst sister chromatid cohesion is only established during DNA replication (Uhlmann and Nasmyth 1998). The ring-like structure of cohesin is thought to embrace the duplicated DNA molecules (Haering et al. 2008; Nasmyth 2011) and its loading onto the DNA relies on ATP hydrolysis (Arumugam et al. 2003). An additional complex, referred to as adherin (Furuya et al. 1998), or kollerin (Nasmyth 2011), is further required for cohesin recruitment. The adherin/kollerin complex is formed of two subunits, Scc2-Scc4 in budding yeast (Ciosk et al. 2000), or NIPBL-MAU2 in mammals (Visnes et al. 2014). It is believed that a transient opening of the cohesin ring facilitates its loading (Gruber et al. 2006), whilst its establishment during S-phase is mediated by the essential acetyltransferase activity of Eco1 (ESCO1/2 in mammals) **(Fig. 1.3b)** (Hou and Zou 2005; Ben-Shahar et al. 2008; Skibbens et al. 1999; Tóth et al. 1999). Once fully established, cohesin then ensures cohesion of sister chromatids until its timely release during mitosis. Without such stable association between duplicated sisters, equal segregation of chromosomes would be severely affected. Therefore, along with condensin, cohesin also ensures correct chromosome organisation.

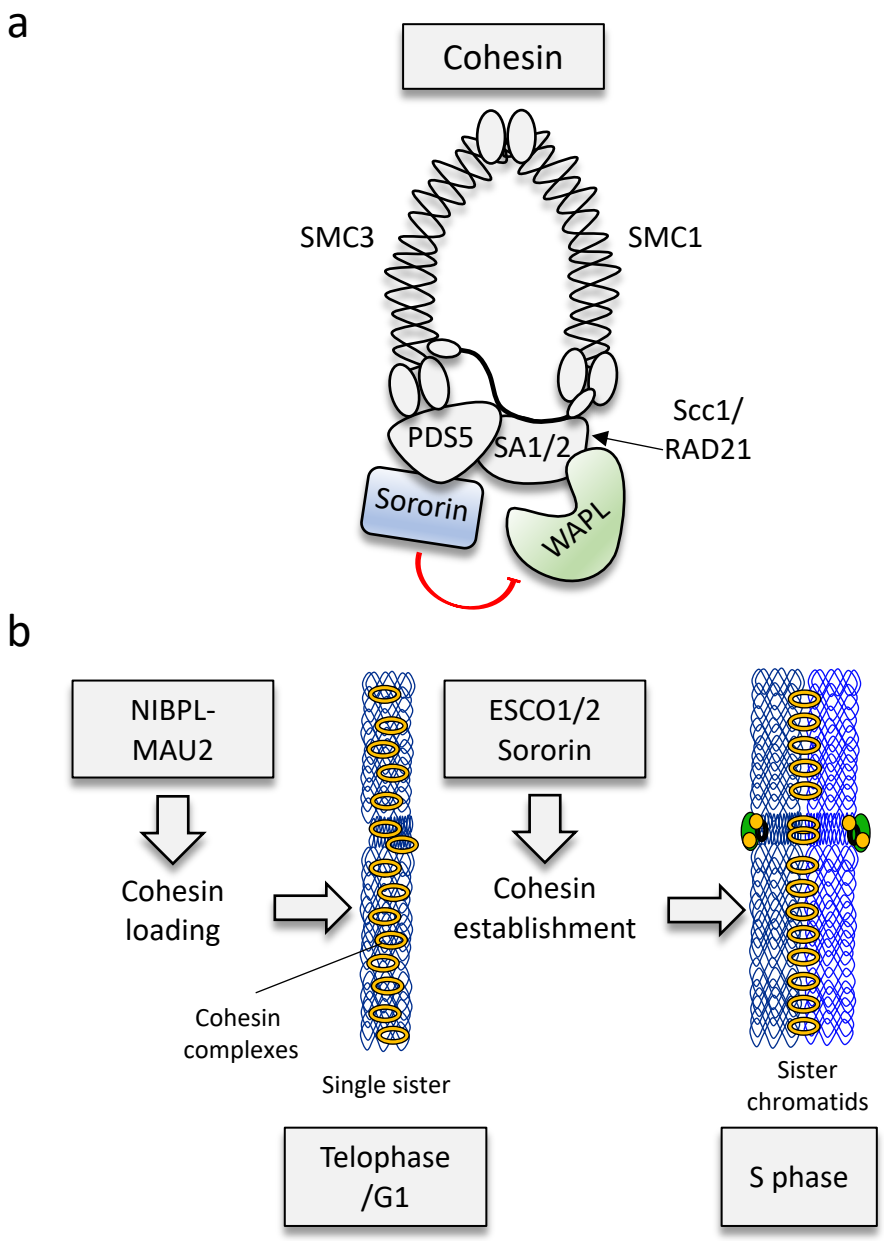

Figure 1.3. Sister chromatid cohesion is established and maintained by cohesin.
a) Diagram shows the key structural components of the SMC complex, cohesin. **b)** Loading and establishment of sister chromatid cohesion. NIBPL-MAU2 promotes cohesin loading during telophase/G1. Acetylation of cohesin by ESCO1/2 acetyltransferase during S phase leads to cohesin establishment. Sororin acts to inhibit WAPL-dependent cohesin release (diagrams adapted from Gligoris & Löwe 2016; Peters and Nishiyama 2012).

1.3.3 A two-step process of cohesin removal during mitosis

The cohesin mediated connection that arises between sister chromatids must be disconnected during mitosis, allowing each sister to be transported to opposite poles of the cell during anaphase. In vertebrates, the removal of cohesin complexes occurs in a two-step process. The majority of arm cohesin is removed during early mitosis, during a process referred to as the 'prophase pathway' (Waizenegger et al. 2000). In contrast, centromeric cohesin continues to remain established during early mitosis (Waizenegger et al. 2000). Only following the onset of anaphase do cells allow the timely cleavage of centromeric cohesin, along with any remaining arm cohesin complexes via the activation of a protein called separase (Uhlmann et al. 1999, 2000). Therefore, cohesin maintains chromosome structure throughout S-phase and ensures a stable connection between sisters for equal separation during anaphase **(Fig. 1.4a, b)**.

1.3.4 Dissociation of cohesin during the 'prophase pathway'

Cohesin removal during interphase and early mitosis is dependent on the activity of WAPL (Gandhi et al. 2006; Kueng et al. 2006). Sororin, which acts as an inhibitor of WAPL, antagonises WAPL-dependent cohesin removal (Nishiyama et al. 2010; Rankin et al. 2005). Sororin is thought to displace WAPL from interacting with PDS5 and the resulting conformational change to the cohesin complex is thought to prevent WAPL-dependent release of cohesin **(Fig. 1.4a)** (Nishiyama et al. 2010). WAPL is thought to remain connected to the cohesin complex as there are no reports to suggest that it totally dissociates. This may allow cohesin to be rapidly loaded and released, without physical cleavage of cohesin subunits **(Fig. 1.4a)**. This mechanism of cohesin release occurs throughout interphase, as WAPL depletion during this time leads to increased time of cohesin association to the DNA (Kueng et al. 2006).

Cohesin release during prophase is regulated by WAPL and phosphorylation of the SA2 subunit (Hauf et al. 2005). This is achieved by the action of the mitotic kinase PLK1

(Sumara et al. 2002), although additional kinases such as CDK1 and Aurora B may also contribute **(Fig. 1.4a)** (Losada et al. 2002). Therefore, during mitosis the mitotic kinases dictate the release of cohesin, through activation of the 'prophase pathway'. WAPL is antagonised by sororin and sororin inactivation is also dependent on phosphorylation (Nishiyama et al. 2010). This has been reported to be achieved by both PLK1 (Zhang et al. 2011) and CDK1 (Dreier et al. 2011). Therefore, mitotic kinases promote a reduction in sororin activity during mitosis, which leads to an increase in WAPL-dependent cohesin release and subsequently activation of the 'prophase pathway' **(Fig. 1.4a)**.

In addition, the adherin/kollerin complexes are also removed from chromosomes during prophase (Gillespie and Hirano 2004; Watrin et al. 2006), suggesting that cohesin is prevented from being loaded onto the DNA during this stage. Therefore, mitotic kinases influence both the WAPL-dependent release of cohesin, and cohesin complex recruitment. This allows cells to achieve rapid cohesin release during the prophase pathway, although some cohesin must remain, in particular centromeric cohesin.

1.3.5 Centromeric cohesin is cleaved by separase

Centromeric cohesin is critical for the bipolar orientation that chromosomes adopt during metaphase. The majority of arm cohesin is removed during the prophase pathway, whilst centromeric cohesin is maintained (Waizenegger et al. 2000). Centromeric cohesin is protected by shugoshin activity, which ensures the maintenance of centromeric cohesion until the onset of anaphase **(Fig. 1.4a)**. Shugoshin (SGO1) is a centromeric protein, which was shown to influence chromosome segregation and depletion experiments demonstrated its protective role in maintaining centromeric cohesion (Kitajima et al. 2005; Salic et al. 2004).

Unlike the WAPL-dependent release of cohesin during the prophase pathway, centromeric cohesin requires cleavage by a protein called separase (Uhlmann et al. 1999, 2000). Centromeric cohesin is protected from WAPL-dependent release by

shugoshin (SGO1) in a complex with protein phosphatase 2A (PP2A) (Kitajima et al. 2006). The SGO1-PP2A protein complex is recruited to centromeres, where SGO1 shields centromeres from WAPL, whilst PP2A counteracts the phosphorylation of cohesin subunits by the mitotic kinases **(Fig. 1.4a)** (Gutiérrez-Caballero et al. 2012). These phosphorylation events would ordinarily promote cohesin release during the prophase pathway (see above). However, SGO1-PP2A functions to protect against this and ensures centromeric cohesin is maintained until anaphase. Centromeric cohesin can only be removed by the action of separase. Separase cleaves the Scc1/RAD21 subunit of cohesin and thereby triggers the release of cohesin through the physical opening of its ring-like structure (Uhlmann et al. 1999, 2000). Separase activity is suppressed by the inhibitory action of its interacting partner securin (Esp1 in *S. cerevisiae*). Removal of the inhibitory signal by securin on separase is associated with anaphase onset (Uhlmann et al. 2000) and this is intricately linked to the activation of the mitotic checkpoint **(Fig. 1.4a, b)**.

1.3.6 Centromere cohesin cleavage is linked to the mitotic checkpoint

Faithful chromosome segregation during anaphase requires the timely cleavage of centromeric cohesin by seperase (Hauf et al. 2001). This is only achieved when all chromosomes are aligned correctly during metaphase, thereby satisfying the mitotic checkpoint. The mitotic checkpoint, otherwise referred to as the spindle assembly checkpoint (SAC), functions to survey the status of kinetochore-microtubule (KT-MT) attachments (Lara-Gonzalez et al. 2012). Errors in KT-MT attachment maintains activation of the SAC, thereby ensuring that cells do not enter anaphase prematurely (Rieder et al. 1995). Hence, cells are protected against possible chromosome missegregation events due to KT-MT attachment errors and premature segregation.

The SAC is comprised of a group of proteins known as MAD (mitotic-arrest deficient) (Li and Murray 1991) and BUB (budding uninhibited by benzimidazole) (Hoyt et al. 1991). These are MAD1, MAD2 and BUBR1 (MAD3), along with BUB1 and BUB3. The SAC is

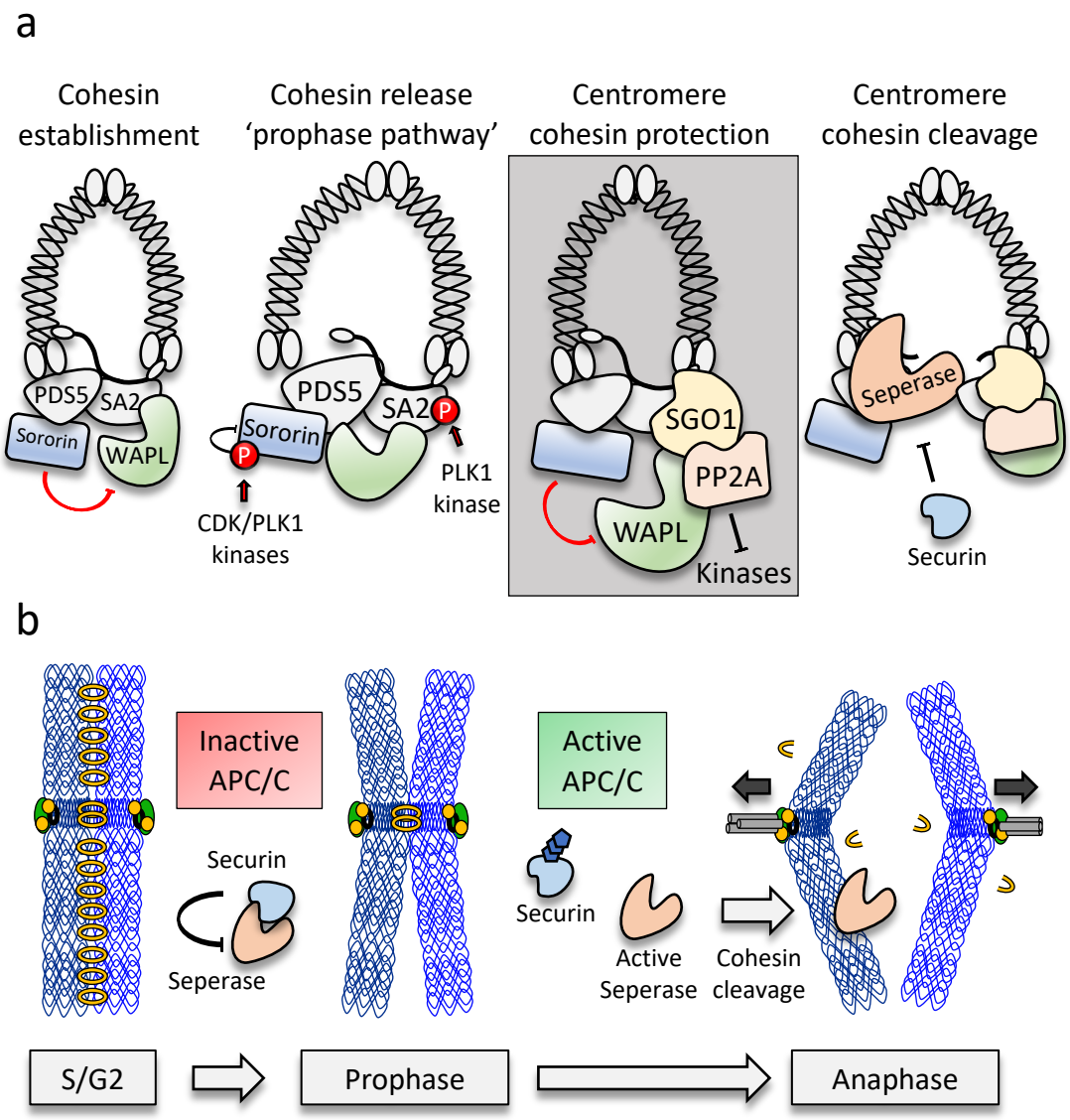

Figure 1.4. Cohesin release by WAPL and cleavage by seperase.
a) Following cohesin establishment during S-phase, cohesin is released during prophase via a WAPL-dependent mechanism during the 'prophase pathway'. The mitotic kinases CDK1 and PLK1 influence WAPL-dependent release of cohesin, by targeting both the SA2 and sororin subunits of cohesin. In contrast, centromeric cohesin remains established until anaphase onset. SGO1-PP2A counteracts mitotic kinase phosphorylation at the centromere, ensuring centromere cohesin remains until commitment to anaphase. Commitment to anaphase is achieved via the activation of the anaphase promoting complex/cyclosome (APC/C), which triggers the release of securin, thereby enabling seperase-dependent cleavage of centromere cohesin. **b)** Schematic diagram to represent cohesin release and cleavage during mitotic progression. During S/G2 phase cohesin remains established. During prophase the WAPL-dependent cohesin release at chromosome arms occurs, due to the activation of the prophase pathway. The APC/C remains inactive and securin prevents seperase activity. Commitment to anaphase leads to APC/C activation and seperase dependent cleavage of centromere cohesin (diagram adapted from Peters and Nishiyama, 2012).

active during early mitosis and its primary function is to prevent the precocious separation of sister chromatids (Lara-Gonzalez et al. 2012; Musacchio and Salmon 2007; Taylor et al. 2004). Specifically, the SAC functions to negatively regulate the anaphase promoting complex/cyclosome (APC/C), an E3-ubiquitin ligase that targets proteins for degradation via the 26S proteasome (Lara-Gonzalez et al. 2012). The SAC achieves this by targeting the APC/C co-activator CDC20, via protein phosphorylation (Ciosk et al. 2000; Musacchio and Salmon 2007). SAC targeting of CDC20 renders the APC/C unable to ubiquitinate its target proteins, thereby preventing them from being signalled for proteasomal degradation **(Fig. 1.5a)**.

Once stable bipolar attachment is achieved cells commit to anaphase. At this point SAC signalling becomes diminished and the APC/C^{CDC20} complex forms, which begins to target proteins for ubiquitin-dependent proteasomal degradation. One protein that is targeted is the separase inhibitor securin. Securin degradation leads to separase activation, which promotes the cleavage of the remaining cohesin complexes, in particular centromeric cohesin **(Fig. 1.5b)** (Musacchio and Salmon 2007). Therefore, centromeric cohesin cleavage is intricately linked to the mitotic checkpoint and APC/C^{CDC20} activation.

PLK1 (Cdc5) dependent phosphorylation of the cohesin subunit Scc1/RAD21 acts as a regulatory mark for cohesin cleavage (Alexandru et al. 2001). This provides another example of how kinases such as PLK1, can play key roles in maintaining correct chromosome organisation, through regulating the timely removal of cohesin complexes during mitosis.

Overall, accurate chromosome assembly and organisation is achieved by the action of both condensin and cohesin complexes, whilst their activity is essential for maintaining faithful chromosome segregation. Both complexes are tightly regulated by phosphorylation by various kinases, in particular PLK1. This demonstrates how kinase function can aid in the regulation of chromosome assembly and maintenance.

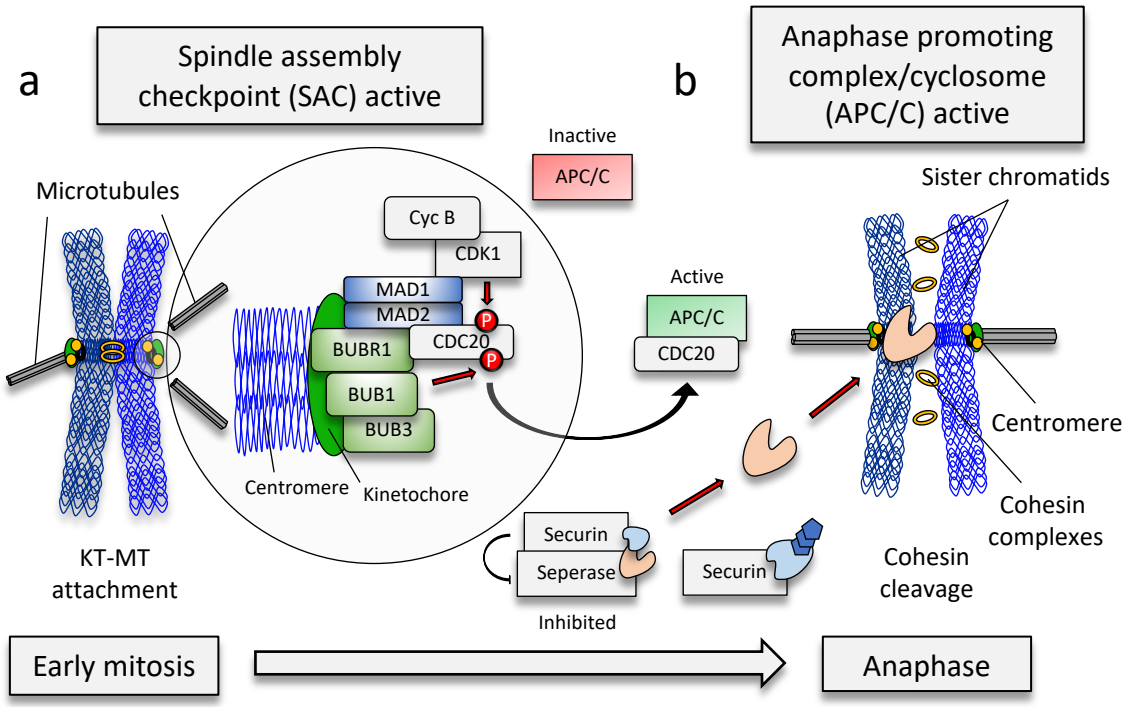

Figure 1.5. The spindle assembly checkpoint (SAC) and the regulation of the anaphase promoting complex (APC).

a) During early mitosis, various components of the SAC function to monitor the status of kinetochore-microtubule attachments. If KT-MT attachments remain absent or unstable, the SAC prevents the activation of the APC/C, via phosphorylation of of its co-activator, CDC20. When the APC/C remains inactive, securin ensures that the activity of seperase remains inhibited. **b)** Following stable KT-MT attachment (metaphase), the SAC becomes satisfied and no longer phosphorylates CDC20. This allows CDC20 to bind with its partner, the APC/C, and promotes anaphase progression. The APC/C^{CDC20} E3-ubiquitin ligase targets securin for proteasomal degradation, thereby allowing the release of seperase. Seperase can then actively cleave centromeric cohesin allowing for sister chromatid separation during anaphase.

However, despite extensive efforts to understand how both condensin and cohesin function to maintain chromosome arrangement, the various multifaceted mechanisms that regulate chromosome assembly and arrangement remain a challenge. Future studies may help to reveal how chromosome segregation errors arise, whilst the centromere and kinetochore remain key targets for further study, as they provide the platform for correct chromosome segregation.

1.4 Centromere assembly

Faithful chromosome segregation relies on a distinct region within each chromosome called the centromere. Centromeres dictate chromosome segregation by acting as a connection point for the attachment of the mitotic spindle. They achieve this by providing a foundation for the recruitment and assembly of the macromolecular protein complex, the kinetochore. The kinetochore forms at opposite sides of the core centromere and during microtubule spindle attachment, the kinetochore becomes the key player involved in directing chromosome segregation (McKinley and Cheeseman 2016).

In the majority of eukaryotes, centromeres are established by the presence of highly repetitive DNA arrays, such as tandemly repeated satellites or transposable elements. In particular, human centromeres contain α-satellite repeats, which can extend for several megabases (Mb) and contribute to a large percentage of the overall genome (Barra and Fachinetti 2018; McKinley and Cheeseman 2016). Although repetitive sequence arrays are important for centromere assembly, they are not sufficient for centromere identity. Instead, centromere identity relies on epigenetic arrangement, which is dictated by the presence of specialised nucleosomes that contain the histone H3 variant, CENP-A (centromere protein A) (Earnshaw et al. 2013; Earnshaw and Rothfield 1985).

In general, defects to centromere assembly lead to chromosome missegregation and aneuploidy (Barra and Fachinetti 2018; McKinley and Cheeseman 2016). Thus, emphasising the importance of correct centromere assembly. Errors in centromere assembly can lead to numerical chromosome alterations and centromere dysfunction can also lead to chromosomal structural alterations. Centromeres have an intrinsic fragility that can lead to chromosome breakage. This fragility is probably due to the highly repetitive DNA sequence arrangement at the centromere, which requires extensive organisation (Barra and Fachinetti 2018). Inaccuracies in centromere

organisation can lead to centromeric breakage, which can result in chromosome rearrangement, a common feature of several cancer cells (Knutsen et al. 2010). Therefore, centromere integrity is key to maintaining chromosome stability and faithful segregation.

Cyril Darlington, who first defined the term centromere in 1936, spoke of how centromeres "[they] must be considered in terms of function rather than form, since the function is evident and the form elusive" (Darlington and Hall 1936). This statement continues to resonate with centromere biologists. Despite extensive studies, many molecular features of the centromere remain unclear and ongoing work continues to uncover greater detail and better understanding of centromere function.

1.4.1 Centromere structure: monocentric (point & regional)

Most eukaryotes, including humans, contain monocentric chromosomes. These are identified by the assembly of a single localised centromere structure along each chromosome. This is distinctly different to organisms such as the nematode (*Caenorhabditis elegans*), which feature holocentric chromosomes. Holocentric chromosomes are comprised of a diffuse centromere that covers the whole chromosome, a characteristic phenomenon referred to as holocentricity (Mandrioli and Carlo Manicardi 2012). Instead, monocentric chromosomes are distinguished by two key variants, either by the formation of point centromeres or alternatively regional centromeres.

Point centromeres contain short DNA sequence specific elements that define the location of the centromere. These DNA elements are both necessary and sufficient for proper kinetochore assembly **(Fig. 1.6a)**. The most studied example of point centromere assembly comes from the budding yeast *Saccharomyces cerevisiae* **(Fig. 1.6a)** (Clarke and Carbon 1980). Various studies have demonstrated that removal or mutation of the centromere specific sequence elements promotes chromosome missegregation

(Carbon and Clarke 1984; Clarke and Carbon 1983; McGrew et al. 1986). Whereas, exchange or orientation change of centromere specific DNA elements is sufficient to promote normal chromosome segregation (Carbon and Clarke 1984). Therefore, point centromeres rely heavily on DNA sequence for their function.

The majority of regional centromeres also contain repetitive DNA sequences. However, unlike point centromeres, the repetitive sequences alone are insufficient for centromere function (McKinley and Cheeseman 2016). Regional centromeres are built on highly repetitive α-satellite arrays or retro transposons (Lower et al. 2018). In particular, human regional centromeres consists of 171bp α-satellite repeat monomers that are A-T rich in sequence **(Fig. 1.6a)**. These monomers are arranged tandemly in a head-to-tail orientation and each monomer can form further higher order repeats (HORs) (Vissel and Choo 1987; Waye and Willard 1985). Blocks of multiple HORs can then produce larger domains, which in turn can be repeated several thousands of times. This extensive arrangement then gives rise to the Mb sized core centromere (Barra and Fachinetti 2018; McKinley and Cheeseman 2016). In addition to the core centromere, a heterochromatic pericentromere also forms. This flanks the core centromere and consists of less ordered satellite repeats **(Fig. 1.6b)** (McKinley and Cheeseman 2016). Therefore, DNA sequence, although not sufficient for centromere assembly, remains an important factor for centromere organisation.

Interestingly, α-satellite arrays contain only one identified sequence specific binding protein, CENP-B (centromere protein B). The CENP-B protein binds to a 17bp sequence specific motif within the α-satellite repeats, termed the CENP-B box **(Fig. 1.6b)** (Masumoto et al. 1989; Muro et al. 1992). CENP-B has been shown to directly stabilise and influence CENP-A nucleosomes (Fujita et al. 2015). Moreover, other studies have suggested a possible redundant function(s) for CENP-B, in order to maintain chromosome segregation in the absence CENP-A (Hoffmann et al. 2016). Additionally, CENP-B may influence other centromere binding proteins, such as CENP-C, to ensure

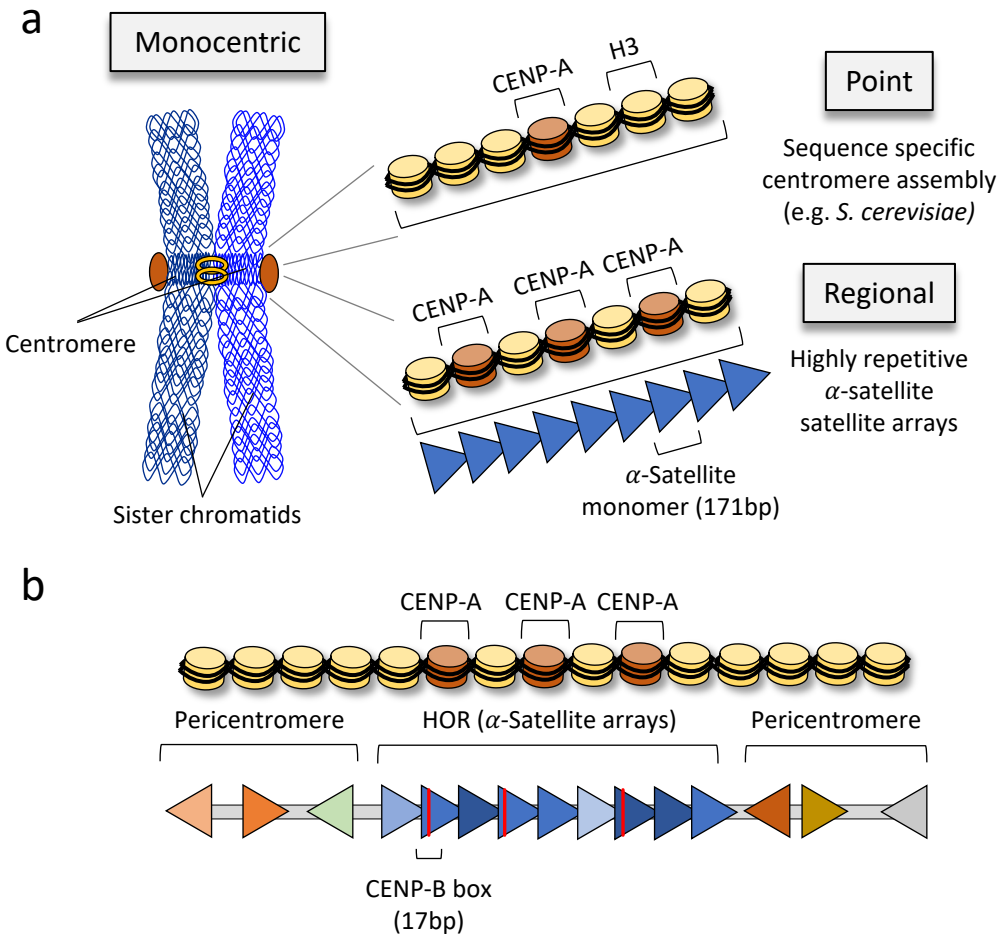

Figure 1.6. Characteristics of monocentric centromeres, including both point and regional centromeres.
a) Monocentric centromeres are assembled at a single distinct region of the chromosome. There are two types of monocentric centromere. Either Point centromeres, which are determined by sequence specific identity (e.g. *S. cerevisiae*); or alternatively, Regional centromeres, which contain repetitive DNA arrays (α-satellite DNA) and multiple CENP-A containing nucleosomes. **b)** Regional centromere α-Satellite arrays assemble to form higher order repeat (HOR) structures, which arrange to form even larger domains to build the core centromere. These are bound by α-Satellite array sequence specific binding protein, called CENP-B. In addition, heterochromatin regions of less ordered satellite repeats flank the core centromere region, forming the pericentromere (diagrams adapted from McKinley 2016; Jansen 2004; McKinley 2014).

correct kinetochore function (Fachinetti et al. 2015). However, it remains uncertain how important CENP-B is to centromere structure and function.

CENP-B is not well conserved among different species and it has been shown to be non-essential in mice (Perez-Castro et al. 1998). Furthermore, CENP-B binding is absent from the male Y chromosome (Earnshaw et al. 1987; Masumoto et al. 1989). This has led to questions around its importance in centromere biology. However, although it may not be absolutely essential, CENP-B and the underlying repetitive α-satellite arrays are undoubtedly required to enhance the fidelity of chromosome segregation.

1.4.2 Centromere identification by CENP-A

Although centromere structure relies on α-satellite arrays, this sequence is not sufficient to identify centromere assembly. Instead, the formation of centromeres in most, if not all eukaryotic cells is largely reliant on the epigenetic arrangement of CENP-A containing nucleosomes (McKinley and Cheeseman 2016). CENP-A was first described following its identification as a centromere specific antigen that was recognised by auto-antibodies from patients with a multisystem connective disorder known as CREST syndrome (Earnshaw and Rothfield 1985). During this time, CENP-A was established as a component of chromatin (Palmer et al. 1987; Palmer and Margolis 1985). CENP-A was later confirmed as a histone variant, displaying similarity to histone H3 (Palmer et al. 1991; Sullivan et al. 1994). Despite disagreements surrounding its nomenclature (Earnshaw et al. 2013; Talbert et al. 2012), CENP-A (or CenH3) is acknowledged as a centromere-specific histone variant.

CENP-A can be considered as an epigenetic marker for centromere location. CENP-A is found at neocentromeres, which are atypical centromeres capable of forming outside the canonical α-satellite arrays (Marshall et al. 2008; Voullaire et al. 1993). The existence of CENP-A at these sites suggested that CENP-A is a critical element for centromere function (Marshall et al. 2008; Tyler-Smith et al. 2002). However, its critical role in

centromere function has been questioned by the finding that certain insects, including the butterfly and moth, have no CENP-A/(CenH3) (Drinnenberg et al. 2014). Despite this, CENP-A is considered crucial for the initial identification of centromeres. Additionally, CENP-A plays an essential role in centromere inheritance. The correct inheritance of centromeres following cell division must be maintained in order to prevent spurious centromere formation, which could otherwise promote erroneous chromosome segregation.

1.4.3 Centromere inheritance & regulation of CENP-A deposition

CENP-A nucleosomes epigenetically identify the position of centromeres on each chromosome. Therefore, the stability of CENP-A is key to maintaining this mark following rounds of cellular division. Importantly, unlike other nucleosomes, CENP-A is not exchanged once incorporated at centromeres. Instead, CENP-A nucleosomes are conservatively partitioned between the newly replicated sister chromatids during DNA replication (Jansen et al. 2007). This was demonstrated by the development of a sophisticated fluorescent labelling technique (SNAP-tagged CENP-A), that allowed for the direct visualisation of CENP-A association throughout the cell-cycle. The use of this technique revealed that CENP-A does not turnover at centromeres once assembled. Instead, CENP-A remains associated to centromeres, even during S phase and has been shown to dilute between sister chromatids during DNA replication. During telophase and early G1, newly synthesised CENP-A is re-deposited (Jansen et al. 2007). This cycle of CENP-A propagation ensures that centromere inheritance is maintained following cell division **(Fig. 1.7a)**. The deposition of CENP-A at centromeres, also requires the co-ordinated action of various assembly factors to maintain this inheritance.

CENP-A has a dedicated chaperone. Two-groups simultaneously identified the Holliday junction recognition protein (HJURP) as a CENP-A chaperone, which promotes the deposition of new CENP-A (Dunleavy et al. 2009; Foltz et al. 2009). Alongside HJURP, a tri-subunit complex, known as the MIS18 complex, was also identified as a factor for

CENP-A deposition. The MIS18 complex consists of MIS18α, MIS18β and MIS18BP1 (MIS18-binding Protein-1; also known as KNL2), and this complex has been shown to further aid in CENP-A deposition (Fujita et al. 2007). The MIS18BP1 subunit also interacts with the CENP-A binding protein CENP-C, which becomes an essential interaction for MIS18 complex binding during CENP-A deposition (Dambacher et al. 2012; Moree et al. 2011) **(Fig. 1.7b)**.

This complex assembly of factors involved in the deposition of CENP-A, has been shown to be regulated by protein phosphorylation. In human cells, CDKs negatively regulate CENP-A deposition. Phosphorylation of MIS18BP1 by CDKs, reduces its potential to localise to centromeres outside of G1 (Silva et al. 2012), whilst CDK phosphorylation of HJURP has also been reported to disrupt HJURP localisation to centromeres (Müller et al. 2014). Despite these negative regulatory phosphorylation events by CDKs, CENP-A deposition has also been shown to require a licensing step. Again, phosphorylation plays a key role in this, as PLK1-dependent phosphorylation of the MIS18 complex promotes MIS18 localisation and stimulates licensing of CENP-A deposition **(Fig. 1.7b)** (McKinley and Cheeseman 2014). Bypassing both regulation of CENP-A deposition, by CDK and PLK1 phosphorylation, by constitutively targeting the MIS18α subunit was able to promote CENP-A deposition throughout the cell cycle, leading to severe mitotic defects (McKinley and Cheeseman 2014). Therefore, inheritance of CENP-A deposition also requires strict regulation in order to suppress chromosome missegregation.

In addition to CENP-A's role in centromere identification and assembly, it is also required for kinetochore assembly (Carroll et al. 2009, 2010; Fachinetti et al. 2013; Guse et al. 2011; Hori et al. 2013; Regnier et al. 2005). Artificial targeting of CENP-A to ectopic loci, has been shown to be sufficient to drive kinetochore formation and microtubule attachment. Cells were also subsequently shown to undertake chromosome segregation (Barnhart et al. 2011; Heun et al. 2006). Therefore, CENP-A appears crucial for centromere identity and function, whilst also bridging the gap between the centromere and kinetochore assembly.

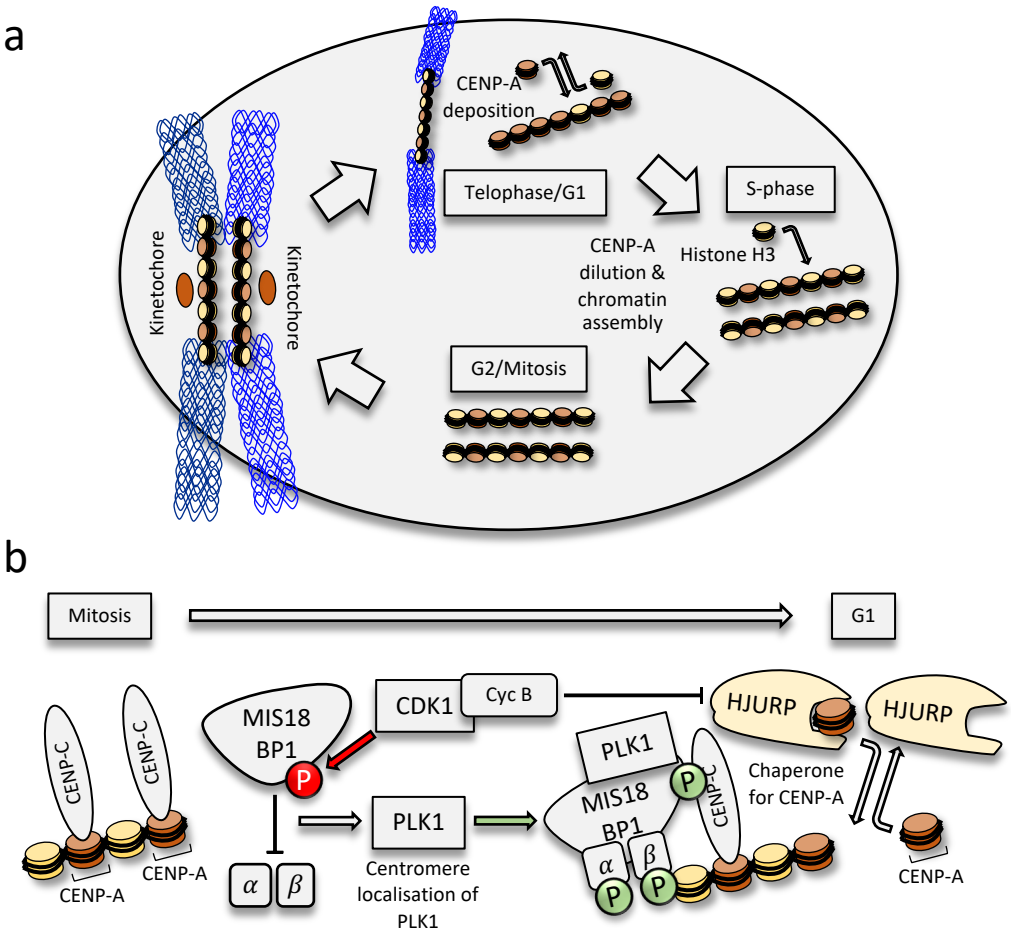

Figure 1.7. The centromere is identified by CENP-A deposition during telophase/G1.
a) Following kinetochore assembly and chromosome segregation, new CENP-A deposition occurs during telophase & G1. CENP-A nucleosomes are partitioned between the newly replicated sisters during S-phase and subsequently become diluted (Histone H3 occupies the gaps). CENP-A nucleosomes then mark the position of centromeres for kinetochore assembly (G2/Mitosis). **b)** CENP-A deposition relies on MISBP1 and its dedicated chaperone HJURP. Outside of G1 (e.g. mitosis), CDK1 prevents MIS18BP1 complex assembly and HJURP recruitment to centromeres. During G1, PLK1 binds to the MIS18 complex to promote CENP-A deposition at centromeres along with HJURP (diagrams adapted from McKinley 2016; Jansen 2004; McKinley 2014).

1.5 Kinetochore assembly

The pivotal role of centromeres, in promoting faithful chromosome segregation, is established by their role in the assembly of the kinetochore complex. This macromolecular protein complex is the attachment site of microtubules of the mitotic spindle and acts as a hub for chromosome segregation during mitosis (Cheeseman and Desai 2008). It is estimated that a human kinetochore is comprised of more than 100 proteins (Cheeseman 2014). Hence, kinetochore architectural assembly is not only essential for correct chromosome segregation, but also possesses a very complex structure. A key element in kinetochore assembly is the establishment of the centromere by the centromere specific histone variant CENP-A, which acts as the foundation for the building kinetochore complex. Various additional CENP factors are recruited to CENP-A, constructing the formation of the inner kinetochore. These additional CENP factors form a multi-layered protein complex, referred to as the CCAN (constitutive centromere associated network). The CCAN functions to support the establishment of further protein recruitment, which helps to build the extending kinetochore complex. Outer kinetochore assembly is largely formed of another multi-layered complex of proteins, termed as the KMN network (KNL-1/MIS12 complex/NDC80 complex). This network of proteins is then able to support kinetochore-microtubule attachment and ensures that chromosome segregation occurs with high levels of accuracy.

1.5.1 The CCAN forms the link between the centromere and kinetochore

The CCAN identifies the centromere-kinetochore interface and constitutes a group of 16 proteins that localise to centromeres throughout the cell-cycle (Cheeseman and Desai 2008). CCAN components have been entitled with alphabetically designated CENP-names (CENP-C, CENP-H, CENP-I, CENP-K, CENP-L, CENP-M, CENP-N, CENP-O, CENP-P, CENP-Q, CENP-U, CENP-R, CENP-T, CENP-W, CENP-S and CENP-X) (Amano et al. 2009; Foltz et al. 2006; Hori et al. 2008; Okada et al. 2006).

The CCAN components can be further classified into five groups. These form either the CENP-C and CENP-L-N complex (Carroll et al. 2009); the CENP-H-I-K-M complex (Foltz et al. 2006; Okada et al. 2006); the CENP-O-P-Q-U-R complex (Hori et al. 2007); and finally, the CENP-T-W-S-X complex (Nishino et al. 2012). Collectively these proteins function to recognise centromeric chromatin and bridge the gap between the centromere and the building kinetochore complex.

1.5.2 CENP-C/T (inner kinetochore) links to the outer kinetochore (KMN)

CCAN assembly at the centromere provides a platform for the association of the outer kinetochore components. Both CENP-C and CENP-T (inner kinetochore) form parallel pathways for the recruitment of the KMN network (KNL-1/MIS12/NDC80) (outer kinetochore) (Malvezzi et al. 2013; Nishino et al. 2013; Screpanti et al. 2011).

CCAN protein recruitment is tightly regulated, thereby limiting the CCAN's ability to build a full kinetochore complex prior to mitosis. This regulation is achieved via protein phosphorylation. The assembly of CENP-C and MIS12 is promoted by Aurora B kinase activity (Kim and Yu 2015). CDK phosphorylation of the NDC80 complex, which is sequestered outside the nucleus throughout interphase and therefore incapable of CCAN interaction, promotes direct interaction with CENP-T **(Fig. 1.8a)** (Gascoigne and Cheeseman 2013). Again, these examples demonstrate the important role(s) that mitotic kinases have on influencing centromere and also kinetochore assembly.

1.5.3 The KMN network links to microtubules

The outer kinetochore KMN network of proteins adds further complexity to centromere-kinetochore biology and broadens the number of proteins involved in kinetochore-microtubule attachment. It consists of three sub complexes. The KNL-1 complex consists

of KNL-1 (or Blinkin), and ZWINT (Obuse et al. 2004); whilst, the MIS12 complex consists of MIS12, NSL1, PMF1 and DSN1 (Hinshaw and Harrison 2018; Kline et al. 2006). Finally, the tetramer NDC80 complex is comprised of NDC80 (HEC1), NUF2, SPC24 and SPC25 (McCleland et al. 2004). The KMN network associates with kinetochores during prophase and dissociates from kinetochores during telophase (Varma and Salmon 2013). The outer end of NDC80, (NUF2/NDC80-(HEC1)), is the primary site for the extending microtubule binding. In contrast, the inner region of NDC80 (SPC24/25) provides the attachment site to the centromere, via the CCAN **(Fig. 1.8a)** (DeLuca and Musacchio 2012; Hori and Fukagawa 2012).

KNL-1 has also been reported to bind to NDC80, at both outer and inner locations, interacting directly with kinetochore-microtubules, or the MIS12 complex, respectively (Petrovic et al. 2010). CENP-C links the MIS12 complex to CENP-A chromatin (Hori and Fukagawa 2012), whilst both the NDC80 and KNL1 extend outwards from their junctions with CENP-T or MIS12 **(Fig. 1.8a)** (Wan et al. 2009). A number of additional proteins bind to the periphery of the outer kinetochore domain, largely dependent on KMN network binding. These additional proteins include microtubule-associated proteins (motor proteins such as dynein), plus various proteins that control the spindle assembly checkpoint (SAC) (Kops and Shah 2012). Hence, kinetochore assembly is very complex, largely due to the vast number of proteins involved.

In summary, kinetochores provide the primary site for spindle microtubule connection, a pre-requisite for faithful chromosome segregation **(Fig. 1.8b)**. Centromere and subsequent kinetochore assembly, are critical for ensuring chromosome biorientation during mitosis. However, attachment of spindle microtubules to kinetochores, may also lead to erroneous connections. The cell must first detect and destabilise inaccurate connections, whilst also suppressing anaphase onset. This sophisticated system ensures chromosomes can correctly undergo segregation. A failure to achieve this can result in chromosome instability, through errors in faithful chromosome separation.

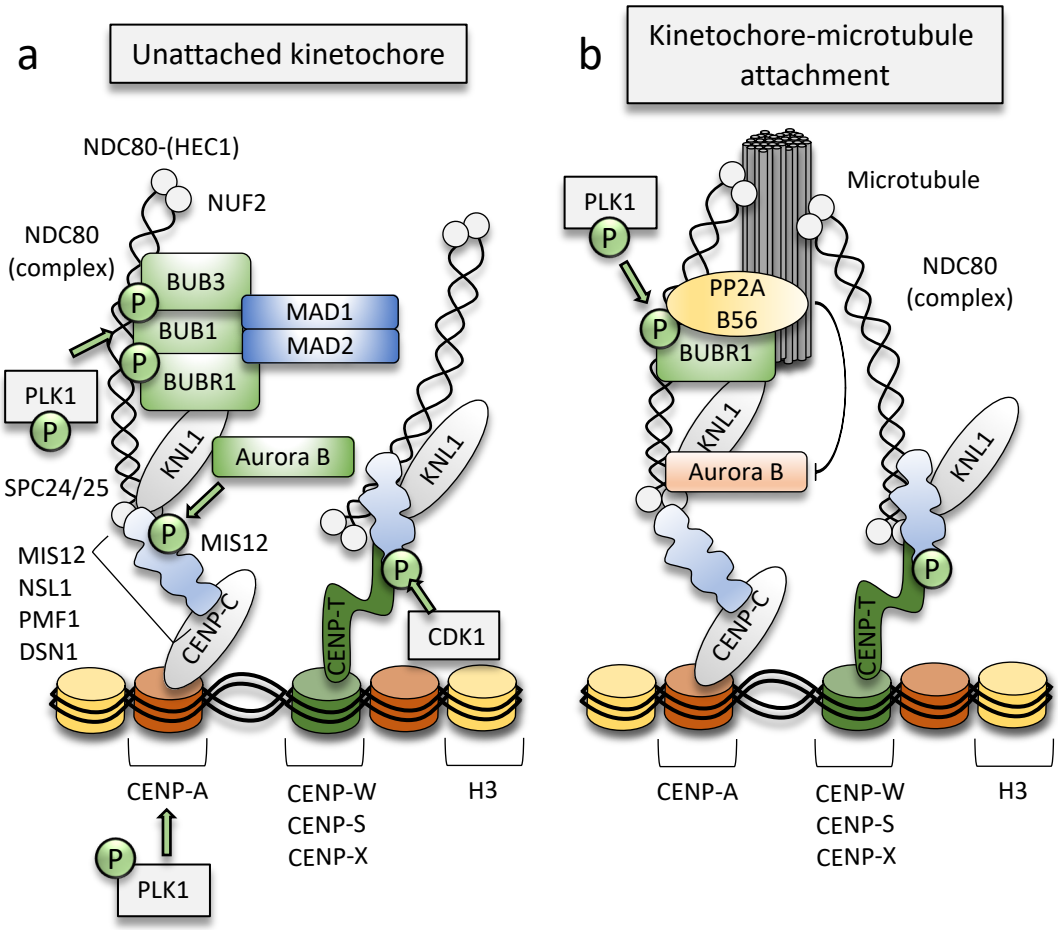

Figure 1.8. Complex assembly of the centromere-kinetochore axis.
a) The CENP-A nucleosomes determine the centromere region. The constitutive centromere-associated network (CCAN) is made up of 16 CENP-derived proteins and associates with CENP-A throughout the cell cycle. During mitosis the CCAN subunits CENP-C and CENP-T recruit the kinetochore microtubule network (KMN), consisting of KNL1, MIS12 and the NDC80 complex. CDK1 phosphorylation of CENP-T may regulate KMN binding to CCAN. **Unattached kinetochore:** The spindle assembly checkpoint proteins (SAC), MAD1/2, BUB1/BUB3 and BUBR1 recruit to regions of the KMN and propagate SAC activation, before correct microtubule binding. PLK1 may be involved in CENP-A licencing and also is involved in phospho-dependent MCC complex regulation. Finally, Aurora B kinase phosphorylates several targets, including MIS12 of the KMN network, to propagate SAC signalling. **b) Attached kinetochore:** The KMN serves as the key kinetochore receptor for spindle microtubule attachment. Binding of microtubules to the KMN may displace SAC proteins. PLK1 may also promote PP2A phosphatase recruitment and counteract Aurora B dependent phosphorylation in order to stabilise MT-KT attachment (diagrams adapted from McKinley 2016; Jia, et al. 2013; Zitouni, et al. 2014).

1.6 Kinetochore-microtubule (KT-MT) error correction and SAC activation

In order for cells to achieve stable chromosome biorientation, and therefore promote error-free segregation, the KT-MT attachments that occur prior to biorientation, must have a certain level of plasticity. Not only do KT-MT connections have to ensure sufficient grip between the KT and the MT framework, they also have to be capable of releasing KT-MT attachments during stages of inaccurate connection(s) **(Fig. 1.9a)**. Therefore, cells not only have to suppress cell cycle progression during inaccurate KT-MT attachment, but also have to destabilise the erroneous attachments, supporting KT-MT error correction. When chromosomes either lack, or encounter inaccuracies in KT-MT attachments, the SAC remains active. This blocks cell cycle progression and allows the cell time to resolve the inaccuracies in KT-MT attachment (Lara-Gonzalez et al. 2012). A primary function of the SAC is to prevent the activation of the anaphase promoting complex/cyclosome-CDC20 complex (APC/C^{CDC20}). Suppression of the APC/C^{CDC20} prevents anaphase onset and gives cells time to achieve correct bipolar kinetochore attachment. Thus, inaccuracies in SAC activation can lead to undetected errors in KT-MT attachment, which in turn can promote missegregation of chromosomes. Therefore, the intrinsic link between correct KT-MT attachment and SAC activation, is essential for maintaining faithful chromosome segregation.

1.6.1 The mitotic checkpoint complex (MCC)

During prometaphase, kinetochores are targeted for capture by the extending mitotic spindle. Consequently, at this early stage of mitosis, the SAC remains active, as kinetochores generally remain unattached or unstably attached. The existence of unattached kinetochores catalyses the formation of the mitotic checkpoint complex (MCC). The MCC is made up of BUBR1, BUB3, MAD2, and the APC/C activator CDC20. The assembly of this complex at unattached kinetochores promotes SAC activation (Lara-Gonzalez et al. 2012). Subsequently, the SAC suppresses the activation of the APC/C^{CDC20}, allowing cells time to establish correct KT-MT attachments (Morrow 2005).

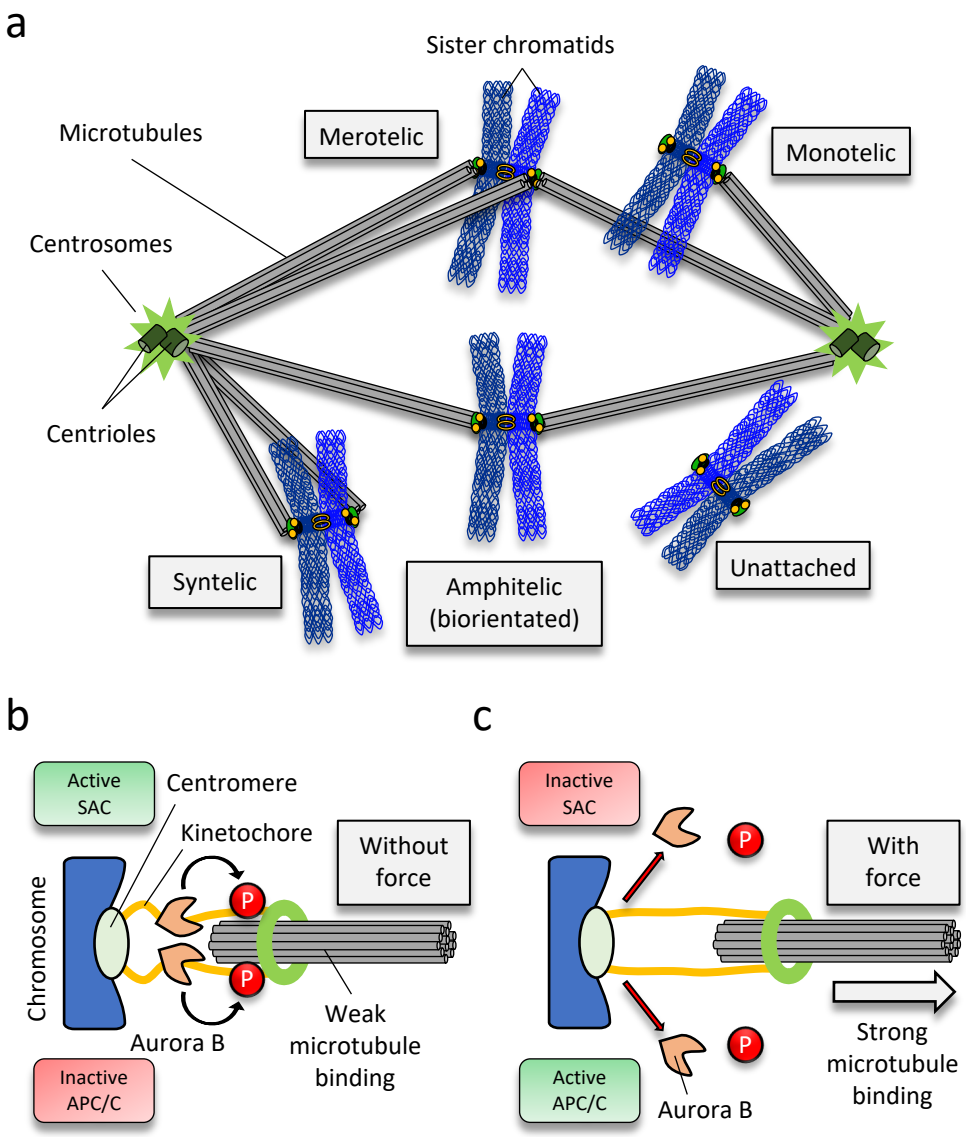

Figure 1.9. KT-MT attachment and Aurora B dependent KT-MT regulation.
a) MT-KT mis-attachment errors include syntelic, merotelic and unattached chromosomes. Monotelic attachment is regarded as an intermediately phase before complementary sister-kinetochore attachment takes place and correct amphitelic attachment is achieved. **b)** Aurora B kinase functions to regulate the status of MT-KT attachment during chromosome biorientation. Unstable or incorrect KT-MT-attachment promotes Aurora B kinase activity, which phosphorylates KT substrates and promotes the release of unstable MT attachments. Following stable KT-MT attachment, pulling forces are generated, which promotes Aurora B kinase to be expelled, leading to APC/C activation and anaphase onset (diagram adapted from Sarangapani and Asbury 2014).

Surveillance by the mitotic checkpoint is considered so robust, that even a single unattached kinetochore is capable of preventing anaphase onset (Rieder et al. 1995) .

Alongside the MCC, additional components help to maintain SAC signalling. These include MAD1 and the kinases BUB1, MPS1 (multipolar spindle-1), and in particular Aurora-B. The main function of these additional proteins is to amplify the SAC signal (Abrieu et al. 2001; De Antoni et al. 2005; Kallio et al. 2002; Tang et al. 2004).

SAC proteins concentrate at unattached kinetochores (Chen et al. 1996, 1998). In contrast, their dramatic reduction coincides with microtubule attachment (Howell et al. 2000; Waters et al. 1998). Concurrently, bipolar spindle attachment leads to SAC inactivation, demonstrated by a depletion of detectable SAC protein localisation (Howell et al. 2004). However, kinetochore capture can lead to erroneous KT-MT attachments. These attachments must be destabilised, whilst also maintaining SAC activation. A key protein involved in the regulation of KT-MT error correction is the highly conserved protein kinase, Aurora B (Sarangapani and Asbury 2014).

1.6.2 Spindle tension and MT-KT error correction by Aurora B

Inappropriate KT-MT attachment leads to a prolonged activation of the SAC. One key reason for this is thought to be due to tension across the centromere-kinetochore axis (Nicklas et al. 1995). Following correct bipolar attachment, spindle pulling is thought to cause the stretching of centromeric chromatin, leading to an increase in inter-kinetochore distance. This tension is understood to enhance the stabilisation of KT-MT attachment, whereas, the opposite can occur in the absence of tension. Incorrect KT-MT attachment is thought to limit the tension that can build across the KT-MT axis, and therefore, microtubule destabilisation occurs. This is believed to be regulated by the action of Aurora B kinase.

The current hypothesis states that the increasing inter-kinetochore distance, during correct bipolar KT-MT attachment, prevents the inner-centromere located Aurora B kinase from acting on kinetochore components (Lampson and Cheeseman 2011; Liu et al. 2009). In contrast, during incorrect KT-MT attachment, insufficient tension across the centromere-kinetochore axis allows Aurora B to target its substrates at the centromere/kinetochore. In turn, this allows Aurora B dependent destabilisation of KT-MT attachment to occur **(Fig. 1.9b)** (Lampson et al. 2004; Tanaka et al. 2002). However, a precise mechanism to explain Aurora B function during SAC maintenance remains a debated topic (Krenn and Musacchio 2015). Nevertheless, tension and Aurora B kinase, play a fundamental role in correcting KT-MT mis-attachment.

During prometaphase, the MCC complex; including CDC20 and all other SAC proteins, localise to kinetochores, in order to propagate the mitotic checkpoint signal. This remarkable surveillance system monitors the status of spindle attachment at kinetochores and prevents anaphase onset (Lara-Gonzalez et al. 2012). Once stable chromosome biorientation is achieved, chromosome segregation can then advance. This demonstrates another sophisticated mechanism to maintain chromosome segregation fidelity. Moreover, this complex mechanism is again regulated by the activity of several kinases.

1.7 Sister chromatid disjunction and the formation of UFBs

As emphasised throughout this thesis, correct chromosome segregation relies on complex and intrinsically linked processes for its success. These processes begin with the accurate duplication of the genome, whilst also maintaining appropriate chromosome organisation (cohesin and condensin activity) and structural features (centromere & kinetochore assembly). Thus, defects in any of these, can hinder proper chromosome disjunction and may also lead to chromosome instability (CIN). Chromosome missegregation is a feature of CIN and in general, it can be observed as erroneous chromosome separation during mitosis. These inaccuracies often give rise to anaphase DNA bridges or lagging chromosomes (Levine and Holland 2018).

Anaphase bridges form due to a failure of complete separation of chromosomes, whereas lagging chromosomes often form when errors in KT-MT attachment occur (Cimini et al. 2015; Levine and Holland 2018). Both of these features have been used extensively as indicators for the detection of missegregation events. More recently, a previously undetected DNA structure has also been visualised in cells that undergo errors in chromosome segregation. These structures were termed ultra-fine DNA bridges (UFBs) and link errors in DNA replication to mitotic non-disjunction (Baumann et al. 2007; Chan et al. 2007).

1.7.1 Classification of ultra-fine DNA bridges (UFBs)

UFBs are a form of stretched DNA linkage that arise during the separation of sister-chromatids. They are believed to be caused by DNA replication and repair, which can promote DNA entanglements that require appropriate resolution. UFBs are not detected by conventional staining methods, such as DAPI. Instead, UFBs become apparent by the detection of the proteins that associate along them (Baumann et al. 2007; Chan et al. 2007). Two major proteins were originally attributed to UFB-binding. These were the PLK1-interacting checkpoint helicase (PICH) (Baumann et al. 2007) and

the Bloom's syndrome helicase (BLM) (Chan et al. 2007). Both PICH and BLM decorate the entire length of UFB structures. Additional proteins have subsequently been found to be associated with UFBs. These include topoisomerase IIIα (TOP3A) and the RecQ-mediated genome instability protein 1 (RMI1) (Chan et al. 2007). BLM, TOP3A and the RMI1/2 heterodimer have been shown to form a complex, commonly referred to as the BTR-complex (Xu et al. 2008). This complex has been reported to drive branch migration of Holliday junctions (HJ) during homologous recombination and repair, whilst also promoting resolution of the resulting hemi-catenane, in a pathway called "dissolution" (Wu and Hickson 2003). The RIF1 protein has also been identified as a factor for UFB binding and resolution (Hengeveld et al. 2015). RIF1 was originally identified as a telomere binding protein, but has subsequently been shown to regulate replication through the recruitment of PP1 (Hiraga et al. 2014).

It is generally accepted that UFB-binding proteins function in the resolution of ultra-fine DNA linkages, which can materialise during chromosome segregation. This prevents potential chromatin damage from being transmitted into offspring cells, as the depletion of these factors not only increases UFB formation, but also leads to transgenerational DNA lesions. These inheritable lesions are marked in daughter cells by 53BP1 nuclear bodies in G1 (Harrigan et al. 2011; Lukas et al. 2011). Therefore, UFB resolution and repair presents as another key factor for ensuring the maintenance of chromosome stability during cellular division.

1.7.2 Types of UFBs

Different types of UFB formation have been described and classified based on their underlying structure and distinctive origins. The primary UFB structure is believed to be either (1) unresolved double-stranded DNA (dsDNA) catenanes; (2) late replication intermediates (LRIs); or, (3) homologous recombination (HR) structures **(Fig. 1.10a, b)** (Chan et al. 2018; Tiwari et al. 2018). UFBs form at four main genomic regions. UFBs form at centromeres (C-UFBs), which are the most common site for their formation **(Fig.**

1.10b) (Baumann et al. 2007; Chan et al. 2007). C-UFBs are believed to represent a form of unresolved dsDNA catenane structure, which persists due to a lack of topoisomerase IIα (TOP2A) decatenation activity. TOP2A is a type II topoisomerase that relieves the topological stress that builds up following DNA unwinding during DNA replication. It achieves this by creating transient dsDNA breaks in the DNA and passing one DNA strand through another **(Fig. 1.10a, b)** (Nitiss 2009). However, C-UFBs may escape TOP2A-mediated decatenation prior to anaphase onset, due to a persistence of sister chromatid cohesion (Baumann et al. 2007; Chan et al. 2007; Wang et al. 2008, 2010). Therefore, this makes C-UFBs a common feature of chromosome segregation and demonstrable in every mitosis (early anaphase). However, UFBs may not exclusively be due to unresolved DNA catenation as many originate from replication intermediates.

Telomeric UFBs (T-UFBs) can form due to an interference of DNA replication of the telomere, or by overexpression of the shelterin component, TRF2, which induces end-to-end telomere fusions **(Fig. 1.10b)** (Barefield and Karlseder 2012; Nera et al. 2015). UFBs have also been shown to form at ribosomal DNA (rDNA) loci (R-UFBs), colocalising with UBF, a marker for sites of rDNA **(Fig. 1.10b)** (Nielsen and Hickson 2016). Finally, UFBs also form at fragile site loci (FS-UFBs) and these arise due to late replication intermediates; in particular at common fragile site (CFS) regions of the genome. CFSs have been defined as late replicating regions of the genome, which are difficult to replicate due to their complex DNA structure and/or long genes (Glover et al. 2017). Replication of CFS is often delayed, especially under conditions of replicative stress, such as during treatment with the DNA polymerase inhibitor aphidicolin (APH). Therefore, APH can induce FS-UFBs and these FS-UFBs are distinctly marked by the presence of the Fanconi anaemia protein FANCD2 at their termini **(Fig. 1.10b)** (Chan et al. 2009).

More recently, unresolved DNA intermediates, due to homologous recombination (HR), were also shown to identify a new class of UFB, termed as HR-UFBs. This newly defined HR-dependent UFB structure was absent of FANCD2 foci, showing it to be distinct from replication stress induced UFB formation. This was confirmed by a reduction in FANCD2 negative UFBs, after depletion of the HR components RAD51 or BRCA2, whilst FANCD2-

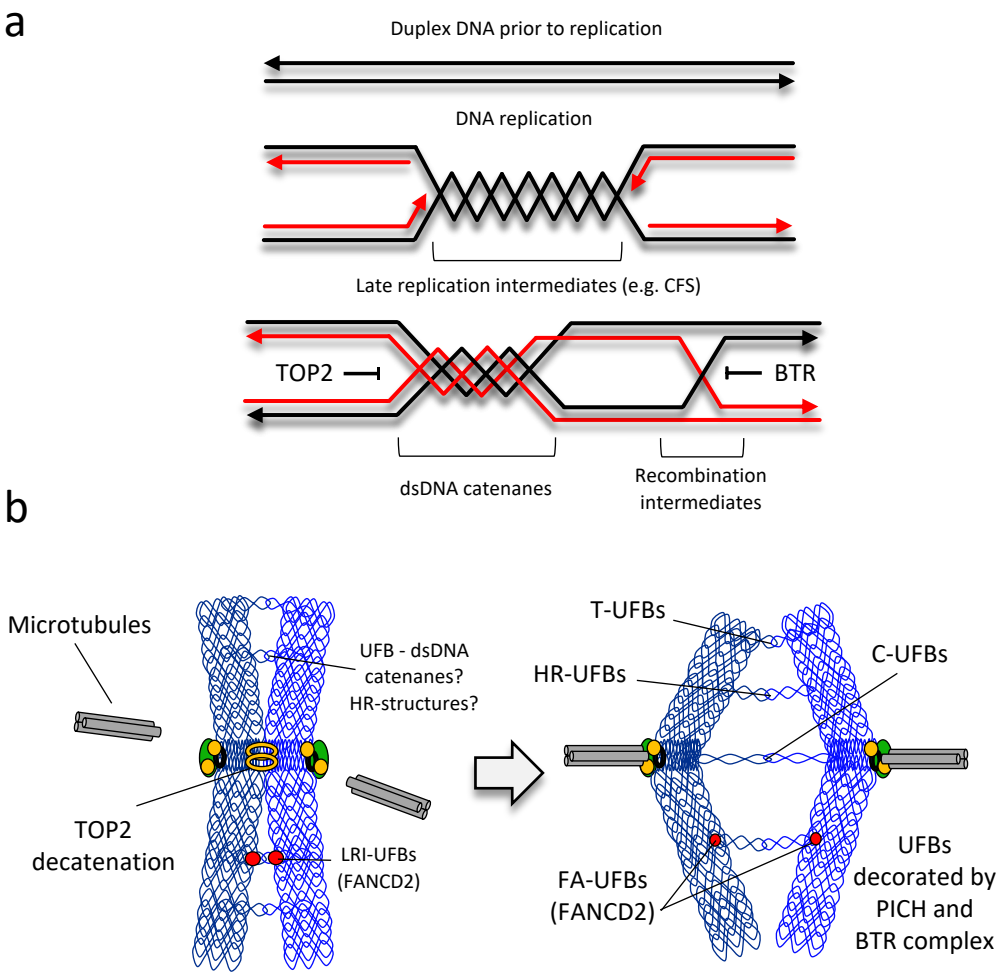

Figure 1.10. Resolution of DNA intertwinements by the UFB binding complex maintains faithful chromosome segregation.

a) DNA intertwinements can arise following DNA replication and recombination. Double stranded DNA (dsDNA) catenanes form due to replication intermediates that require processing by topoisomerase II (TOP2) activity. Alternatively, recombination intermediates can be resolved by the action of the BTR-complex (BLM, topoisomerase III-alpha and RMI1/2). **b)** Anaphase UFBs arise as a result of unresolved DNA intertwinements caused by DNA replication or homologous recombination. A failure to deal with such DNA intertwining structures prior to mitosis, leads to the BTR (BLM, TOP3 and RMI1) complex and PICH associating with UFBs to resolve them. Nucleolytic cleavage can also occur by structure-specific nucleases, such as MUS81 and GEN1 (diagrams adapted from Fernández-Casañas 2018; Fernandez-Vidal 2017).

positive UFBs increased (Chan et al. 2018; Tiwari et al. 2018). Therefore, the formation of these FANCD2-negative UFBs is dependent of HR, as RAD51 and BRCA2 are crucial elements for HR.

1.7.3 PICH (Plk1-interacting checkpoint helicase)

PLK1-interacting checkpoint helicase, PICH, was originally identified through interaction studies with the protein kinase PLK1 (Baumann et al. 2007). PICH has been shown to co-localise with PLK1 at kinetochores, early in mitosis, whilst it is spatiotemporally regulated and remains excluded from the nucleus until nuclear envelope breakdown (NEBD). PICH is a member of the SNF2 family of SWI/SNF chromatin remodellers and has ATPase activity **(Fig. 1.11a)** (Baumann et al. 2007). Despite PICH being referred as a helicase (Baumann et al. 2007), *in vitro* studies have demonstrated that PICH is unable to catalyse strand unwinding of duplex DNA (Biebricher et al. 2013; Ke et al. 2011). Instead, the actual catalytic function of PICH is as a translocase. Using an *in vitro* DNA triplex assay, PICH was found to translocase along dsDNA molecules and displace a radiolabelled ssDNA oligo substrate from a DNA triplex structure **(Fig. 1.11b)** (Biebricher et al. 2013). PICH DNA translocase activity is dependent on ATP binding or hydrolysis, as a mutation within its ATP binding motif (K128A) abolishes its catalytic activity (Biebricher et al. 2013). During the same study, PICH was also shown to be unable to bind ssDNA. Instead, it was only capable of binding to dsDNA substrates, even if the dsDNA end was not 'free'. PICH was also reported to translocate Holliday junction substrates, promoting branch migration of the four-way junction; a characteristic feature of homologous recombination (Biebricher et al. 2013). However, the significance of this remains unclear.

Despite an increasing amount of knowledge on the catalytic function of PICH, its precise cellular role(s) remain less clear. Following its original discovery, PICH was thought to regulate the activity of the SAC (Baumann et al. 2007). However, this was later shown to be incorrect and previous conclusions made were instead attributed to off-target

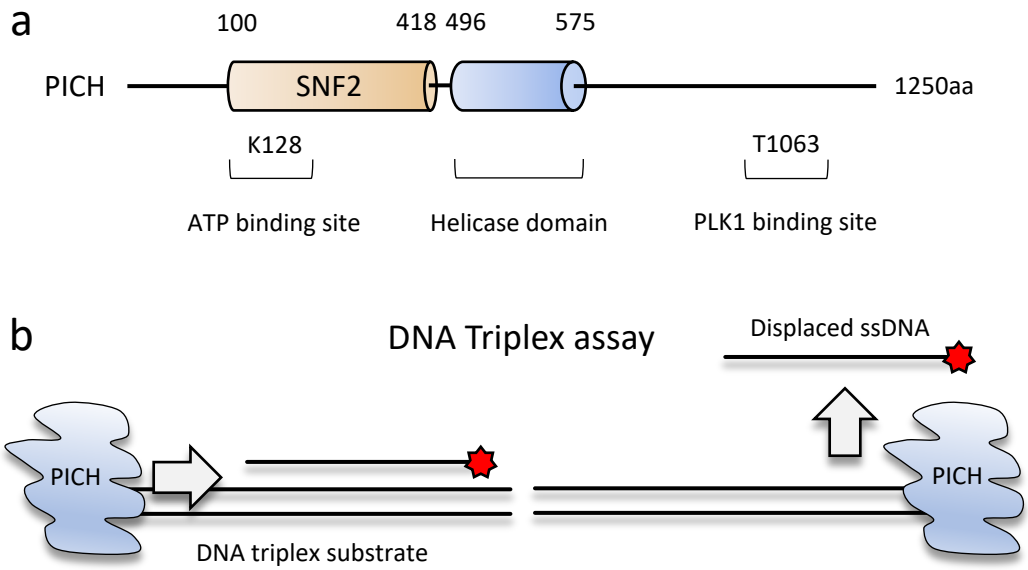

Figure 1.11. PICH an ATP-dependent DNA translocase.
a) Schematic representation of the structural domains of PICH. Amino acid residue K128 denotes the site of ATP-binding, whilst phosphorylation at T1063 enables PLK1 to interact with PICH. **b)** A diagram to represent PICH's translocase activity. PICH has been shown to displace ssDNA from a triplex DNA substrate, rather than unwind dsDNA substrates (diagrams adapted from Pitchai, et al. 2017 & Biebricher, et al. 2013).

effects of siPICH oligonucleotides, which inadvertently targeted the SAC protein MAD2 (Hübner et al. 2010). PICH has also been reported to promote chromatin remodelling, showing a possible histone displacement capability. As mentioned previously, UFBs are regarded as histone negative. However, histone positive UFBs were detected during PICH depletion, leading to the suggestion that PICH was contributing to the displacement of histones at UFB structures (Ke et al. 2011). Nonetheless, this original claim was not reproducible by a different group, and therefore, doubts remain regarding its ability to participate in histone displacement (Biebricher et al. 2013).

An interesting feature of PICH, is demonstrated by its ability to sense tension. Using single-molecule *in vitro* studies, two groups have demonstrated that PICH binds more effectively to dsDNA substrates, following the application of tension (Biebricher et al. 2013; Sarlós et al. 2018). Notably, tension is almost certain to build between sites of stable KT-MT attachment. In addition, during early anaphase onset, tension will build between sister chromatids that remain intertwined by catenation. Therefore, it is conceivable that the recruitment of PICH to UFBs is influenced by spindle tension (Biebricher et al. 2013).

PICH is considered as the primary sensor for UFB assembly. Alongside that, it probably plays a role in the recruitment of other UFB binding proteins, as a depletion of PICH has been shown to abolish both BLM and RIF1 binding at UFBs (Hengeveld et al. 2015). Recent *in vitro* reports have also highlighted PICH's potential as a stimulator of TOP2 decatenation activity. This may explain a functional role for PICH, through mediating TOP2-dependent decatenation of unresolved intertwining DNA molecules between sister chromatids, during the metaphase-to-anaphase transition (Nielsen et al. 2015). However, whether this is the principal role for PICH on stretched DNA molecules, such as UFBs, remains unconfirmed.

It has also been reported that an absence of PICH is embryonically lethal in mice (Albers et al. 2018); although, knockout cell lines have been described in both chicken DT40 and

human HeLa cells (Nielsen et al. 2015). However, in all cases of PICH absence or depletion, DNA metabolism is affected (e.g. mis-segregation errors, condensation defects, hypersensitivity to TOP2 inhibition). Therefore, PICH is regarded as a vital protein involved in the safeguarding of chromosome segregation and this makes it an intriguing protein for further study.

1.7.4 BLM (Bloom's syndrome helicase)

The Bloom's syndrome (BS) gene product, BLM helicase, is also found abundant on UFBs. BLM is a member of the RecQ family of DNA helicases, with a 3'-5' directionality **(Fig. 1.12a)** (Karow et al. 1997). BLM has been shown to function during DNA replication and homologous recombination (Bachrati and Hickson 2008). Germline loss of function mutations of the BLM gene causes Bloom's syndrome (BS) (Ellis et al. 1995), which was first described in 1954 and named after its discoverer; the dermatologist David Bloom (Bloom 1954). It is a rare autosomal recessive genetic disorder that is characterised by prenatal and postnatal growth deficiency. It is associated with short stature, photosensitive skin changes, immune deficiency, insulin resistance and an increased risk of early onset cancer (Bloom 1954; German 1997; German et al. 1965). Diagnostically BLM cells display an increase in sister-chromatid exchanges (SCE) and chromosome breaks (Chaganti et al. 1974). SCE's are a cross-over product, formed between sister chromatids and are dependent on HR activity. This highlights that BLM plays a key role in HR-mediated DNA repair. Importantly, BLM-deficient cells also display an increase in chromosome missegregation, most notably through the formation of bulky anaphase bridges, UFBs and lagging chromatin (Chan et al. 2007).

BLM forms a sub-complex with its partner proteins, topoisomerase IIIα (TOP3A) and the RecQ-mediated genome instability complex 1 and 2 (RMI1/BLAP75; RMI2/BLAP18), which forms the BTR-complex (Mankouri and Hickson 2007; Singh et al. 2008; Xu et al. 2008). It is thought that BLM is stabilised by its partner proteins, RMI1 and RMI2 (Raynard et al. 2006), whilst RMI1 has also been found to associate to UFBs (Chan et al.

2007). BTR complex formation facilitates a unique DNA resolution event (dissolution), which is catalysed by the action of topoisomerase IIIα (TOP3A) **(Fig. 1.12b)**.

TOP3A is a type 1 topoisomerase, which catalyses the transient breakage and re-joining of ssDNA substrates. This action relieves the torsional stress that is generated by duplex DNA unwinding, particularly following BLM-dependent helicase activity. An example of this action is demonstrated by an event where BLM acts in concert with TOP3A in order to resolve double-Holliday junctions (dHJs). These unique recombination structures are generated during HR-mediated repair of dsDNA breaks, or by fork regression during DNA replication (Wu and Hickson 2003). The BLM/TOP3-dependent dHJ dissolution pathway exists as a two-step process. First, the BLM helicase within the BTR-complex, catalyses a branch migration reaction on the dHJ recombination structure. This promotes the formation of a hemi-catenane DNA intermediate, which is then decatenated by TOP3-(RMI1/2). This dissolution reaction, unlike the cleavage of HJs, exclusively produces non-crossover recombination products (Wu and Hickson 2003). Therefore, BLM helicase activity, along with the rest of the BTR-complex, plays a key role in maintaining genome stability.

The DNA unwinding activity of BLM is enhanced by the presence of replication protein A (RPA) (Brosh et al. 2000), a single stranded DNA (ssDNA) binding protein. Interestingly, RPA is also present at UFB structures and its loading has been shown to be dependent on BLM helicase activity (Chan et al. 2018; Hengeveld et al. 2015). More recently, *in vitro* single molecule analysis, using optical tweezers, revealed that RPA binding is exclusive of the PICH/BTR complex (Sarlós et al. 2018). Therefore, providing further evidence to support the idea that BLM is responsible for the physical unwinding of UFBs and the generation of ssDNA, which thereby promotes RPA binding. However, a precise mechanism to explain how the UFB-binding complex (PICH/BTR-complex) resolves DNA bridging structures remain uncertain.

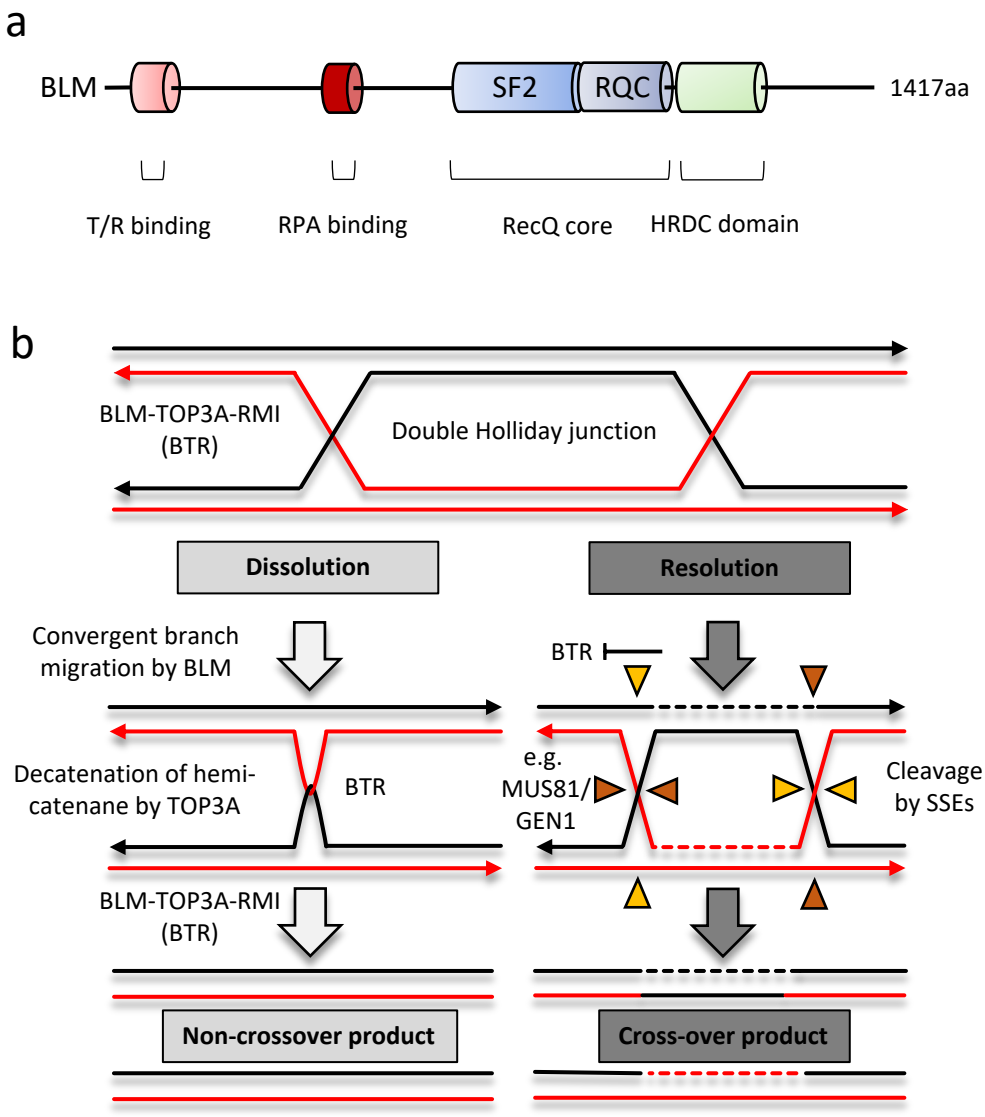

Figure 1.12. BLM helicase promotes double Holliday junction (dHJ) dissolution.
a) A **s**chematic representation of the core structural domains of BLM. The RecQ core region contains the super family-2 helicase domain (SF2) and a RecQ conserved domain (RQC). The T/R site denotes the region of BLM that interacts with topoisomerase IIIα and RMI1-2. The helicase and RNAse D carboxy-terminal domain (HRDC) identifies the region of BLM that is required for double Holliday junction binding and dissolution reaction. **b)** BLM and topoisomerase IIIα and RMI1-2 catalyse the dissolution of dHJ recombination intermediates, favouring the generation of non-crossover products. Minimising the chance of loss of heterozygosity (LOH), and preventing inappropriate genomic rearrangements. Alternatively, in the absence of BLM, Holliday junction resolution is mediated by cleavage by structure-specific endonucleases (SSEs). This can result in the generation of both cross-over and non-crossover products (not shown), encouraging possible genomic rearrangement (diagrams adapted from Bizard & Hickson 2014; Martin, et al. 2019).

Nevertheless, despite uncertainty regarding the precise molecular mechanism of UFB resolution, it is conceivable that PICH acts as the primary detector for the presence of tension derived UFBs. This in turn may promote the recruitment of BLM and the remaining BTR-factors. It is then tempting to speculate that TOP3A decatenation activity aids in UFB resolution. However, whether TOP3A is responsible for ssDNA decatenation of UFBs remains unclear. A recent study has reported the clinical appearance of a BS-like disorder, from patients identified with mutations in either TOP3 or RMI1. The patient derived cells displayed increased frequencies of mitotic defects, compared to both control and parental cells, including an increase in the detection of UFBs, micronuclei and transgenerational lesions, marked by 53BP1 nuclear bodies (Martin et al. 2018). These findings highlight the significance of the whole BTR-complex in maintaining genomic stability.

Overall, this section has highlighted how faithful transmission of the genome relies on various processes for its attainment. To ensure the accurate transmission of genetic material, cells require the action of a large number of molecular machineries. These facilitate the appropriate organisation and arrangement of chromosomes, in order to promote correct chromosome biorientation and faithful chromosome segregation. These processes require coordination and regulation. A recurring component involved in many different aspects of mitotic stability and chromosome segregation, is the action of protein phosphorylation. In particular, this is influenced by the activity of the mitotic kinase PLK1, which will be discussed further in the next section.

1.8 The mitotic regulator polo-like kinase 1 (PLK1)

Commonly regarded as the master regulatory mitotic kinase, mammalian PLK1 plays a multitude of roles in regulating mitotic progression. PLK1, or '*Polo*' as it was described following its original discovery in *Drosophila Melanogaster* (Llamazares et al. 1991; Sunkel and Glover 1988), has been shown to function throughout various stages of mitosis. This includes mitotic entry, centrosome maturation, bipolar spindle formation, chromosome congression and segregation, cytokinesis and mitotic exit (Archambault and Glover 2009; Zitouni et al. 2014). Given the multifunctional roles identified for PLK1 during mitosis, it is not surprising that PLK1 has many cellular substrates. Some of these substrates have been largely studied, whilst others undoubtedly remain unidentified.

The activation and recruitment of PLK1 is regulated by its C-terminal polo-box domain (PBD), which binds to and recognises phosphorylated serine/threonine residues within target proteins (Elia, Cantley, et al. 2003; Elia, Rellos, et al. 2003). Thus, PLK1 substrates generally require a 'priming' reaction, which refers to the addition of a phosphate group, allowing for subsequent PLK1 recruitment. Priming is commonly achieved, although not exclusively, by the action of CDK1. However, PLK1 does not always depend on a priming reaction for substrate recruitment. Instead, the PBD domain of PLK1 is also capable of binding to both non-phosphorylated peptides, and also previous PLK1 phospho-peptide sequences (self-priming) (Archambault et al. 2008; Elia, Cantley, et al. 2003). Phosphorylation by PLK1 can lead to various outcomes for PLK1 targets. Although, in general, PLK1 promotes either the inhibition or stimulation of target protein activity (Archambault and Glover 2009; Zitouni et al. 2014).

PLK1 protein level and activity appears to peak on mitotic entry. Thus, studies have largely concentrated on exploring the roles of PLK1 during mitosis. Notably, a loss of PLK1 has been shown to cause severe mitotic defects. These include abnormal centrosome formation and a failure of mitotic cells to correctly undergo chromosome biorientation (Barr et al. 2004). How PLK1 facilitates these processes is still not fully

understood. Therefore, PLK1 remains an intriguing protein to study, with great potential, as many unidentified roles are yet to be determined.

1.8.1 PLKs a family of serine/threonine kinases

PLK1 belongs to a family of serine/threonine protein kinases (PLKs), which function to perform vital roles involved in cellular progression. There are five mammalian PLK paralogues, PLK1-5 **(Fig. 1.13)**. PLK1 is generally recognised as the principal member of this kinase family and has been implicated in various aspects of cellular regulation, including DNA replication and mitotic fidelity (Schmucker and Sumara 2014; Song, Liu, and Liu 2012; Yim and Erikson 2009). Much less is known about the other PLK members.

PLK2 is primarily expressed in G1 and has been suggested to provide a functional role(s) in the G1-S phase transition of the cell cycle, through centriole duplication. PLK2 may also have links to cytokinesis progression (Simmons et al. 1992; Warnke et al. 2004). PLK3 is continuously expressed throughout the cell cycle. Therefore, it has been suggested that PLK3 may support a role(s) in G1-S phase transition, along with a possible DNA replication function. PLK3 has also been reported to function during cellular stress responses, including the DNA damage response (Xie et al. 2001). PLK4 has a role in centriole biogenesis, acting as a centriole assembly factor. It is only present in species that contain centrioles (Habedanck et al. 2005). Finally, PLK5 is abundant in non-proliferative cells, such as neurons. Hence, PLK5 is largely found expressed in the brain. PLK5 contains an inactive kinase and lacks important residues for substrate recognition within its polo-box domain (de Cárcer, Escobar, et al. 2011; de Cárcer, Manning, et al. 2011). Therefore, the biological function(s) of PLK5 may be distinctly different from other PLK family members (PLK1-4).

Structurally, all PLK members display similarities in their protein domain architecture (Jana et al. 2012). This includes an amino-terminal serine/threonine kinase domain and a carboxy-terminal polo-box domain (PBD). The PBD of each PLK contains either one or

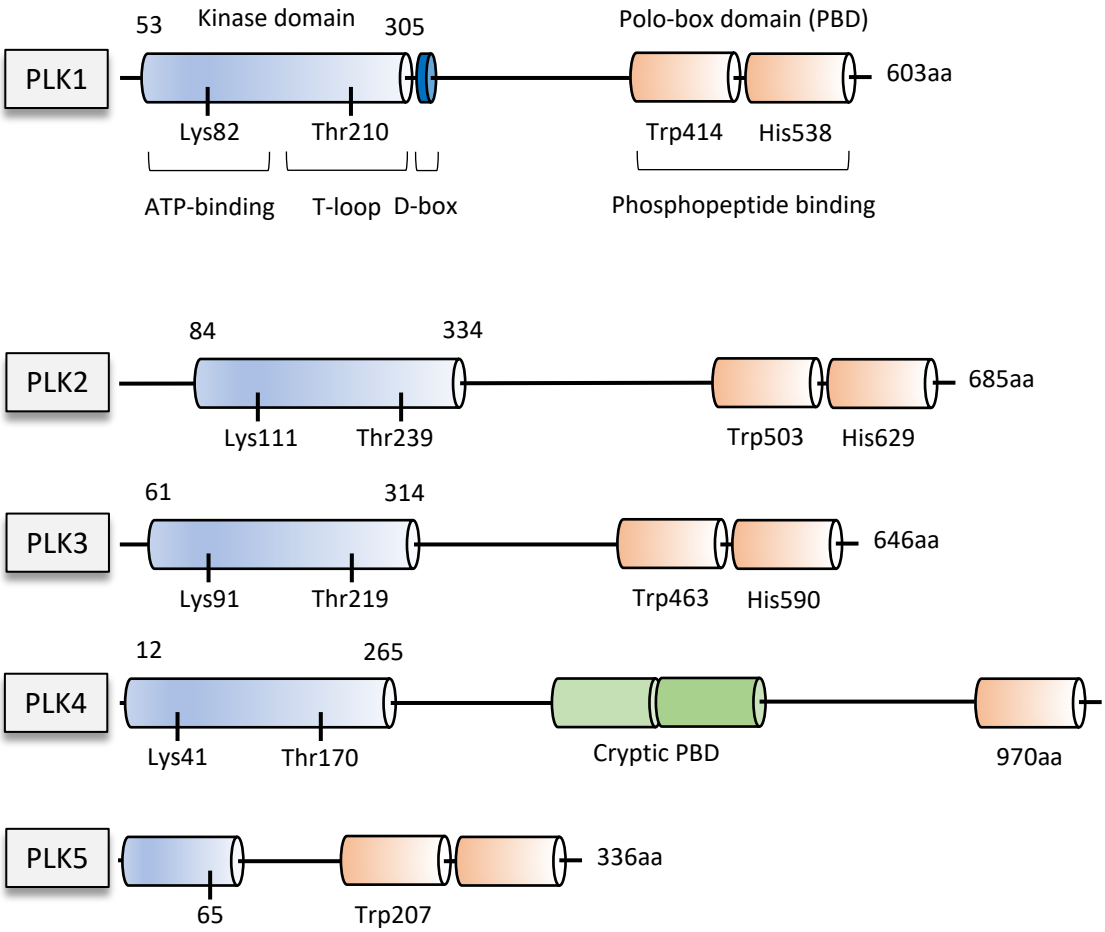

Figure 1.13. The structural domains of PLK1-5.
In general PLK's are structurally very similar. Each contain a catalytic core (helicase domain), and either one or two polo-box domains (PBD). These are required for PLK substrate targeting. PLK1-3 have the most similar kinase domains among the PLK's, whilst PLK4 has a divergent sequence and PLK5 features a pseudo-kinase domain, absent of catalytic activity. PLK1 also features a destruction box (D-box) sequence, which is essential for PLK1 degradation (diagram adapted from Zitouni, et al. 2014).

two polo-box domains. The kinase domains of PLK1-3 are considered the most similar among the PLK family. In contrast, PLK4 has a divergent sequence within its kinase domain, and PLK5 contains a pseudo-kinase domain (Zitouni et al. 2014). The structural similarities within the kinase domain of PLK1-3 means they can all display sensitivity to small-molecule competitive inhibitors of ATP. This includes a potent PLK1 inhibitor, known as BI2536 (IC_{50} = 0.83nM) (Lénárt et al. 2007). Therefore, despite the substantial specificity to PLK1, the use of such inhibitors (i.e. BI2536) may affect the catalytic activity of all three kinases (PLK1-3) at once. Overall, PLKs, and in particular PLK1, are critical kinases in order to promote cellular progression and survival. Thus, their catalytic activity is highly regulated.

1.8.2 Regulation of PLK1 activity

The activation cycle of PLKs is largely understood from studies examining PLK1. Therefore, only the regulatory processes of PLK1 activation will be discussed in detail. PLK1 is largely activated during the G2-M transition and its activity is maximised during mitosis. PLK1 activation involves phosphorylation at two key residues, which are positioned within the catalytic domain or 'T-loop' (Thr210) and the hinge region of the kinase domain (Ser137) (Bruinsma et al. 2012, 2013). In general, Aurora A, along with its co-factor BORA, are responsible for PLK1 activation.

The cytoplasmic scaffold BORA binds to Aurora A and PLK1, which promotes PLK1 T-loop phosphorylation (Thr210). BORA functions to 'unlock' the access of the T-loop of PLK1, thus promoting Aurora A dependent phosphorylation of PLK1 at Thr210 **(Fig. 1.14a)** (Macůrek et al. 2008; Seki, Coppinger, Jang, et al. 2008). Active PLK1 is then able to phosphorylate several mitotic entry network factors, including CDK1, which functions to promote mitotic entry (Lindqvist et al. 2009). In addition, CDK1 activation also determines a positive feedback loop involved in PLK1 activation. It does this by phosphorylating BORA (priming) at the PBD-docking site and facilitates the PLK1-BORA interaction. Subsequently, Aurora A dependent phosphorylation of PLK1 is promoted

(Vigneron et al. 2018). Surprisingly, the activation of PLK1 also stimulates bulk BORA degradation, via PLK1 dependent phosphorylation of BORA, despite BORA acting as an activator of PLK1. PLK1 phosphorylation generates a phospho-degron signal on BORA, which is recognised by the S phase Kinase associated Protein 1 (SKP1)-cullin-1-F-box β-Transducin repeat Containing Protein (βTrCP) ($SCF^{\beta TrCP}$). This E3-ubiquitin ligase complex targets BORA for proteasomal degradation prior to mitotic entry (Seki, Coppinger, Du, et al. 2008). Thus, mitotic entry relies on a two-tiered control of PLK1 and Aurora A, which is dependent on BORA activity. This culminates in the activation of PLK1 and CDK1, with the concomitant degradation of BORA. PLK1 'T-loop' phosphorylation (Th210) remains throughout mitosis and is therefore refractory to de-phosphorylation, despite Aurora A depletion. A small level of BORA remains, which is considered sufficient to maintain the required level of PLK1 activity throughout mitosis (Bruinsma et al. 2013).

Apart from being the primary substrate recruitment site for PLK1 localisation, the PBD is also responsible for controlling the catalytic activity of PLK1. The PBD functions to achieve this via an auto-inhibitory mechanism. The PBD binds to the catalytic domain of PLK1 in such a conformation to result in the mutual inhibition of both of their functional activities **(Fig. 1.14a)** (Bruinsma et al. 2012). Currently, it is understood that PLK1 kinase activity is suppressed through three identified regulatory methods. One is through the PBD itself, which functions to reduce the flexibility of the hinge region of the kinase domain, where Ser137 is located. Subsequently, phosphorylation at Ser137, achieved by activating kinases, such as Aurora A/BORA, allows for PLK1's inhibitory signal to be released. Secondly, PLK1 kinase activity can be inhibited by the Inter-domain Linker (IDL). This links the kinase domain with the PBD and sequesters access to the T-loop (Thr210). Conversely, the prevention of T-loop sequestration, by protein partner binding of the PBD, can prevent this inhibition of PLK1 activity. Finally, studies using the *Drosophila melanogaster Polo*, have revealed that binding of an inhibitory protein, called MAP205, to the PBD of *Polo,* can also regulate the catalytic activation of *Polo* (Archambault et al. 2008; Xu et al. 2013). Alleviation of the inhibitory effect on *Polo* by MAP205 can be achieved by phosphorylation of MAP205 itself **(Fig. 1.14a)**. However, it is important to note, currently no orthologue of MAP205 has been identified in human

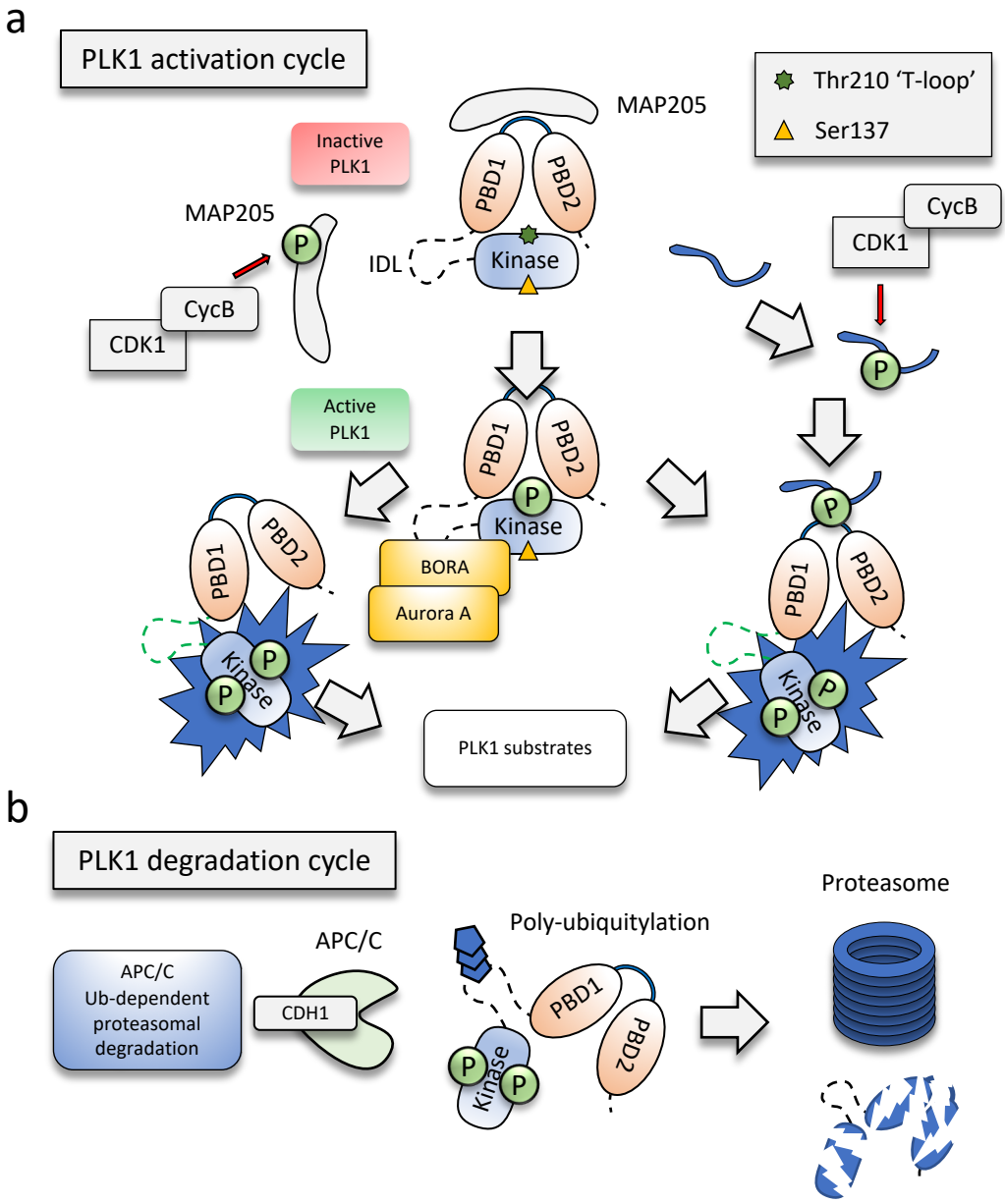

Figure 1.14. The activation and degradation cycle of PLK1.
a) Inactive PLK1: In the resting state, PLK1 is inactive. The PBD domains bind to the kinase domain in such a way that it sequesters access to two key residues of PLK1, which are required for its activation, Thr210 and Ser137. In addition, MAP205 may bind to PLK1 and also inhibit PLK1's catalytic activity. Release of MAP205 inhibition on PLK1 requires CDK1-dependent phosphorylation of MAP205. **Active PLK1:** Activation of PLK1 is achieved via phosphorylation of key residues, Thr210 ('T-loop') and Ser137 by Aurora A kinase (maybe also Aurora B). Aurora A, along with its binding partner BORA, encourages a conformational change in the structure of PLK1 and release of the PBD from the catalytic core, allowing Aurora A-dependent phosphorylation of PLK1. Alternatively, PLK1 can become active via pre-primed (CDK1) phospho-peptide binding, which encourages release of the PBD and subsequently Aurora A kinase dependent activation. **b)** During exit from mitosis, PLK1 is signalled for degradation via the APC/C^{CDH1} dependent ubiquitination pathway, which signals PLK1 for destruction via the 26S proteasome. (Diagrams adapted from Zitouni, et al. 2014)

cells (Normandin et al. 2016). Despite the absence of MAP205 in human cells, ectopic expression of MAP205 in HEK293T cells, has been shown to effectively inhibit PLK1 activity. To alleviate this inhibition on PLK1, MAP205 requires phosphorylation by CDK1 for its displacement (Normandin et al. 2016), much like in *Drosophila melanogaster Polo* MAP205 regulation. Therefore, PLK1 regulation contains various levels of control in order for its activation, whilst its degradation cycle is also highly ordered.

In the resting state, PLK1 remains inactive. However, during mitosis, the independent or sequential phosphorylation of Thr210 and Ser137, leads to either partially or fully active PLK1. Phosphorylation by Aroura A, along with the recruitment of the Aurora A cofactor BORA, promotes a conformational change to the PBD of PLK1 and induces the release of the kinase domain away from the PBD; thereby triggering the activation of PLK1 (Zitouni et al. 2014). In contrast, during mitotic exit, PLK1 proteolytic degradation begins. This is triggered by the activation of a ubiquitin-dependent proteasomal degradation pathway, that targets PLK1 for destruction. The E3-ubiquitin ligase, APC/C, works in conjunction with its co-factor CDH1 (APC/C^{CDH1}). Together they recognise a destruction box (D-box) signal within PLK1. Ubiquitylation of PLK1 by APC/C^{CDH1} at this D-box marks PLK1 for proteasomal degradation and subsequently, PLK1 protein levels dramatically fall during exit from mitosis **(Fig. 1.14b)** (Lindon and Pines 2004).

Overall, PLK1 activity is considered essential for mitotic progression. Once active, PLK1 has been implicated in various processes involved in mitotic advancement. In particular, PLK1 influences centrosome maintenance and also supports KT-MT attachment, two key features that if compromised, can affect the status of accurate chromosome alignment.

1.8.3 PLK1 function during centrosome maturation

In its original identification in *Drosophila melanogaster* (*Polo*), PLK1 was shown to localise to centrosomes (Golsteyn et al. 1995). This highlights PLK1's probable functional influence on centrosome maintenance. Centrosomes are small cytoplasmic organelles

that consist of a pair of barrel-shaped centrioles, which are surrounded by pericentriolar material (PCM) (Conduit et al. 2015). Centrosomes act as the microtubule (MT) organising centre for microtubule nucleation. Microtubules are responsible for the capture and alignment of chromosomes during mitosis, which is a key process of mitotic fidelity.

The centrosome is duplicated during S phase and creates a pair of centrosomes that begin separating during prophase (Conduit et al. 2015). Each separated centrosome positions itself at opposing sides of the chromosome mass and act as the two poles for the mitotic spindle. This promotes the bipolar arrangement of chromosomes during metaphase (chromosome biorientation), whilst also supporting equal chromosome segregation. Although the role of centrosomes in acting as the organising centre for the mitotic spindle is well established, its precise contribution to cell division remains a debated topic. Cells ablated of centrosomes have been reported to still be capable of undergoing chromosome biorientation (Khodjakov et al. 2000). This suggests that cells may have a centrosome-independent bipolar spindle formation capacity. However, a disruption to centrioles and therefore, a disruption to correct centrosome biogenesis, has also been shown to lead to defects in bipolar spindle assembly (Sir et al. 2013). Despite these differences in conclusions, it is generally understood that centrosomes provide a robustness to bipolar spindle formation and chromosome segregation, whilst PLK1 has been reported to provide a functional role to support this.

Centrosomes go through a process of maturation, which involves the recruitment of γ-tubulin. This occurs during prophase and is essential for microtubule nucleation from mitotic centrosomes. PLK1 is involved in centrosome maturation and is believed to facilitate γ-tubulin recruitment (Casenghi et al. 2005; Lane and Nigg 1996; Oshimori et al. 2006). PLK1 inactivation commonly leads to a disruption in γ-tubulin detection at centrosomes, highlighting an essential role for γ-tubulin during centrosome maturation. It also suggests that PLK1 activity influences both centrosome establishment and maintenance (Lénárt et al. 2007; Peters et al. 2006; Santamaria et al. 2007). In addition,

an absence of PLK1 activity has also been shown to prevent bipolar spindle formation, with cells displaying a prometaphase-like stage arrest (van Vugt et al. 2004). This implies that PLK1 provides a function that influences microtubule nucleation from centrosomes, which is likely to ensure correct mitotic spindle formation.

Contrasting reports have suggested that centrosomes can function normally, despite an ablation of PLK1's PBD domain, which subsequently causes an absence of PLK1 recruitment to centrosomes (Hanisch 2006). However, the same study also reported defects in chromosome congression when PLK1 activity was compromised (Hanisch 2006). Therefore, despite the contradictory studies regarding PLK1 function during centrosome maintenance, PLK1 is required for accurate chromosome alignment.

1.8.4 PLK1 function in kinetochore-microtubule attachment stability

PLK1 has also been shown to accumulate at kinetochores during early mitosis (Seong et al. 2002). Kinetochores function as the molecular platforms for which microtubules attach to chromosomes during chromosome congression. Moreover, PLK1 localisation at KTs has led to the suggestion that PLK1 plays a functional role in KT-MT maintenance. In support of this, PLK1 inactivation studies have shown that microtubule attachment at kinetochores are affected when PLK1 is inactivated. Studies using indirect fluorescent microscopy techniques were able to demonstrate a decline in stable KT-MT attachment (K-fibres), following the inactivation of PLK1 (Hanisch 2006; Lénárt et al. 2007; Santamaria et al. 2007).

In addition, PLK1 activity has been reported to affect the regulation of the mitotic checkpoint. The inactivation of PLK1, using the small-molecule inhibitor BI2536 (IC_{50} = 0.83nM), has been shown to prolong SAC activation, due to the existence of unattached kinetochores (Lénárt et al. 2007; Steegmaier et al. 2007). Therefore, increasing evidence implies that PLK1 is required for KT-MT attachment and probably also for its maintenance.

The expression of PLK1 begins during S phase and peaks during mitosis, whilst its detection at sister-kinetochores can occur during the G2 phase of the cell cycle (Hamanaka et al. 1994; Kang et al. 2006). PLK1 recruitment to kinetochores has been shown to be dependent on PBIP1 (CENP-50) (Kang et al. 2006). It has been reported that PLK1 'self-primes' PBIP1 via protein phosphorylation and in doing so, PLK1 generates its own docking site (T78) for PBD binding. This subsequently supports PLK1's recruitment to kinetochores. PLK1 is also reported to promote the degradation of PBIP1 early in mitosis, despite PLK1 persisting at kinetochores until telophase (Kang et al. 2006). Therefore, it is conceivable that additional factors may contribute to PLK1 stabilisation at kinetochores.

The SAC protein, BUB1 (kinase), has been shown to interact with PLK1 following an initial 'priming' reaction by CDK1. This phospho-dependent interaction is believed to influence PLK1 recruitment to kinetochores (Qi et al. 2006). PLK1 has also been shown to interact with INCENP, a member of the chromosomal passenger complex (CPC) (Goto et al. 2006). The CPC is made up of INCENP, Aurora B, Borealin and survivin. Its primary functions include KT-MT attachment maintenance and SAC activation (Carmena et al. 2012). This suggests that PLK1 localisation to kinetochores depends on several factors. However, elucidating the role each factor plays remains challenging. For example, depletion of BUB1 can lead to secondary effects, such as kinetochore structural alterations (Meraldi and Sorger 2005). Therefore, these potential effects may indirectly influence PLK1 localisation. Also, self-priming by PLK1 on different proteins may be a factor for PLK1 localisation to kinetochores, much like the mechanism of PBIP1-dependent kinetochore localisation of PLK1. Thus, PLK1 activity and multiple factors are likely responsible for PLK1 localisation to kinetochores.

Kinetochore complexes are made up of over 100 different proteins (Cheeseman 2014). Therefore, following PLK1 localisation to kinetochores, PLK1 can phosphorylate a vast repertoire of targets. In addition to BUB1, obvious targets of PLK1 phosphorylation

would be additional components of the SAC. PLK1 levels have been shown to increase at kinetochores that remain unattached (Ahonen et al. 2005). Therefore, it is conceivable that PLK1 plays a role in regulating the activity of the SAC. PLK1 has also been shown to phosphorylate BUBR1, another recognised member of the SAC (Elowe et al. 2007). However, this phosphorylation is probably independent of SAC regulation, because PLK1 inactivation studies have demonstrated that the SAC remains active in the absence of PLK1 (Lénárt et al. 2007; Santamaria et al. 2007; Sumara et al. 2004). Therefore, PLK1 is not directly responsible for SAC activation. Instead, the PLK1-dependent phosphorylation of BUBR1 has been shown to indirectly link PLK1 to ensuring correct KT-MT attachment. PLK1 dependent phosphorylation of BUBR1 generates a binding site on BUBR1, supporting the recruitment of the protein phosphatase-2A-B56α complex (PP2A-B56α) (Suijkerbuijk et al. 2012). The recruitment of PP2A-B56α at kinetochores acts to counteract Aurora B-mediated phosphorylation of the KMN-network. This promotes the stabilisation of KT-MT attachments (Kruse et al. 2013), as Aurora B phosphorylation of the KMN-network reduces MT-binding affinity to kinetochores, thereby encouraging KT-MT error correction (Lampson and Cheeseman 2011). Thus, PLK1 and Aurora B activity may act antagonistically to achieve bipolar spindle attachment. Phosphorylation of substrates by Aurora B acts to destabilise MT-KT attachment, whilst PLK1-dependent phosphorylation may indirectly act to stabilise MT-KT attachment.

PLK1 also interacts with the 'tension sensing' protein PICH (Baumann et al. 2007). PICH has been shown to colocalise with PLK1 at KTs following NEBD (Baumann et al. 2007), although the significance of this PICH-PLK1 interaction remains unclear. PICH was originally identified as a SAC effector, however, the same group later confirmed this to be incorrect (Hübner et al. 2010). Therefore, a precise function for PICH at KTs continues to remain elusive. However, because of its localisation and interaction with PLK1 at KTs, PLK1 presents as a strong candidate for the regulation of PICH.

PICH stabilisation at kinetochores has been reported to be dependent on PLK1. Depletion, or expression of a kinase inactive version of PLK1, led to PICH re-localisation

away from kinetochores and recruitment along the chromosome arms (Baumann et al. 2007). This is supported by an independent study which showed that both PICH and PLK1 became localised to chromosome arms during PLK1 inactivation, using a then novel PLK1 inhibitor; ZK-Thiazolidinone (Santamaria et al. 2007). This led to the suggestion that PICH might target PLK1 to chromosome arms, when PLK1 activity becomes compromised. PICH is able to target PLK1 to chromosome arms, dependent on phosphorylation of PICH at T1063 (Leng et al. 2008). The significance of this PLK1-PICH re-localisation away from kinetochores to chromosome arms remains unclear, but it highlights a possible regulatory link between PLK1 and PICH.

Both PLK1 and PICH are required to ensure stable chromosome alignment and segregation during mitosis. A disruption to the activity of either protein leads to mitotic defects, including errors in KT-MT attachment and chromosome mis-segregation (Lénárt et al. 2007; Nielsen et al. 2015). Thus, further studies of PLK1 and its interacting proteins, may help to uncover how cells ensure correct chromosome alignment and faithful segregation.

1.9 Summary

Faithful chromosome segregation relies on an extremely complex series of processes, both prior to and after mitotic entry. These include DNA duplication and the establishment of sister chromatid cohesion, whilst commitment to mitosis also requires the refined manipulation of chromosome architecture through chromosome condensation. In addition, intricate processes are involved in the identification and assembly of the centromere and building of the kinetochore complex. A sophisticated surveillance system also exists in order to monitor kinetochore attachment, by the microtubules that emanate from spindle poles. This ensures correct chromosome bipolarity, before sister chromatid disjunction can occur. Cells also rely on molecular machinery to 'decatenate', or 'resolve' DNA intertwining structures that can link sister chromatids. The recruitment of the UFB-binding complex to DNA linkages that appear during anaphase, promotes chromosome disjunction and prevents further genome damage. Understanding how each of these processes are activated and regulated remains an ongoing topic for scientific discovery. However, it seems clear that most, if not all of these processes involve PLK1 kinase activity.

Therefore, this project aimed to further investigate the roles of PLK1, in particular during mitotic progression, whilst also considering the potential regulatory role of its interacting proteins, including PICH and BLM. This research has led to the discovery that PLK1 plays an unexpected function in the protection of centromere integrity (Addis Jones et al. 2019). Inhibition of PLK1 kinase activity leads to a mis-regulation of the UFB-binding complex at the centromere, which results in catastrophic DNA breakage of centromeric chromatin. In particular, both BLM helicase and PICH translocase have been implicated as key drivers for this catastrophic centromere destruction (Addis Jones et al. 2019). We hypothesis that PLK1 activity prevents such deformation via direct phospho-dependent regulation of the UFB-binding complex, although this is yet to be confirmed. Additionally, PLK1 may play a role in DNA structural integrity and in its absence, centromeric DNA can become weak and susceptible to deformation.

Overall, the results detailed within this thesis highlight the importance of PLK1 kinase, to ensure the maintenance of genomic stability, via a previously undescribed pathway for the protection of centromeres.

Chapter 2: Materials & Methods

2.1 DNA plasmid construction

All cloning reactions involved the use of chemically competent *E. coli* DH5α cells (New England Biolabs). Either High- or Sub-cloning efficiency DH5α cells were used, depending on the cloning application.

2.1.1 DNA plasmids

eGFP-C1-BLM

eGFP-C1-BLMQ672R

eGFP-C1-PICH

eGFP-C1-PICHK128A

siRES-PICH(GeneArt)

pSYC-181 – psCMV-NLS-eGFP-P2A-NEO-T7-SV40pA (Neomycin cassette inserted)

2.1.2 Oligonucleotides for cloning

Primer number	Primer name	Sequence
1	GFP_BLM_F-AscI	GCTACCTTGGCGCGCCATGGTGAGCAAGG
2	GFP_BLM_R-AgeI	GAGATTCGGACCGGTTGAGAATGCATATGAAGGC
3	siRES_PICH_F-AfiII	CCTAATGGACCTACTTAAGAGG
4	siRES_PICH_R-SacI	TCCTCGATTGTAAAGAGCTC
5	GFP_PICH_F-AgeI	CTAGCGCTACCGGTCGCCA
6	GFP_PICH_R-SmaI	GTGGATCCCGGGTGAATTGTTATTAAG

2.1.3 Bacterial transformation

All bacterial transformation reactions followed the manufacturers protocol involving the use of chemically competent *E. coli* DH5α cells (New England Biolabs). In brief, chemically competent *E. coli* DH5α cells (50µl) were thawed on ice and incubated with the required amount of purified DNA for 30 mins. Cells were then heat shocked at 42°C for exactly 30 seconds, before returning them back on ice for 5 minutes. 450µl of SOC media was added to the cells and then incubated at 37°C for up to 60 minutes, whilst shaking in an Eppendorf thermomixer. Finally, cells were plated on to pre-warmed LB-Agar plates (supplemented with the required antibiotic for selection) at varying dilutions and incubated overnight at 37°C.

2.1.4 Plasmid preparation and purification

Preparation of plasmid DNA was achieved by selecting a single transformed bacterial colony and inoculating in 5ml of LB (Luria-Bertani) media, supplemented with the necessary antibiotics. The inoculated colonies were incubated overnight at 37°C, whilst shacking at 220rpm in a C25 incubating shaker (New Brunswick Scientific). The following day, 500µl of the culture was collected and added to 500µl of 50% glycerol in cryo-vials (Thermo Fisher), in order to prepare bacterial glycerol stocks (stored at -80°C). The remaining culture was then harvested by centrifugation at >4000rpm for 5 minutes at room temperature. The pelleted cells were then directly used for plasmid extraction, following the manufacturers protocol using either a QIAprep Spin Mini or Midi prep kit (Qiagen), depending on the required DNA amount and downstream application(s). The DNA concentration was measured using a NanoDrop (ND-1000 UV-Vis Spectrophotometer) and the purified plasmid DNA was stored at -20°C.

2.1.5 Restriction enzyme digestion

Restriction enzyme digestion was performed using New England Biolab restriction enzymes, alongside the recommended buffer composition, according to the manufacturers guidelines (NEB). Typically, for a 25μl reaction, 2.5μl of the recommended 10x buffer was used with around 1μg of purified plasmid DNA. 0.5-1μl of restriction enzyme was added and incubated at 37°C for 15-60 minutes, before analysing on an agarose gel.

2.1.6 Thermocycling (Polymerase Chain Reaction)

All polymerase chain reactions (PCR) were performed using an Eppendorf PCR machine. PCR primer oligonucleotides were purchased from Eurofins Genomics and dissolved for use in all PCR reactions at a concentration of 10μM in ultra-pure water. All DNA fragment amplification reactions were performed using Phusion polymerase (New England Biolabs), following the manufacturer's guidelines.

2.2 Human Cellular assays

2.2.1 Human cell culture

Unless stated, all human cell lines used were obtained from the Cell Bank at the Genome Damage & Stability Centre, which were originally purchased from ATCC. All cell lines passed regular testing for mycoplasma contamination (Lonza Mycoplasma testing kit). RPE1 (PLK1as cells) derivative cell lines were a gift from Mark Burkard (University of Wisconsin). HAP1 and knockout BLM (HAP1) cells were a gift from Marcel van Vugt (University of Groningen). Stable cell lines created during this study include:

Cell line name	Parental
GFP-BLM	DeltaBLM-HAP1
GFP-BLM(Q672R) - Helicase dead	DeltaBLM-HAP1
GFP-PICH-(siRES)	HCT116
GFP-PICH(K128A)-(siRES) - Translocase dead	HCT116

In brief, all human cell lines were maintained at 37°C in a humidified incubating chamber, containing 5% CO_2. All cell lines were grown in their necessary growth medium (see table, 2.3.2), supplemented with foetal calf serum (FCS) and antibiotics (Penicillin-Streptomycin). To maintain healthy cell growth, cells were passaged every two-three days. In brief, cells were washed in PBS before adding 0.25% Trypsin-EDTA (Sigma T4049). Cells were then incubated at 37°C for 1-2 minutes to allow cells to detach from the cell culture flasks. Cells were then neutralised with fresh pre-warmed medium and centrifuged at 1200rpm for 2 minutes. Cells were then resuspended in fresh culture medium and plated into new flasks at a low-medium density.

2.2.2 Cell lines (parental)

Cell line	Morphology	Culture medium	Karyotype	Origins
RPE1 hTERT	Epithelial (like)	DMEM F12 15% FCS Pen-Strep	46 (Diploid)	Normal
HCT116	Epithelial	McCoys 5A 15% FCS Pen-Strep	46 (Diploid)	Colorectal carcinoma

HeLa	Epithelial	DMEM 10% FCS L-Glutamine Pen-Strep	70-164 (Polyploid)	Adenocarcinoma
HAP1	Fibroblast-like	IMDM 10% FCS Pen-Strep	23 (Haploid)	Chronic myelogenous leukaemia (CML)

2.2.3 Drugs & Inhibitors

Drug/Inhibitor	Target/Function	Source	Concentration
3-MB-PP1	ATP-analogue	Abcam	1μM
BI2536	PLK1	Cayman chemical	60nm/250nm
G418	Antibiotic	Sigma	0.6-1.2mg/ml
Nocodazole	Microtubule spindle poison	Sigma	100ng/ml
ProTAME	APC/C	R&D systems	12μM
Thymidine	G1/S arrest	Sigma	2mM

2.2.4 Transfection of human cells

2.2.4.1 Electroporation (transient & stable transfection)

Cells were trypsinised at 37°C for approximately 2-5 minutes, before neutralisation with fresh medium. Cells were centrifuged at 1200rpm for 2 minutes and the pellet resuspended in 5-10ml of fresh medium for counting. The volume required for $4x10^5$ cells was taken and washed in 5ml of PBS, before again pelleting via centrifugation. After

removing the supernatant, cells were resuspended in 20μl of Buffer R (pre-warmed to RT). A range of between 1-5μg/μl of purified DNA was added to the cells in a maximum of 2.5μl volume. Using the Neon Transfection System 10μl kit (ThermoFisher, MPK1025), the DNA mixture was pipetted into the needle and electroporated at 1350V, for 20ms with 2 pulses, and added to a 6-cm dish containing 5ml of pre-warmed culture medium. This was repeated for a second time and the DNA complex again added to the culture medium, before the cells were incubated at 37°C in a 5% CO_2 cell culture incubator. Cells were either examined after 24-48 hours of transfection (transient plasmid expression) or, alternatively, for stable cell line creation, cells were re-plated after approximately 48 hours and allowed to re-adhere to the surface (16-24 hours). Once recovered the cells were then subjected to antibiotic selection pressure for 2-14 days, depending on the antibiotic used (Puromycin 2-3 days, G418 a minimum of 10-14 days). Following antibiotic selection, cells were either seeded at a very low density (500-2000 cells) in a large cell culture dish (e.g. 15cm) for single colony selection, or alternatively, sorted using a BD Melody cell sorter (see below, Flow Cytometry 2.3).

2.2.4.2 Lipid mediated delivery (transient & stable transfection)

FuGENE HD (Promega) was used to transfect plasmid DNA into human cells, if electroporation was not required. The manufacturers guidelines were used for all FuGENE HD transfections. In brief, cells were plated in a 6-well dish (approximately $2x10^5$ cells) a day before transfection (approximately 16 hours before). In general, 2μg of purified plasmid DNA was used for transfection at a 3:1 or 4:1 ratio of transfection reagent to DNA. Cells were either examined after 24-48 hours post transfection (transient expression), or alternatively, re-plated in a larger cell culture dish and subjected to antibiotic selection pressure for up to 14 days (see stable cell line creation, 2.2.5). Successful clones were either isolated by single colony isolation or by FACS cell sorting, using a BD Melody cell sorter.

2.2.4.3 Protein depletion using RNA interference (RNAi)

Depletion of proteins was achieved by using Lipofectamine RNAi MAX transfection reagent (ThermoFisher, 13778075), whilst following the manufacturers guidelines. In brief, following cell seeding (approximately 75% confluency), cells were transfected with siRNA oligos (see RNAi oligo sequences, 2.2.4.4) using RNAi MAX, for up to 24-72 hours in order to deplete the target protein. Fresh siRNA-RNAi MAX complex was added for transfections over 24 hours every 24-48 hours. Protein depletion was measured via Western Blot or Immunofluorescent analysis.

Culture dish	siRNA (20μM)	RNAi MAX	OPTI-MEM	Final volume
6-well plate	1.25μl	1.25μl	250μl (each)	2ml
6cm plate	2.5μl	2.5μl	500μl (each)	4ml
10cm plate	6.25μl	6.25μl	1250μl (each)	10ml

2.2.4.4 RNA interference Oligonucleotide sequences

RNAi Target	Sequence	Supplier
BLM	GGAUGACUCAGAAUGGUUA	Dharmacon ON-TARGET plus Individual (J-007287-08-0005)
CTRL	UGGUUUACAUGUCGACUAA; UGGUUUACAUGUUGUGUGA; UGGUUUACAUGUUUUCUGA; UGGUUUACAUGUUUUCCUA	Dharmacon ON-TARGET plus Non-targeting Pool (D-001810-10-05)
PICH	AAUUCGGUAAACUCUAUCCACAGCU	Invitrogen

PLK1	GCACAUACCGCCUGAGUCU; CCACCAAGGUUUUCGAUUG; GCUCUUCAAUGACUCAACA; UCUCAAGGCCUCCUAAUAG	Dharmacon ON-TARGET plus SMARTpool (L-003290-00-0005)
RAD51	CCACCAGACCCAGCUCCUUUAUCAA	Invitrogen
SGO1	CAGCCAGCGUGAACUAUAA; GUUACUAUCUCACAUGUCA; AAACGCAGGUCUUUUAUAG; GUGAAGGAUUUACCGCAAA	Dharmacon ON-TARGET plus SMARTpool (L-015475-00-0005)

2.2.5 Stable cell line generation

2.2.5.1 Complementation of WT & helicase dead (Q672R) GFP-BLM

DeltaBLM (HAP1) cells were created by PCR amplifying the GFP-BLM sequence from the GFP-BLM bacterial plasmid (see bacterial plasmids, 2.1.2). Oligos were designed to include restriction enzymes in both the forward and reverse direction (AscI & AgeI, respectively), whilst also removing the stop codon from the GFP-BLM sequence (see oligo sequences 2.1.3). The PCR fragment was then used for restriction cloning into the pSYC-181(NEO) vector, using the AscI & AgeI sites. In brief, both the PCR fragment (2-5μg DNA of GFP-BLM & GFP-Q672R) and vector (10μg DNA of pSYC181-(NEO)) were digested in a 50μl reaction for 6-8 hours, using AscI & AgeI restriction enzymes according to the manufacturers reaction guidelines (NEB). The digested PCR product was PCR purified (QIAquick PCR purification Kit, Qiagen), whilst the digested vector was then de-phosphorylated with (5μl) Antarctic phosphatase (NEB) and gel extracted, according to the manufacturer's guidelines (QIAquick Gel Extraction Kit, Qiagen). The digested products were then ligated together in a 1:3 ratio of vector (500ng) to insert using T4 DNA Ligase (NEB). The ligation reaction was heat de-activated at 65°C for 10mins, before 3μl of ligated RXN mixture was then transformed into High-efficiency DH5α cells (New England Biolabs). Following transformation and successful isolation of clones via sanger

sequencing (ATGC), purified plasmid DNA (MIDI prep) was then transfected into DeltaBLM (HAP1) cells using FuGENE transfection reagent, following the manufacturers guidelines. After 48hours of transfection, antibiotic selective pressure in the form of G418 was applied to the cell medium, for a minimum of 2 weeks (1.2mg/ml). After 2 weeks of antibiotic selection, cells were then sorted for GFP expression using the BD Melody FACS cell sorter, which isolated a polyclonal population of GFP-BLM or GFP-BLM (Q672R) cells.

2.2.5.2 PICH RNAi resistant stable cell line

In order to generate an RNAi resistant copy of the PICH gene for stable cell expression, it was necessary to change the DNA sequence that the PICH siRNA oligo targeted (see RNAi oligo sequences, 2.2.4.4), whilst maintaining the original amino acid sequence. A gene synthesis service by Thermo Fisher (Gene Art) was used to generate a 589bp sequence of the PICH gene, which contained 10 nucleotide variations within the 20 nucleotide RNAi targeting region, whilst maintaining the same amino acid sequence. The synthesised DNA sequence was also designed to include flanking restriction enzymes (AfiII & SacI, New England Biolab, NEB) for further cloning needs. The synthesised sequence was then PCR amplified and digested (2-5μg DNA in a 50μl RXN for 6-8hrs), targeting the AfiII and SacI sites for downstream cloning. Alongside this the GFP-PICH & GFP-K128A vectors were digested with AfiII and SacI (10μg DNA in a 50μl RXN for 6-8hrs) and then de-phosphorylated using 5μl of Antarctic phosphatase (NEB). The PCR product was purified (QIAquick PCR purification Kit, Qiagen) and the vector underwent gel extraction (QIAquick Gel Extraction Kit, Qiagen). The vector (~8Kb) and insert (~500bp) fragment were then ligated using T4 DNA Ligase (NEB) according to the manufacturer's guidelines in a 1:3 ratio, using 500ng of vector DNA for 2hrs at RT. The ligation reaction was heat de-activated at 65°C for 10mins, before 3μl of the ligation RXN mixture was transformed into High-efficiency DH5α cells (New England Biolabs). Following mini-preparation of plasmid DNA, GFP-PICH & GFP-K128A (including the mutated RNAi targeting site) plasmids were PCR amplified with specific oligos (see oligonucleotides, 2.1.3), which contained both AgeI & SmaI restriction enzyme sites, whilst also removing

the stop codon. This fragment was then cloned into the pSYC-181(NEO) vector using restriction enzyme digestion (AgeI & SmaI, NEB) and T4 DNA ligase (NEB). Following transformation and confirmation of clones via sanger sequencing (ATGC), purified plasmid DNA (MIDI prep) was then transfected into HCT116 cells using FuGENE. After 48hours of transfection antibiotic selection pressure in the form of G418 (0.7mg/ml) was applied to cell medium for 2 weeks. After 2 weeks of antibiotic selection, cells were then sorted for GFP expression using the BD Melody FACS.

2.3 Flow cytometry and fluorescent activated cell sorting (FACS)

2.3.1 Flow cytometry cell cycle analysis

In order to analyse cell cycle profiles, cells were subjected to propidium iodine (PI) staining and Flow Cytometry analysis (BD Accuri C6). In brief, cell culture medium was collected and cells were then washed in PBS. Again, this was collected, before cells were trypsinised at 37°C for approximately 2-5 minutes. The collected medium was used to neutralise the cells before centrifugation at 1200 rpm for 2 minutes. Cells were then resuspended in 5-10ml PBS and centrifuged again. The S/N was removed before cells were gently resuspended by flicking. Cells were then fixed in 1ml of Ice cold EtOH (70%), adding dropwise whilst vortexing at high force. Samples were stored at -20°C O/N and then stained in FACS-PI buffer. For PI staining, fixed cells were centrifuged at 4000 rpm in a 1.5ml Eppendorf tube for 5 minutes. The S/N was then removed and cells were resuspended in (300-800µl) FACS-PI staining buffer (9.5ml 1x PBS, 400µl Propidium Iodine solution [1mg/ml] & 100µl RNAseA [10mg/ml]). The resuspended cells were then passed through a Falcon cell strainer, into a 5ml round bottom tube (Falcon Corning, 352235) ready for Flow Cytometry analysis. The BD Accuri C6 machine was used for cell cycle analysis, following the manufacturer's instructions. A minimum of 20,000 events were recorded for each sample.

2.3.2 Cell sorting (FACS)

Cell sorting was used to isolate a population of cells stably expressing a detectable protein (e.g. GFP-tagged protein). Following successful transfection (see Human cell transfection, 2.3.4) cells were subjected to FACS cell sorting using a BD Melody cell sorter. In brief, cells were trypsinised at 37°C for approximately 2-5 minutes. Cells were then neutralised in fresh medium before centrifugation at 1200 rpm for 2 minutes. Cells were then resuspended in fresh medium containing only 1% serum (FCS), and passed through a Falcon cell strainer into a 5ml round bottom tube (Falcon Corning, 352235), ready for FACS. A 5ml Polystyrene collection tube was also needed (Falcon Corning, 352003), containing approximately 2-3ml of fresh pre-warmed medium (containing the full amount of serum e.g. 10-15%). First, the parental cell line (prior to fluorescently-tagged protein transfection) was passed through the machine to examine any background fluorescence. Next, the fluorescently tagged expressing cell line was passed through the machine and the detection of GFP was gated and collected into the collection tube. Cells were then added to fresh pre-warmed medium to amplify the isolated fluorescently expressing stable cell line and incubated at 37°C in a humidified incubating chamber, containing 5% CO_2. Cells were also quarantined and examined for mycoplasma testing following each FACS experiment (all samples passed testing).

2.4 Antibodies

2.4.1 Primary Antibodies (Immunofluorescence & Western blot)

Immunofluorescence

Antibody	Host species	CAT Number	Source	Dilution
BUB1	Mouse	ab54893	Abcam	1:400
BLM	Goat	C-18	Santa Cruz	1:100
BLM	Rabbit	ab2179	Abcam	1:100

CENP-A	Mouse	Ab13939	Abcam	1:100
CENP-B	Rabbit	Ab25734	Abcam	1:400
γH2AX	Mouse	JBW-301	Millipore	1:400
GFP-Atto488	Nanobody	GBA488	Chromotek	1:200
PICH	Mouse	H00054821-B01P	Abnova	1:100
PICH	Rabbit	H00054821-D01P	Abnova	1:100
SMC2	Rabbit	A300-058A	Bethyl	1:200
TOP2-α	Goat	(S20)-5348	Santa Cruz	1:100
RPA-(32)	Mouse	ab2175	Abcam	1:200
RPA-(70)	Rabbit	Ab79398	Abcam	1:200
PLK1	Mouse	(E2)-55504	Santa Cruz	1:100
α-tubulin	Rabbit	Ab18251	Abcam	1:600
Centromere	Human	HCT-0100	Immuno Vision	1:400
Pericentrin	Rabbit	Ab4448	Abcam	1:400
NUF2	Rabbit	Ab122962	Abcam	1:200
FLAG	Mouse	M2	Sigma	1:400

Western blotting

Antibody	**Host species**	**CAT Number**	**Source**	**Dilution**
PICH	Mouse	H00054821-B01P	Abnova	1:500
BLM	Goat	C-18	Santa Cruz	1:300
BLM	Rabbit	ab2179	Abcam	1:1000
KU80	Rabbit	Ab80592	Abcam	1:8000

β-actin	Mouse		Sigma	1:5000
GFP	Rabbit	Ab290	Abcam	1:2000
RAD51	Rabbit	Ab63801	Abcam	1:1000

2.4.2 Secondary Antibodies (Immunofluorescence & Western blot)

Immunofluorescence

Target IgG	Host species	Conjugation	Source	Dilution
Mouse	Donkey	Alexa Fluor 488	Invitrogen	1:500
Rabbit	Donkey	Alexa Fluor 488	Invitrogen	1:500
Goat	Donkey	Alexa Fluor 488	Invitrogen	1:500
Mouse	Donkey	Alexa Fluor 555	Invitrogen	1:500
Rabbit	Donkey	Alexa Fluor 555	Invitrogen	1:500
Goat	Donkey	Alexa Fluor 555	Invitrogen	1:500
Human	Goat	Alexa Fluor 550	Abcam	1:500
Mouse	Donkey	Alexa Fluor 647	Invitrogen	1:500
Rabbit	Donkey	Alexa Fluor 647	Invitrogen	1:500
Human	Goat	Alexa Fluor 650	Abcam	1:500

Western blotting

Target IgG	Host species	Conjugation	CAT Number	Source	Dilution
Mouse	Goat	Horseradish peroxidase (HRP)	Ab6789	Abcam	1:25000
Rabbit	Donkey	Horseradish peroxidase (HRP)	NA92340	ECL	1:20000
Goat	Rabbit	Horseradish peroxidase (HRP)	P0160	Agilent	1:10000

2.5 Western blotting

Cells were washed in PBS before trypsinisation at 37°C for approximately 2-5 minutes. Cells were then neutralised in fresh medium, before centrifugation at 1200 rpm for 2 minutes. Cells were washed in 5-10ml of PBS and again pelleted. Cells were then lysed on ice for 10-15mins in ice cold lysis buffer (50mM Tris pH 7.5, 300mM NaCl, 5mM EDTA, 1% Triton X-100, 1.25 mM DTT, 1mM PMSF and cOmplete^{TM} protease inhibitor cocktail). After 10-15mins of lysis, cells were then centrifuged at 15,000rpm for 20mins, at 4°C. The S/N was added to pre-chilled Eppendorf tubes and the protein concentration was measured using a Bradford Assay (Bio-Rad). In brief, BSA [1mg/ml] was added (0, 2, 4, 6, 8μl) to a final volume of 800μl of ultra-pure water to plastic cuvettes, to generate a standard curve. 1μl of each protein lysate was added to a final volume of 800μl of ultra-pure water, into individual plastic cuvettes. Finally, 200μl of Bradford reagent was added to each cuvette and vortexed to mix. A spectrophotometer (595nm λ) was used to measure light absorption and this was then calculated to protein concentration, using GraphPad Prism 7 software against the standard curve. Protein lysates were then diluted in 4x Laemmli sample buffer (Bio-Rad, 1610747), with 5% β-mercaptoethanol (Sigma,

M6250), so that each lysate contained the same protein concentration. Around 30-75μg of protein was loaded into SDS-Page gels, using a Tris/Glycine/SDS buffer for protein separation at 80-120V for 1-3hours, depending on protein size and separation required. Separated proteins were then transferred onto Amersham Hybond PVDF membranes, 0.2μm (GE Healthcare Lifesciences, 10600021). Protein transfer was performed for 60-90mins at 100V in ice cold Tris/Glycine buffer, containing 15% MeOH. Following protein transfer, membranes were then blocked in 10% Milk PBS-T (0.1% Tween-20) for 1-1.5 hours. In general, primary antibody incubations were performed O/N at 4°C in 10% Milk PBS-T, whilst rotating slowly. A minimum of 5 washes were performed in 1% Milk PBS-T whilst shacking (medium-fast). Secondary antibody incubations were performed for 30-45mins in 10% Milk PBS-T whilst rotating slowly. Again, washing was performed a minimum of 5 times in 1% Milk PBS-T, before a final wash in PBS-T. Proteins were then detected using chemiluminescent Clarity Western ECL substrate reagents (Bio-Rad, 1705060S) and developed using X-ray film.

2.6 High resolution microscopy

2.6.1 Immunofluorescent staining (including Pre-extraction protocol)

Typically, immunofluorescent staining involved seeding cells (2-4x10^5 cells) onto #1.5 or 1.5H coverslips (0.16-0.19mm or 0.17-0.18mm, respectively). In brief, cells were fixed in 4% PFA, containing Triton X-100 (250mM HEPES pH7.4, 1xPBS, 0.1% Triton X-100 & 4% methanol-free paraformaldehyde) at 4°C for 20mins. Cells that required pre-extraction prior to fixation were submerged into ice-cold pre-extraction buffer for 10-15 seconds, whilst remaining on ice (20mM HEPES pH7.4, 0.5% Triton X-100, 50mM NaCl, 3mM $MgCl_2$, 300mM sucrose). Following pre-extraction, cells were then fixed in 4% PFA (250mM HEPES pH7.4, 1xPBS & 4% methanol-free paraformaldehyde) at RT for 10mins. All PFA fixed cells were then washed 4-5 times in 1xPBS to remove any remaining PFA. Cells were then permeabilised for 20mins at RT (1x PBS, 0.5% Triton X-100 & 0.5% FCS) and washed a further 4-5 times in 1x PBS. Following washing, cells were then blocked for 20-30 minutes at RT (1x PBS & 0.5% FCS) before primary antibody staining. Primary

antibodies were prepared in blocking solution at the required dilution (see primary antibodies, 2.4.1) and incubated at 37°C for approximately 1.5hrs. Cells were then washed a further 5 times in 1xPBS, before secondary antibody incubation. Again, secondary antibodies (see secondary antibodies, 2.4.2) were prepared in blocking solution and incubated at RT for approximately 30 mins. Finally, cells were washed in 1xPBS, before a final submersion in ultra-pure water and coverslips were airdried before mounting using Vectashield (Vectashield) containing DAPI.

2.6.2 DNA bridge immunofluorescent staining

Immunostaining for ultrafine DNA structures followed the rule as described previously for all immunofluorescent staining procedures. However, to minimise the loss of mitotic cell populations (less adherent), agitation during washing was kept to a minimum, with a slow rotating action of a 6-well plate after addition of 1xPBS.

2.6.3 K-fibre immunofluorescent staining

To immunostain for K-fibre attachment (kinetochore attached tubulin fibres), prior to fixing the cells, a 6-well plate containing cells seeded onto coverslips (previously described, 2.6.1) was placed on ice for 10 mins. Coverslips were then carefully pre-extracted and fixed as previously described and immunostained as before.

2.6.4 5-Ethynyl-2'-deoxyuridine (EdU) Click-iT staining

In order to detect replicating cells (S-phase), the thymidine analogue 5-Ethynyl-2'-deoxyuridine (EdU) was added to cell cultures, prior to fixation. The incorporated EdU could then be later detected during microscopy. Following fixation and cell permeabilisation, EdU Click-iT chemistry was performed according to the manufacturer's instructions. Immunofluorescent staining was also performed on cells after EdU Click-iT chemistry, before fluorescent microscopy analysis.

2.6.5 Acquisition of immunofluorescent imaging

All image acquisition was carried out using a Zeiss Axio Observer Z1 epifluorescence microscope, using either a 40x / 1.3NA, 60x / 1.4NA or 100x / 1.4NA oil Plan-Apochromat objective for fluorescent imaging. The Zeiss Axio Observer Z1 microscopy system is fitted with a Hamamatsu ORCA-Flash 4.0 LT camera and is aligned and calibrated using 200nm diameter Tetra Speck microsphere beads (Thermo Fisher). Typically, all imaging involved covering a range of 2-8μm, using a varying range of Z-stack intervals at 0.2μm. Post processing of images involved the use of both ZEN Blue (Zeiss) software and ImageJ (FiJI).

2.6.6 Widefield live cell microscopy

Cells were seeded into 2-or 4- well on cover glass II chamber slides (2-3 x 10^5 cells) (Sarstedt). In order to stain nuclei, SiR-DNA (Spirochrome) was added to the cell culture medium (1:1000) for a minimum of 4 hours before imaging. Cell cycle progression was monitored by using a Zeiss Axio Observer Z1 microscopy system, equipped with a heating (37°C) and CO_2 chamber (5%) and fitted with a Hamamatsu ORCA-Flash 4.0 LT camera for image acquisition. Image acquisition relied on the use of either a 40x/0.6 Plan-Neofluar or 40x/1.3 oil Plan-Apochromat objective, whilst acquiring images every 5-7 minutes. A maximum of 6 z-stacks with 2μm intervals were used to cover the cell depth and analysed using both ZEN Blue (Zeiss) and ImageJ (FiJI) software.

2.6.7 Deconvolution (Huygens professional)

Image deconvolution was carried out using Huygens Professional (SVI Huygens) deconvolution software, using a measured point spread function (PSF), generated using the 200nm diameter Tetra Speck microsphere beads. Minimal iteration sampling was used between 10-60, with a range of 20-50 signal-to-noise being applied.

2.7 Cytogenic analysis

2.7.1 Chromosome spread preparation

Typically, a 10cm dish was used for chromosome spread preparation with the cell medium being collected into 15ml Falcon tubes (Falcon Corning) before washing the cells in PBS. Again, this was collected prior to trypsinisation at 37°C, for approximately 2-5 minutes. Cells were then neutralised with the collected medium and centrifuged at 1000 rpm for 5 mins. Approximately 500µl of the S/N was kept to allow for cells to be resuspended by gentle tapping of the pellet. Cells were then subjected to pre-warmed hypotonic solution (7ml, 0.075M KCL, 37°C) in a dropwise motion whilst also being gently mixed and allowed to incubate at 37°C for approximately 5-10mins. Again, cells were centrifuged at 1000rpm for 5mins before again approximately 500µl of the S/N was kept to allow for cells to be resuspended by gentle tapping of the pellet. Cells were then fixed and washed with 7ml of a 3:1 ratio of Methanol:Acetic acid solution, again in a dropwise motion whilst gently mixing. Cells were again centrifuged at 1200 rpm for 5 mins and washed/fixed in Methanol:Acetic acid solution a further two times. After the final wash, cells were then resuspended in up to 1ml of fresh Methanol:Acetic acid solution and dropped onto glass slides for analysis or stored at -20°C.

2.7.2 Centromere & Telomere FiSH (ctFiSH)

Peptide nucleic acid (PNA) probe hybridisation of pre-aged (minimum 2-3 days) chromosome spreads followed the manufacturers guidelines (DAKO Agilent & PNAbio). In summary, chromosome spreads were washed in TBS before being fixed in 3.7% PFA and dehydrated using an increasing ethanol wash series (ice cold 70%, 90%, 100%EtOH). Slides were then air-dried prior to PNA probe addition to the spread. A small coverslip (18x18mm) was added to the probe and the slide was co-denatured at 80°C for 1min to 1min 15 seconds and incubated in a humidifying chamber for 1-3 hours at RT. Spreads were then wash (65-70°C) and dehydrated again in the ice-cold ethanol series, before air drying and mounting and counterstaining using Vectashield with DAPI.

Chapter 3: PLK1 activity promotes metaphase maintenance

3.1 Introduction

A key cellular feature of transformed cells, such as cancer cells, is their tendency to mis-segregate their chromosomes during mitosis (Funk et al. 2016). This often leads to the unequal distribution of genetic material, which consequently results in changes of ploidy. This imbalanced distribution of chromosome number is referred as aneuploidy and is a characteristic feature of both cancer and rare congenital disease. How cells acquire such genomic instability remains a long-unanswered question.

A strong case can be made for further investigation into chromosome alignment itself, or chromosome biorientation. Cells rely on a complex series of events to successfully orientate their chromosomes during mitosis. Crucially, correct chromosome alignment requires the stable capture of each and every centromere by mitotic spindle microtubules (MT). These emanate from opposite centrosomes and manoeuvre each chromosome in order to establish the metaphase plane. In addition, centromere capture also requires the prior assembly of kinetochores (KT) at each centromere. This macromolecular protein complex assembles at both sides of the core centromere, forming sister kinetochores (Cheeseman 2014). Apart from KT assembly at centromeres, chromosome biorientation also relies on several other molecular mechanisms for its accomplishment. These include maintaining sister chromatid cohesion and the regulation of the mitotic checkpoint machinery (Hengeveld et al. 2017; Musacchio and Salmon 2007). Sister chromatid cohesion is mediated by cohesin complexes, which physically embrace sister chromatids until anaphase, and this supports bipolar MT attachment. The mitotic spindle checkpoint or spindle assembly checkpoint (SAC), monitors spindle mis-attachments and acts as a protective surveillance system, that functions to prevent cells from prematurely initiating anaphase, if for example KT-MT attachment errors exist (Musacchio and Salmon 2007). Activation of the SAC is achieved by the disruption of stable bipolar microtubule spindle attachment to kinetochores, and

its regulation is so robust that even a single unattached kinetochore is enough to trigger its activation (Rieder et al. 1995). Without such a system, cells are likely to enter anaphase with misaligned chromosomes, which can lead to chromosome mis-segregation and unequal distribution of genetic material in the subsequent daughter cells; a prominent cause for cellular disease progression, such as cancer (Funk et al. 2016). Chromosome biorientation is also facilitated by another regulatory mechanism, the chromosomal passenger complex (CPC). The CPC consists of INCENP, survivin, borealin and Aurora B kinase. Its primary function is to detect and resolve improper KT-MT attachments through phosphorylation of multiple kinetochore associated proteins by Aurora B kinase. However, the precise mechanism for the role of Aurora B during erroneous KT-MT attachment remains a debated topic (Hengeveld et al. 2017; Krenn and Musacchio 2015).

Another key protein influencing stable KT-MT attachment, is the mitotic kinase, Polo-like kinase 1 (PLK1) (Krenn and Musacchio 2015; O'Connor et al. 2016). PLK1 activity is required to phosphorylate factors associated with the activation and maintenance of the SAC (Elowe et al. 2007; Lénárt et al. 2007). Inhibition of PLK1 activity leads to severe chromosome misalignment patterns, which have been attributed to a failure of accurate KT-MT attachment and maintenance (Lénárt et al. 2007). This was highlighted by the evidence of defects in chromosome congression and the direct detection of unattached kinetochore complexes, which was concomitant with the accumulation of SAC proteins at KTs (Lénárt et al. 2007). Depletion of PLK1 using RNAi results in unattached kinetochores, with cells displaying strong MAD2 signals at their kinetochores; a hallmark feature of SAC activation (Hanisch 2006). However, despite these observations, it remains uncertain how PLK1 precisely functions during metaphase establishment. Orthologs of the mammalian PLK1, including the yeast Cdc5 (*S. cerevisiae*) and Plo1 (*S. pombe*), are not required for kinetochore function (Lee et al. 2005). This reflects the differences of PLK1's spatiotemporal regulation and function across different species, and highlights that PLK1 function(s) may not be necessarily limited to KT-MT stabilisation. Therefore, it is of great interest to study PLK1 activity during chromosome alignment.

This basic overview of the regulation and complex protein involvement during KT-MT attachment, demonstrates the importance of chromosome biorientation to guarantee faithful chromosome segregation. Chromosome biorientation is not only key to equal chromosome distribution, but also provides a safeguarding mechanism for mitotic progression. PLK1 loss of function experiments have widely implicated PLK1 to be responsible for stabilising KT-MT attachment, during chromosome biorientation. However, understanding how PLK1 promotes the stable KT-MT attachment required to support chromosome biorientation remains uncertain. This study has focused on further understanding the role(s) of PLK1 during mitotic progression, in particular, exploring the effects of the loss of PLK1 activity during chromosome congression and biorientation.

3.2 Results

3.2.1 Inhibition of PLK1 by a small-molecule inhibitor, BI2536, arrests cells in mitosis

A small-molecule inhibitor, BI2536 was used to study the loss of function(s) of PLK1 during mitosis (Lénárt et al. 2007; Steegmaier et al. 2007). This very potent and largely specific PLK1 inhibitor has been previously reported to effectively prevent PLK1 kinase activity in nanomolar concentrations (IC_{50} = 0.83nM) (Lénárt et al. 2007; Steegmaier et al. 2007). A recognised phenotype of PLK1 inactivation is a mitotic arrest. Therefore, to confirm that BI2536 was effectively inhibiting PLK1 kinase activity, and cells were arresting in mitosis, cell cycle analysis of RPE1 hTERT cells was performed using FACS. Asynchronously growing RPE1 cells showed an expected cell cycle profile during FACS analysis **(Fig. 3.1, i)**. In order to enrich for a mitotic population for study, cells were treated with thymidine [2mM] to initially arrest them at the G1/S boundary before release **(Fig. 3.1, ii)**. Following release from a thymidine arrest (G1/S arrest), it was possible to demonstrate that the majority of cells were successfully progressing through S phase **(Fig. 3.1, iii)**. To examine whether BI2536 arrested cells in a mitotic stage, BI2536 [60nm] was added after 6 hours release from a thymidine arrest and fixed after 8 hours. FACS analysis confirmed that BI2536 treated cells were arresting at the G2/M stage of the cell cycle **(Fig. 3.1, iv)**. Notably, BI2536 was added at 6 hours after a thymidine arrest and release, to ensure that the majority of cells had completed S phase before the addition of the PLK1 inhibitor. To confirm that cells were arresting at the G2/M boundary after BI2536 treatment, an additional sample was fixed after 10 hours **(Fig. 3.1, v)**. The resulting FACS data confirmed that BI2536 treatment led to an enrichment of cells at the G2/M phase of the cell cycle. This was consistent with a previous study using BI2536 in HeLa cells (Steegmaier et al. 2007). Additionally, a control sample (DMSO treated) showed that cells were capable of re-entering G1, after releasing them from a thymidine arrest **(Fig. 3.1, vi)**. Therefore, BI2536 is an effective way of inhibiting PLK1 kinase activity for future PLK1 loss of function studies. Furthermore, as this dosage of BI2536 [60nm] used showed effective signs of a mitotic arrest, the majority of further experiments were completed using this concentration.

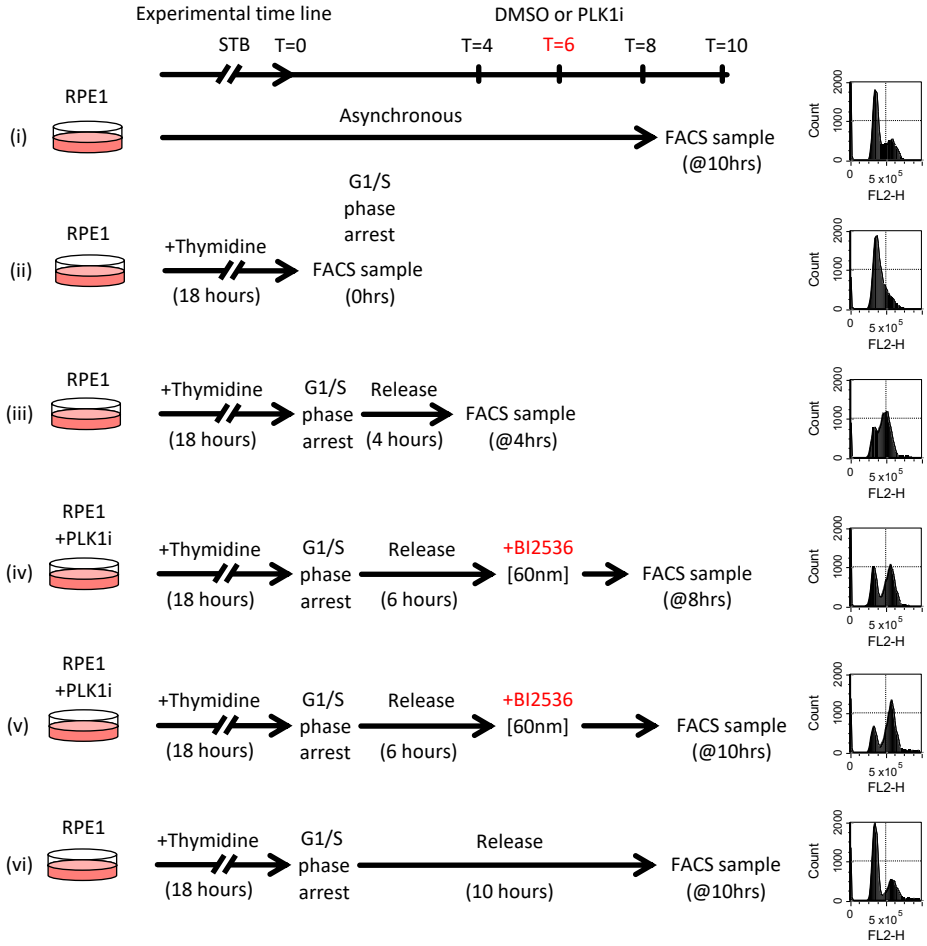

Figure 3.1. BI2536 arrests cells in G2/M.
Experimental outline to describe the cell-cycle progression of RPE1 hTERT cells after a single thymidine block and release; or after a mitotic arrest using BI2536 treatment. FACS experimental design and cell-cycle profile of **(i)** Asynchronous RPE1 cells; **(ii)** G1/S arrest after single-thymidine block (STB) treatment; **(iii)** S-phase progression after 4hrs post release from STB; **(iv & v)** mitotic arrest and enrichment after the addition of BI2536 at 6 hrs and FACS at either 8hrs, or 10hrs post release from STB; **(vi)** re-entry into G1 10hrs after STB in the absence of PLK1i.

3.2.2 Cells remain capable of metaphase establishment when PLK1 activity is inhibited

Typically, studies exploring the mitotic function of PLK1 have used fixed samples for their analysis. However, the use of live-cell time lapse microscopy may uncover the temporal detail regarding the fate of cells entering mitosis when PLK1 activity is inhibited by BI2536. In particular, it would be possible to examine chromosome arrangement as cells enter and progress through mitotic stages. Therefore, to enrich for a large mitotic population for study, RPE1 hTERT cells were synchronised at early G1/S using thymidine. Following release into fresh media, the cells were treated with different mitotic inhibitors in order to examine the fate of mitotic entry and progression **(Fig. 3.2a)**. As expected, control cells (DMSO treated) were able to proficiently enter mitosis and segregate their chromosomes without any obvious signs of impairment **(Fig. 3.2b, c)**. In contrast, cells treated with nocodazole, the microtubule spindle poison, arrested in a prometaphase like stage and showed no sign of further mitotic progression (Vasquez et al. 1997). Cells treated with the APC/C inhibitor, ProTAME, progressed through the early stages of mitosis (prophase-prometaphase), before arresting at metaphase **(Fig. 3.2b, c)** (Zeng and King 2012). Live-cell imaging confirmed that BI2536 treated cells arrested in mitosis, however, unexpectedly the majority of these cells showed signs of competent chromosome alignment during early stages of mitosis **(Fig. 3.2b, c)**.

BI2536 treated RPE1 cells displayed normal mitotic entry and progression through prophase. They were also able to progress past prometaphase and undergo chromosome alignment during metaphase. Remarkably, of the BI2536 treated cells analysed, approximately 80% of them appeared to align their chromosomes at metaphase **(Fig. 3.2c)**. This led to the speculation that in contrast to previous studies (Lénárt et al. 2007; Steegmaier et al. 2007), PLK1 may not be completely required in order for cells to establish bipolar KT-MT attachments. However, BI2536 treated cells did eventually display signs of metaphase collapse. Intriguingly, the collapsed cells showed a distinctly different collapse pattern to what had previously been described as the “polo” chromosome morphology (Lénárt et al. 2007). Instead, what was observed

was a chromosome misalignment pattern that resembled a 'figure-of-8' like shape **(Fig. 3.2b, e.g. BI2536 treated cells T=152 and Fig.3.3c for further examples)**. Therefore, it could be possible that PLK1 plays a role in the long-term stability, or maintenance of KT-MT attachment, in addition to its proposed establishment function.

BI2536 treated cells also showed signs of a prolonged metaphase stage (chromosome alignment), when compared against untreated cells (DMSO treated) **(Fig. 3.2d)**. This finding supports the idea that RPE1 cells are capable of forming bipolar spindle attachment during metaphase, despite the absence of PLK1 activity. As expected, cells treated with ProTAME displayed with even more extended metaphase alignment durations **(Fig. 3.2d)**. Therefore, these observations suggested that PLK1 activity is required for mitotic progression, but may not be essential for metaphase establishment, at least in RPE1 hTERT cells. This led to further questions regarding the status of mitotic cells, when PLK1 kinase activity was absent.

Previous studies reported that PKL1 inactive cells result in a "polo" stage mitotic arrest (Lénárt et al. 2007; Steegmaier et al. 2007). This has largely been attributed to cells being unable to undergo stable bipolar KT-MT attachment, as a result of either monopolar spindle attachment, or a complete absence of KT-MT attachment altogether. However, the results of the live-cell imaging data suggested that cells were capable of establishing bipolar attachment, despite the absence of PLK1 activity. Therefore, to further support this, analysis of bipolar spindle attachment was also investigated in fixed cells.

RPE1 hTERT cells were enriched in mitosis by synchronisation at early G1/S using thymidine. Following release into fresh media, cells were treated with either DMSO or BI2536, before being subject to indirect immunofluorescence staining analysis **(Fig. 3.3a)**. As expected, K-fibre staining, which identify stably bound KT-MT attachments in fixed cells, confirmed that BI2536 treated cells were capable of establishing bipolar spindle attachment, similarly to untreated cells **(Fig. 3.3b)**. Therefore, this analysis, taken together with the live-cell imaging data, would suggest that PLK1 activity is not

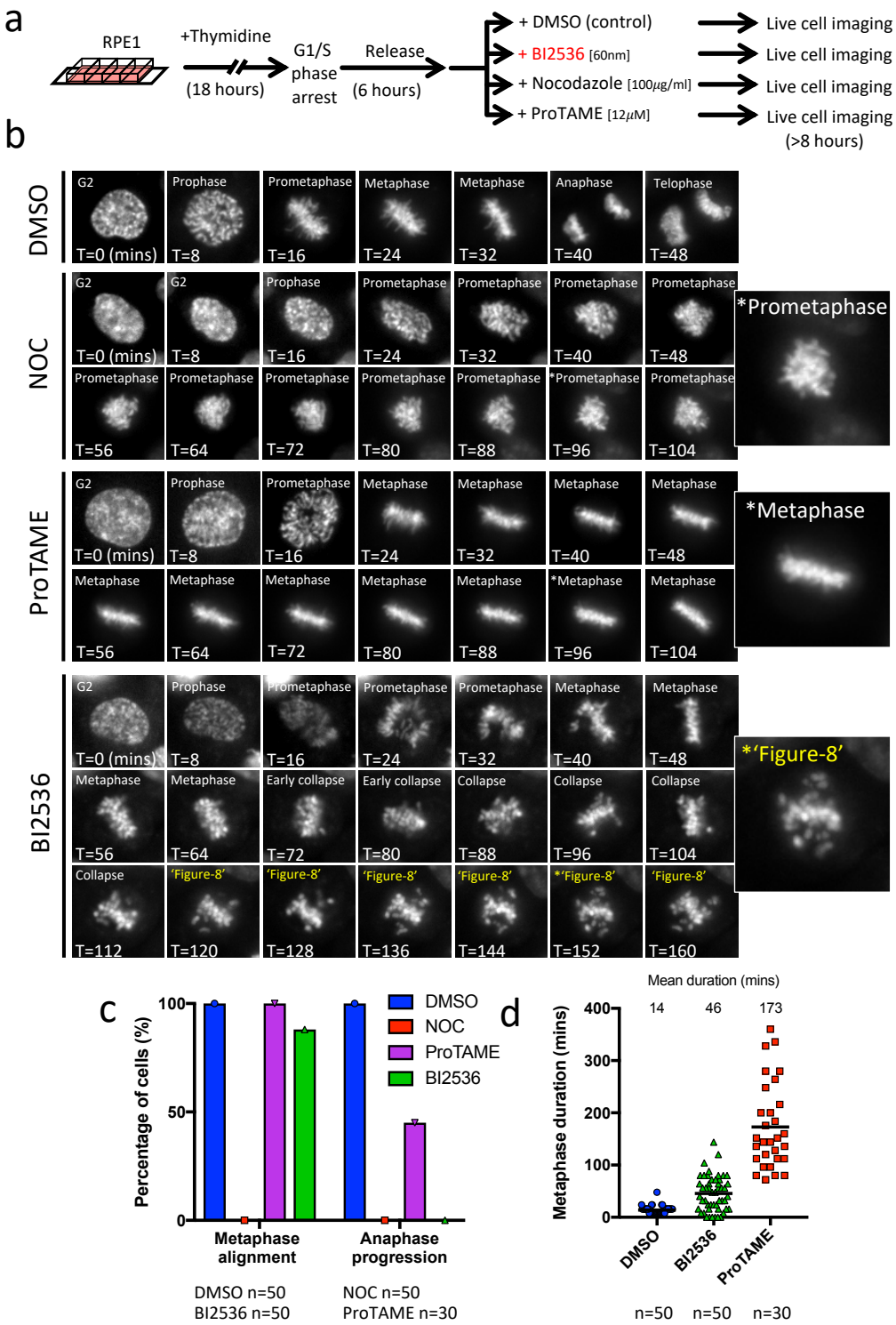

Figure 3.2. Cells fail to maintain metaphase alignment during PLK1 inhibition.
a) Experimental outline of cell-synchronisation and live-cell time lapse microscopy, after addition of indicated inhibitor treatment. **b)** Examples of live-cell time lapse microscopy image stills after indicated inhibitor treatment ('Figure-8' (yellow) metaphase collapse after BI2536 treatment is shown). **c)** Analysis of metaphase establishment and anaphase progression after indicated inhibitor treatment. **d)** Analysis of metaphase duration after indicated inhibitor treatment. A maximum of 50 frames after prophase establishment was recorded (overall mean is shown; n=number of cells analysed).

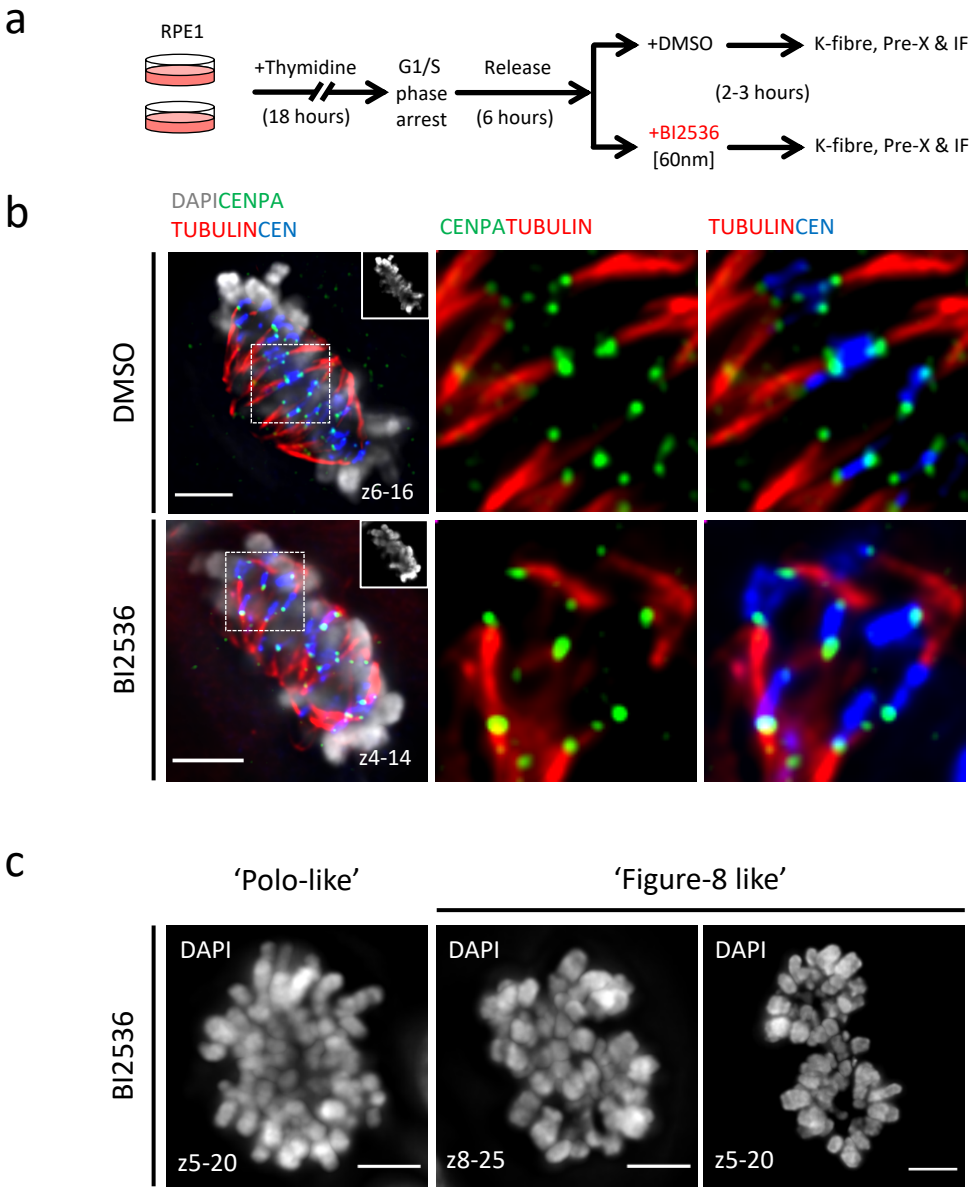

Figure 3.3. Bipolar spindle attachment during PLK1 inhibition.
a) Experimental outline of cell-synchronisation, plus and minus BI2536; and K-fibre immunofluorescent staining. **b)** Representative images of K-fibre attachment in cells that have established chromosome biorientation and show KT-MT attachment using the centromere specific histone CENPA (Green), α-tubulin (Red) and centromere (Blue) antibodies. **c)** DAPI stained nuclei of collapse metaphases, demonstrating either a 'polo-like' or 'figure-8' chromosome morphology.

absolutely required for the initial formation of KT-MT attachment, at least in RPE1 cells. Although, it cannot be ruled out that these results could be due to incomplete PLK1 inhibition when using BI2536. However, a consistently observed feature of PLK1 inhibition, during BI2536 treatment, showed that cells eventually do succumb to a form of metaphase collapse, implying that PLK1 activity is compromised. The metaphase collapse pattern resembled either the previously reported "polo" chromosome morphology (Lénárt et al. 2007), or the newly described 'figure-of-8' like pattern **(Fig. 3.3c)**. Most interestingly, further examination of the 'figure-of-8' collapse pattern led to an unexpected observation. This unexpected observation will be discussed below.

3.2.3 PLK1 inactivation leads to a DNA linkage during metaphase collapse

In an attempt to better understand what might be happening during the observed 'figure-of-8' metaphase collapse, during PLK1 inhibition, the localisation of the PLK1 protein at different stages of mitosis was examined. Previous studies identified PLK1s recruitment patterns during mitosis; in particular its recruitment to centrosomes and kinetochores (Golsteyn et al. 1995; Seong et al. 2002). However, to confirm PLK1 protein association during mitosis in this study, immunofluorescent staining for PLK1 was performed on RPE1 hTERT cells. Untreated mitotic cells showed the expected localisation patterns of PLK1 at both centrosomes and kinetochores **(Fig. 3.4a, b)**. In anaphase, surprisingly it was also possible to observe PLK1 localising to PICH positive UFBs **(Fig. 3.4a, b)**. This is believed to be the first report of PLK1 localising directly to UFBs. These DNA structures arise during sister-chromatid separation and remain undetectable by conventional DNA staining methods, such as DAPI. Instead, they are only detectable by protein association (Baumann et al. 2007; Chan et al. 2007). PLK1 appeared to localise alongside the recognised UFB binding protein, PICH (Polo-like kinase 1 interacting checkpoint helicase), which was originally identified through its interaction with PLK1 (Baumann et al. 2007). This could therefore imply that PLK1 has a role in regulating UFB proteins such as PICH. However, this currently remains as speculation, as it could be argued that PLK1 is simply associating to inter-polar spindles. However, there are no reports to suggest that PICH binds to microtubule structures and

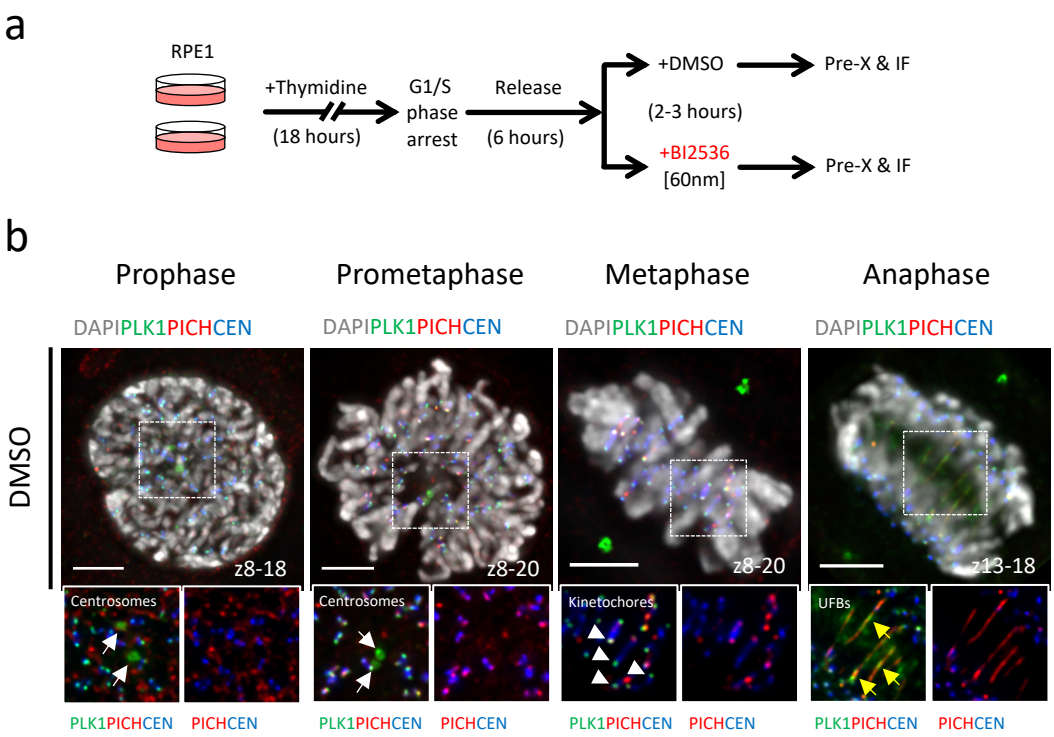

Figure 3.4. PLK1 recruits to ultra-fine DNA bridges (UFBs) during anaphase.
a) Experimental outline of cell-synchronisation and immunofluorescent staining, plus and minus BI2536 treatment. **b)** Immunofluorescent images of untreated (DMSO) mitotic RPE1 cells. Cells show antibody staining for PLK1 (Green), PICH (Red) and centromeres (Blue). PLK1 localises to centrosomes (white arrows), centromere/kinetochore (arrowheads) and anaphase UFBs (yellow arrows). Enlarged regions show PLK1 and PICH co-localisation patterns.

therefore, due to the PLK1-PICH localisation pattern displayed, it is likely that PLK1 is a component of the UFB binding complex.

Most remarkably, immunofluorescent staining of PLK1 in BI2536 treated cells, where PLK1 activity is inhibited, showed that the PLK1 protein was unexpectedly associating to structures that inter-linked the chromatin of mitotic cells **(Fig. 3.5a, b)**. In general, this occurred in cells that presented with the 'figure-of-8' metaphase collapse shape. Alongside PLK1, both PICH and the single-stranded DNA (ssDNA) binding protein, RPA (Replication protein A), were also shown to associate along these chromatin linking structures **(Fig. 3.5a, b)**. Further still, it was also apparent that PLK1 and PICH localisation appeared to overlap with each other, whereas RPA detection was generally shown to be exclusive of PICH localisation **(Fig. 3.5a, b)**.

The presence of PICH and RPA suggested that these inter-linking structures consisted of DNA molecules, as both proteins bind to double- and single-stranded DNA substrates, respectively. RPA binds ssDNA regions, especially during DNA replication and repair (Wu et al. 2016). The PICH protein has been reported to be capable of DNA manipulation and preferentially localises to DNA that encounters tension (Biebricher et al. 2013). Therefore, it is conceivable that the inter-linking structures are DNA assemblies, which have generated due to PLK1 inactivation. In addition, these DNA linkage structures originate from centromeres as they were positive for centromere staining at their termini **(Fig. 3.5a, b)**. Since the centromere is the principal point of tension during chromosome biorientation, it was speculated that spindle tension influenced the formation of these unexpected DNA linkages, during PLK1 inactivation.

We hypothesised that the structures were a result of centromeric DNA being aberrantly revealed due to the inhibition of PLK1 activity. PICH, RPA, and from this study also PLK1, have been identified as factors that associate to UFB structures during anaphase. This suggested that they function to aid in their resolution. We therefore tested whether additional UFB-binding proteins also localise to these DNA assemblies, during PLK1

inhibition. Both BLM helicase and its partner protein topoisomerase III alpha (TOP3A) were also shown to localise along these DNA assemblies **(Fig. 3.5c)**. Again, as with PICH, RPA localisation was largely exclusive of BLM or TOP3A **(Fig. 3.5c)**, implying that ssDNA was exposed along these DNA assemblies.

Despite these new DNA assemblies showing similarities to the previously described UFB structures that arise during anaphase, it is important to note that these cells are unable to enter anaphase, due to the chemical inhibition of PLK1 during BI2536 treatment. Therefore, it was decided to term these new structures as 'pre-anaphase DNA threads', in order to distinguish them from the previously reported anaphase UFBs.

3.2.4 Pre-anaphase DNA threads are not a result of protein mis-localisation to cellular cytoskeleton structures

The surprising formation of pre-anaphase DNA threads led to many questions regarding their validity. Thus, it was important to confirm that the appearance of pre-anaphase DNA threads during PLK1 inactivation, was not due to artefactual antibody staining, or as a result of protein mis-localisation. Therefore, firstly, to confirm that pre-anaphase DNA threads were not due to artefactual antibody staining, an RPE1 cell line that stably expressed a GFP-tagged PLK1 protein was examined. Under control conditions (DMSO treatment), the GFP-tagged PLK1 protein was shown to localise to known PLK1 subcellular recruitment sites during early mitosis (i.e. the centrosomes and kinetochores) **(Fig. 3.6a, b)**. In addition, the GFP-PLK1 protein was also shown to localise to the midzone and cleavage furrow, during anaphase and telophase, respectively **(Fig. 3.6b)**. This confirmed that the recruitment pattern of GFP-PLK1 resembles the known PLK1 subcellular recruitment pattern seen using only a PLK1 antibody. Importantly, following treatment with BI2536, GFP-PLK1 protein localisation displayed a similar pattern of recruitment, as in control cells (centrosome and kinetochore recruitment) **(Fig. 3.6b)**. It was also possible to detect GFP-PLK1 protein localisation along pre-anaphase DNA threads, following metaphase collapse **(Fig. 3.6b)**. Therefore, these

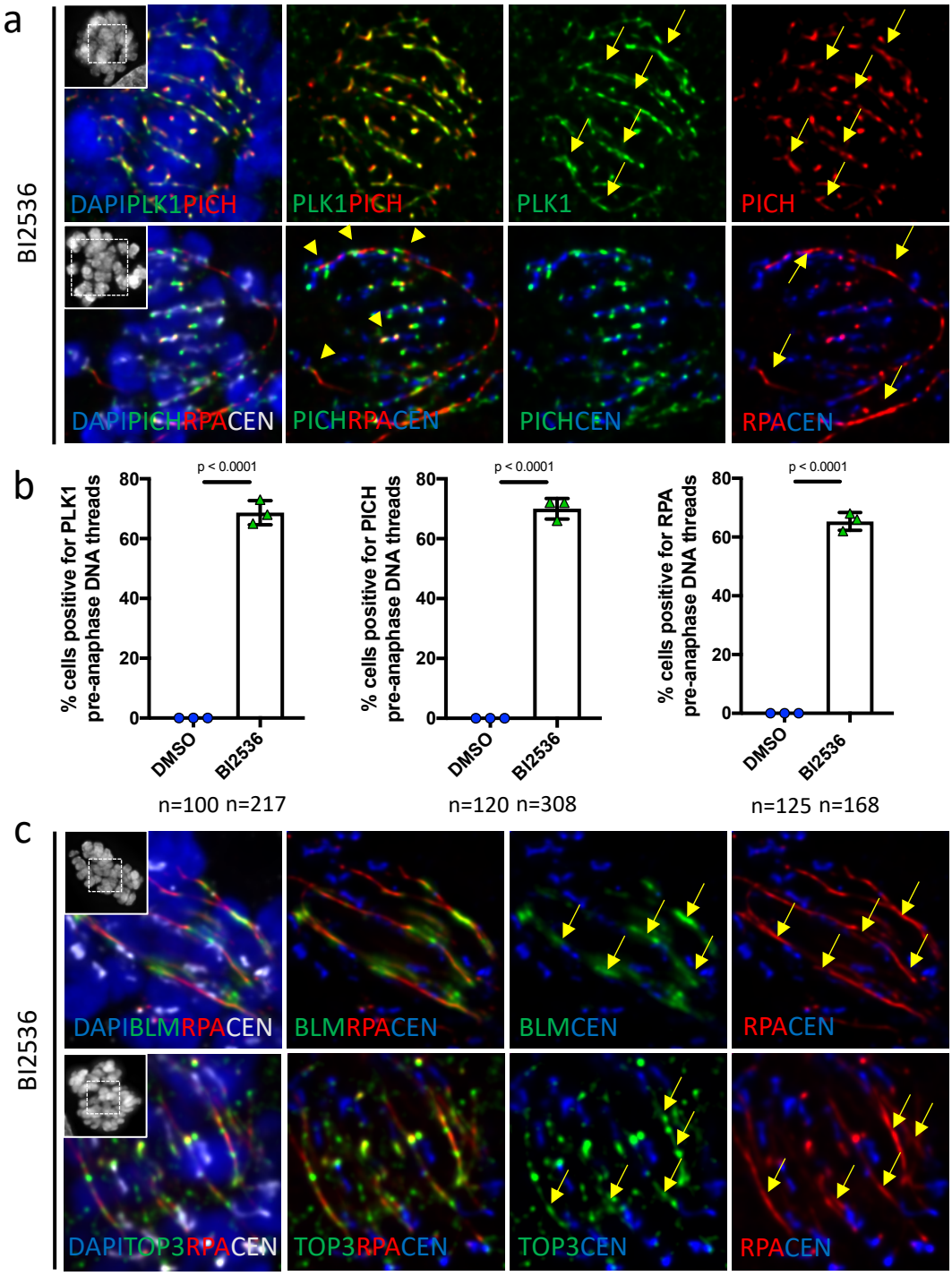

Figure 3.5. PLK1, PICH, RPA, BLM and TOP3A decorate centromere linkages during PLK1 inhibition.

a) Immunofluorescent images of BI2536 treated mitotic RPE1 cells (experimental outline of cell-synchronisation and immunofluorescent staining as of **(Fig. 3.4a)**). Pre-anaphase RPE1 cell (above) after BI2536 treatment, showing PLK1 (Green) and PICH (Red) associated inter-chromatin linkage (arrows). RPE1 cell (below) after BI2536 showing PICH (Green) and RPA (Red) (arrows) associated inter-chromatin linkage between centromeres (Blue) (arrowheads). **b)** Quantification of different protein associated centromeric inter-chromatin linkages (PLK1, PICH or RPA), termed 'Pre-anaphase DNA threads' in RPE1 cells (mean ±SD is shown from three independent experiments; student t-test was used for p-value calculation; n=number of cells analysed; scale bar 5μm). **c)** RPE1 cell (above) after BI2536 treatment, showing BLM (Green) and RPA (Red) associated inter-chromatin linkage (arrows). RPE1 cell (below) after BI2536, showing TOP3A (Green) and RPA (Red) associated inter-chromatin linkage (arrows).

findings ruled out that PLK1 recruitment to pre-anaphase DNA threads is due to artefactual immunofluorescent staining of PLK1 protein.

Next, it was important to rule out that pre-anaphase DNA threads were due to PLK1 protein mis-localisation, during its inactivation. Notably, PLK1 has also been reported to associate to cytoskeletal structures, including the microtubule based central spindle (Burkard et al. 2007). Thus, it was envisaged that pre-anaphase DNA threads may be caused by PLK1 protein mis-localisation to cytoskeletal structures, particularly when its catalytic activity was compromised. However, it was also possible to exclude this idea, as GFP-PLK1 protein localisation, in cells treated with BI2536, was distinctly different when compared to alpha-tubulin staining patterns **(Fig. 3.6b)**. Further still, the ssDNA binding protein, RPA, was also shown to display distinct localisation patterns when compared with alpha-tubulin. RPA was shown to localise distinctly on pre-anaphase DNA threads, which had arisen due to PLK1 inactivation **(Fig. 3.6c)**.

Therefore, based on these findings, it was concluded that PLK1 functions to suppress metaphase collapse. In its absence, cells suffer from the formation of centromeric pre-anaphase DNA threads, which are bound by various factors of the UFB-binding complex.

3.2.5 Pre-anaphase DNA thread formation is not cell type specific

As all of the previous experiments were performed using RPE1 hTERT cells, it was also of interest to confirm whether pre-anaphase DNA thread formation, during BI2536 treatment, was cell line specific. Thus, alternative cell lines were also examined for their ability to form pre-anaphase DNA threads, following synchronisation using thymidine and subsequent BI2536 treatment **(Fig. 3.7a)**. Both HCT116 (cancer) and 82-6 hTERT (non-cancerous) cells also displayed PICH and RPA positive pre-anaphase DNA threads during BI2536 treatment, although their frequencies did vary **(Fig. 3.7b, c)**. A possible explanation for this may be the different dependencies on the activity of PLK1, between different cell lines. However, there remains a lack of evidence to support this idea.

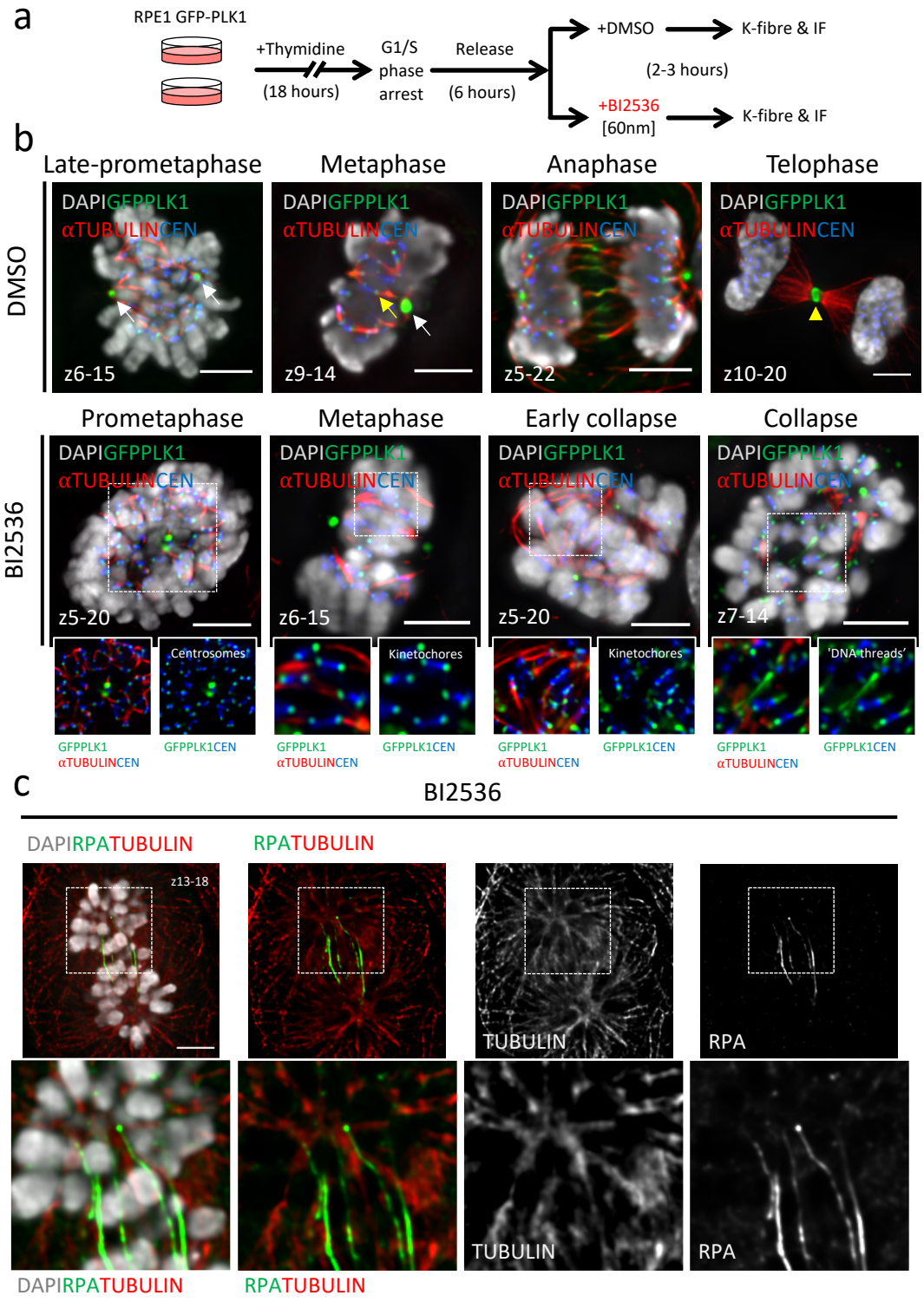

Figure 3.6. Centromere linkages are protein coated DNA structures.
a) Experimental outline for K-fibre immunofluorescent staining using either RPE1 GFP-PLK1; or wild-type RPE1 cells. **b)** Immunofluorescent images of mitotic RPE1 GFP-PLK1 cells, either untreated (above) or after BI2536 treatment (below). Antibody staining for DAPI (Grey), GFP-PLK1 (Green), α-tubulin (Red) and centromeres (Blue). Enlarged regions show distinct patterns of GFP-PLK1 localisation compared with α-tubulin after BI2536 treatment, and GFP-PLK1 pre-anaphase DNA threads (arrows) after metaphase collapse. **c)** Immunofluorescent images of RPE1 hTERT positive for RPA pre-anaphase DNA threads. Antibody staining DAPI (Grey), RPA (Green), α-tubulin (Red). Enlarged regions show distinct patterns of RPA localisation compared with α-tubulin after BI2536 treatment.

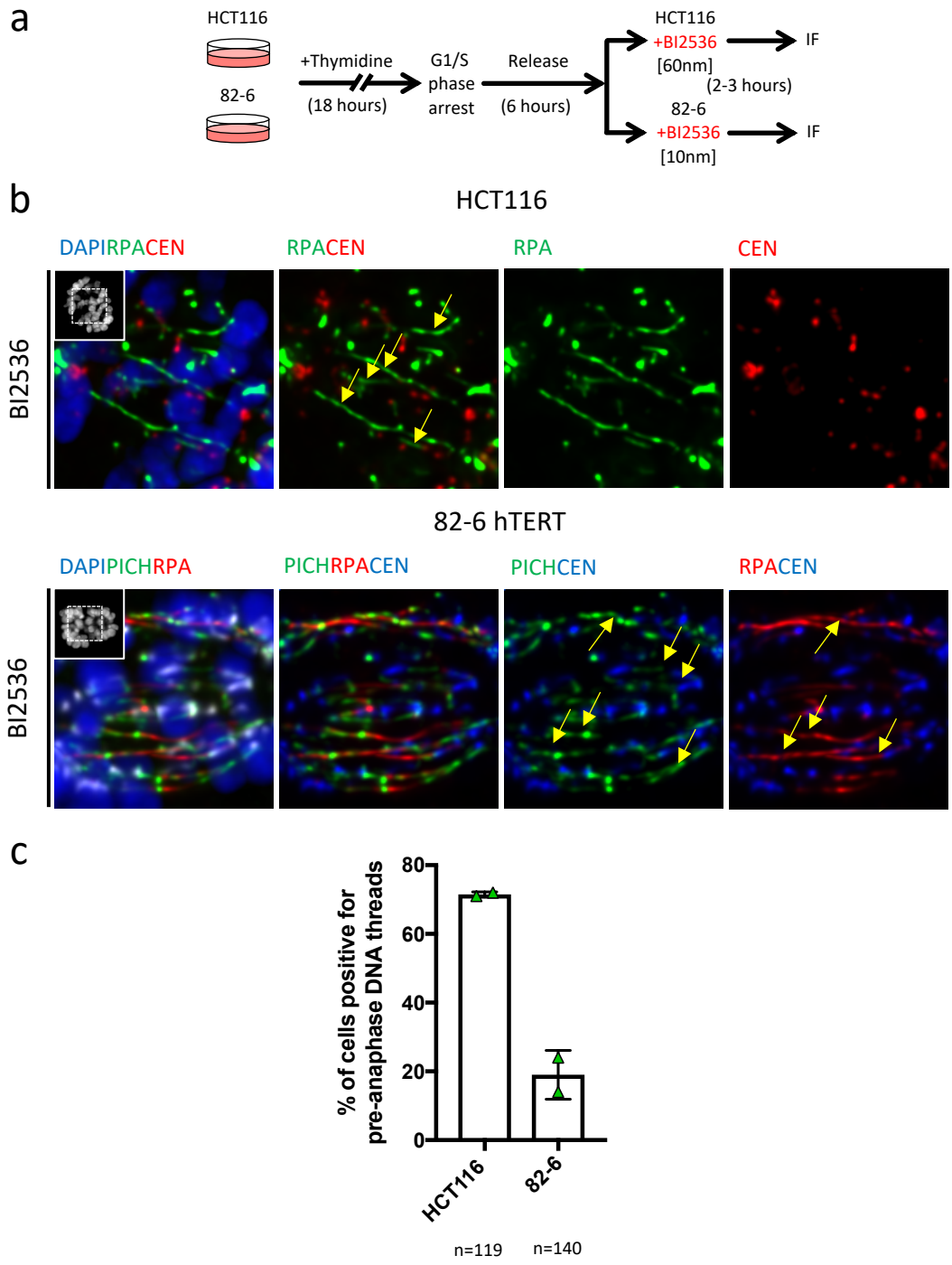

Figure 3.7. PLK1 suppresses pre-anaphase DNA threads in various different cell lines.
a) Experimental outline of cell-synchronisation and immunofluorescent staining using HCT116 (cancer cells) and 82-6 hTERT (non-cancerous cells). **b)** Immunofluorescent images of BI2536 treated HCT116 (above) & 82-6 cells (below). Antibody staining for PICH (Green), RPA (Red) and centromeres (Blue). Enlarged regions show pre-anaphase DNA thread formation (arrows). **c)** Quantification of pre-anaphase DNA threads after BI2536 treatment in HCT116 & 82-6 hTERT cells (mean ±SD is shown from two independent experiments; n=number of cells analysed; scale bar 5μm)

Despite this, it is tempting to speculate that certain cell lines may rely more on PLK1 kinase activity. Hence, when considering the current findings, it would be inviting to suggest that 82-6 hTERT cells are more dependent on PLK1 kinase activity, when compared with RPE1, or HCT116 cells. The 82-6 hTERT cells may have an intrinsic weakness in maintaining stable KT-MT attachments, in particular during PLK1 inactivation. Thus, an absence of PLK1 activity in 82-6 hTERT cells may prevent stable KT-MT attachment and thereby preclude the formation of pre-anaphase DNA threads. Furthermore, the hypothesis that cells may rely on different levels of PLK1 activity for mitotic function(s), could also explain earlier reports that suggested that PLK1 inactivation leads to errors in KT-MT establishment (Lénárt et al. 2007; Steegmaier et al. 2007). PLK1 inhibition using BI2536 in HeLa cells led to a "polo" mitotic state. This was attributed to the cells inability to form stable KT-MT attachments, due to PLK1 inactivation. Thus, it is possible that like 82-6 hTERT cells, HeLa cells also rely more on the activity of PLK1 to establish and maintain stable KT-MT attachments. During this study, RPE1 cells also displayed evidence of the typical "polo" collapse. Therefore, a balance of requirement for PLK1 may exist, which could explain a role of PLK1 activity in the long-term stability of KT-MT attachment during mitosis.

3.2.6 PLK1 inhibition causes both centromere and kinetochore disassembly

Immunofluorescent staining experiments showed that pre-anaphase DNA threads arise from centromeric regions. Consequently, further examination of the kinetochore/centromere complex was performed. It was speculated that pre-anaphase DNA threads may be centromeric DNA, which becomes disorganised and protrudes out from the centromere during PLK1 inactivation. If this prediction was correct, the centromere and/or kinetochore complex may display signs of disassembly during metaphase. Therefore, RPE1 hTERT cells were synchronised and treated with BI2536 and analysed for possible centromere/kinetochore disassembly **(Fig. 3.8a)**. Both the outer kinetochore component, NUF2, and the centromere specific histone variant, CENP-A, were used to examine the status of centromeres/kinetochores during PLK1 inactivation. As expected, both NUF2 and CENP-A localised as pairs on each centromere,

in both control cells (DMSO) and BI2536 treated mitotic cells, during the early stages of mitosis (prometaphase-metaphase) **(Fig. 3.8b, c)**. However, following the examination of BI2536 treated cells after metaphase (collapse), both CENP-A and NUF2 began to display an abnormal distribution at the centromeres and kinetochores, respectively **(Fig. 3.8b, c)**. This abnormal distribution at the centromere, was generally displayed with the loss of one side of the sister kinetochore signal, either NUF2 or CENP-A. These observations could imply that the centromeres, and/or kinetochores, were suffering from disassembly during PLK1 inactivation. Moreover, the loss of NUF2 or CENP-A signal generally coincided with a strong focus of either PICH or RPA, which was predicted to be the start of pre-anaphase DNA thread formation **(Fig. 3.8b, c)**.

Additionally, although very rare, the outer kinetochore component NUF2 was shown to remain attached to a short PICH thread that also remained attached to the core centromere **(Fig. 3.8d)**. It is predicted that this pattern of protein localisation may represent the early signs of aberrant centromere protrusion, whilst also suggesting that MT-tension may directly promote this centromeric aberration. Therefore, cells absent of PLK1 may be unable to counteract microtubule spindle forces and promptly result in centromere/kinetochore disassembly, which eventually displays as pre-anaphase DNA threads.

It was also speculated that centromeric DNA damage may occur during metaphase collapse during BI2536 treatment. Therefore, to test this, RPE1 cells were again enriched in mitosis, before being treated with BI2536 **(Fig. 3.9a)**. The DNA damage response marker, γH2AX (Rogakou et al. 1998), was used to determine possible centromeric DNA damage, following PLK1 inactivation. There was only a minimal detection of γH2AX at the centromere of cells examined during prometaphase (~26%). However, as the cells progressed into metaphase, when kinetochores became subjected to spindle pulling forces, nearly all cells showed γH2AX foci forming at their centromeres (~81%) **(Fig. 3.9b, c)**. All the collapsed cells that were positive for pre-anaphase DNA threads, displayed with γH2AX foci at their centromeres.

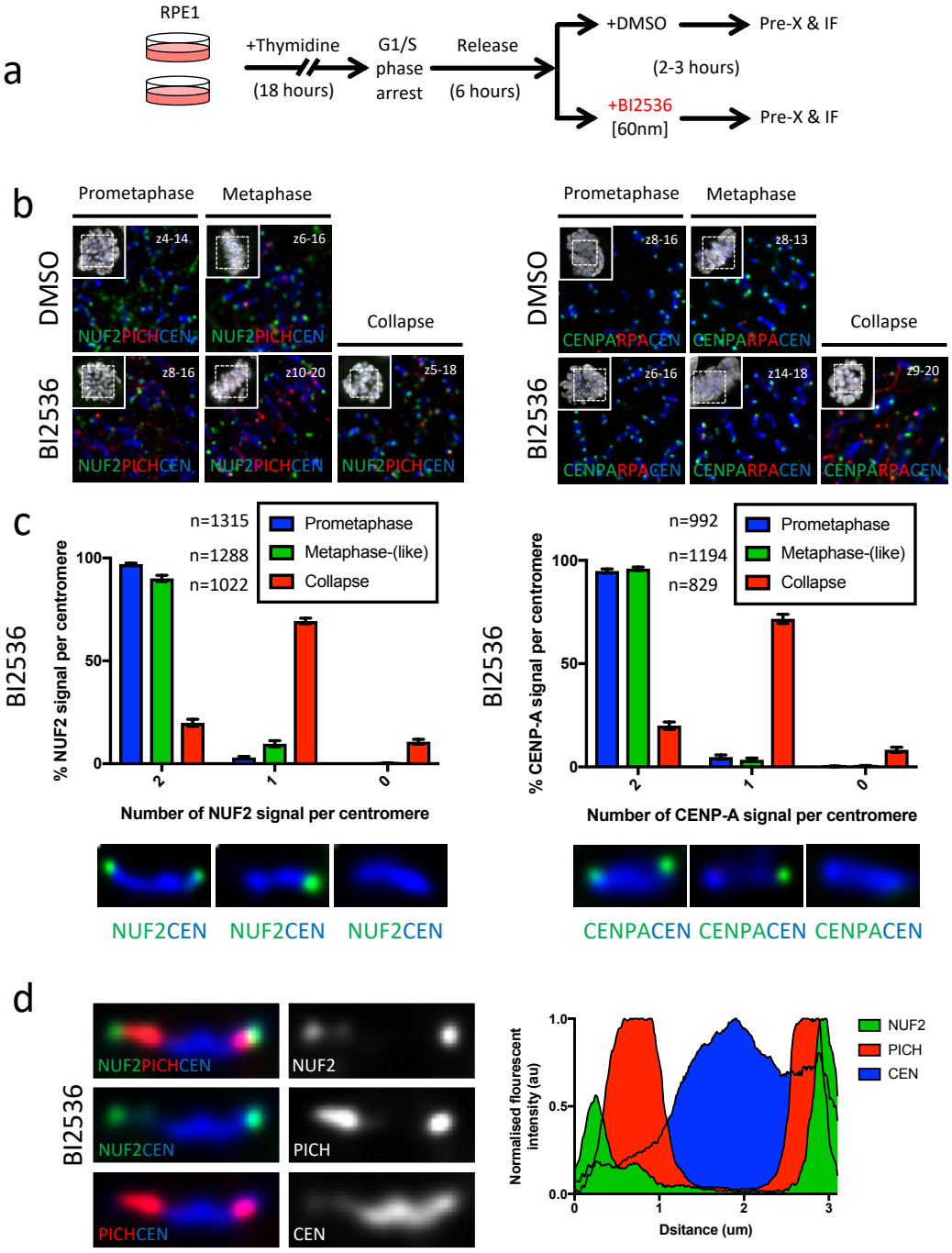

Figure 3.8. Kinetochores disassemble after metaphase following PLK1 inhibition.
a) Experimental outline of cell-synchronisation and immunofluorescent staining using RPE1 cells. **b)** Immunofluorescent images of both untreated (DMSO) and BI2536 treated mitotic cells. (Left) Antibody staining for NUF2 (Green), PICH (Red) and centromeres (Blue); (Right) Antibody staining for CENPA (Green), RPA (Red) and centromeres (Blue); DAPI (Grey) was used to stain chromosomes. Enlarged regions demonstrate NUF2 or CENPA recruitment to kinetochore complexes. **c)** Quantification of CENPA or NUF2 detection at centromeres after BI2536 treatment. Images below demonstrate either 2, 1 or 0 kinetochore signal detection (mean ±SD is shown from three independent experiments; n=number of kinetochore signals analysed; Ankana Tiwari completed an experimental replicate of CENP-A analysis) **d)** Enlarged cropped image of kinetochore complex NUF2 (Green) being pulled out from the centromere (Blue), whilst remaining attached by PICH (Red). A plot-profile of the fluorescent intensity is also shown.

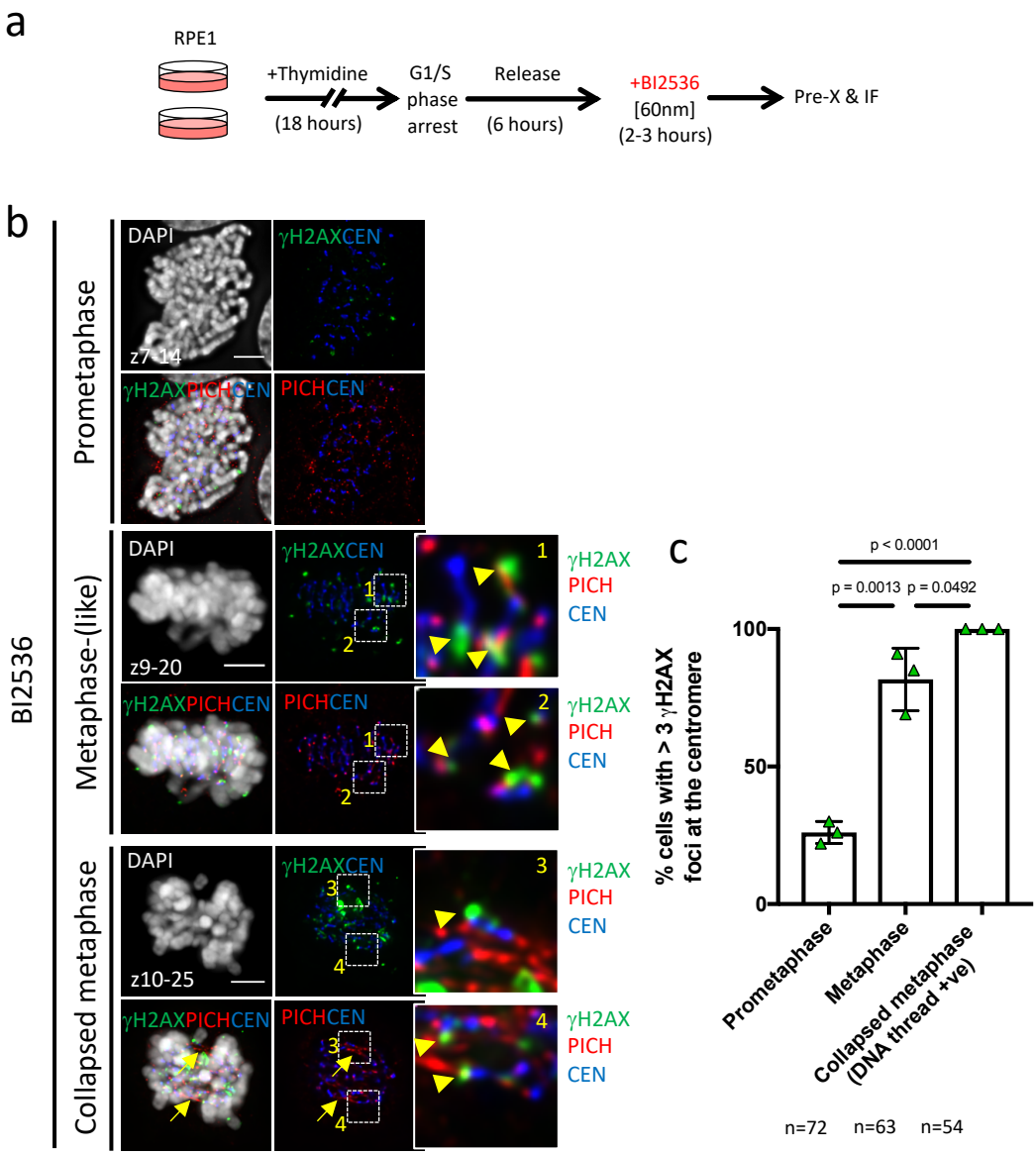

Figure 3.9. PLK1 inhibition promotes centromere DNA damage during mitosis.
a) Experimental outline of cell-synchronisation and immunofluorescent staining using RPE1 cells. **b)** Immunofluorescent images of BI2536 treated mitotic RPE1 cells. Antibody staining for γH2AX (Green), PICH (Red) and centromeres (Blue). Enlarged regions highlight γH2AX (Green) signal (arrowheads) at centromeres (Blue). Pre-anaphase DNA threads (arrows) are also shown after metaphase collapse. **c)** Quantification of different mitotic stages in RPE1 cells with >3γH2AX foci at the centromere, after BI2536 treatment (mean ±SD is shown from three independent experiments; student t-test was used for p-value calculation; n=number of cells analysed; scale bar 5μm).

Thus, these data suggest that in the absence of PLK1 kinase activity, kinetochores/centromeres suffer from disassembly, which can also trigger a DNA damage response, as observed by the detection of γH2AX foci at the centromere. Therefore, it is predicted that PLK1 functions to suppress a centromere deformation pathway and enables cells to maintain chromosome biorientation during metaphase.

3.2.7 A mitotic function of PLK1 suppresses centromere deformation

Although PLK1 is largely regarded as a mitotic regulator, it has also been reported to be involved in various processes throughout earlier stages of the cell cycle. For example, PLK1 has also been identified as a promoting factor in order to initiate DNA replication at dormant origins, in particular during conditions of replicative stress (Song, Liu, Davis, et al. 2012). Therefore, it was speculated that pre-anaphase DNA thread formation, after PLK1 inactivation, maybe due to a potential interference of an S-phase function(s) of PLK1. Thus, PLK1 inhibition may be affecting DNA replication, in particular at centromeres, and therefore in its absence, centromeric pre-anaphase DNA threads may form. Centromeres are difficult regions of the genome to replicate (Barra and Fachinetti 2018). Thus, it is possible that PLK1 function(s) could be required for their efficient duplication. Another consideration was that throughout previous experimental set-ups, cell-synchronisation by thymidine was used and thymidine is known to induce low levels of replicative stress (Darzynkiewicz et al. 2011). Therefore, thymidine addition could conceivably influence pre-anaphase DNA thread formation during PLK1 inactivation.

Therefore, to rule out that thymidine was responsible for pre-anaphase DNA thread formation during PLK1 inhibition, a control experiment was performed. Asynchronously growing RPE1 hTERT cells were treated with BI2536 for just 1 hour, before fixation and immunofluorescent analysis **(Fig. 3.10a)**. In the absence of thymidine, around 14% (n=115) of mitotic pre-anaphase cells were positive for centromeric PICH/RPA pre-anaphase DNA threads **(Fig. 3.10b)**. This implies that thymidine is not a determining

influence on the formation of pre-anaphase DNA threads during PLK1 inactivation. However, the frequency of pre-anaphase DNA thread formation was much lower when compared to synchronised cells **(ranges from 50-75% in RPE1 hTERT cells; see previous Fig. 3.5 for comparison)**. This could be due to the short treatment of BI2536, as late mitotic cells may be able to bypass PLK1 inhibition and progress into anaphase, thereby reducing the chance of observing pre-anaphase DNA thread formation in that population of cells. Although, it cannot be ruled out that thymidine may also exacerbate pre-anaphase DNA thread formation, during PLK1 inactivation.

Next, in order to determine whether a disruption to PLK1 activity during S-phase was a contributing factor to the formation of pre-anaphase DNA threads, an experiment was designed to analyse only mitotic cells that had completed S-phase, prior to the addition of BI2536. In order to achieve this, RPE1 hTERT cells were pre-synchronised as before, and released into fresh medium. Based on earlier cell-cycle analysis profiles after thymidine release, it was predicted that at 6 hours post G1/S release, the majority of cells would be in either late S-phase, or G2/M stage **(for cell cycle profiles see previous Fig. 3.1)**. Therefore, at this time, both BI2536 and the thymidine analogue, EdU, were added to cell cultures and incubated for a further 2-3 hours. Cells were then fixed and subjected to immunofluorescent staining, combined with Click-iT EdU detection **(Fig. 3.10c)**. EdU incorporates into the nascently replicating DNA. Therefore, it was used as a determinant for cells that remained in S-phase, during BI2536 addition. Analysis showed that 69% (±4%) of cells (n=385) remained positive for pre-anaphase DNA threads, but absent for EdU detection **(Fig. 3.10d)**. Therefore, this result implies that PLK1 inactivation during S phase, is not the principal cause of pre-anaphase DNA thread formation during metaphase collapse. Instead, PLK1 function(s) is required during either G2 or M, in order to suppress pre-anaphase DNA thread formation.

Further experiments were able to dissect a more precise mitotic stage in which PLK1 function is required to suppress metaphase collapse and pre-anaphase DNA thread formation. By arresting cells at metaphase, using the APC/C inhibitor ProTAME, and adding BI2536 for just 30 mins before fixing the cells **(Fig. 3.11a)**, it was possible to

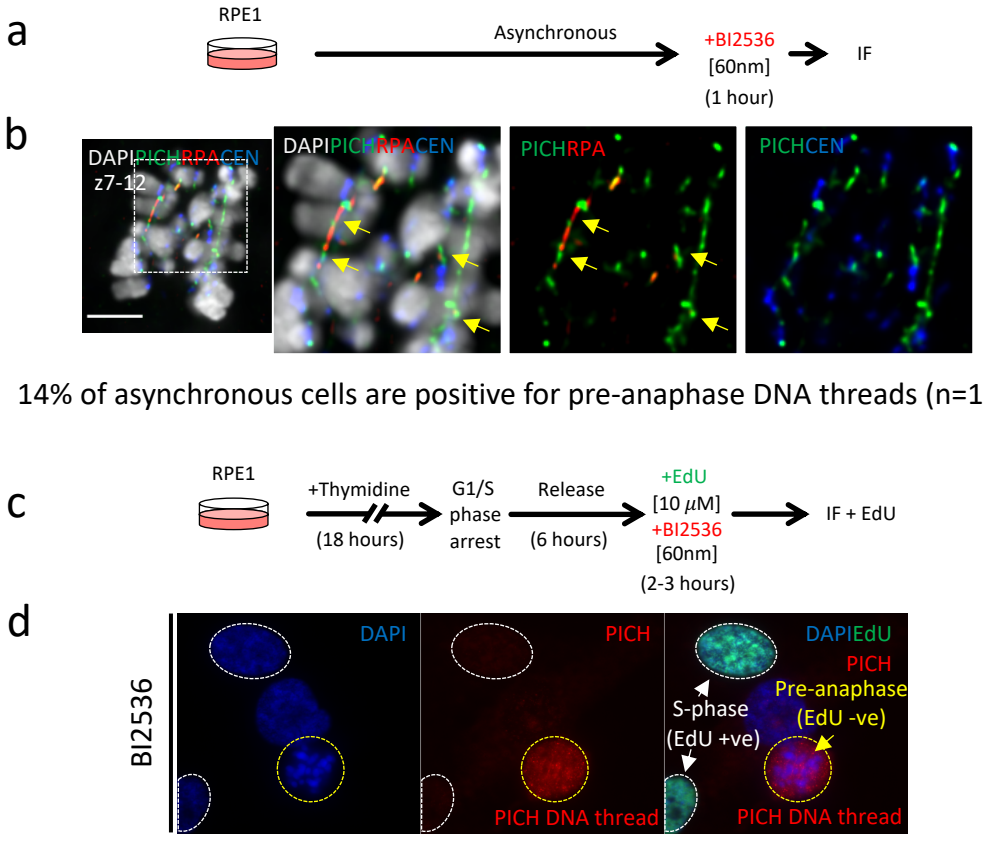

Figure 3.10. Pre-anaphase DNA threads are not due to interference of S-phase functions of PLK1.

a) Experimental outline and immunofluorescent staining using asynchronous RPE1 cells. **b)** Immunofluorescent images of a representative pre-anaphase RPE1 cells containing pre-anaphase DNA treads after treatment with BI2536 for 1hr. Antibody staining for PICH (Green), RPA (Red) and centromeres (Blue). Pre-anaphase DNA threads are shown (arrows) (n=number of cells analysed; scale bar 5μm). **c)** Experimental outline of cell-synchronisation and immunofluorescent staining combined with EdU Click-iT detection, using RPE1 cells. **d)** Representative example of EdU positive (Green) and negative mitotic cells. EdU negative cells were analysed for PICH (Red) pre-anaphase DNA threads (yellow arrow) after BI2536. 69±4% scored positive for PICH pre-anaphase DNA threads (mean ±SD is shown from three independent experiments; n=number of cells analysed).

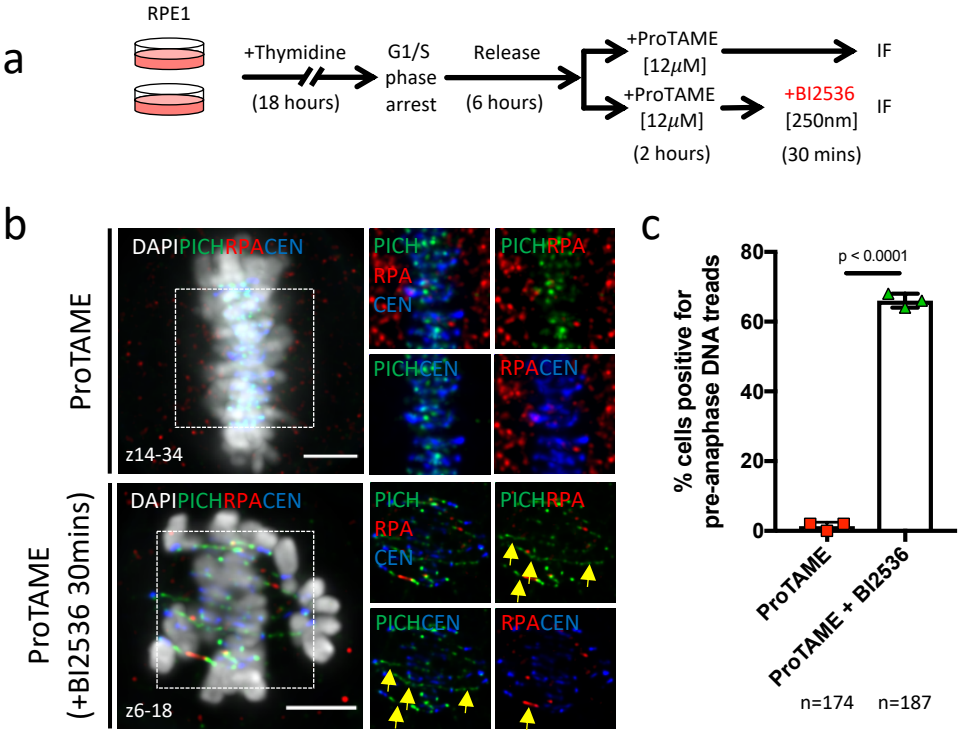

Figure 3.11. PLK1 supresses pre-anaphase DNA thread formation in established metaphase cells.

a) Experimental outline of cell-synchronisation and immunofluorescent staining using RPE1 cells. **b)** Immunofluorescent images of metaphase arrested RPE1 cells using ProTAME, plus and minus BI2536. Antibody staining for PICH (Green), RPA (Red) and centromeres. Pre-anaphase DNA threads are shown after BI2536 treatment (arrows). **c)** Quantification of pre-anaphase DNA thread formation after ProTAME alone, or after addition of BI2536 for 30 minutes (mean ±SD is shown from three independent experiments; student t-test was used for p-value calculation; n=number of cells analysed; scale bar 5μm).

address the question of whether PLK1 inactivation was sufficient to promote pre-anaphase DNA thread formation in fully established metaphase cells. The resulting immunofluorescent analysis showed that BI2536 addition for just 30 minutes in established metaphase cells, is sufficient to drive cells into a metaphase collapse and promote the formation of pre-anaphase DNA threads, positive for PICH/RPA **(Fig. 3.11b, c)**.

Overall, these data strongly suggest that pre-anaphase DNA thread formation is not due to an effect of PLK1 inactivation on PLK1s possible role(s) during S-phase. Instead, it suggests that PLK1 activity is required during mitosis for metaphase maintenance and stability.

3.2.8 Bipolar spindle attachment promotes centromere deformation during PLK1 inhibition

Experiments were then designed to further dissect the mechanism(s) behind pre-anaphase DNA thread formation. A consistent feature of previous findings is that MT-KT attachment and possibly tension remain, despite the inhibition of PLK1 kinase activity. In particular, this was highlighted during experiments that observed both centromere and kinetochore disassembly, where the pulling out of one side of the kinetochore complex was seen, whilst also remaining attached to the core centromere **(see Fig. 3.8d)**. Consequently, it was predicted that spindle pulling forces may be the basis for pre-anaphase DNA thread formation during PLK1 inactivation.

To investigate this further, RPE1 cells were synchronised as before and treated with BI2536, or a combined treatment of BI2536 and the microtubule spindle poison nocodazole **(Fig. 3.12a)**. Immunofluorescent analysis demonstrated that spindle pulling forces are necessary for pre-anaphase DNA thread formation as pre-anaphase DNA thread formation was completely absent in cells co-treated with BI2536 and nocodazole **(Fig. 3.12b-d)**.

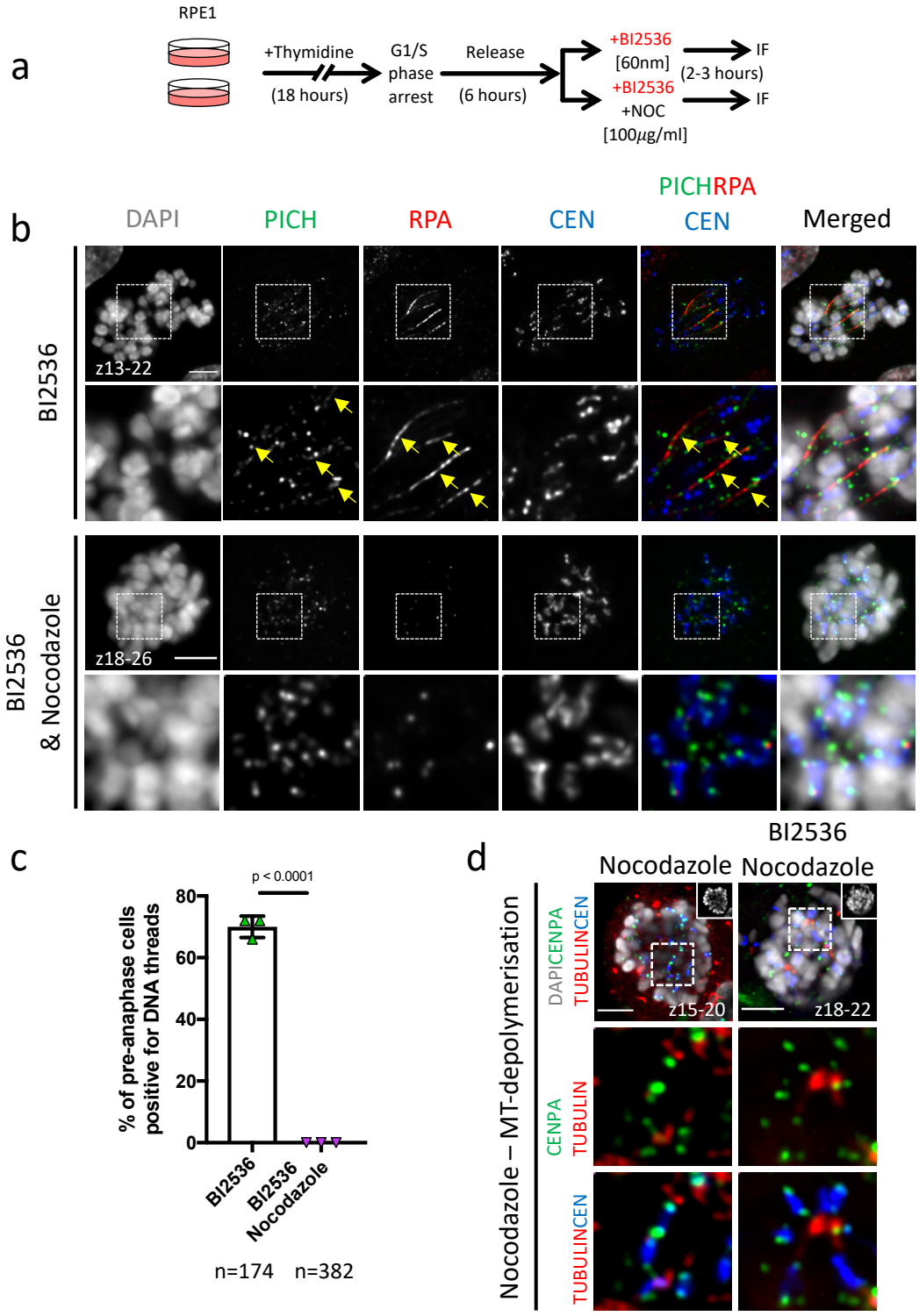

Figure 3.12. Microtubule forces promote pre-anaphase DNA thread formation during PLK1 inhibition.

a) Experimental outline of cell-synchronisation and immunofluorescent staining using RPE1 cells. **b)** Immunofluorescent images of mitotic RPE1 cells after either BI2536; or BI2536 and Nocodazole treatment. Enlarged regions demonstrate the presence or absence of pre-anaphase DNA thread formation (arrows) following each indicated inhibitor treatment. **c)** Quantification of DNA threads observed in pre-anaphase RPE1 cells after indicated inhibitor treatment. **d)** K-fibre staining displays an absence of tubulin after nocodazole addition (mean ±SD is shown from three independent experiments; student t-test was used for p-value calculation; n=number of cells analysed; scale bar 5μm).

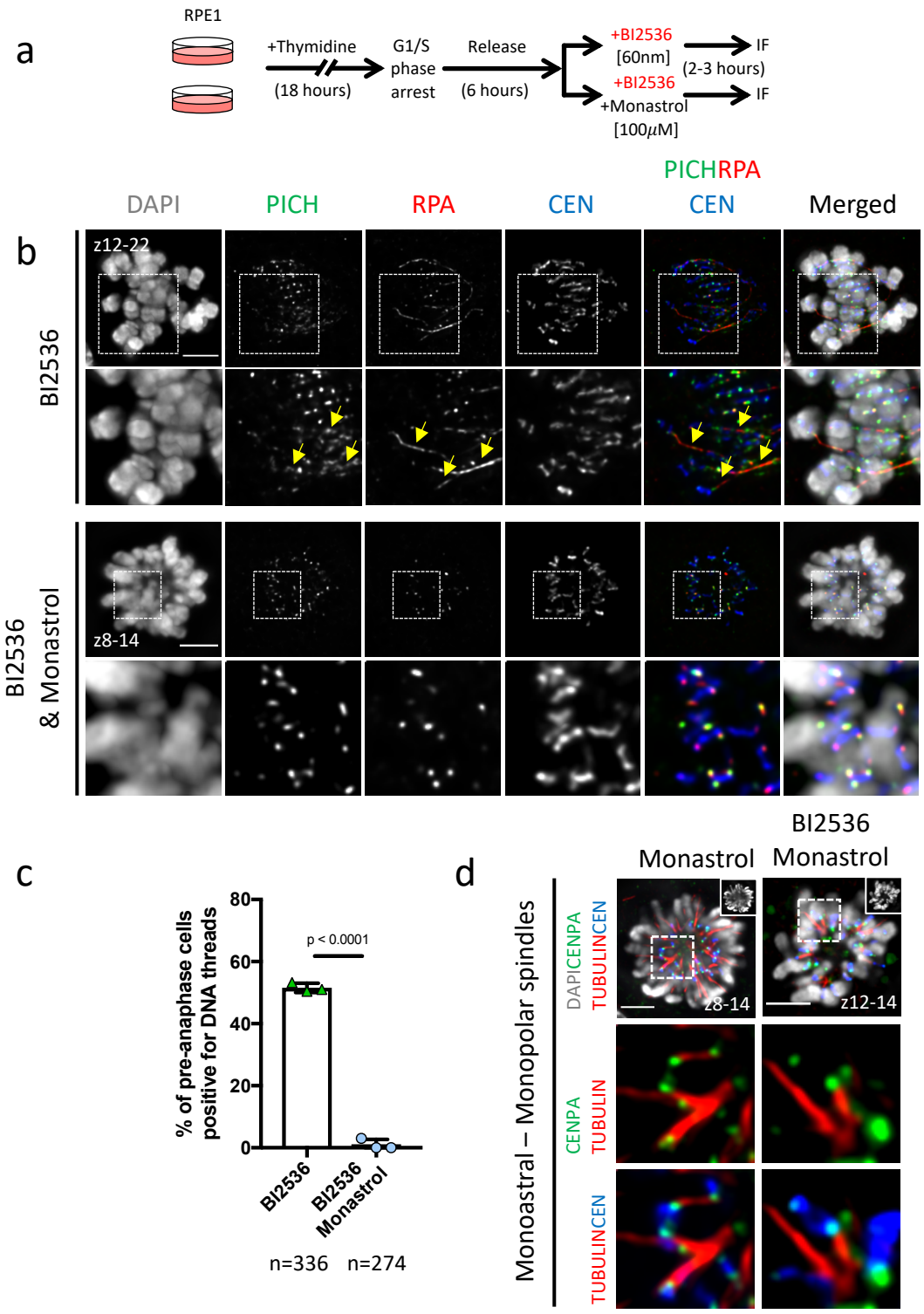

Figure 3.13. Bipolar spindle-attachment is required for pre-anaphase DNA thread formation.

a) Experimental outline of cell-synchronisation and immunofluorescent staining using RPE1 cells. **b)** Immunofluorescent images of mitotic RPE1 cells after either BI2536; or BI2536 and Monastrol treatment. Enlarged regions demonstrate the presence or absence of pre-anaphase DNA thread formation (arrows) following each indicated inhibitor treatment. **c)** Quantification of DNA threads observed in pre-anaphase RPE1 cells after indicated inhibitor treatment. **d)** K-fibre staining displays monopolar attachment of centromeres after monastrol addition (mean ±SD is shown from three independent experiments; student t-test was used for p-value calculation; n=number of cells analysed; scale bar 5μm).

This experiment was unable to confirm that microtubule attachment is sufficient to promote pre-anaphase DNA thread formation, during BI2536 treatment. Therefore, to investigate whether spindle-attachment alone was sufficient for pre-anaphase DNA thread formation following BI2536 treatment, cells were pre-synchronised as before and treated with BI2536, or BI2536 and monastrol **(Fig. 3.13a)**. Monastrol acts as a kinesin-Eg5 inhibitor, which prevents the ATP turnover of the spindle motor protein kinesin-Eg5. This leads to monopolar spindle attachment at the centromere (Mayer et al. 1999). Immunofluorescent analysis of BI2536 and monastrol treated cells showed the complete absence of pre-anaphase DNA thread formation, in contrast to control cells (BI2536), which continued to display pre-anaphase DNA thread formation **(Fig. 3.13b-d)**. Thus, it can be concluded that pre-anaphase DNA thread formation requires both bipolar spindle attachment and MT-tension, in concert with PLK1 inactivation.

Interestingly, despite the abolishment of pre-anaphase DNA threads after BI2536 in monastrol co-treated cells, strong RPA foci were detected at the centromeres **(Fig. 3.13b)**. This observation was not apparent during the analysis of BI2536 and nocodazole co-treated cells, suggesting that MT-attachment alone may be sufficient to initiate centromere deformation. Further investigation of this idea will be examined in later chapters.

3.3 Discussion

Experiments discussed in this chapter confirm that PLK1 activity provides an essential role(s) for the maintenance of mitotic progression. Previous reports have suggested that PLK1 activity is crucial for both the establishment and maintenance of chromosome biorientation, during metaphase (Lénárt et al. 2007; Steegmaier et al. 2007). However, unexpectedly, this study revealed that in RPE1 hTERT cells, PLK1 activity may not be absolutely required for the initial establishment of chromosome biorientation, as the majority of cells absent of PLK1 activity were able to achieve this (~80%). Despite this, RPE1 hTERT cells did eventually display evidence of metaphase collapse, during PLK1 inactivation. However, the metaphase collapse pattern largely exhibited the newly reported "figure-of-8" chromosome morphology, rather than the previously reported "polo" pattern (Lénárt et al. 2007). The "polo" chromosome morphology is attributed to errors in KT-MT attachment when PLK1 activity was inhibited. This implies that PLK1 was required for metaphase establishment. Fundamentally in agreement to previous reports, this study suggests that PLK1 may be necessary for the long-term maintenance of chromosome biorientation, rather than biorientation establishment. However, a precise mechanism remains unclear.

More remarkably, this study revealed that PLK1 activity is required for the suppression of a previously unreported centromere deformation phenotype. An absence of PLK1 activity during mitosis leads to cells exhibiting a DNA linkage structure, which was shown to originate from the centromere of cohesed chromatin. These aberrant DNA structures have been referred to as 'pre-anaphase DNA threads', which are seen during metaphase collapse. Pre-anaphase DNA threads become apparent via the direct recruitment of the PLK1 protein itself. PLK1 has been shown to decorate along these centromeric DNA structures, alongside various other factors of the UFB-binding complex (including PICH, BLM, TOP3A, RPA), indicating that the DNA make-up of pre-anaphase DNA threads may be similar to that of anaphase UFBs.

This study has also described how the centromere/kinetochore may suffer from disassembly, which occurs concomitantly with the formation of pre-anaphase DNA thread formation. Thus, following a metaphase collapse during PLK1 inactivation, both the centromere component CENP-A and the outer kinetochore protein NUF2 become largely undetectable. In particular, one side of each sister kinetochore displays signs of CENP-A, or NUF2 absence. Therefore, it is proposed that the centromere/kinetochore disassembly, during the inactivation of PLK1, could be the underlying cause of the formation of pre-anaphase DNA threads.

Pre-anaphase DNA thread formation was shown to be dependent on spindle tension, which supports the idea that spindle pulling forces influence any potential centromere/kinetochore disassembly, when PLK1 activity is compromised.

Overall, these unexpected observations have led to some key fundamental questions. First, how does PLK1 activity suppress such a drastic centromere deformation pathway? Secondly, why do cells not encounter such spindle-tension dependent centromere impairment when PLK1 remains active? In an attempt to answer these questions, previously reported functions of PLK1 may help to elucidate why pre-anaphase DNA threads form when PLK1 activity is compromised and are discussed below.

PLK1 has been implicated in various processes involved in mitotic progression, including bipolar spindle formation, chromosome congression and chromosome segregation (Archambault and Glover 2009; Zitouni et al. 2014). In its absence or catalytic inactivation, unwanted cellular outcomes arise, such as the previously reported mitotic arrest phenotype and KT-MT mis-attachment issues (Lénárt et al. 2007; Steegmaier et al. 2007). It is now tempting to include the novel centromere deformation pathway, which has been shown to promote the formation of pre-anaphase DNA threads.

Apart from PLK1 itself, pre-anaphase DNA thread formation leads to the recruitment of various UFB-binding proteins, notably PICH. Based on the current knowledge

surrounding the function of PICH, it is tempting to speculate that PICH recruitment to pre-anaphase DNA threads, occurs because the DNA make-up is similar to anaphase UFBs. However, it is worth noting that the precise DNA make-up of both anaphase UFBs, and the newly reported pre-anaphase DNA threads, remains unconfirmed. A plausible explanation for PICH recruitment to pre-anaphase DNA threads and/or anaphase UFBs, is the preference of PICH to recruit to DNA that is subject to tension (Biebricher et al. 2013). During PLK1 inactivation, pre-anaphase DNA thread formation was shown to be dependent on MT-spindle pulling forces. Therefore, MT-spindle pulling forces may lead to an increase in DNA tension at the centromere and also explain the recruitment of PICH to centromeres during unperturbed conditions. However, a precise function for PICH at the centromere remains unconfirmed. Nevertheless, the loss of PLK1 activity, alongside building MT-spindle tension during chromosome biorientation, promotes the formation of centromeric pre-anaphase DNA threads, which PICH is subsequently able to recruit to.

The question remains as to why an interference of PLK1 activity promotes such centromere-specific deformation in the first place. One possible suggestion is that centromere compaction, or condensation, is affected during the absence of PLK1 activity. It is generally accepted that mitotic chromosome assembly and organisation is primarily accomplished by the action of condensin proteins (T. Hirano 2005). Additionally, phosphorylation of condensin complexes is reported to promote their activity (Bazile et al. 2010). In particular, PLK1 has been reported to influence mitotic chromosome compaction, via phosphorylation of the non-SMC subunit of condensin II, CAP-H2 (Kagami et al. 2017). Therefore, correct centromere compaction may become affected during PLK1 inactivation, culminating in the formation of pre-anaphase DNA threads, due to a lack of condensation activity. Also, centromeric chromatin is known to consist of tandem arrays of repeating α-satellite DNA, which is further organised to form extensive higher order repeat (HOR) structures (McKinley and Cheeseman 2016). Hence, it is also conceivable that the centromere region requires extensive compaction for its correct assembly. Therefore, PLK1 inactivation may compromise correct chromosome

compaction at the centromere, which may be required in order to withstand MT-spindle tension, in particular, during chromosome biorientation.

In support to this hypothesis, depletion of condensin has been shown to result in similar outcomes to the phenotypes during PLK1 inactivation. Previous condensin depletion experiments have been shown to effect overall mitotic chromosome assembly (Ono et al. 2003). More specifically, centromere structural alterations have been described. In particular, following the depletion of condensin in HeLa cells (Samoshkin et al. 2009). This later study showed that both the core centromere and outer kinetochore are susceptible to stretching, following the depletion of condensin (SMC2). Most importantly, this centromere stretching was also dependent on spindle microtubule pulling forces (Samoshkin et al. 2009). These findings could therefore provide support to the idea that continual compaction of centromeric DNA, by the action of condensin complexes, may be required to counteract the forces applied by microtubule spindle pulling at the centromere. However, it is also worth noting that the centromere stretching phenotype reported after condensin depletion, is relatively mild compared to the formation of pre-anaphase DNA threads during PLK1 inactivation. Therefore, although condensin may provide essential function(s) for the correct assembly of mitotic chromosomes and centromere architecture, it may not be the single factor that is required to ensure the suppression of pre-anaphase DNA threads, following PLK1 inactivation.

Since PLK1 inactivation and pre-anaphase DNA thread formation maybe caused by multifactorial processes, another key observation worth discussion is the apparent disassembly of the centromere and in particular CENP-A.

CENP-A is key to specifying centromere identity, and therefore also kinetochore establishment. Its deposition is cell cycle dependent, occurring only after mitosis and primarily during the G1 phase of the cell-cycle (Jansen et al. 2007). Interestingly, a report has suggested a role for PLK1 during new CENP-A deposition. This study describes how

PLK1 activity is crucial for the localisation of the MIS18 complex, and the HJURP chaperone to centromeres, both of which aid in ensuring that new CENP-A deposition occurs during G1 (McKinley and Cheeseman 2014). However, despite this PLK1 dependent role for CENP-A deposition, it is unlikely that this represents a determining factor to explain the centromere disassembly observed in this study, as it was shown that even a transient inactivation of PLK1 (30 minutes), in fully established mitotic chromosomes, is sufficient to trigger pre-anaphase DNA thread formation. Thus, centromere disassembly cannot be explained by an effect on the regulation of CENP-A deposition by PLK1. Although, at this stage, it cannot be ruled out that PLK1 may have an influence on the maintenance of CENP-A during mitosis. It could be proposed that during an absence of PLK1 activity, centromeres become fragile, possibly due to a break down in the maintenance of CENP-A stability, or through a lack of chromosome compaction. Either of which may lead to centromeres being unable to withstand MT-spindle pulling tension, and therefore leading to centromere deformation.

This study has also shown that centromeric regions exhibit a DNA damage response, when PLK1 activity is compromised as γH2AX foci were detected at centromeric regions after BI2536 treatment. This occurs prior to and post pre-anaphase DNA thread formation. This suggests that centromeres exhibit some form of fragility during PLK1 inactivation. However, it remains uncertain what causes this apparent weakness.

Therefore, in order to gain further insight into the effects of centromere deformation during the inactivation of PLK1, cytogenetic analysis of isolated chromosomes was performed. This led to new revelations to further explain the fate of centromeres during PLK1 inactivation, which will subsequently be discussed in the next chapter.

Chapter 4: PLK1 suppresses whole chromosome arm breakage

4.1 Introduction

The formation of pre-anaphase centromeric DNA threads and various other signs led to the suggestion that centromeres were being subjected to extensive DNA strain, following the inactivation of PLK1. In particular, the detection of γH2AX foci at centromeres, following PLK1 inhibition, strongly implied that a DNA damage response was elicited. The H2A histone variant, H2AX, becomes phosphorylated at serine-139 in order to generate γH2AX, which is regarded as a cellular indicator for the presence of DNA double-stranded breaks (DSBs) (Rogakou et al. 1998). Phosphorylation of H2AX is achieved by the activation of the phosphatidylinositol 3-kinase related kinases (PIKKs), including ATM (ataxia-telangiectasia mutated); ATR (ataxia-telangiectasia and Rad3 related); or DNA-PKcs (DNA-dependent protein kinase catalytic subunit). The resulting phosphorylation event that generates γH2AX leads to signal amplification at the site of damage, and this acts as a docking site for the accumulation and initiation of key DNA damage response proteins (Ciccia and Elledge 2010). Therefore, γH2AX detection is widely linked to DNA damage and its appearance can be associated with the generation of DNA DSBs.

During this study, following the inactivation of PLK1, cells were shown to display an increasing formation of γH2AX foci at centromeric regions, when cells progressed through mitosis. This increase in the formation of γH2AX foci was thought to be caused by PLK1 inactivation, combined with the building microtubule spindle forces at centromeres, during chromosome biorientation. In support of this prediction, by the time cells had progressed to metaphase, around 75% of centromeres displayed γH2AX foci. The detection of γH2AX foci at the centromere could imply that the centromeric DNA was subjected to damage, possibly in the form of DNA breakage. This DNA damage may promote centromere fragility and lead to centromere breakage. However, to directly show this by using conventional immunofluorescent imaging was an impossible

challenge. In general, fixed cells for immunofluorescent analysis maintain their mitotic chromosome arrangement. Consequently, this results in a large mass of mitotic chromosomes sitting directly on top of each other, making it almost impossible to identify any specific chromosomal breakage patterns. To overcome this technicality, cytogenetic analysis was performed. This method allows for the examination of individual chromosomes, to determine whether PLK1 inactivation was promoting centromeric breakage. Cytogenetic analysis of chromosomes is widely used in both clinical and basic research science, and it provides an intricate level of detail of various potential chromosome abnormalities. This can include karyotypic changes, chromosomal breakage patterns and even chromosomal translocations. Cytogenetic analysis is also commonly paired with the technique of fluorescent *in situ* hybridisation (FISH). This method can provide visual identification of site-specific regions within the genome (such as centromeres), through the hybridization of specific DNA probes. Therefore, chromosomal analysis, combined with FISH, was used to determine whether PLK1 kinase inactivation promoted centromere chromosome damage.

4.2 Results

4.2.1 PLK1 kinase activity is required to suppress chromosome fragmentation

To determine the status of individual isolated chromosomes during PLK1 inactivation, mitotic chromosome spreads were prepared, using RPE1 hTERT cells treated with or without BI2536. RPE1 cells maintain a near diploid karyotype (46 chromosomes) (Bodnar et al. 1998), which is unlike many cancer-derived cell lines that can display considerable fluctuations in ploidy (Nicholson and Cimini 2013). Thus, as expected, analysis of mitotic chromosome spreads following a thymidine-block and release, showed that control cells exhibited average chromosome numbers very close to a diploid karyotype (DMSO=46.5 & nocodazole=45.5 per spread) **(Fig. 4.1a-c)**. Notably, due to the synchrony of mitotic entry after a thymidine-block and release, colcemid treatment, which acts as a non-reversible mitotic arresting agent was omitted and deemed unnecessary during preparation.

Surprisingly, close examination of mitotic spreads following BI2536 treatment showed that the average number of chromosomes per spread was significantly increased (BI2536=58.5; mean chromosome number per spread) **(Fig. 4.1a-c)**. This led to the suggestion that the loss of PLK1 activity induce a form of chromosome fragmentation. In mitotic spreads co-treated with BI2536 and nocodazole, fragmentation rescue was evident, as chromosome numbers reverted to a near diploid karyotype, much like control cells (BI2536+NOC=48.3) **(Fig. 4.1a-c)**. Importantly, none of the 90 chromosome spreads analysed for chromosome counting after BI2536, displayed signs of sister-chromatid separation **(Fig. 4.1d)**. This rules out the possibility that the increase in chromosome numbers after BI2536 treatment is a result of counting individual sisters, rather than cohesed chromosomes.

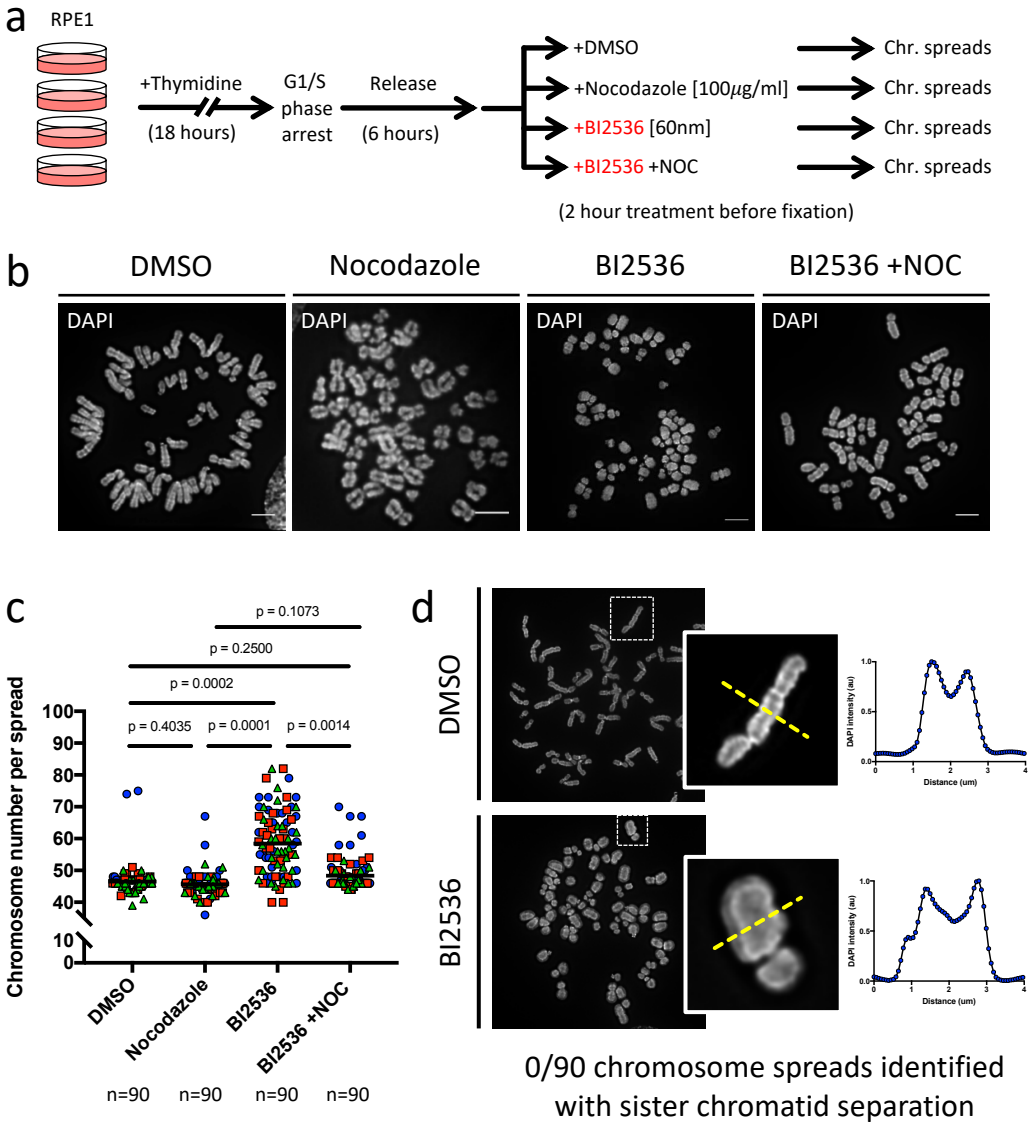

Figure 4.1. PLK1 inhibition causes chromosome fragmentation.
a) Experimental outline of cell-synchronisation and chromosome spread preparation, following indicated inhibitor treatments. **b)** Examples of chromosome spread images following indicated inhibitor treatments. DAPI was used to stain chromosomes. **c)** Quantification of chromosome number per spread after indicated inhibitor treatment (overall mean is shown from three independent experiments; student t-test was used for p-value calculation; n=number of cells analysed; scale bar 5μm; different colours indicate each experiment). **d)** Enlarged example image of a single chromosome, and DAPI intensity scanline plot profile, after either DMSO or BI2536 treatment (0/90 chromosome spreads showed evidence of sister-chromatid separation).

Overall, these data supported the idea that PLK1 kinase activity functions to suppress a form of chromosome fragmentation, which seems to be mediated by microtubule spindle pulling forces.

4.2.2 PLK1 suppresses centromere breakage - 'centromere dislocation'

Since PLK1 inactivation leads to pre-anaphase centromeric DNA thread formation and centromere/kinetochore distortion, it was speculated that the fragmentation of chromosomes may be caused by damage at centromeric chromatin. Therefore, to further investigate this idea, chromosome spreads from cells treated with or without BI2536, were subject to centromere and telomere fluorescent *in situ* hybridisation (ct-FISH) **(Fig. 4.2a)**.

Analysis of chromosome spreads after ct-FISH clearly showed that the breakage of chromosomes after BI2536 treatment was not a random event. As predicted, following nocodazole treatment, chromosome spreads displayed an absence of chromosome fragmentation. Each chromosome analysed appeared as expected, displaying two pairs of telomere signals at each chromosome termini, whilst also containing an obvious centromere signal, within the flanking telomere signals **(Fig. 4.2b-d)**. In contrast, BI2536-treated chromosome spreads displayed a centromere specific breakage pattern **(Fig. 4.2b-d)**, strongly implying that PLK1 was required to suppress this chromatin damage phenomena.

The breakage pattern was classified into two distinct classes. BI2536 treatment could result in a complete centromere breakage pattern, which resembled the formation of telocentric chromosomes. This was shown as a centromere signal at one chromosome terminus and a pair of telomere signals at the opposite end **(Fig. 4.2d)**. This breakage pattern was referred to as 'centromere dislocation', emphasising the complete separation of the short and long arm of individual chromosomes. In addition, BI2536 treatment led to 'partially' separated centromeres. In contrast to the complete

centromere breakage pattern (centromere dislocation), 'partially' separated chromosomes presented as stretching of the centromere, with both the short and long arm of the chromosome clearly remaining tethered together **(Fig. 4.2d)**. This stretching scenario was categorised as distinctly different from the complete breakage pattern (centromere dislocation). It was tempting to predict that the 'partial' separation of centromeres resembled the initial stage of centromere breakage, during PLK1 inhibition.

Based on these current findings, it was proposed that the spindle-mediated tension applied to centromeres during chromosome biorientation, promoted deformation or fragility at the centromere, when PLK1 function is compromised. In support of this, following the co-treatment of BI2536 and nocodazole, centromere dislocation was largely reduced **(Fig. 4.2b-d)**. This implies that spindle-mediated tension and PLK1 inactivation are able to promote centromere deformation. Additionally, these results were consistent with the earlier experiments, which showed pre-anaphase DNA threads were abolished, following the co-treatment of BI2536 and nocodazole **(see previous Fig. 3.12)**. Therefore, it was concluded that MT spindle attachment and MT pulling forces, influenced the centromere deformation pathway following the inactivation of PLK1.

In order to confirm that PLK1 inactivation leads to chromatin breakage, specifically at the core centromere, all broken chromosomes were closely examined for the existence of a centromere FISH signal at their termini. Over 300 individual centromeres were examined and approximately 99% of each broken chromosome displayed a centromeric FISH signal at one end **(Fig. 4.3a-c)**. Hence, it was concluded that PLK1 is required to suppress the formation of a (peri)-centromere specific DNA breakage pattern.

4.2.3 Centromere deformation is specifically suppressed by the activity of PLK1

Throughout this study, all experimental analysis investigating the loss of PLK1 activity, was performed using the small-molecule inhibitor BI2536. Despite being reported as a

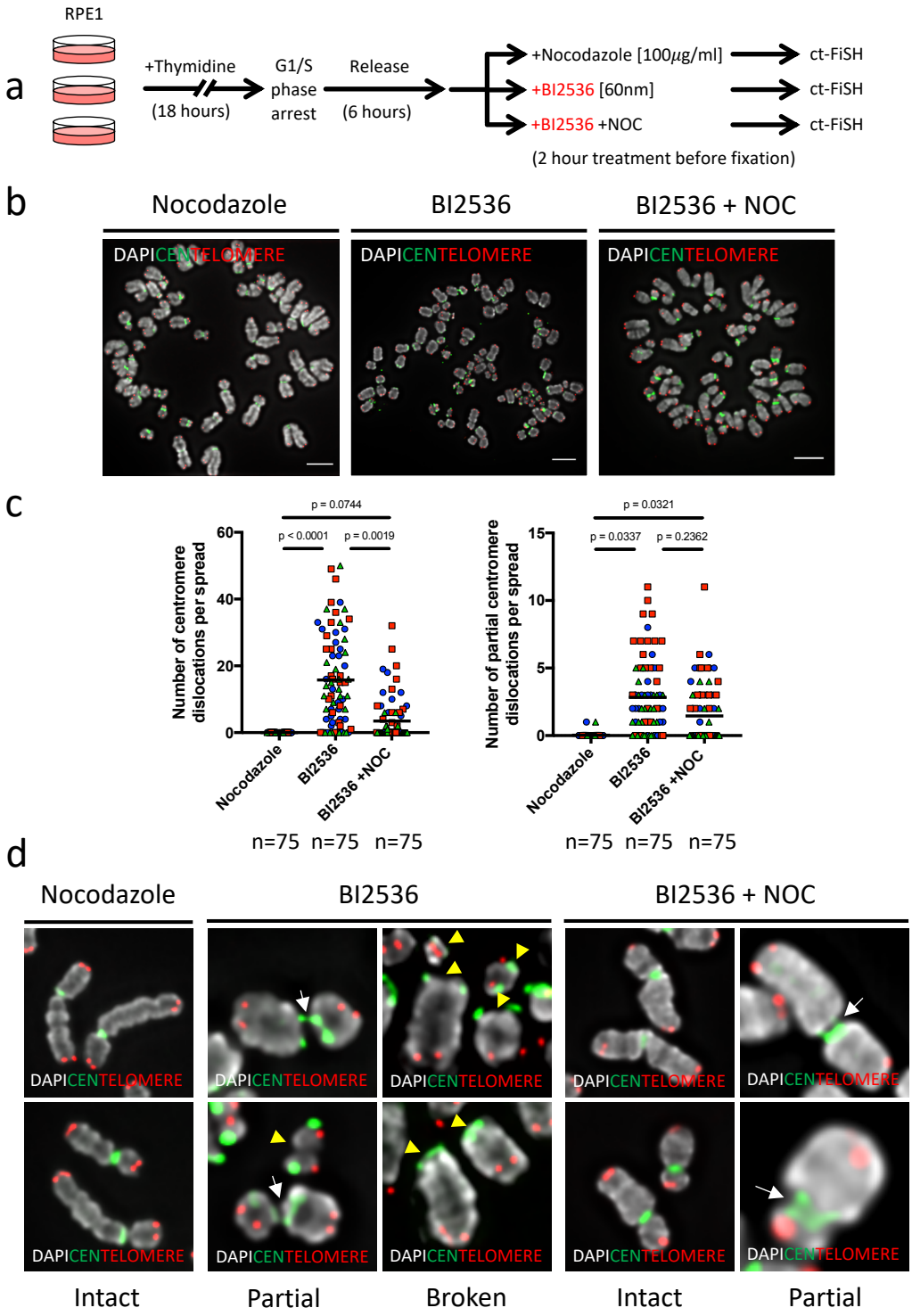

Figure 4.2. PLK1 inhibition causes 'centromere dislocation'.
a) Experimental outline of cell-synchronisation and chromosome spread preparation following indicated inhibitor treatments. **b)** Examples of chromosome spread images following centromere-telomere FISH (ctFISH), and treatment with indicated inhibitors. DAPI was used to stain chromosomes; centromeres (Green) and telomeres (Red) were detected using specific FISH probes. **c)** Quantification of 'centromere dislocations' (left), or 'partially splitting' (right) chromosome arms (overall mean is shown from three independent experiments; student t-test was used for p-value calculation; n=number of cells analysed; scale bar 5μm; different colours indicate each experiment; Ankana Tiwari assisted with quantifications of both centromere dislocations and partial centromere dislocation counting). **d)** Enlarged examples from ctFISH chromosome spread images showing either intact (left), partially split (arrows), or broken (arrowheads) chromosomes.

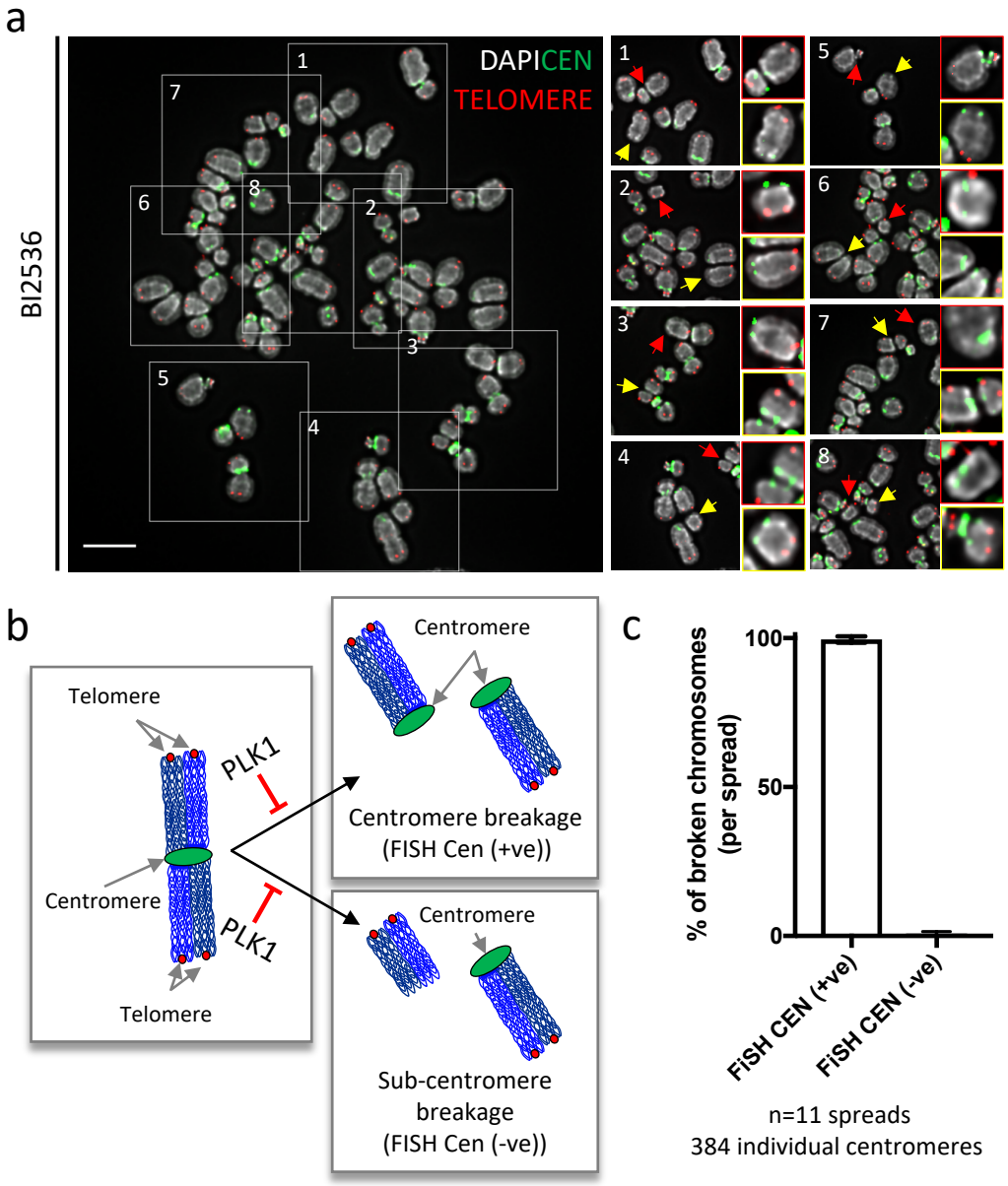

Figure 4.3. Centromere dislocation results in chromatin breakage specifically within centromeric DNA.

a) Example of a single chromosome spread image following centromere-telomere FISH (ctFISH) and treatment with BI2536. Enlarged regions (1-8) show 'centromere dislocations' (arrows), paired with cropped images of enhanced contrast centromere FISH signals (red arrows=above; yellow arrows=below). DAPI was used to stain chromosomes; centromeres (Green) and telomeres (Red) were detected using specific FISH probes. **b)** Diagram to explain how 'centromere dislocation' could be either due to a centromeric breakage (Centromere signal at the termini of all broken arms = FISH CEN +ve), or alternatively a sub-centromere breakage (Only half of all broken chromosomes show a centromere signal at their termini = FISH CEN -ve). **c)** Quantification of broken chromosome arms either positive, or negative for centromere FISH signal at one terminus (Error bars indicate SD; n=number of spreads analysed; scale bar 5μm).

highly potent and specific inhibitor of PLK1 activity (IC_{50} = 0.83nm), it may also non-specifically interfere with the activity of other family members of Polo-like kinases, for instance PLK2 and PLK3 (Lénárt et al. 2007; Steegmaier et al. 2007). Therefore, it was important to confirm that the centromere deformation phenotypes reported during this study, were not due to off-target effects of BI2536, or unwanted effects that may be caused by trapping of inactive PLK1 to it substrates.

To determine whether the suppression of centromere deformation was specifically dependent on PLK1 function, the effects of inhibiting PLK1 activity using a previously developed RPE1 PLK1 analogue sensitive (PLK1as) cell line was investigated (Burkard et al. 2007). The RPE1 PLK1as cell line was developed by conditional targeting of wild-type PLK1, and replacement with a GFP-tagged PLK1as mutant allele **(Fig. 4.4a)**. Amino acid substitutions at PLK1's gatekeeper residue that lines the ATP-binding pocket (L130G), in combination with a suppressor mutation in the amino-terminal of the ATP-binding pocket (C67V), results in an increase in the size of the catalytic ATP-binding pocket of PLK1. This renders PLK1as cells sensitive to large bulky purine analogues, such as 3-MB-PP1. However, due to the size increase of the ATP-binding pocket in the mutant PLK1as protein, small-molecule inhibitors – including BI2536, are no longer effective at inhibiting PLK1 activity, as they are unable to be retained within the catalytic site of PLK1as. Therefore, by analysing mitotic RPE1 PLK1as cells during treatment with the large purine analogue 3-MB-PP1, it would be possible to determine whether PLK1 activity was required to suppress the centromere deformation phenotypes reported **(Fig. 4.4b)**.

Both RPE1 wild-type and RPE1 PLK1as cells were synchronised as before, and treated individually with either BI2356, or 3-MB-PP1 **(Fig. 4.5a)**. As expected, during BI2536 treatment, pre-anaphase DNA threads were shown to form in wild-type RPE1 cells, but not in RPE1 PLK1as cells **(Fig. 4.5b, c)**. PLK1as cells were insensitive to BI2536 and instead were able to progress through mitosis and successfully underwent anaphase, demonstrating that BI2536 is unable to influence PLK1as protein activity **(Fig. 4.5b, c)**. Importantly, during 3-MB-PP1 addition, wild-type RPE1 cells displayed no evidence of

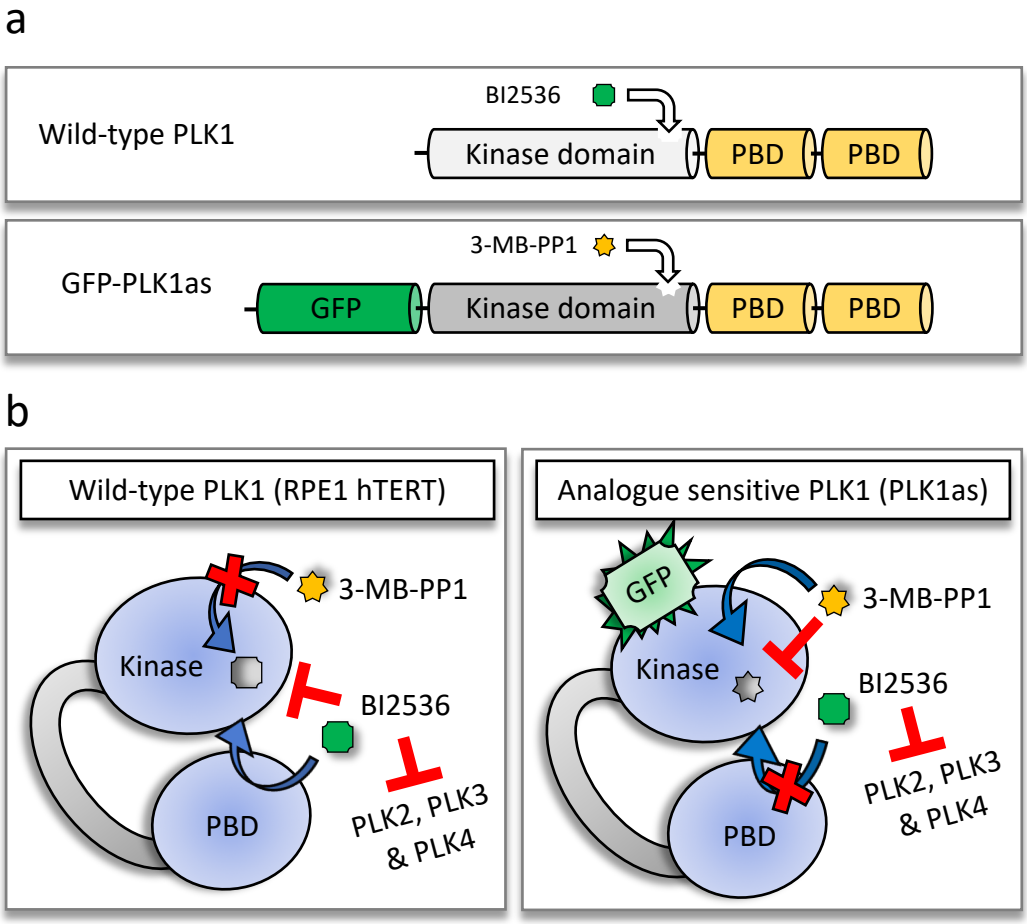

Figure 4.4. An alternative approach at targeting PLK1 kinase activity using PLK1as cells. **a)** A diagram to demonstrate how RPE1 hTERT cells, which contains wild-type PLK1, are sensitive to the small-molecule inhibitor BI2536. However, wild-type PLK1 is insensitive to the large bulky ATP analogue, 3-MB-PP1. The RPE1 PLK1as cells are only sensitive to the large bulky 3-MB-PP1 molecule and insensitive to the small-molecule BI2536. **b)** A schematic to demonstrate that wild-type RPE1 cells contain two copies of PLK1, which each have a kinase domain (sensitive to BI2536) and a PBD domain. PLK1as RPE1 cells have two copies of a GFP-tagged PLK1 analogue sensitive PLK1. PLK1as cells have a functional mutant kinase domain (sensitive to 3-MB-PP1) and a PBD domain.

pre-anaphase DNA thread formation, whereas the RPE1 PLK1as cells were shown to exhibit them **(Fig. 4.5b, c)**. This confirmed that RPE1 PLK1as cells treated with 3-MB-PP1, recapitulate the effects of treating wild-type RPE1 cells with BI2536. Importantly, it further supports the hypothesis that PLK1 activity is specifically required to suppress DNA thread formation and the phenotypes are not due to an interference to other kinases.

These data do not rule out that PLK1 inactivation via either BI2536, or 3-MB-PP1 may cause trapping of PLK1 to its substrates, and thus lead to the centromere deformation phenotypes. Accordingly, to rule out that trapping of PLK1 to its targets may promote pre-anaphase DNA thread formation, PLK1 protein depletion using RNAi was performed. This could show whether an absence of PLK1 protein is sufficient to promote metaphase collapse and pre-anaphase DNA thread formation.

RPE1 cells were treated with specific siRNA oligo sequences that target PLK1 mRNA. The targeting of PLK1 by RNAi was performed for a short period before, and during cell-synchronisation using thymidine, in order to achieve sufficient depletion **(Fig. 4.6a)**. Following ~25 hours of RNAi treatment, RPE1 cells were released into fresh media, prior to fixation and indirect immunostaining analysis. Cells are known to arrest in mitosis following the interference of PLK1 activity, either through chemical inhibition, or via protein depletion. As anticipated, the majority of RPE1 cells began to display a mitotic arrest after ~25 hours of RNAi treatment, thus implying an effective depletion of PLK1. This was confirmed by indirect immunostaining of the PLK1 depleted cells, which showed the majority of cells were absent for PLK1 detection **(Fig. 4.6b)**. The mitotic cells also displayed a metaphase collapse, which resembled that observed after BI2536 treatment, whilst also displaying PICH positive pre-anaphase DNA thread formation **(Fig. 4.6b)**. Taken together, these results strongly suggested that the activity of PLK1 is responsible for suppressing the formation of pre-anaphase DNA threads. It therefore rules out that pre-anaphase DNA thread formation is due to an interference of other PLKs (i.e. PLK1-3), or trapping of PLK1 to its substrates.

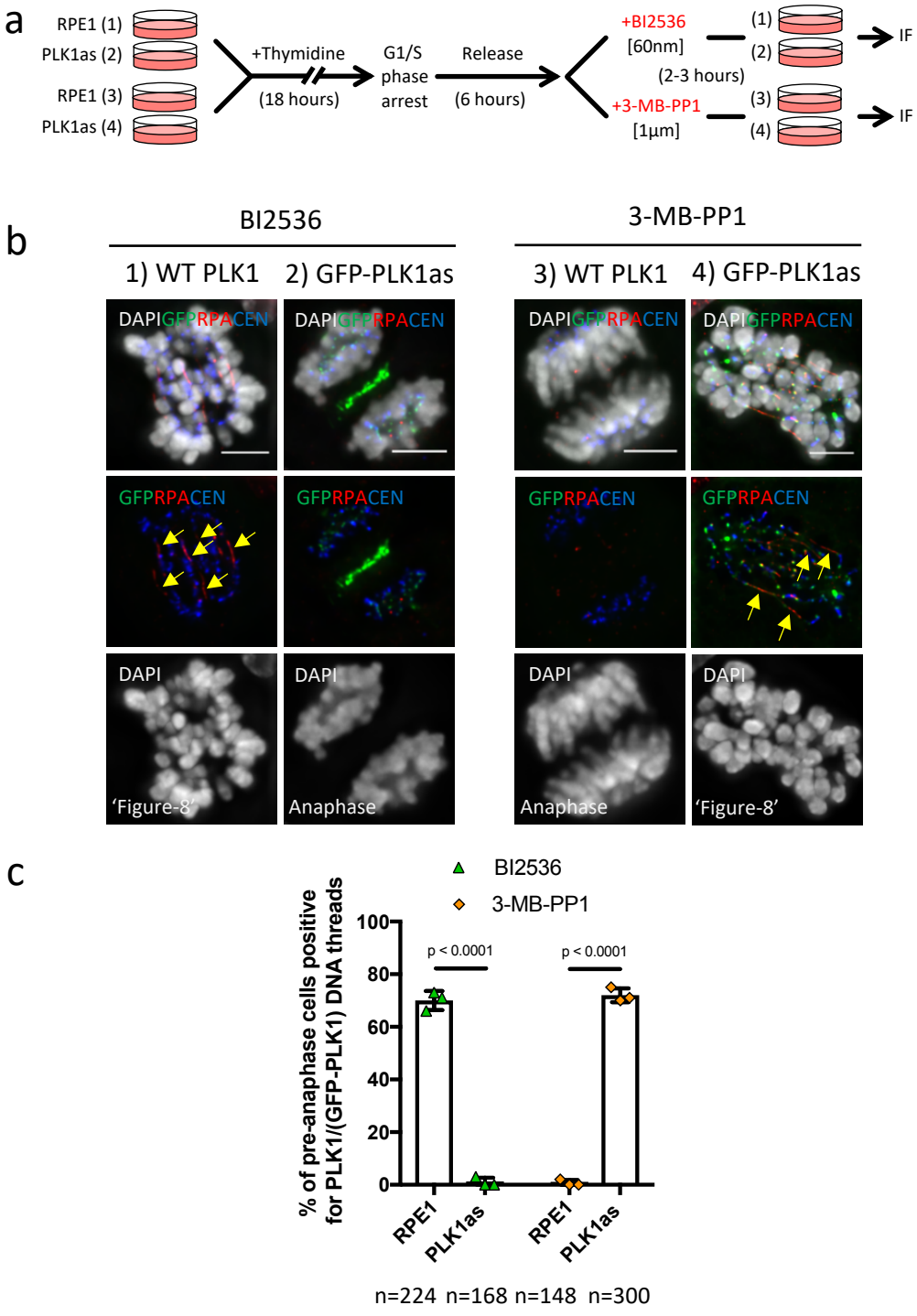

Figure 4.5. PLK1 kinase activity supresses pre-anaphase DNA thread formation.
a) Experimental outline of cell-synchronisation and immunofluorescent staining using wild-type, or PLK1as, RPE1 cells. **b)** Immunofluorescent images of either BI2536, or 3-MB-PP1 treated mitotic RPE1 and PLK1as cells. Cells positive for pre-anaphase DNA threads are indicated (arrows). Antibody staining for GFP-PLK1 (Green), RPA (Red) and centromeres (Blue). **c)** Quantification of DNA threads observed in indicated cell lines, treated with either BI2536, or 3-MB-PP1 (mean ±SD is shown from three independent experiments; student t-test was used for p-value calculation; n=number of cells analysed; scale bar 5μm).

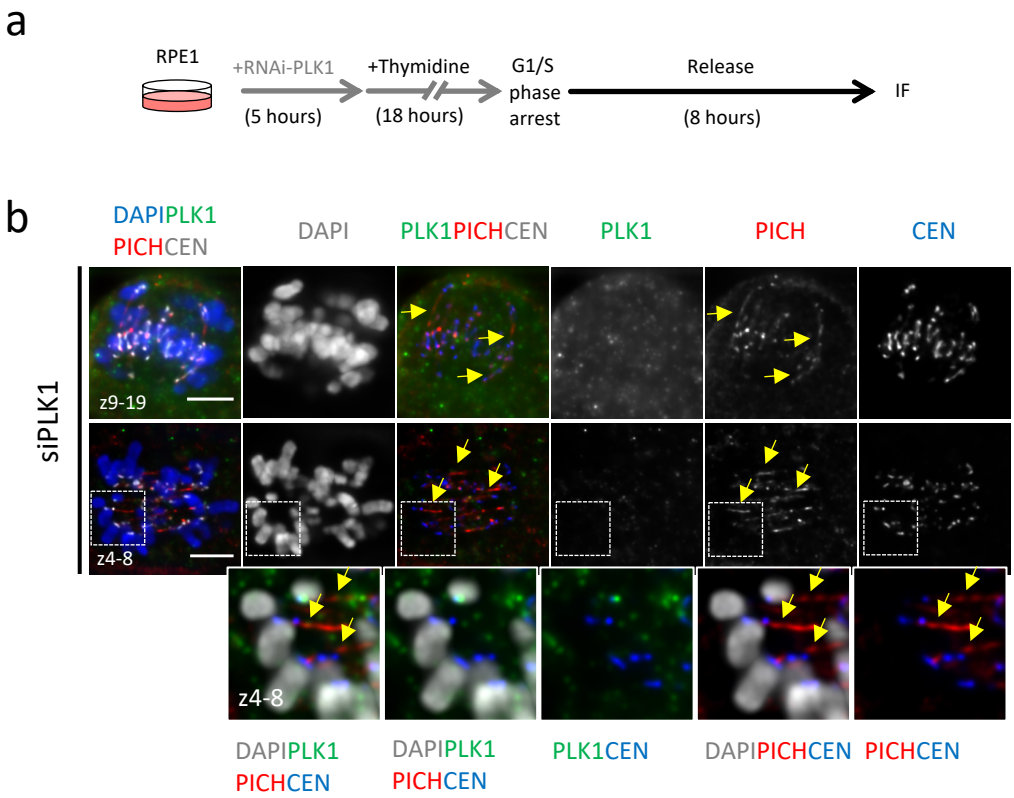

Figure 4.6. Centromere deformation is not caused by trapping inactive PLK1 to its substrates.

a) Experimental outline of RNAi targeting of PLK1, cell-synchronisation and immunofluorescent staining using RPE1 cells. **b)** Immunofluorescent images of mitotic RPE1 cells after PLK1 depletion show pre-anaphase DNA threads (arrows). The absence of antibody staining for PLK1 (Green) highlights protein depletion, whilst PICH (Red) and centromere (Blue) signal remain. Enlarged regions show a PICH-positive (Red) pre-anaphase DNA threads associated with the centromere (Blue) (scale bar 5μm).

4.2.4 Artificial tethering of PLK1 to the centromere/kinetochore fails to rescue centromere deformation

In order to further validate that cells require PLK1 activity to suppress centromere deformation, ectopic expression of wild-type PLK1 protein in the analogue sensitive RPE1 PLK1as cells (Lera et al. 2016), during 3-MB-PP1 treatment was tested, as it would be predicted to suppress centromere deformation **(Fig. 4.7a, b)**. Pre-anaphase DNA threads were shown to form in the RPE1 PLK1as cells, following the addition of 3-MB-PP1, whilst the stable ectopic expression of a wild-type PLK1 protein (PLK1as + WT) suppressed pre-anaphase DNA thread formation **(Fig. 4.8a-c)**. This further emphasises the important role that PLK1 plays in preventing centromere deformation.

PLK1 is known to require its PBD domain for substrate targeting and its downstream function(s). Therefore, it was predicted that an interference to PLK1's PBD domain will render cells sensitive to centromere deformation phenotypes (i.e. pre-anaphase DNA thread formation). Examination of RPE1 PLK1as+ΔPBD cells, which ectopically expressed a modified PLK1 protein, containing a wild-type kinase domain but with a mutant PBD domain **(see previous Fig. 4.7a, b)**, showed them to no longer be capable of suppressing pre-anaphase DNA thread formation during 3-MB-PP1 treatment **(Fig. 4.8b, c)**. Therefore, these data show that the catalytic function of wild type PLK1, along with its PBD domain, is required to suppress pre-anaphase DNA thread formation.

Throughout mitosis, PLK1 has been reported to localise and function within discrete regions along the centromere/kinetochore axis (Lera et al. 2016). Therefore, it was speculated that in order to suppress centromere deformation, PLK1's catalytic activity may be required to function at specific site(s) along this centromere/kinetochore axis. In an attempt to define the specific site, three previously developed RPE1 PLK1as cell lines were examined for their ability to suppress pre-anaphase DNA thread formation during 3-MB-PP1 treatment (Lera et al. 2016). Each modified RPE1 PLK1as cell line featured a catalytically active form of PLK1, which was artificially tethered to either BUBR1 (PLK1-Δ^{c}-BubR1 – outer kinetochore region); KIF2c (PLK1-Δ^{c}-Kif2c – outer

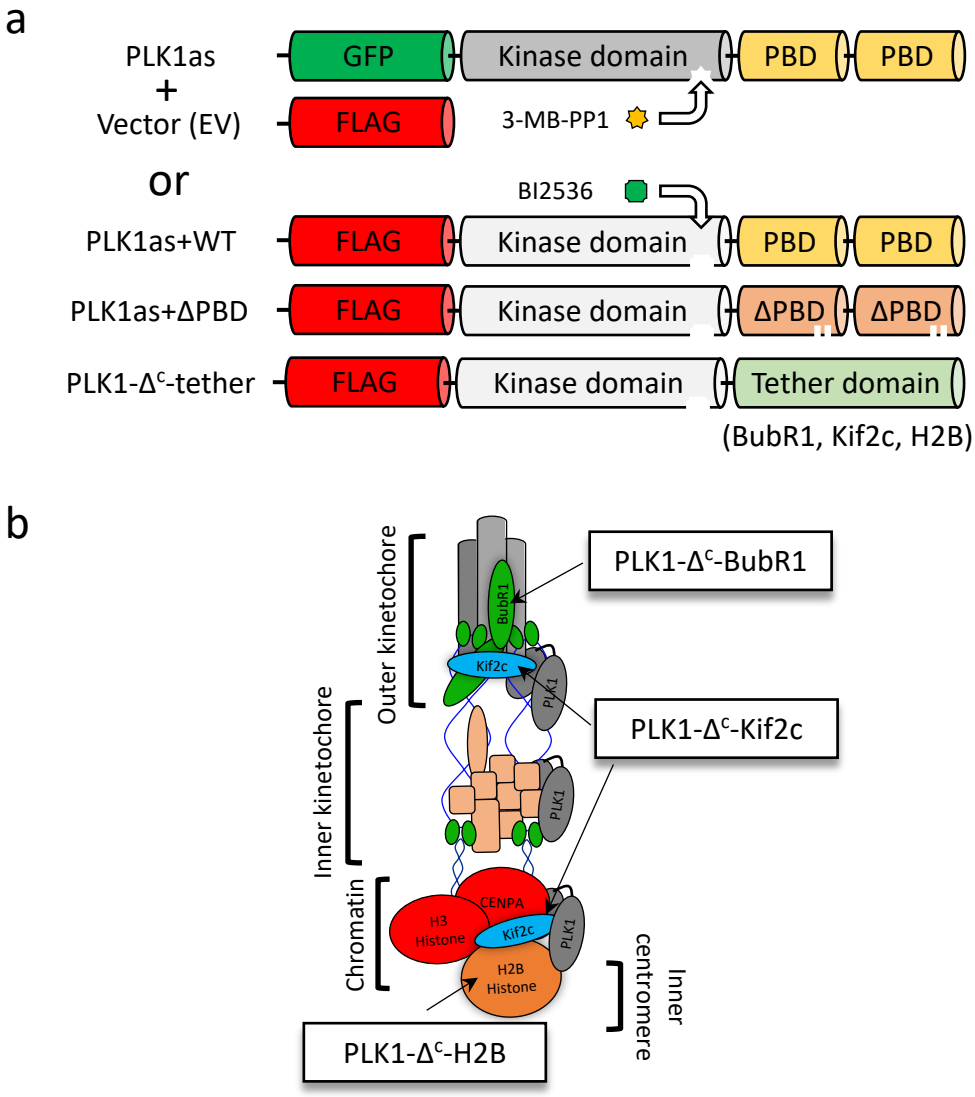

Figure 4.7. Schematic of domain structure & localisation of centromere tethered PLK1as cell lines.

a) A schematic diagram of the different PLK1as cell lines. PLK1as cells were stably infected with either an empty FLAG vector (PLK1as EV), or with a FLAG-tagged PLK1 (PLK1as+WT), a FLAG-tagged PLK1 that has a mutated PBD domain (PLK1as+ΔPBD); or finally a variety of derivatives that have a FLAG-tagged kinase domain, absent of their PBD and instead tethered to either -BubR1, -Kif2c or -H2B. Note that both alleles of PLK1as(EV) are sensitive to 3-MB-PP1, whereas all further cell line derivatives have one copy of the PLK1as allele, which is sensitive to 3-MB-PP1, and the other copy (wild-type PLK1 kinase domain) is sensitive to BI2536. **b)** A schematic diagram of the centromere/kinetochore axis, highlighting the localisation of the PLK1-Δ^{c}-tethered constructs.

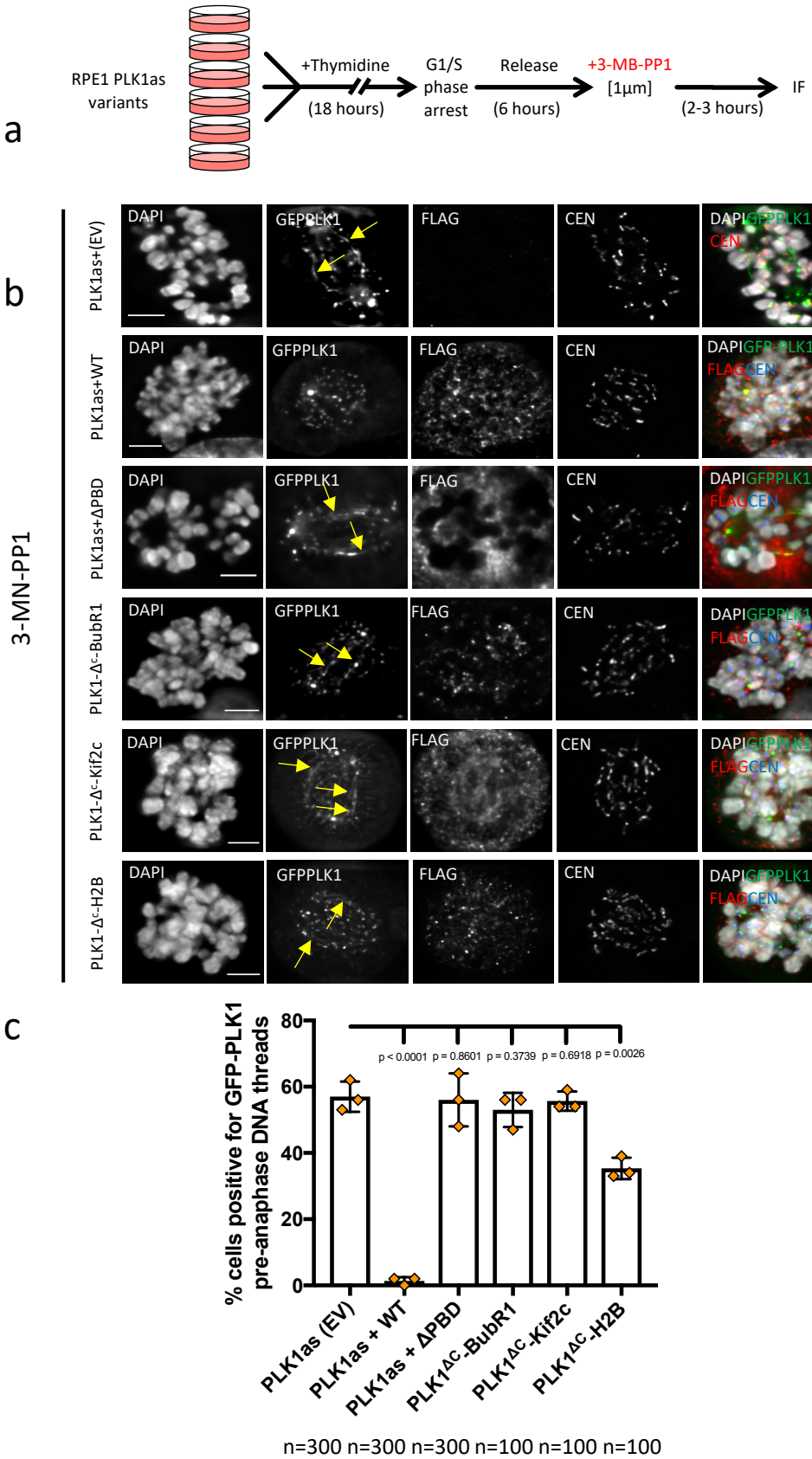

Figure 4.8. Centromere tethered PLK1 is insufficient to prevent centromere deformation. **a)** Experimental outline of cell-synchronisation and immunofluorescent staining using RPE1 PLK1as cells and derivates. **b)** Immunofluorescent images of GFP-tagged PLK1as (EV) and derivatives, PLK1as+WT, PLK1as+ΔPBD, PLK1-Δ^{c}-BubR1, PLK1-Δ^{c}-Kif2c and PLK1-Δ^{c}-H2B, after 3-MB-PP1 treatment. Pre-anaphase DNA threads are indicated (arrows). Antibody staining for GFP-PLK1 (Green), FLAG (Red) and centromeres (Blue). **c)** Quantification of GFP-PLK1 pre-anaphase DNA threads observed in each cell line after treatment with 3-MB-PP1 (mean ±SD is shown from three independent experiments; student t-test was used for p-value calculation; n=number of cells analysed; scale bar 5µm).

kinetochore and inner centromere); or, histone H2B (PLK1-Δ-H2B – chromatin) **(see previous Fig. 4.7a, b)**. The artificial tethering of an active form of PLK1 to either BUBR1, KIF2c or H2B was tested to determine if it could suppress centromere deformation, when PLK1as activity was compromised by 3-MB-PP1 treatment.

Indirect immunofluorescent analysis showed none of each of the tethered PLK1-Δ^{c}(-BubR1, -Kif2c or -H2B) cell lines could fully suppress pre-anaphase DNA thread formation, during the addition of 3-MB-PP1 **(Fig. 4.8b, c)**. Interestingly, PLK1-Δ-H2B cells did display a significant reduction in the percentage of mitotic cells positive for pre-anaphase DNA threads, when compared to control cells (PLK1as) **(Fig. 4.8b, c)**. This could suggest that PLK1 is required to function at the level of chromatin, in order to suppress pre-anaphase DNA thread formation.

In addition to the indirect immunofluorescent analysis, cytogenetic examination of each of the RPE1 PLK1as cell lines was also performed in order to determine centromere dislocation frequencies. Mitotic chromosome spreads were prepared during 3-MB-PP1 treatment, for each of the PLK1as cell lines (including all derivatives) and subjected to ct-FISH.

As expected, during 3-MB-PP1 treatment, PLK1as cells displayed an increase in centromere dislocation patterns, whilst PLK1as+WT cells showed a significant reduction in centromere dislocations **(Fig. 4.9a, b)**. These results supported previous findings on pre-anaphase DNA thread formation in the same cell lines. Consistent with previous findings, PLK1as+ΔPBD cells displayed high numbers of centromere dislocations, whilst each of the three PLK1-tethered cell lines (PLK1-$_{\Delta}{}^{C}$-BubR1, PLK1-$_{\Delta}{}^{C}$-Kif2c and PLK1-$_{\Delta}{}^{C}$-H2B) also showed significant levels of centromere dislocation, during 3-MB-PP1 treatment **(Fig. 4.9a, b)**. This confirms that PLK1 activity is crucial to suppress centromere dislocations, whilst fusion of an active form of PLK1 to BUBR1, KIF2c or H2B, appears insufficient to suppress centromere deformation.

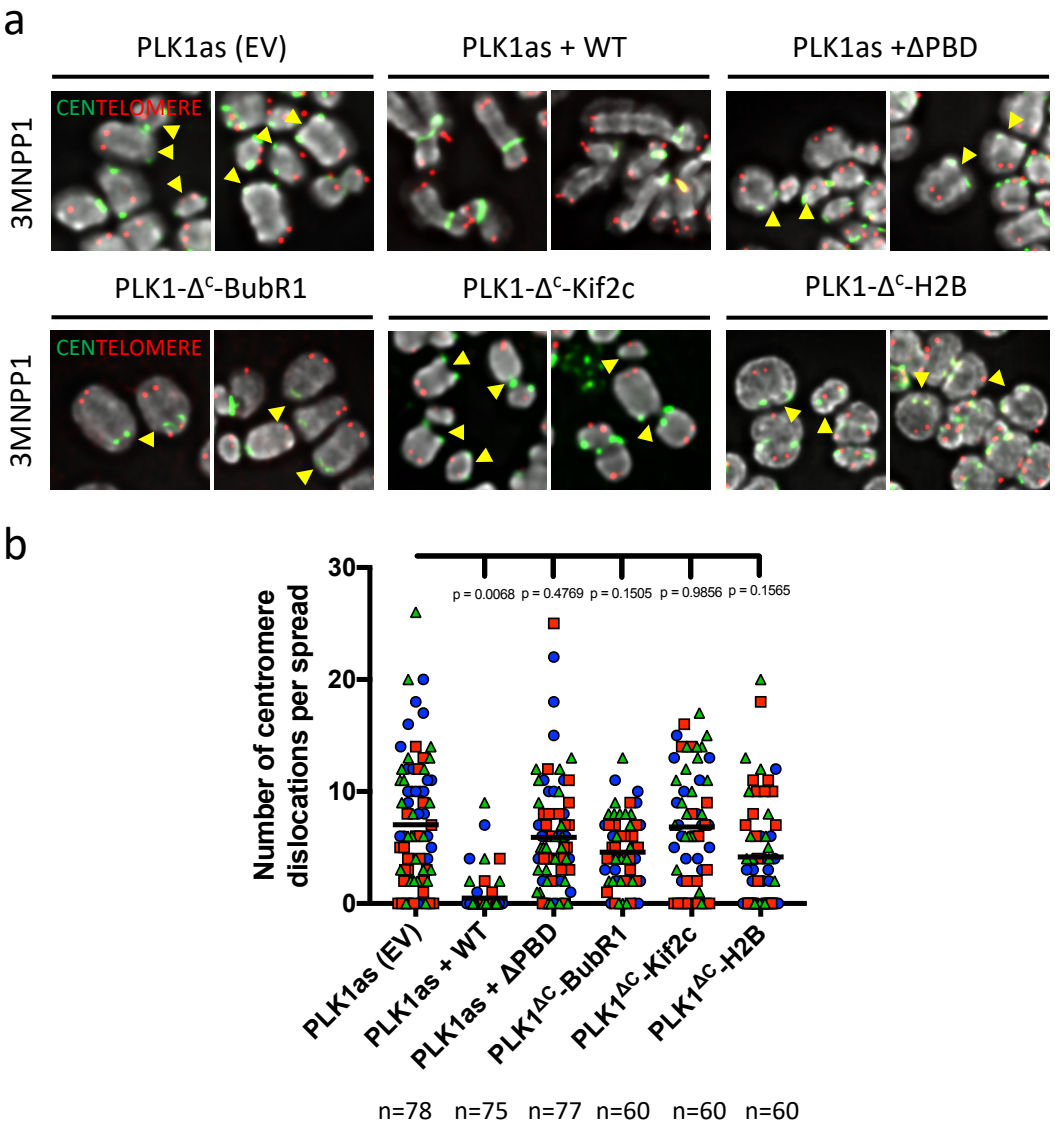

Figure 4.9. Tethering PLK1 to the centromere is insufficient to prevent centromere dislocations.

a) Examples of chromosome spread images after 3-MB-PP1 treatment, and ctFISH, using GFP-tagged PLK1as (EV) and its derivatives PLK1as+WT, PLK1as+ΔPBD, PLK1-Δ^c-BubR1, PLK1-Δ^c-Kif2c and PLK1-Δ^c-H2B. Enlarged regions highlight 'centromere dislocations' (arrowheads). DAPI was used to stain chromosomes; specific FISH probes were used for centromere (Green) and telomere (Red) detection; cells were synchronised as before from **(Fig. 16a)**. **b)** Quantification of 'centromere dislocations' of chromosome arms (overall mean is shown from three independent experiments; student t-test was used for p-value calculation; n=number of cells analysed; scale bar 5μm).

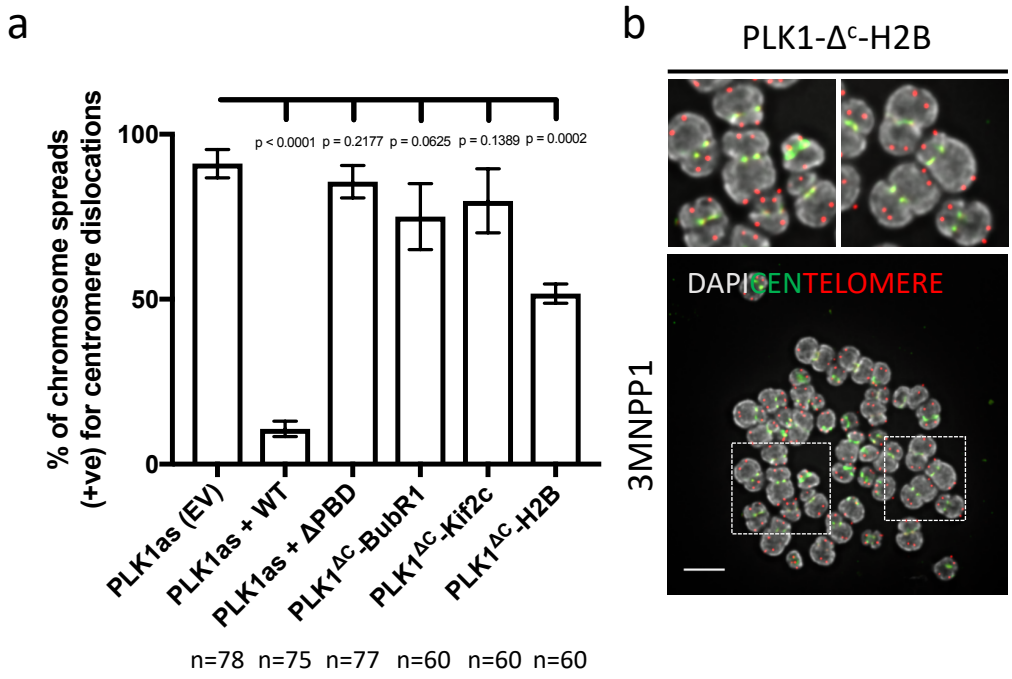

Figure 4.10. Tethering PLK1 to chromatin partially rescues centromere dislocations.
a) Quantification of the percentage of spreads showing ≥1 'centromere dislocation' per spread (mean ±SD is shown from three independent experiments; student t-test was used for p-value calculation; n=number of spreads analysed; scale bar 5μm). **b)** Example of chromosome spread after 3-MB-PP1 treatment, and ctFISH, using PLK1-Δc-H2B cells. Enlarged regions show no centromere dislocations, whilst chromosomes remain hyper-condensed. DAPI was used to stain chromosomes; specific FISH probes were used for centromere (Green) and telomere (Red) detection; cells were synchronised as before.

Interestingly, following close examination of the PLK1-Δ^{C}-H2B cell line, it was noticed that a significantly lower percentage of chromosome spreads were positive for one or more centromere breakages, when compared to control cells (PLK1as) **(Fig. 4.10a, b)**. Therefore, fusion of PLK1 to the histone variant H2B, can lead to a mild suppression of centromere deformation phenotypes, despite overall PLK1 inactivation during 3-MB-PP1 treatment. Thus, these findings support the suggestion that PLK1 functions at the level of chromatin in order to suppress centromere deformation. However, further investigation into the possible substrate targets of PLK1 is needed to elucidate the mechanism of centromere deformation suppression by PLK1.

4.3 Discussion

In this chapter, careful cytogenetic analysis has demonstrated that the loss of PLK1 activity can lead to an unexpected spindle-mediated centromere breakage phenomenon during mitosis, which is referred to as 'centromere dislocation'. In Chapter 3, earlier immunofluorescent experiments suggested that centromeres suffer from serious DNA damage, as revealed by the presence of γH2AX foci at centromeres, following the inhibition of PLK1 activity **(see previous Fig. 3.9b, c)**. This suspected centromere damage was confirmed by detailed chromosome examination, using centromere and telomere FISH (ct-FISH). Here, we show that whole chromosome arm breakage is displayed after PLK1 inhibition and this can be largely suppressed when spindle attachment and tension is abolished using nocodazole **(Fig. 4.2b-d)**. This highlights that MT-spindle forces influence centromere breakage during PLK1 inactivation.

In addition, the whole chromosome arm breakage pattern is non-random, with the break point specific to the core-centromere region(s). Therefore, it is tempting to suggest that centromere dislocation is the culmination of pre-anaphase DNA thread breakage, although the mechanistic process of this remains uncertain. Whether pre-anaphase DNA thread formation, and the resulting centromere breakage phenomenon, induced by PLK1 inactivation, is simply due to microtubule spindle forces or the result of additional factors/active mechanisms, remains to be discovered. Further analysis into the possible PLK1 substrates at the centromere may help to uncover greater detail and to explain how PLK1 functions to suppress such centromere deformation.

The study of cell lines artificially tethering PLK1 to various sites of the centromere-kinetochore axis was inconclusive, but continues to hold promise. Further studies are required to investigate the effects of tethering PLK1, either directly to chromatin, or alternatively to additional sites along the centromere/kinetochore axis. This may help

to uncover possible PLK1-kinase targets that function to suppress centromere deformation.

The lack of centromere deformation rescue using the current selection of PLK1 tethered cell lines (PLK1-Δ^C-BubR1, PLK1-Δ^C-Kif2c and PLK1-Δ^C-H2B), may be due to various factors. Each PLK1 tethered cell line has been reported to be kinase active, but it remains to be seen whether they are fully capable of mimicking wildtype PLK1 function and/or localisation (Lera et al. 2016). Therefore, the PLK1-tethered cell lines examined may not be sufficient to suppress such centromere deformation. PLK1 is anticipated to have multiple targets at the centromere. Hence, current PLK1-tethered cell lines may not be able to satisfy the full plethora of PLK1 targets required to suppress centromere deformation. Thus, future examination into different locations of PLK1 tethering, or even tethering active PLK1 to multiple sites, may help to dissect how PLK1 functions in centromere maintenance.

Interestingly, tethering PLK1 to the histone variant, H2B showed a partial rescue of centromere deformation. Despite cells displaying centromere breakage following PLK1 kinase inhibition using 3-MB-PP1, there was a significant reduction in centromere dislocations. This mild rescue of centromere breakage may imply that PLK1 acts directly at the level of chromatin in order to suppress centromere deformation. Thus, it is speculated that PLK1 may actively phosphorylate histones in order to provide rigidity to chromatin structure, particularly at the centromere. Subsequently, PLK1-dependent phosphorylation of histones may ensure centromeric chromatin rigidity, which could be required in order to counteract the microtubule-spindle pulling forces encountered during KT-MT attachment and chromosome biorientation. However, it must be emphasised that this is speculation and PLK1 is most likely required to phosphorylate multiple factors in order to suppress centromere deformation.

Results presented in this chapter could imply that microtubule-spindle pulling forces may not be the only factor responsible for centromere deformation, during PLK1

inactivation. Previous immunofluorescent experiments showed that pre-anaphase DNA threads are abolished when cells were co-treated with BI2536 and either the microtubule spindle-poison, nocodazole, or the Eg-5 inhibitor, monastrol **(Fig 3.12-3.13)**. This would imply that microtubule spindle tension may drive the formation of pre-anaphase DNA threads, during the inhibition of PLK1 kinase activity. However, cytogenetic analysis during this chapter has revealed a more detailed outlook. Through careful analysis of centromere FISH signals, it was possible to observe two distinct centromere deformation scenarios, either centromere breakage (centromere dislocations); or, partial splitting of the centromere. Notably, the partial splitting phenotype was reminiscent of centromere stretching. Thus, partial separation of the centromere may be attributed to an early stage of centromere deformation, prior to complete breakage (centromere dislocation) **(Fig. 4.2c, d)**.

Intriguingly, experiments investigating the co-treatment of microtubule-spindle poison (nocodazole), alongside PLK1 inhibition, showed that such co-treatment, leads to a significant reduction in centromere dislocations. However, when comparing against PLK1 inactivation alone, partial splitting of the centromere was not significantly reduced, during the co-treatment of BI2536 and nocodazole **(Fig. 4.2c, d)**. Therefore, it was speculated that additional influences may play a role in centromere deformation, independent of MT-spindle pulling forces, and these could promote the initial stages of centromere deformation during PLK1 inhibition.

Consistent with this idea, previous experiments showed that pre-anaphase DNA thread formation could be suppressed during the co-treatment of BI2536 and monastrol (monopolar MT-spindle attachment). However, close analysis of these cells showed RPA focus formation at the centromeres. This was not detected in cells co-treated with BI2536 and nocodazole (no MT-spindle attachment). Therefore, it was speculated that MT-attachment may promote structural changes to centromeric chromatin in the absence of PLK1, which could be sufficient to trigger the initial stages of centromere deformation. However, the centromeric structural alterations that may occur during PLK1 inactivation and MT-spindle attachment remain unknown. Since RPA foci form in

these cells, centromeric DNAs are probably exposed by an active mechanism, which likely results in the formation of ssDNA. This could then promote centromere fragility. Consequently, centromere deformation may not be simply accredited to MT-spindle pulling forces, but additional influences must also be considered.

Chapter 5: Catalytic activity of BLM and PICH promote centromere deformation during PLK1 inactivation

5.1 Introduction

In previous chapters it was shown that mitotic PLK1 activity is required to suppress a centromere deformation pathway, which takes the form of centromeric pre-anaphase DNA threads and centromere specific chromatin breakage. It was established that centromere deformation develops through the co-action of microtubule spindle pulling forces and PLK1 inactivation. Therefore, it is predicted that PLK1 inactivation affects centromeric chromatin structure, which may cause a weakness to the centromere. This potential centromeric weakness is then exposed during mitotic spindle attachment and tension. Based on this prediction, it was necessary to investigate a mechanistic link between centromeric chromatin structural changes and PLK1 inactivation.

Initially, chromosome condensation was predicted to be affected when PLK1 activity became compromised. This was considered a strong candidate to explain the cause of centromere deformation during PLK1 inactivation. Chromosome compaction is achieved via the action of condensin complexes. This function of condensin is considered crucial for the correct assembly of mitotic chromosomes (Ono et al. 2003). It has also been reported that PLK1-dependent phosphorylation of condensin II (CAP-H2 subunit) is required to support the correct assembly of mitotic chromosomes during prophase (Kagami et al. 2017). Therefore, it could be predicted that in the absence of PLK1 activity, mitotic chromosome compaction may become compromised and in particular, at the centromere. This could lead to alterations to centromeric chromatin arrangement, thus promoting centromere fragility. Subsequently, centromeric chromatin may no longer be able to withstand MT-spindle pulling forces. Therefore, cells will display the centromere deformation phenotypes described (pre-anaphase DNA threads and centromere dislocation).

It has been shown that following the depletion of SMC2 (condensin complex), centromere elongation occurs, which resembles a form of centromere stretching (Samoshkin et al. 2009). This centromere stretching, after condensin depletion, could be considered similar to the early formation of pre-anaphase DNA threads during PLK1 inactivation. The same study also reported that centromere stretching after condensin depletion, can be suppressed during the addition of nocodazole, similarly to centromere deformation suppression during PLK1 inactivation. Therefore, based on these findings, it could be speculated that PLK1 functions in regulating condensin activity at the centromere to ensure centromere rigidity. Furthermore, it is anticipated that this rigidity is necessary to counteract MT-spindle pulling forces and facilitate the correct centromere structure during chromosome biorientation.

Other studies have also revealed that condensin depletion can lead to an increase in inter-kinetochore distance following microtubule spindle attachment (Gerlich et al. 2006; Ribeiro et al. 2009). Again, this supports the idea of a centromere-specific role for condensin to sustain centromere rigidity, especially during bipolar spindle attachment and tension. However, despite a probable function for condensin activity in supporting centromere rigidity, there remains a lack of evidence of chromatin rupture following depletion of condensin. This is in contrast to centromere deformation during PLK1 inactivation, where pre-anaphase DNA thread formation and centromere breakage is observed. PLK1 likely has multiple roles at the centromere in order to suppress centromere deformation, but a PLK1-dependent function in regulating condensin activity is worthy of future consideration as part of a centromeric PLK1 function.

In addition, given that centromeric pre-anaphase DNA thread formation is also linked to the recruitment of the ultra-fine DNA bridge (UFB)-binding complex and in particular PICH and BLM, it was predicted that the activity of these proteins may affect centromeric chromatin structure. Therefore, the role that the UFB-binding complex proteins plays in centromere deformation was investigated, with the aim to further explain how centromere deformation may arise during PLK1 inactivation.

The manifestation of UFBs results from DNA replication and repair activities, which can promote DNA entanglements, and these require resolution by the action of the UFB-binding complex (Fernández-Casañas and Chan 2018). Two of the principle UFB-binding factors, PICH and BLM, are required for UFB resolution (Baumann et al. 2007; Chan et al. 2007).

PICH is a member of the SNF2 family of DNA helicase-like proteins and has been shown to co-localise with PLK1 at kinetochores following NEBD during prophase (Baumann et al. 2007). A phospho-specific residue (T1063) in PICH supports an interaction between PICH and PLK1 (Ke et al. 2011). PICH acts as a DNA translocase and requires ATP binding and/or hydrolysis for its activity (Biebricher et al. 2013). This implies a catalytic function for PICH at DNA substrates. However, despite its initial discovery over 10 years ago and knowledge of its biochemical action, the precise function(s) of PICH remain enigmatic. One function of PICH is to support the recruitment of additional proteins at UFB structures (Hengeveld et al. 2015), particularly the BLM helicase.

BLM is a member of the RecQ family of DNA helicase proteins that is capable of unwinding DNA substrates with a 3'-5' directionality (Karow et al. 1997). A major function of BLM is in a unique HR-mediated dissolution pathway, during DNA replication and repair (Wu and Hickson 2003). BLM is also a prominent factor of the UFB-binding complex and displays a matching localisation pattern with PICH along anaphase UFB DNA linkages. Therefore, it is believed that BLM functions in combination with PICH, in the maintenance and resolution of UFB-structures. BLM helicase activity is probably necessary to unwind the ultra-fine DNA structure and aid in their resolution, although a precise mechanism remains uncertain. However, studies have shown that BLM helicase activity promotes UFB unwinding, which triggers the recruitment of another UFB-binding factor; the ssDNA binding protein RPA (Chan et al. 2018; Sarlós et al. 2018).

In this study, RPA foci formed at the centromeres of mitotic cells and co-treated with BI2536 and monastrol **(see previous Fig. 3.13b)**. Cells treated with monastrol have been shown to form monopolar spindle attachments, and therefore MT-spindle pulling forces are limited. RPA was not detected at centromeres of mitotic cells co-treated with BI2536 and nocodazole. This suggests that monopolar spindle attachment, alongside PLK1 inactivation (BI2536 and monastrol treatment), is sufficient to promote the recruitment of RPA to centromeres during mitosis.

This interesting observation was the basis for experiments aimed to uncover why centromeres encounter such severe deformation during PLK1 inactivation. During early mitosis, if PICH and BLM were to inadvertently target tension derived DNA substrates (such as centromeres), when PLK activity is absent, unsolicited processing of centromeric DNA may result. This would suggest a causative link between PLK1 inhibition and the action of the UFB-binding proteins, in particular PICH and BLM, in promoting centromere fragility and subsequent deformation.

This chapter will aim to explore a mechanistic link between centromere deformation during PLK1 inactivation and explain how the action of the UFB-binding complex promotes this unexpected centromere fragility. Specifically, after PLK1 inactivation, the careful analysis of mitotic cells reveals how both BLM and PICH are able to catalytically drive this unexpected centromere deformation.

5.2 Results

5.2.1 PLK1 suppresses the aberrant formation of PICH, BLM and RPA at centromeres during metaphase

It has recently been reported that phospho-RPA can be detected at the centromeres of unperturbed mitotic cells (Kabeche et al. 2018). In contrast, during the current study, RPA was largely undetectable at the centromeres of RPE1 cells during metaphase **(Fig. 5.1a, b)**. However, following the inhibition of PLK1 kinase, abundant levels of RPA foci formation were detected at the centromeres of metaphase cells, implying that ssDNA may be forming at the centromeres **(Fig. 5.1a, b, arrowheads)**. Thus, it was speculated that during PLK1 inactivation additional factors, such as the UFB-binding complex, may be responsible for this unexpected RPA foci formation at centromeres.

To investigate this idea further, the recruitment patterns of BLM helicase were examined during metaphase. BLM has been reported to be a centromere associating factor during mitosis (Rouzeau et al. 2012). However, during this study there was little evidence to suggest that BLM is an abundant centromere-associating protein during mitosis. BLM was shown to be largely undetectable at the centromeres of metaphase cells during unperturbed conditions **(Fig. 5.1c)**. In contrast, following PLK1 inhibition using BI2536, BLM foci were shown to be abundant at the centromeres of metaphase(-like) cells **(Fig. 5.1c, arrowheads)**. This implies that PLK1-inhibition can promote the aberrant recruitment of both RPA and BLM to centromeres.

By co-culturing wild-type RPE1 and RPE1 PLK1as cells, it was possible to determine whether the apparent increase in RPA at the centromeres was dependent on PLK1 activity, and not simply due to immunofluorescent staining variations between samples. As previously described, wild-type RPE1 cells are sensitive to the small-molecule inhibitor BI2536, but insensitive to the ATP-analogue 3-MB-PP1. In contrast, PLK1as cells are sensitive to 3-MB-PP1 and insensitive to BI2536 **(see previous Fig. 4.5)**. Therefore, by co-culturing the two cell types together and treating the cultures with either BI2536

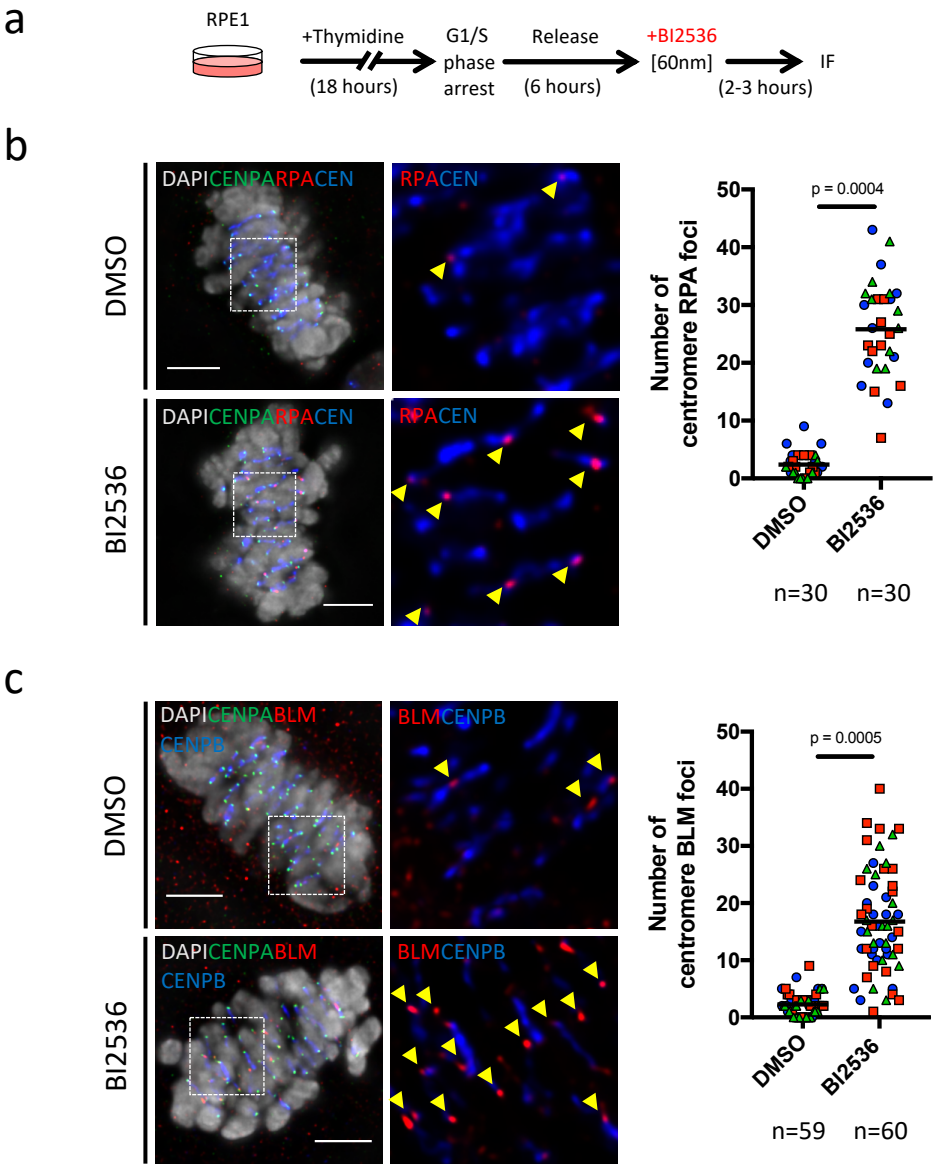

Figure 5.1. PLK1 inhibition promotes recruitment of BLM & RPA at the centromeres during metaphase.

a) Experimental outline of cell-synchronisation and immunofluorescent staining using RPE1 cells. **b)** Immunofluorescent images of metaphase(-like) RPE1 cells after either DMSO, or BI2536 treatment. Enlarged regions demonstrate the presence of RPA foci (arrows). Antibody staining for DAPI (Grey), CENPA (Green), RPA (Red) and centromeres (Blue). Quantification (right) of RPA foci at centromeres. **c)** Immunofluorescent images of metaphase(-like) RPE1 cells after either DMSO, or BI2536 treatment. Enlarged regions demonstrate the presence of BLM foci (arrows). Antibody staining for DAPI (Grey), CENPA (Green), BLM (Red) and CENPB (Blue). Quantification (right) of BLM foci at centromeres (overall mean is shown from three independent experiments; student t-test was used for p-value calculation; n=number of cells analysed; scale bar 5µm).

(targeting only the wild-type RPE1 cells), or 3-MB-PP1 (targeting only the PLK1as cells), it was possible to show that under the same coverslip, only the PLK1 kinase inhibited cells displayed a detectable increase in RPA at the centromeres. The two cell lines are distinguishable because the PLK1as protein is GFP-tagged, unlike the wildtype PLK1 protein. PLK1as cells could be distinguished from wildtype RPE1 cells, through the detection of GFP-PLK1as positive centrosomes **(see examples in Fig. 5.2b, arrows)**.

In agreement with previous findings, detailed examination of the co-culture cells showed that RPA foci formation is aberrantly increased at centromere regions only when PLK1 is inhibited **(Fig. 5.2a-c)**. Consistently, RPA foci was undetectable at centromeres in cells that maintained an active PLK1 kinase **(Fig. 5.2b, c)**. These results provide strong evidence to suggest that PLK1 inactivation leads to the aberrant recruitment of RPA at the centromeres of mitotic cells. This is possibly linked to the regulation of the UFB-binding complex proteins, most likely BLM helicase, due to its DNA unwinding capabilities.

Together with the aberrant recruitment of RPA and BLM at centromeres following PLK1 inhibition, PICH recruitment is also increased at centromeres. PICH is known to recruit to kinetochore/centromeres following NEBD (Baumann et al. 2007). Therefore, unlike with RPA and BLM, it was expected that PICH would be readily detectable at the centromeres. However, following treatment with BI2536, the intensity of centromeric PICH foci appeared to be increased at the centromeres when compared to cells with active PLK1. This suggests that PLK1 may influence the level of PICH recruitment to centromeres. To investigate this further, quantitative imaging was performed using the co-cultured system of RPE1-WT and PLK1as cells. PICH became more readily detectable at centromeres after the inactivation of PLK1 using BI2536 **(Fig. 5.3a-b)**. Furthermore, the fluorescence intensity of PICH focal formation at centromeres was also shown to be increased following PLK1 inhibition **(Fig. 5.3c)**. This implied that PLK1 may negatively regulate the level of PICH recruitment to centromeres, and in its absence, more PICH molecules are loaded to the centromeres following NEBD.

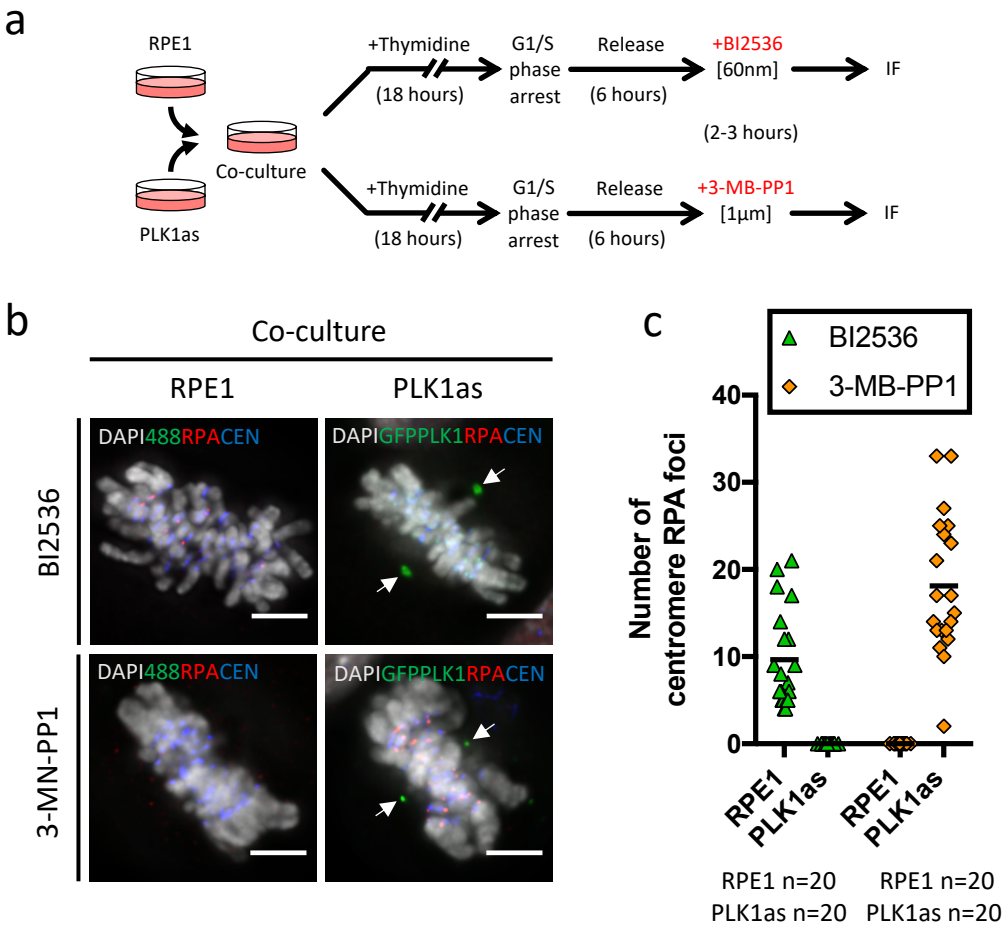

Figure 5.2. PLK1 kinase suppresses aberrant recruitment of RPA at the centromere during metaphase.

a) Experimental outline of cell-synchronisation and immunofluorescent staining, using co-cultures of wild-type RPE1 and GFP-PLK1as cells. **b)** Immunofluorescent images of metaphase(-like) wild-type RPE1 and PLK1as cells, after either BI2536, or 3-MB-PP1 treatment. Positive GFP-PLK1 detection of centrosomes (arrows) distinguish PLK1as cells from wild-type RPE1 cells. Antibody staining for DAPI (Grey), GFP-PLK1 (Green), RPA (Red) and centromeres (Blue). **c)** Quantification of RPA foci at centromeres of metaphase(-like) cells after indicated inhibitor treatment (overall mean is shown; n=number of cells analysed; scale bar 5µm).

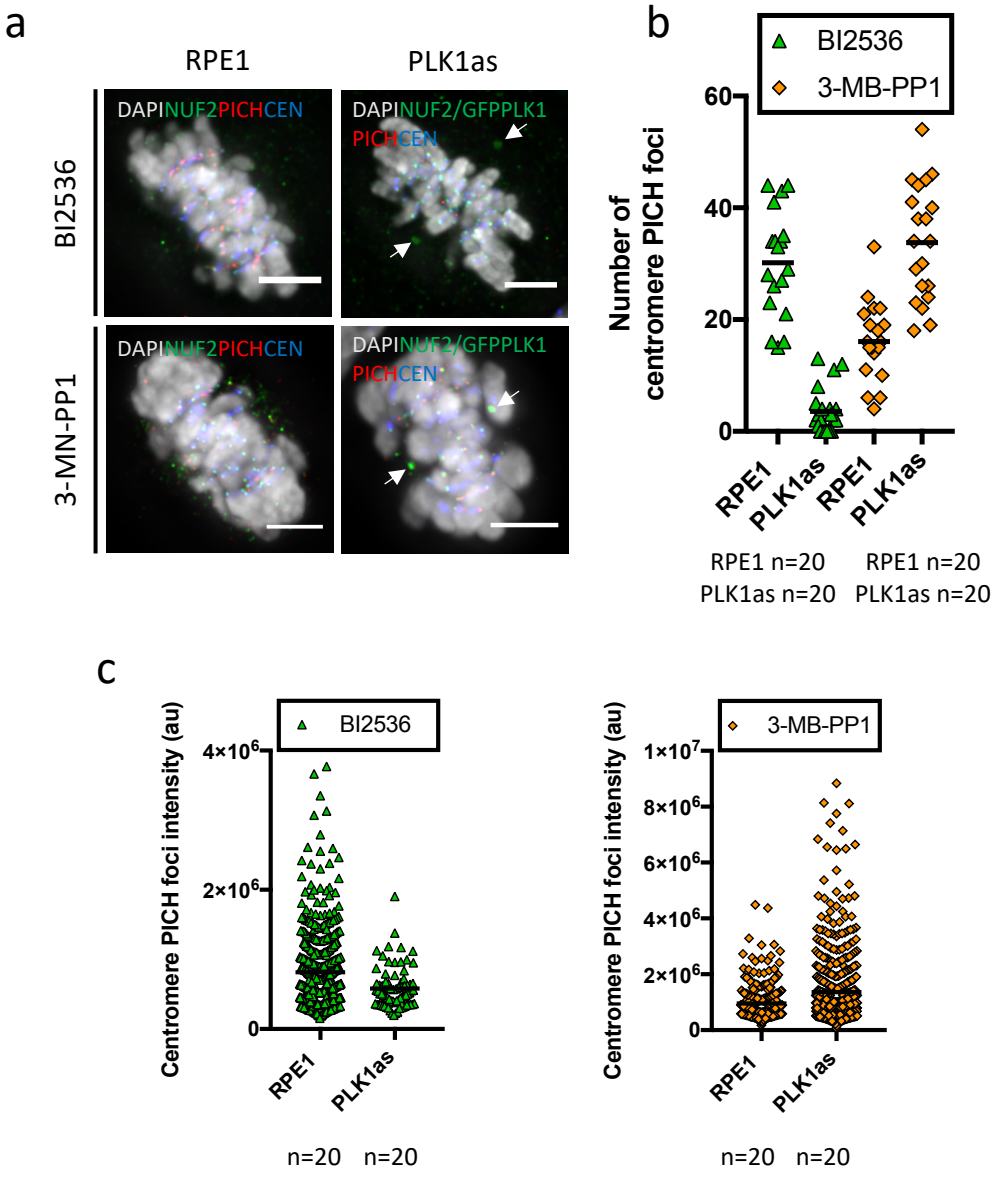

Figure 5.3. PLK1 kinase may limit the loading of PICH at the centromere during metaphase.

a) Immunofluorescent images of metaphase(-like) wild-type RPE1 and PLK1as cells, after either BI2536; or 3-MB-PP1 treatment. Cells were co-cultured and positive GFP-PLK1 detection of centrosomes (arrows) distinguished PLK1as cells from wild-type RPE1 cells. Antibody staining for DAPI (Grey), NUF2 & GFP-PLK1 (Green), PICH (Red) and centromeres (Blue). **b)** Quantification of PICH foci at centromeres of metaphase(-like) cells after indicated inhibitor addition. **c)** Quantification of PICH foci intensity at centromeres of metaphase(-like) cells after BI2536 (left), or 3-MB-PP1 (right) (overall mean is shown; n=number of cells analysed; scale bar 5μm).

Based on these findings, it was speculated that PLK1 activity is required to regulate the recruitment of BLM and PICH at the centromere during mitosis, either directly or indirectly. In addition, it also suggested that BLM activity and possibly PICH, may be responsible for the physical unwinding of centromeric DNA at the centromeres, when PLK1 activity is compromised.

This hypothesis may explain why RPA becomes readily detectable at centromeres during PLK1 inactivation. Unsolicited DNA unwinding at the centromere, due to the aberrant recruitment and activity of BLM and PICH during PLK1 inactivation, may promote centromeric ssDNA formation. This could trigger the loading of RPA for its protection, explaining why RPA is detected at centromeres following PLK1 inhibition. Further experiments were required to test this theory. Additional factors such as MT-spindle tension, together with PLK1 inactivation, should not be overlooked, as they may also be the basis for the aberrant recruitment of RPA and BLM at centromeres.

5.2.2 MT-spindle tension promotes aberrant RPA foci formation at the centromere during PLK1 inhibition

The formation of pre-anaphase DNA threads and centromere breaks during PLK1 inhibition were shown to be dependent on bipolar spindle attachment and MT-tension **(see previous Figs. 3.12 & 3.13)**. Hence, it was predicted that RPA foci formation at the centromere could also be dependent on MT-tension, during the inactivation of PLK1.

To investigate this idea, individual mitotic cells were examined for centromere associated RPA recruitment following BI2536 treatment. Each distinct mitotic stage from prophase to metaphase was analysed and both RPA foci number and fluorescence intensity was recorded. Finally, an additional sample was prepared, which was subject to the co-treatment of both BI2536 and the MT-poison, nocodazole. This would help to

determine whether PLK1 activity and MT-spindle tension are both required for the aberrant formation of RPA at the centromere.

Following cell synchronisation and treatment with BI2536 **(Fig. 5.4a)**, RPA foci formation at the centromeres of mitotic cells was consistent with previous findings. The RPA foci was shown to increase in both number and fluorescence intensity as cells progressed from prophase to metaphase **(Fig. 5.4b-d)**. This could suggest that during PLK1 inactivation, the increasing MT-tension from prophase to metaphase, enhanced the aberrant recruitment of RPA. Abolishing MT-tension by co-treatment of BI2536 and nocodazole led to both a significantly reduced number of RPA foci and fluorescent intensity at their centromeres **(Fig. 5.4b-d)**. This suggested that the reduction in RPA foci following the co-treatment of BI2536 and nocodazole, is most likely due to a lack of spindle attachment and therefore tension.

The same experimental method was used to examine whether the reported increase in PICH loading to centromeres during PLK1 inhibition was also dependent on MT-spindle tension **(Fig. 5.5a)**. PICH foci formation was apparent at the centromeres of mitotic cells and displayed an increasing loading fashion from prophase to metaphase **(Fig. 5.5b-d)**. Both the number of PICH foci and the fluorescent intensity of centromeric PICH was shown to peak during metaphase. However, following co-treatment with BI2536 and nocodazole, PICH foci number and intensity showed no significant change **(Fig. 5.5b-d)**. Therefore, PICH loading to centromeres, during PLK1 inactivation, is unlikely to be enhanced by MT-spindle pulling forces. Instead, the increasing level of detection of PICH at centromeres during mitosis is most likely due to the increased accessibility of PICH to mitotic chromatin, following NEBD during prophase.

It was also possible to examine whether MT-attachment alone was sufficient for the aberrant recruitment of RPA, during PLK1 inhibition. Nocodazole treatment should generate an absence of KT-MT attachments. Therefore, although spindle pulling forces would be abolished during nocodazole treatment, this treatment is unable to disprove

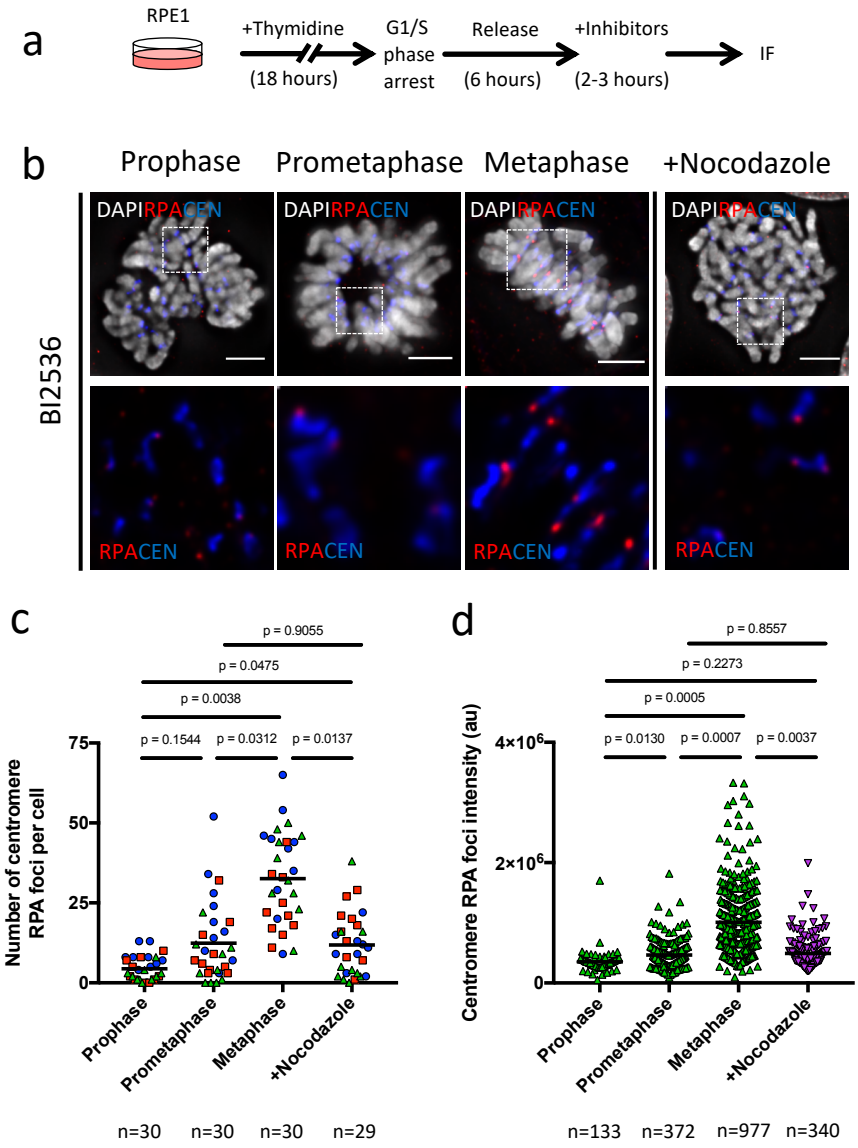

Figure 5.4. The aberrant recruitment of RPA after PLK1 inhibition is dependent on spindle-pulling forces.

a) Experimental outline of cell-synchronisation and immunofluorescent staining using RPE1 cells. **b)** Immunofluorescent images of mitotic RPE1 cells after BI2536 treatment; or BI2536 plus Nocodazole. Antibody staining for DAPI (Grey), RPA (Red) and centromeres (Blue). Enlarged regions highlight centromeres with RPA foci (scale bar 5μm). **c)** Quantification of RPA foci number (left) at centromeres of different mitotic stages during BI2536 treatment; plus, after addition of BI2536 and Nocodazole (different colours indicate each experiment; n=number of cells analysed; overall mean is shown from three independent experiments; student t-test was used for p-value calculation). **d)** Quantification of RPA foci intensity (right) at centromeres of different mitotic stages during BI2536 treatment; plus, after addition of BI2536 and Nocodazole (n=number of RPA foci analysed; overall mean is shown from three independent experiments; student t-test was used for p-value calculation).

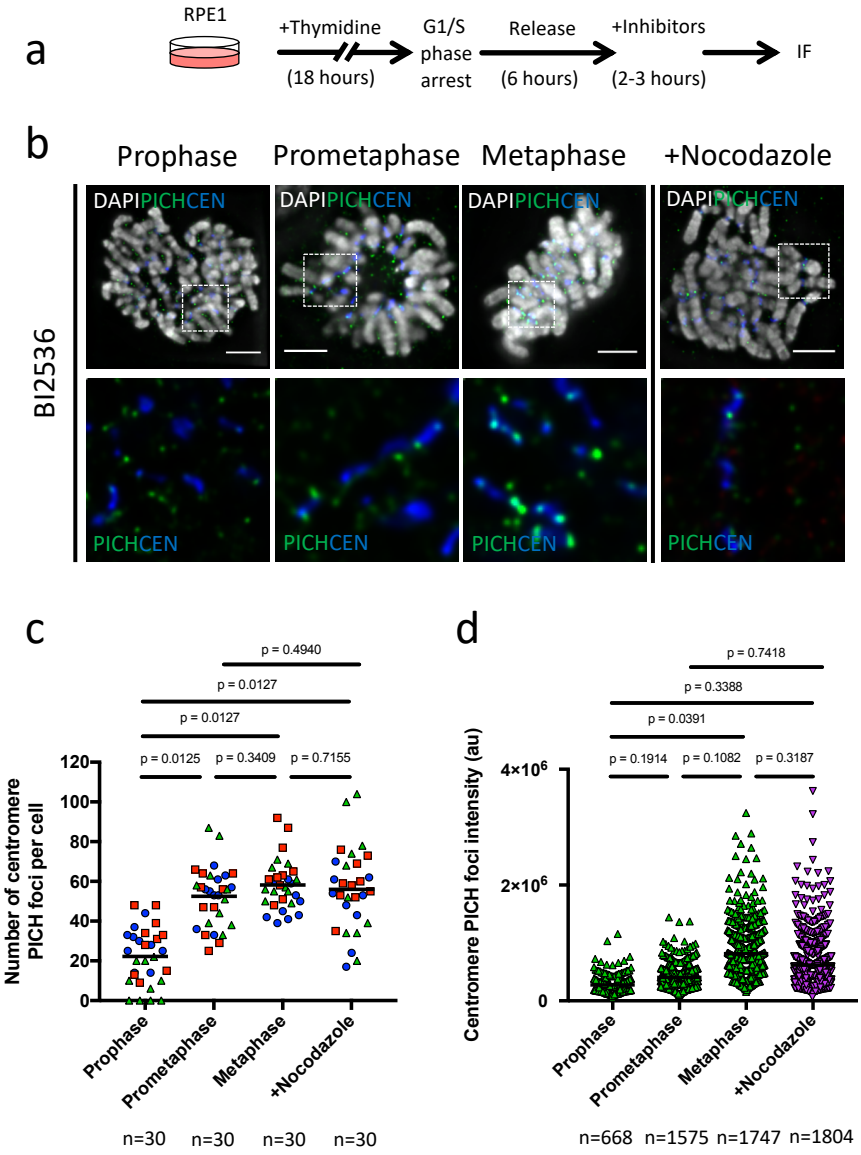

Figure 5.5. The aberrant loading of PICH during PLK1 inhibition is independent on spindle-pulling forces.

a) Experimental outline of cell-synchronisation and immunofluorescent staining using RPE1 cells. **b)** Immunofluorescent images of mitotic RPE1 cells after BI2536 treatment; or BI2536 and Nocodazole. Antibody staining for DAPI (Grey), PICH (Green) and centromeres (Blue). Enlarged regions highlight centromeres with PICH foci. **c)** Quantification of PICH foci number (left) at centromeres of different mitotic stages during BI2536 treatment; plus, after addition of BI2536 and Nocodazole (different colours indicate each experiment; n=number of cells analysed). **d)** Quantification of PICH foci intensity (right) at centromeres of different mitotic stages during BI2536 treatment; plus, after addition of BI2536 and Nocodazole (n=number of PICH foci analysed; overall mean is shown from three independent experiments; student t-test was used for p-value calculation; scale bar 5μm).

the theory that MT-attachment alone may promote centromere deformation during PLK1 inactivation. Therefore, in order to determine whether MT-attachment alone was sufficient to promote the aberrant formation of RPA at centromeres during PLK1 inactivation, mitotic cells were co-treated with BI2536 and monastrol. Consistent with earlier findings, metaphase cells treated with BI2536 displayed clear signs of RPA foci formation at their centromeres **(Fig.5.6a-d)**. Following the co-treatment of BI2536 and monastrol, mitotic cells displayed both a similar overall number and intensity of RPA foci, as cells treated with BI2536 alone **(Fig.5.6a-d)**. In contrast, RPA foci number and fluorescent intensity were both significantly reduced in samples co-treated with BI2536, monastrol and nocodazole, compared to both BI2536 alone, and BI2536 plus monastrol cells **(Fig.5.6a-d)**.

Overall, these data would suggest that mitotic spindle attachment, bipolar or monopolar attachment, during the inactivation of PLK1, promotes the aberrant recruitment of RPA at the centromere. Thus, KT-MT attachment may alter the DNA architecture at the centromere and by doing so, cause BLM to target centromeric DNA, when PLK1 activity is compromised. This idea could begin to explain how centromere deformation originates.

5.2.3 BLM promotes centromere deformation during PLK1 kinase inhibition

The current data would support the suggestion that PLK1 kinase activity functions to suppress the unsolicited unwinding of centromeric DNA, possibly through the regulation of BLM helicase. This prediction is based on data that show that aberrant levels of BLM foci are detected at centromeres during metaphase, when PLK1 is inactivated. Centromeric BLM localisation may promote centromeric DNA unwinding, which could lead to pre-anaphase DNA thread formation during bipolar spindle pulling. Therefore, the depletion of BLM by RNA interference (RNAi) was predicted to abolish centromere deformation, caused by inhibition of PLK1 activity.

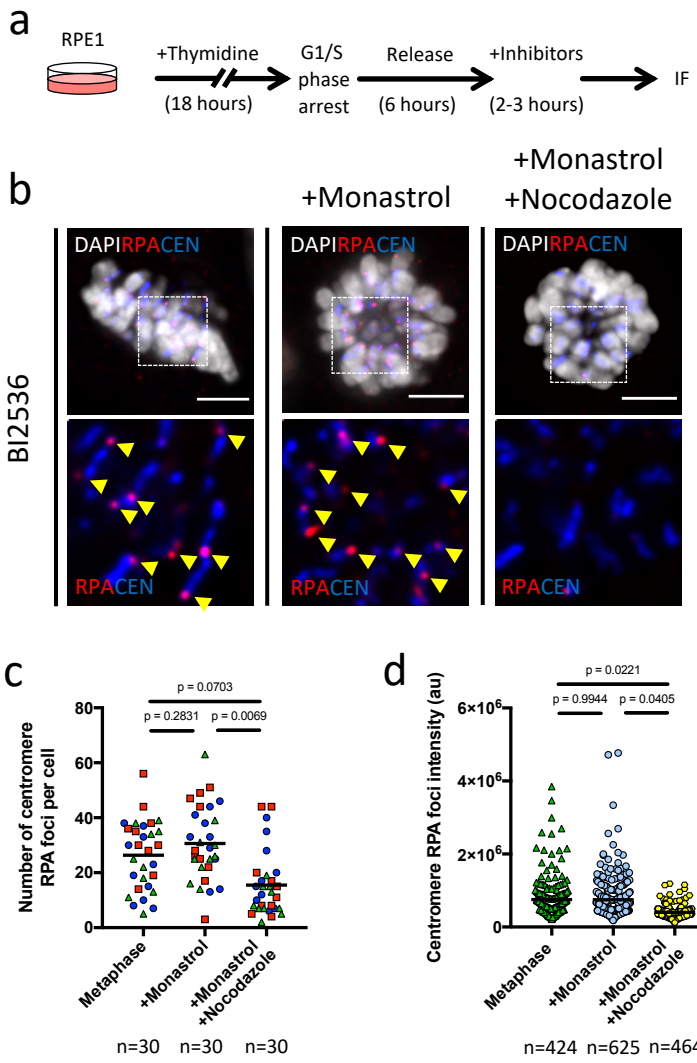

Figure 5.6. KT-MT attachment promotes the aberrant recruitment of RPA at the centromere during PLK1 inhibition.

a) Experimental outline of cell-synchronisation and immunofluorescent staining using RPE1 cells. **b)** Immunofluorescent images of mitotic RPE1 cells after BI2536 treatment (Metaphase), BI2536 and Monastrol, or BI2536, Monastrol and Nocodazole. Antibody staining for DAPI (Grey), RPA (Red) and centromeres (Blue). Enlarged regions highlight centromeres with RPA foci (arrowheads) (scale bar 5μm). **c)** Quantification of RPA foci number (left) at centromeres of different mitotic stages during BI2536 treatment, plus, after addition of Monastrol, and Monastrol plus Nocodazole (different colours indicate each experiment; n=number of cells analysed; overall mean is shown from three independent experiments; student t-test was used for p-value calculation). **d)** Quantification of RPA foci intensity (right) at centromeres of different mitotic stages during BI2536 treatment; plus, after addition of Monastrol, and Monastrol plus Nocodazole (n=number of RPA foci analysed; overall mean is shown from three independent experiments; student t-test was used for p-value calculation).

Initial experiments with siRNA-mediated depletion of BLM for greater than 24 hours, prevented RPE1 cells from entering mitosis. This was predicted to be due to an increase in replicative stress during cell synchronisation using thymidine, which may require BLM activity to overcome this. BLM is required for replication fork restart and recovery, in particular during conditions of replicative stress (Davies et al. 2007). Therefore, BLM depletion, combined with the addition of thymidine, may generate levels of replicative stress that require BLM for effective recovery of replication fork restart. To overcome this, BLM was only partially depleted in RPE1 cells (less than 24 hours), whilst also synchronising the cells at the G1/S border using thymidine **(Fig. 5.7a)**.

The limited depletion time was sufficient to significantly reduce the level of BLM protein, as judged by protein level following western blot analysis **(Fig. 5.7b)**. Crucially, BLM depleted cells displayed a significant reduction in the formation of pre-anaphase DNA threads during BI2536 treatment, when compared to control cells **(Fig. 5.7c)**. In addition, BLM depletion was also shown to suppress centromere breakage, despite the inhibition of PLK1 **(Fig. 5.7d)**. Therefore, these results suggest that BLM is responsible for centromere deformation when PLK1 activity is compromised.

Moreover, BLM depletion was also shown to significantly reduce the number of detectable centromeric RPA foci during metaphase, when compared against control cells during BI2536 treatment **(Fig. 5.8a)**. It is also worth noting that despite a depletion of BLM, metaphase cells remained positive for PICH protein localisation, demonstrating that the depletion of BLM does not disrupt PICH recruitment **(Fig. 5.8b)**.

Together, these data strongly support the idea that BLM participates in centromere deformation during PLK1 inactivation. However, additional influences and/or factors, including PICH, may also be responsible.

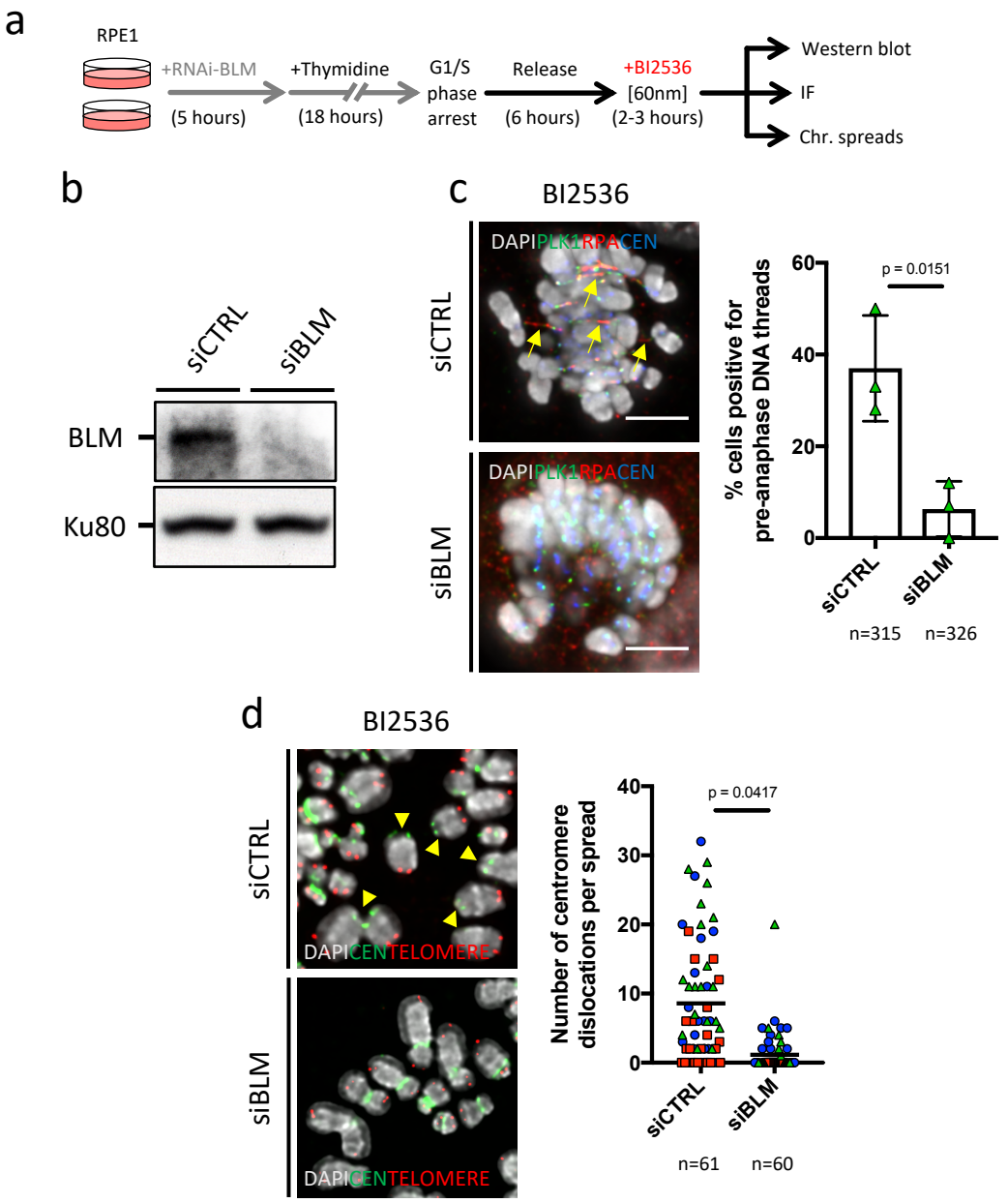

Figure 5.7. BLM-helicase promotes centromere deformation during PLK1 inhibition.
a) Experimental outline of RNAi during cell-synchronisation, western blot analysis, immunofluorescent staining and ctFISH, using RPE1 cells. **b)** Western blot analysis using anti-BLM antibody, showing wild-type BLM levels (siCTRL) and depletion (siBLM) after RNAi. Anti-KU80 was used as a loading control. **c)** Immunofluorescent images of pre-anaphase DNA threads (arrows) in RPE1 cells after either siCTRL, or siBLM, during BI2536 treatment. Antibody staining for DAPI (Grey), PLK1 (Green), RPA (Red) and centromeres (Blue). Quantification shows the percentage of cells positive for pre-anaphase DNA threads after RNAi and during PLK1 inhibition using BI2536 (mean ±SD is shown from three independent experiments). **d)** Chromosome spread and ctFISH images of centromere dislocations (arrowheads) in RPE1 cells after either siCTRL, or siBLM during BI2536 treatment. DAPI (Grey) was used to stain chromosomes, specific PNA FISH probes were used for centromere (Green) and telomere (Red) detection. Quantification of centromere dislocations after RNAi and during PLK1 inhibition using BI2536 (overall mean is shown from three independent experiments; student t-test was used for p-value calculation; n=number of cells analysed; scale bar 5µm; Tomisin Olukoga completed an experimental replicate of both pre-anaphase DNA thread and centromere dislocation analysis).

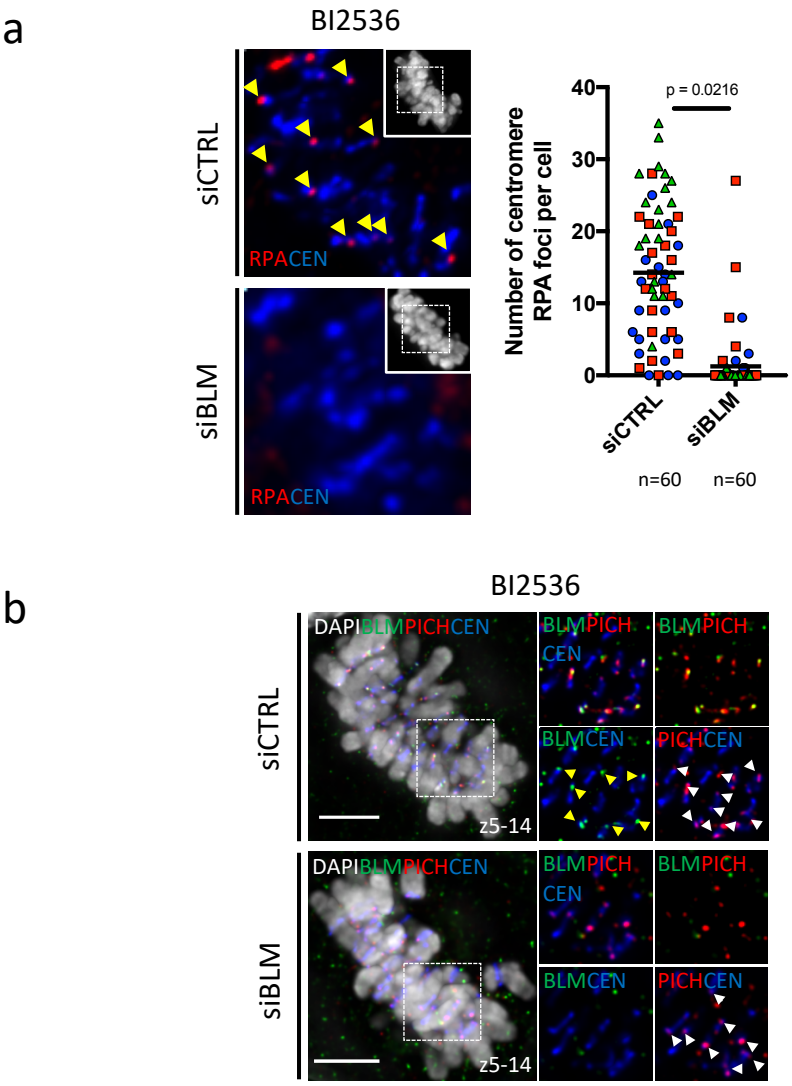

Figure 5.8. The aberrant loading of RPA at centromeres is dependent on BLM during PLK1 inhibition.

a) Immunofluorescent images of RPA foci (arrowheads) at centromeres of metaphase(-like) RPE1 cells after RNAi of either siCTRL, or siBLM during BI2536 treatment. Antibody staining for DAPI (Grey), RPA (Red) and centromeres (Blue). Quantification shows the number of RPA foci at centromeres after RNAi and during PLK1 inhibition, using BI2536 (overall mean is shown from three independent experiments; student t-test was used for p-value calculation; n=number of cells analysed). **b)** Immunofluorescent images of PICH (white arrowheads) and BLM (yellow arrowheads) foci at centromeres of metaphase(-like) RPE1 cells after RNAi of either siCTRL, or siBLM during BI2536 treatment. Antibody staining for DAPI (Grey), BLM (Green), PICH (Red) and centromeres (Blue) (scale bar 5μm).

5.2.4 PICH acts upstream of BLM during centromere deformation

In order to investigate whether PICH was also responsible for promoting centromere deformation during PLK1 inhibition, siRNA targeting of PICH was also performed **(Fig. 5.9a, b)**. Cells depleted of PICH showed an almost complete absence of pre-anaphase DNA thread formation following BI2536 treatment **(Fig. 5.9c)**, whilst the frequency of centromere dislocations were also significantly reduced **(Fig. 5.9d)**.

In addition, similar to results observed after the depletion of BLM, PICH depletion also led to a significant reduction in the number of RPA foci at the centromere of metaphase cells **(Fig. 5.10a)**. This initially implied that along with BLM recruitment, PICH may also be responsible for the formation of RPA at the centromere. However, following the depletion of PICH, BLM became virtually undetectable at the centromeres of metaphase cells **(Fig. 5.10b)**. Therefore, it is likely that PICH acts upstream of BLM, and in its absence, BLM can no longer bind to centromeres during PLK1 inhibition.

These data strongly imply that PLK1 kinase functions to suppress centromere deformation, by preventing the untimely recruitment and/or activity of mitotic BLM, and/or PICH.

5.2.5 PLK1 activity protects against PICH/BLM-dependent metaphase collapse

Since PICH and BLM were identified as key drivers for centromere deformation during PLK1 inhibition, it was predicted that their depletion may suppress metaphase collapse, even in the absence of PLK1 activity. Therefore, to test this theory, live-cell time lapse microscopy was performed to assess the total duration of metaphase stage in RPE1 cells, depleted of either PICH or BLM by RNAi, during treatment with BI2536 **(Fig. 5.11a)**.

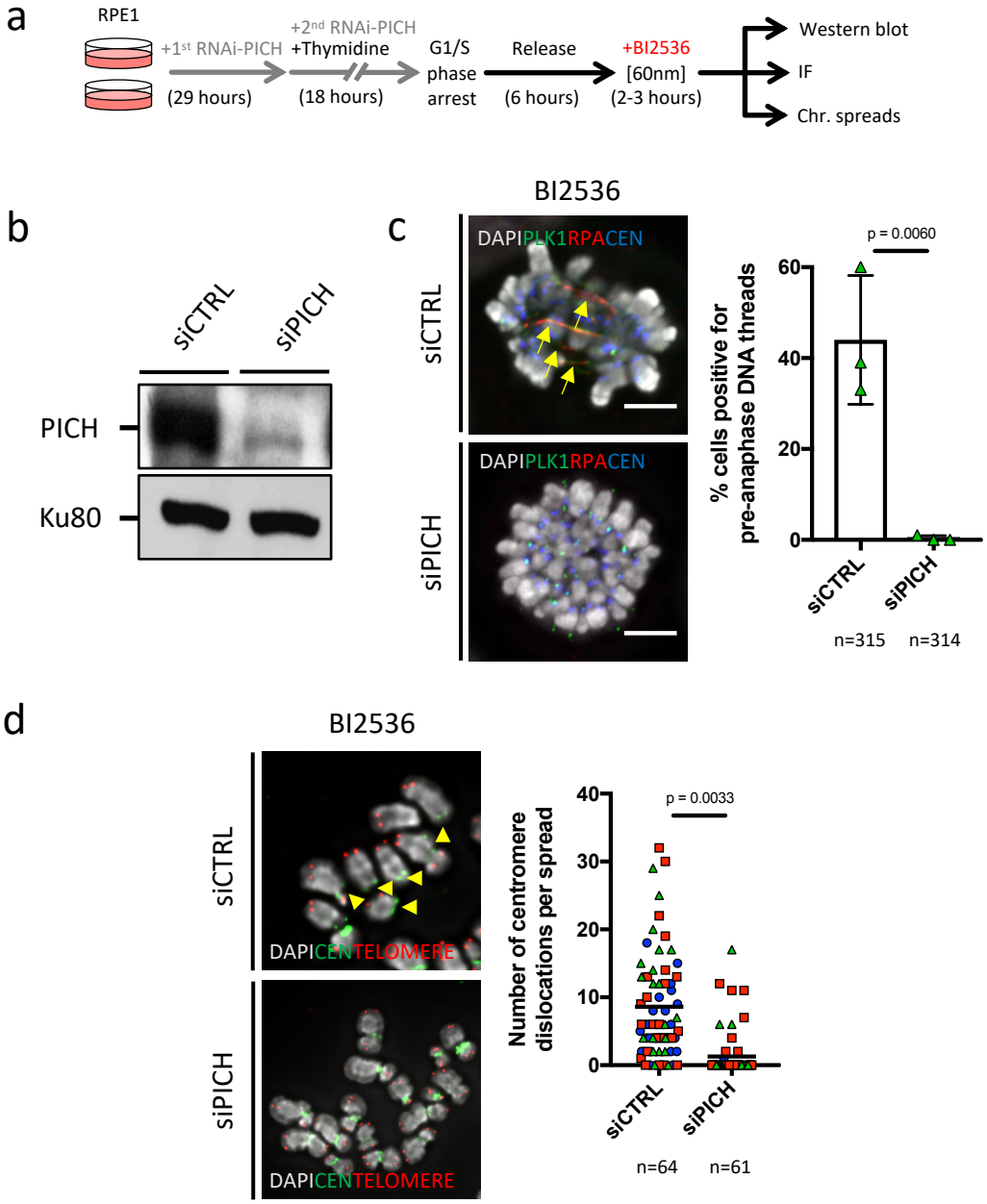

Figure 5.9. PICH promotes centromere deformation during PLK1 inhibition.
a) Experimental outline of RNAi during cell-synchronisation, western blot analysis, immunofluorescent staining and ctFISH, using RPE1 cells. **b)** Western blot analysis using anti-PICH antibody showing wild-type PICH levels (siCTRL) and depletion (siPICH) after RNAi. Anti-KU80 was used as a loading control. **c)** Immunofluorescent images of pre-anaphase DNA threads (arrows) in RPE1 cells after either siCTRL, or siPICH during BI2536 treatment. Antibody staining for DAPI (Grey), PLK1 (Green), RPA (Red) and centromeres (Blue). Quantification shows the percentage of cells positive for pre-anaphase DNA threads after RNAi and during PLK1 inhibition using BI2536 (mean ±SD is shown from three independent experiments). **d)** Chromosome spread and ctFISH images of centromere dislocations (arrowheads) in RPE1 cells after either siCTRL, or siPICH during BI2536 treatment. DAPI (Grey) was used to stain chromosomes, specific PNA FISH probes were used for centromere (Green) and telomere (Red) detection. Quantification of centromere dislocations after RNAi and during PLK1 inhibition using BI2536 (overall mean is shown from three independent experiments; student t-test was used for p-value calculation; n=number of cells analysed; scale bar 5μm; Tomisin Olukoga completed an experimental replicate of both pre-anaphase DNA thread and centromere dislocation analysis).

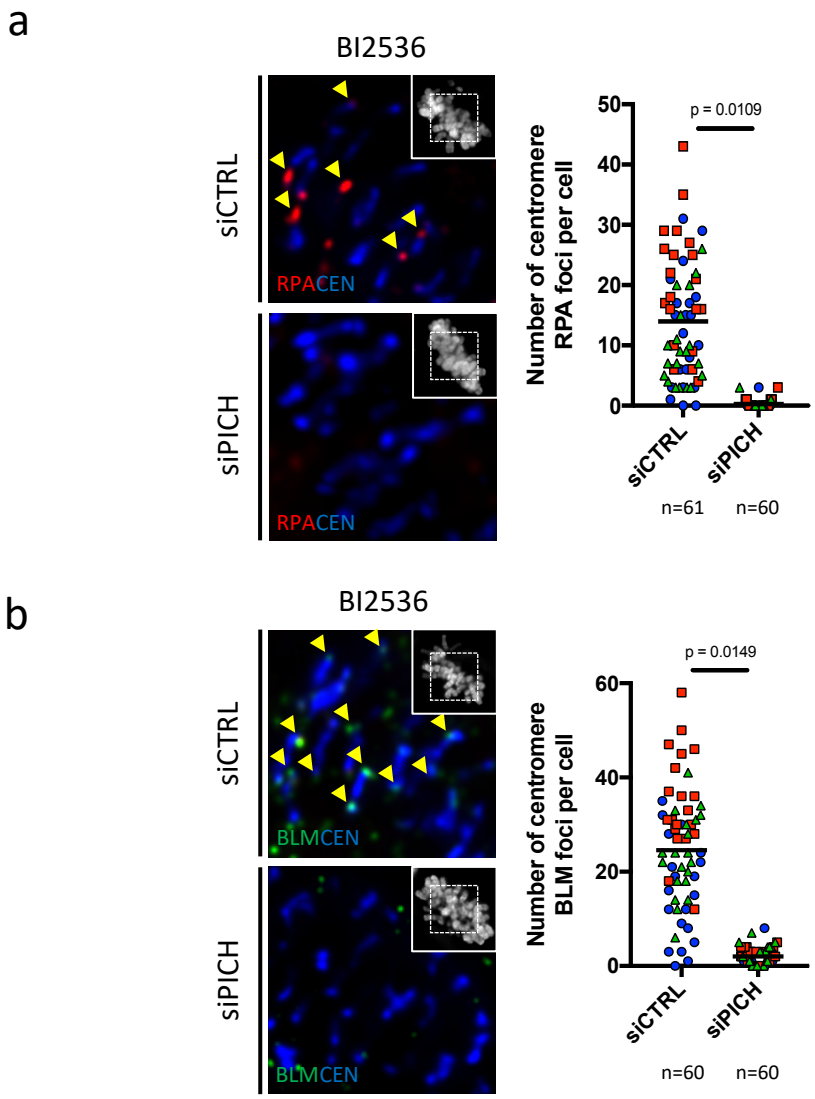

Figure 5.10. PICH functions upstream of BLM during centromere deformation when PLK1 is absent.

a) Immunofluorescent images of RPA foci (arrowheads) at centromeres of metaphase(-like) RPE1 cells after RNAi of either siCTRL, or siPICH during BI2536 treatment. Antibody staining for DAPI (Grey), RPA (Red) and centromeres (Blue). Quantification shows the number of RPA foci at centromeres after RNAi and during PLK1 inhibition, using BI2536. **b)** Immunofluorescent images of BLM foci (arrowheads) at centromeres of metaphase(-like) RPE1 cells after RNAi of either siCTRL, or siPICH, and BI2536 treatment. Antibody staining for DAPI (Grey), BLM (Green) and centromeres (Blue) (overall mean is shown from three independent experiments; student t-test was used for p-value calculation; n=number of cells analysed; scale bar 5μm).

Results showed that metaphase durations were extended in both PICH and BLM depleted cells treated with BI2536, when compared against control cells **(Fig. 5.11b, c)**. This supports the suggestion that centromeres are capable of counteracting MT-spindle pulling forces when PICH or BLM are absent, even if PLK1 activity is compromised.

To further confirm the RNAi results, a knockout BLM cell line (HAP1 ΔBLM) was also investigated for centromere deformation phenotypes, during PLK1 inhibition (Hengeveld et al. 2015). Western blot analysis confirmed the absence of BLM protein expression in ΔBLM cells, when compared against the parental cells (HAP1) **(Fig. 5.12a, b)**.

To investigate centromere deformation phenotypes, cell synchronisation by thymidine block and release were performed as before, and cells were then subject to BI2536 treatment. The parental HAP1 cells showed pre-anaphase DNA thread formation during BI2536 treatment, albeit at a lower frequency (25-30%) when compared to RPE1 cells (50-70%) **(Fig. 5.12c; compared with Fig. 3.5b)**. This variation is consistent with the variation seen in HCT116 and 82-6 hTERT cells **(see previous Fig. 3.7c),** and may reflect a different dependency of PLK1 activity between various cell types.

In contrast, ΔBLM cells showed no signs of pre-anaphase DNA thread formation, following the analysis of mitotic cells during BI2536 treatment **(Fig. 5.12c)**, supporting the BLM depletion results. Additionally, centromere dislocations were almost completely absent in the ΔBLM cells, whilst the parental HAP1 cells showed a significant number of centromere dislocations per spread analysed **(Fig. 5.12d)**. The ΔBLM cells also showed low levels of centromeric and arm breakage, along with the formation of dicentric chromosomes **(Fig. 5.12d)**; reflecting the unstable nature of the cell line. Overall, these results further support the hypothesis that BLM is responsible for driving centromere deformation during mitosis, when PLK1 activity is absent.

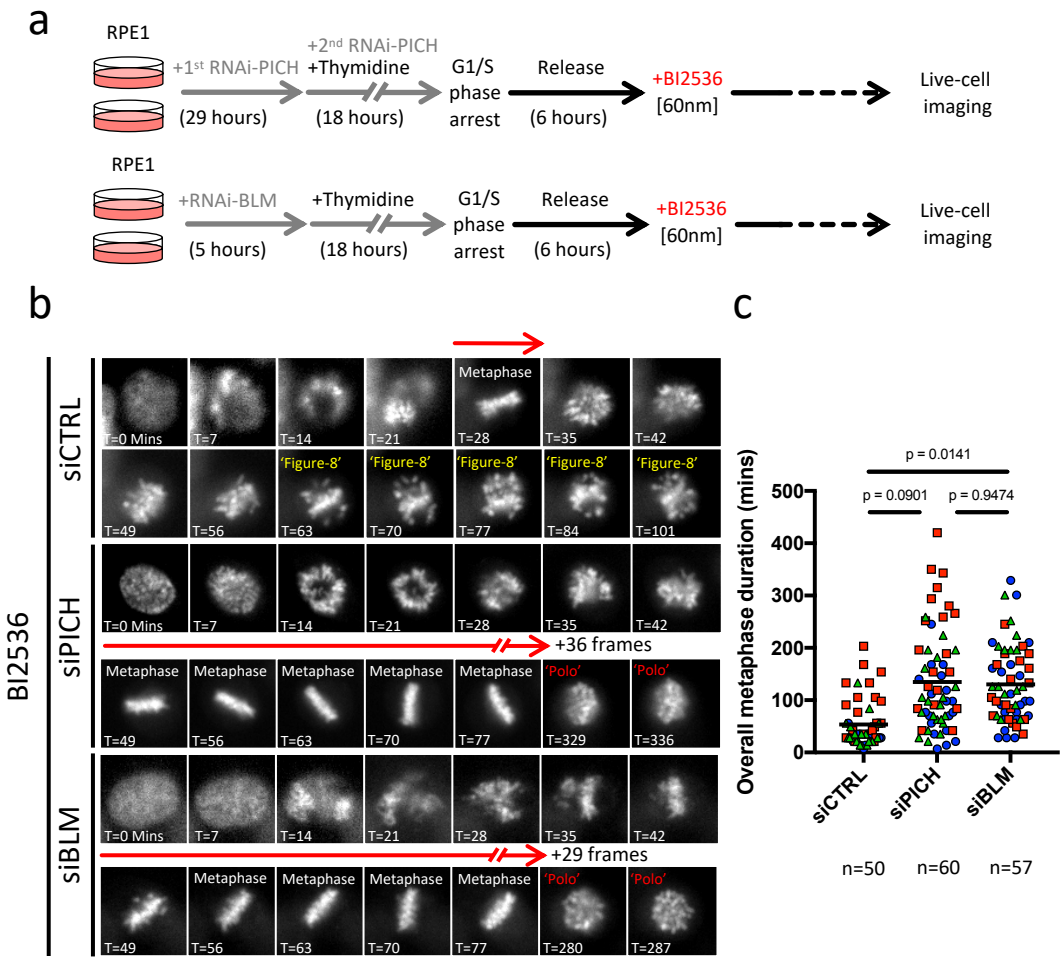

Figure 5.11. Both PICH & BLM promote metaphase collapse during PLK1 inhibition.
a) Experimental outline of RNAi during cell-synchronisation and live-cell time-lapse microscopy, using RPE1 cells. **b)** Examples of live-cell time lapse microscopy image stills after indicated RNAi and BI2536 treatment. Metaphase(-like) durations are indicated by red arrows. Metaphase collapse is indicated by either 'figure-8' or 'polo'-like morphology. **c)** Quantification of the overall duration of metaphase(-like) alignment after indicated RNAi and BI2536 treatment (overall mean is shown from three independent experiments; student t-test was used for p-value calculation; n=number of cells analysed; Tomisin Olukoga completed an experimental replicate of siCTRL, siPICH and siBLM analysis).

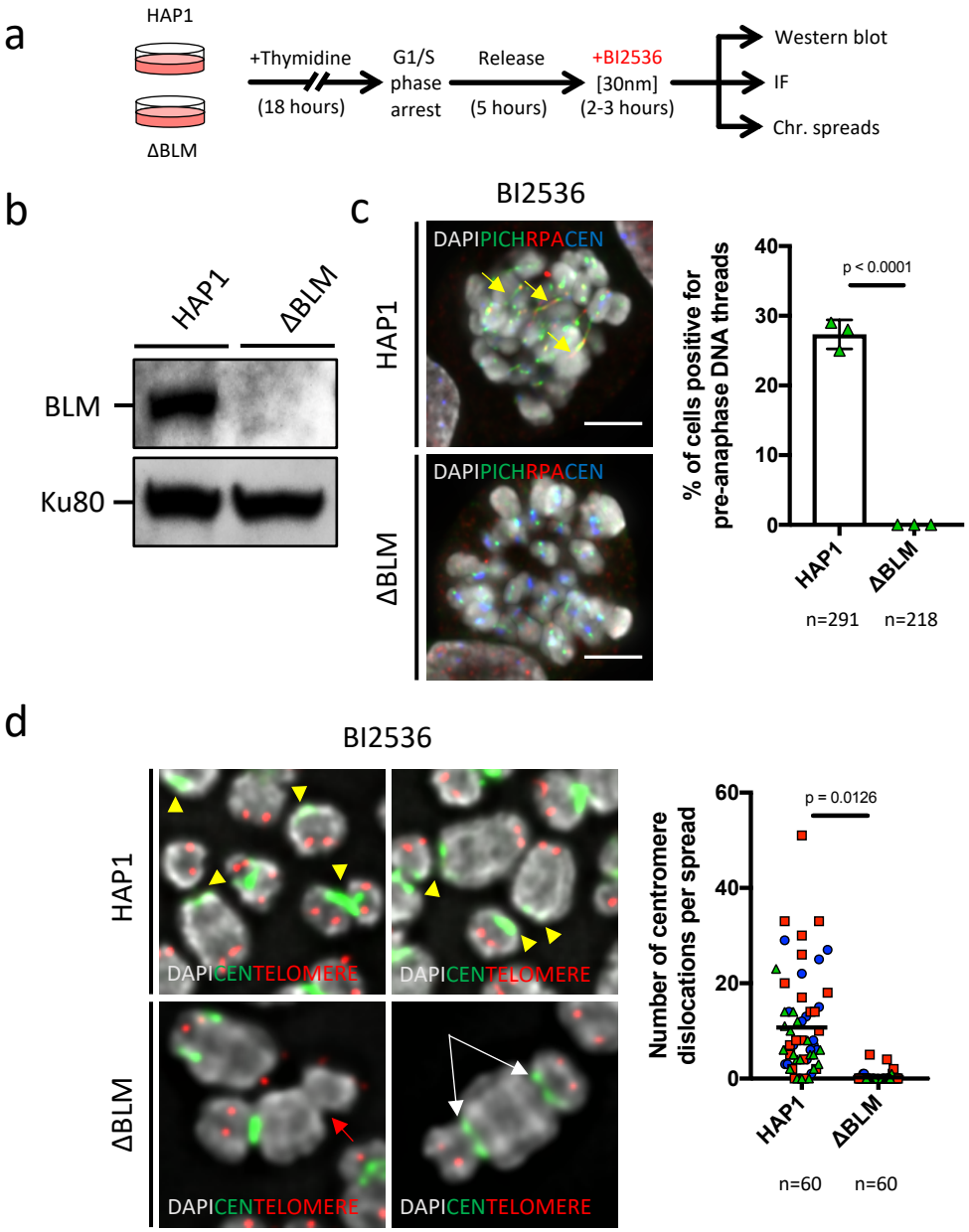

Figure 5.12. BLM promotes centromere deformation during PLK1 inhibition.
a) Experimental outline of cell-synchronisation, western blot analysis, immunofluorescent staining and ctFISH, using HAP1 (wild-type) and knockout BLM (ΔBLM) cells. **b)** Western blot image using anti-BLM antibody showing wild-type BLM levels (HAP1) and absence of BLM detection (ΔBLM) in knockout cells. Anti-KU80 was used as a loading control. **c)** Immunofluorescent images of pre-anaphase DNA threads (arrows) in HAP1 and ΔBLM cells after BI2536 treatment. Antibody staining for DAPI (Grey), PICH (Green), RPA (Red) and centromeres (Blue). Quantification shows the percentage of cells positive for pre-anaphase DNA threads after PLK1 inhibition using BI2536 (mean ±SD is shown from three independent experiments). **d)** Chromosome spread and ctFISH images of centromere dislocations (arrowheads) in HAP1 and ΔBLM cells after BI2536 treatment. Arm breaks (red arrow) and dicentric chromosomes (white arrows) were detected in ΔBLM cells. DAPI (Grey) was used to stain chromosomes, specific PNA FISH probes were used for centromere (Green) and telomere (Red) detection. Quantification of centromere dislocations after BI2536 addition (overall mean is shown from three independent experiments; student t-test was used for p-value calculation; n=number of cells analysed; scale bar 5μm).

5.2.6 BLM helicase activity actively unwinds centromeric DNA during PLK1 inhibition

To test if centromere deformation during PLK1 inactivation was due to the catalytic activity of BLM, the HAP1 ΔBLM cells were complemented with a GFP-tagged wildtype BLM, or a helicase-dead (Q672R) mutant. Initially, protein expression was confirmed in both the complemented cell lines using western blot analysis **(Fig. 5.13a).** In addition, it was also shown that following HU treatment, both cell lines displayed recruitment of GFP-BLM at sites of replication, colocalising with RPA; a known cellular response marker to replicative stress **(Fig. 5.13b)** (Ouyang et al. 2013).

Next the requirement for BLM helicase activity to induce centromere deformation was tested. Each cell line was synchronised as before and examined for their ability to form pre-anaphase DNA threads, during BI2536 treatment **(Fig. 5.14a)**. The expression of a wild-type copy of BLM (GFP-BLM) in the ΔBLM cells; which did not previously exhibit pre-anaphase DNA thread formation, led to the formation of pre-anaphase DNA threads following the addition of BI2536 **(Fig. 5.14b)**. However, in contrast, the ectopic expression of a helicase inactive BLM mutant (Q672R) did not induce the formation of pre-anaphase DNA threads, during BI2536 treatment **(Fig. 5.14b)**. Thus, these results strongly suggested that BLM helicase activity is essential for promoting the formation of pre-anaphase DNA threads, induced by the inhibition of PLK1.

To further test that BLM helicase activity is required for centromere deformation, chromosome spreads were also examined for centromere breakage during BI2536 treatment. Interestingly, a significant reduction in centromere dislocations was observed in the mutant GFP-Q672R cells, when compared to wild-type GFP-BLM cells **(Fig. 5.14c)**. Although, it is worth noting, that the mutant GFP-Q672R complemented cells continued to show signs of the occasional centromere breakage, characteristic of the ΔBLM parental cell line.

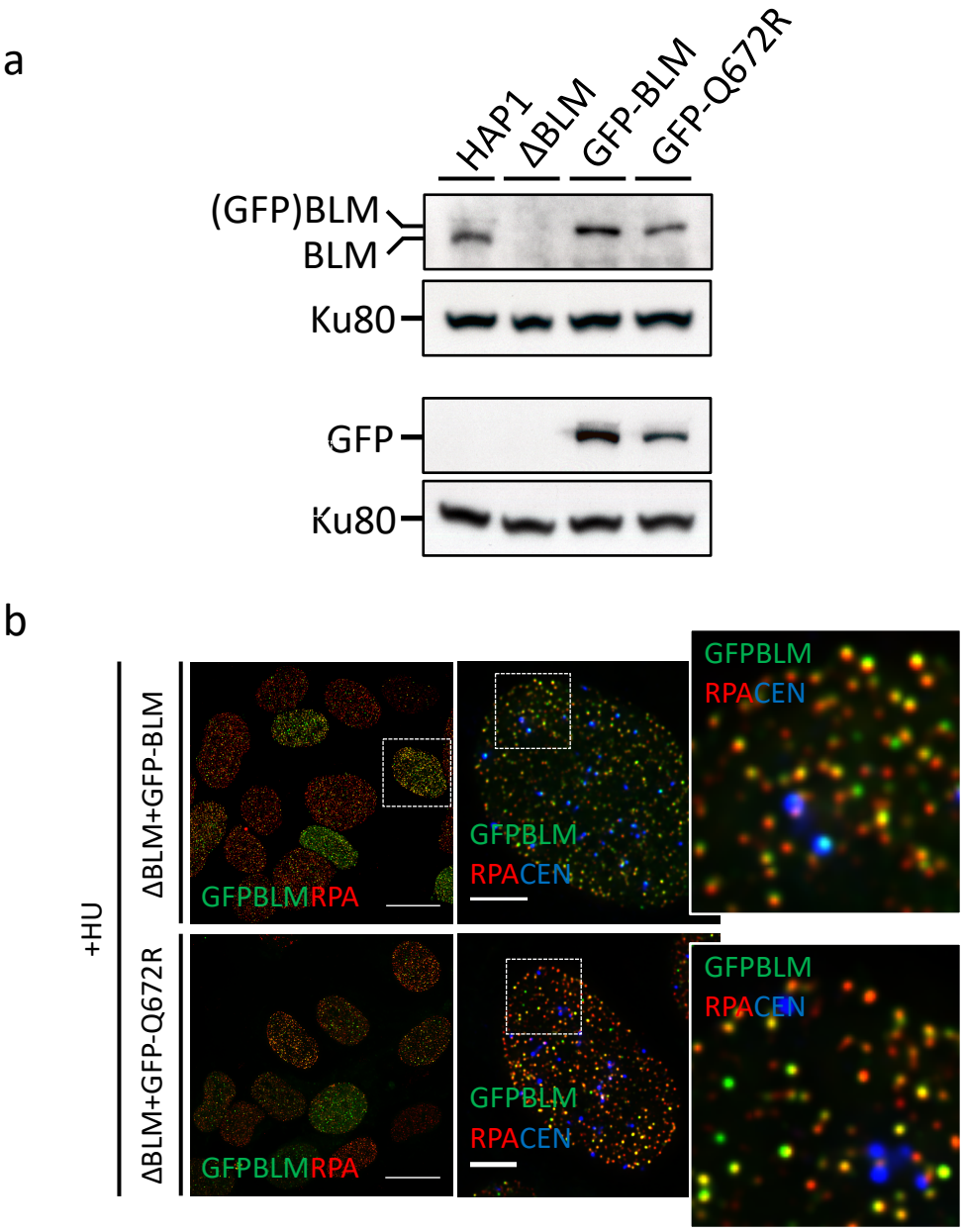

Figure 5.13. Creation of a BLM-helicase inactive stable cell line.
a) Western blot image using anti-BLM antibody (above), showing BLM expression levels in HAP1 cells, GFP-BLM and GFP-Q672R cell lines. Anti-KU80 was used as a loading control. Western blot image using anti-GFP antibody (below), showing GFP expression levels in GFP-BLM and GFP-Q672R cell lines. Anti-KU80 was used as a loading control **b)** Immunofluorescent images of ΔBLM cells stably expressing either a wild-type GFP-BLM (above), or helicase inactive mutant GFP-Q672R (below) after 2mM hydroxyurea (HU) treatment for 16hrs. Enlarged region highlights the co-localisation between GFP-BLM and RPA in both WT GFP-BLM and helicase inactive GFP-Q672R cell lines. Antibody staining for GFP (Green) to detect BLM expression, RPA (Red) and centromeres (Blue) (scale bar 5μm).

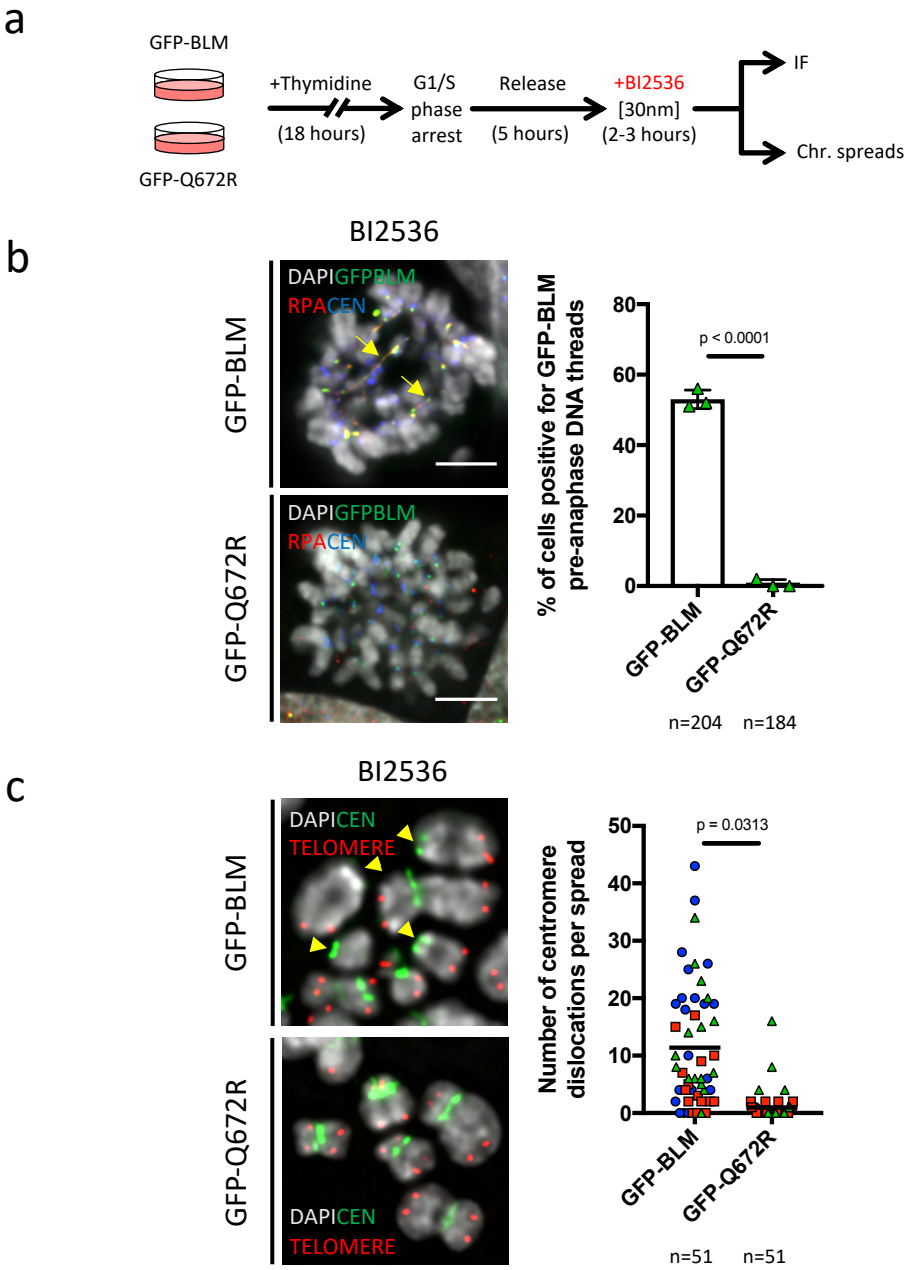

Figure 5.14. BLM helicase activity promotes centromere deformation during PLK1 inhibition.

a) Experimental outline of cell-synchronisation, immunofluorescent staining and ctFISH, using HAP1-ΔBLM+GFP-BLM (wild-type) and HAP1-ΔBLM+GFP-Q672R (helicase inactive mutant) cells. **b)** Immunofluorescent images of pre-anaphase DNA threads (arrows) in GFP-BLM and GFP-Q672R cells after BI2536 treatment. Antibody staining for DAPI (Grey), GFP-BLM (Green), RPA (Red) and centromeres (Blue). Quantification shows the percentage of cells positive for pre-anaphase DNA threads after PLK1 inhibition using BI2536 (mean ±SD is shown from three independent experiments). **c)** Chromosome spread and ctFISH images of centromere dislocations (arrowheads) in GFP-BLM and GFP-Q672R cells after BI2536 treatment. DAPI (Grey) was used to stain chromosomes, specific PNA FISH probes were used for centromere (Green) and telomere (Red) detection. Quantification of centromere dislocations after BI2536 addition (overall mean is shown from three independent experiments; student t-test was used for p-value calculation; n=number of cells analysed; scale bar 5μm).

It was noted that the mutant version of GFP-Q672R protein had lower expression levels, when compared against the expression level of the wild-type GFP-BLM protein **(see previous Fig. 5.13b)**.

To check that this did not influence the observed result, both cell lines were re-sorted using florescence activated cell sorting (FACS). A new population of GFP-BLM cells were selected, which displayed expression levels lower than the endogenous BLM protein expression levels in the parental HAP1 cells. In parallel, mutant GFP-Q672R cells were selected for higher than wild-type GFP-BLM protein expression levels **(Fig. 5.15a)**.

Consistent with the previous results, pre-anaphase DNA threads were shown to be absent in the re-sorted BLM helicase mutant cell line GFP-Q672R (High), whilst wild-type GFP-BLM (Low) cells continued to show pre-anaphase DNA thread formation after BI2536 treatment **(Fig. 5.15b)**. Therefore, it was concluded that the catalytic activity of BLM is required in order to promote centromere deformation, when PLK1 activity is absent.

It was also noticed that both ΔBLM and GFP-Q672R cells were largely absent in RPA foci formation at their centromeres, during PLK1 kinase inhibition. In contrast, the parental HAP1 and GFP-BLM cells were positive for RPA at their centromeres, during BI2536 treatment. The presence of RPA at the centromere supports the idea that BLM helicase activity is responsible for the formation of RPA foci at the centromere, due to centromeric DNA unwinding, during the inhibition of PLK1.

To test this idea, GFP-BLM and GFP-Q672R cells treated with BI2536 were examined for GFP-fluorescent intensity, alongside centromeric RPA-fluorescent intensity, which is more abundant after PLK1 kinase inhibition **(Fig. 5.16a)**.

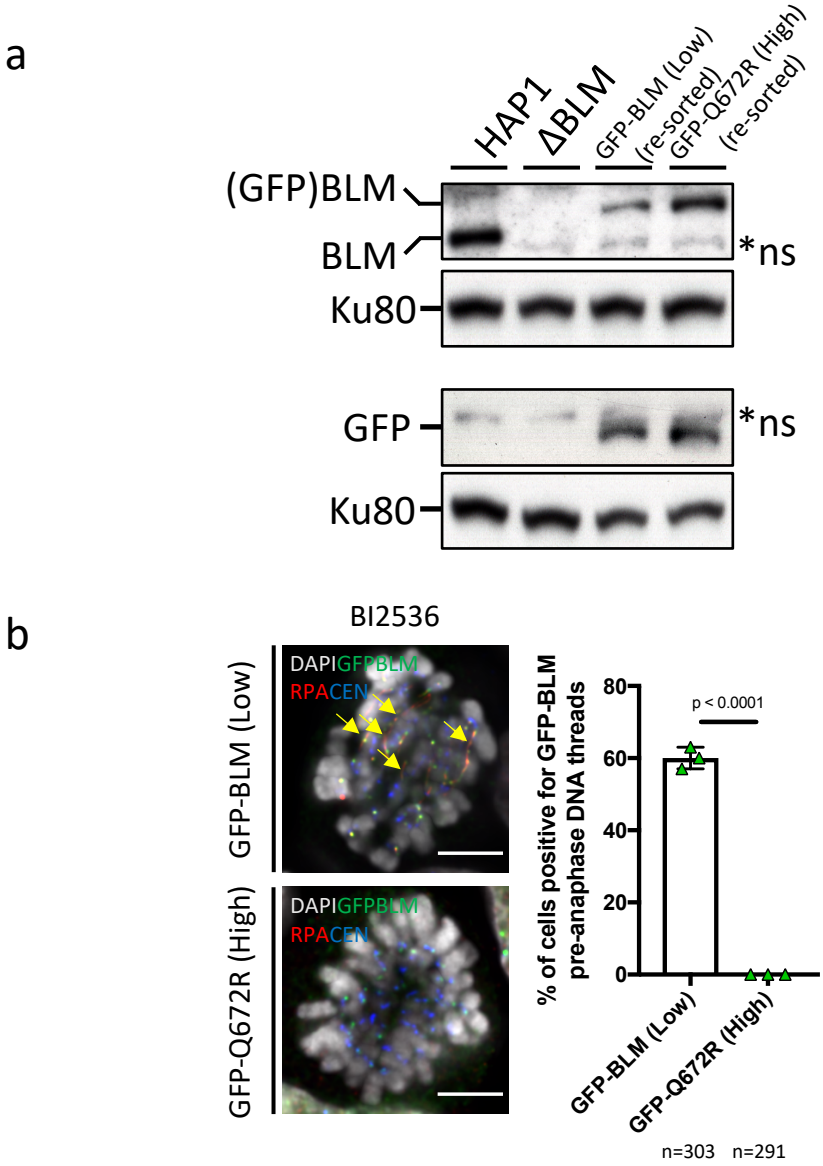

Figure 5.15. Low BLM expression is sufficient to promote centromere deformation during PLK1 inhibition.

a) Western blot image using anti-BLM antibody (above), showing BLM expression levels in HAP1 cells and BLM expression in GFP-BLM (lower than wild-type) and GFP-Q672R FACS re-sorted cell lines. Anti-KU80 was used as a loading control. Western blot image using anti-GFP antibody (below), showing GFP expression levels in GFP-BLM and GFP-Q672R cell lines. Anti-KU80 was used as a loading control (scale bar 5μm). **b)** Immunofluorescent images of pre-anaphase DNA threads (arrows) in GFP-BLM (low expression) and GFP-Q672R (high expression) cells after BI2536 treatment. Antibody staining for DAPI (Grey), GFP-BLM (Green), RPA (Red) and centromeres (Blue). Quantification shows the percentage of cells positive for pre-anaphase DNA threads after PLK1 inhibition using BI2536 (mean ±SD is shown from three independent; student t-test was used for p-value calculation; n=number of cells analysed; scale bar 5μm).

In GFP-Q672R cells there was an overall reduction of GFP-signal intensity at the centromere, although this was minor and not significant when compared to the GFP-BLM cells **(Fig. 5.16b)**. Importantly however, the mutant GFP-Q672R cells showed an almost complete absence of RPA signal intensity at centromeres, whereas the GFP-BLM cells were largely positive for RPA signals **(Fig. 5.16c)**. Therefore, these results would strongly imply that the catalytic activity of BLM, is responsible for the active unwinding of centromeric DNA during BI2536 treatment.

It is also worth noting that even the high expressing GFP-signals in the mutant GFP-Q672R cells showed an absence of RPA signals **(Fig. 5.16c)** (red triangles to the right-hand side of X-axis). In contrast, low GFP-signal intensity in GFP-BLM cells remained positive for RPA signal **(Fig. 5.16c)** (green circles to the left-hand side of X-axis). This suggests that even a low level of catalytically active BLM is able to trigger RPA formation at centromeres, when PLK1 is inhibited.

These findings strongly support the theory that the catalytic activity of BLM is responsible for the unwinding of centromeric DNA, during PLK1 inactivation and this results in RPA loading at the centromere.

5.2.7 BLM and Topoisomerase IIIα (TOP3A) may act together to promote centromere deformation during PLK1 inhibition

While it is clear that BLM's catalytic activity is responsible for driving centromere deformation when PLK1 activity is compromised, additional contributing factors could not be ruled out. As a result of this, attempts were made to investigate whether there were possible secondary factors involved in pre-anaphase DNA thread formation. The obvious candidates to investigate further were other members of the BTR-complex and in particular topoisomerase IIIα (TOP3A). BLM is a recognised component of the BTR-complex, which also includes TOP3A, and both the RecQ-mediated genome instability proteins 1 & 2 (RMI1/2) (Mankouri and Hickson 2007; Singh et al. 2008; Xu et al. 2008).

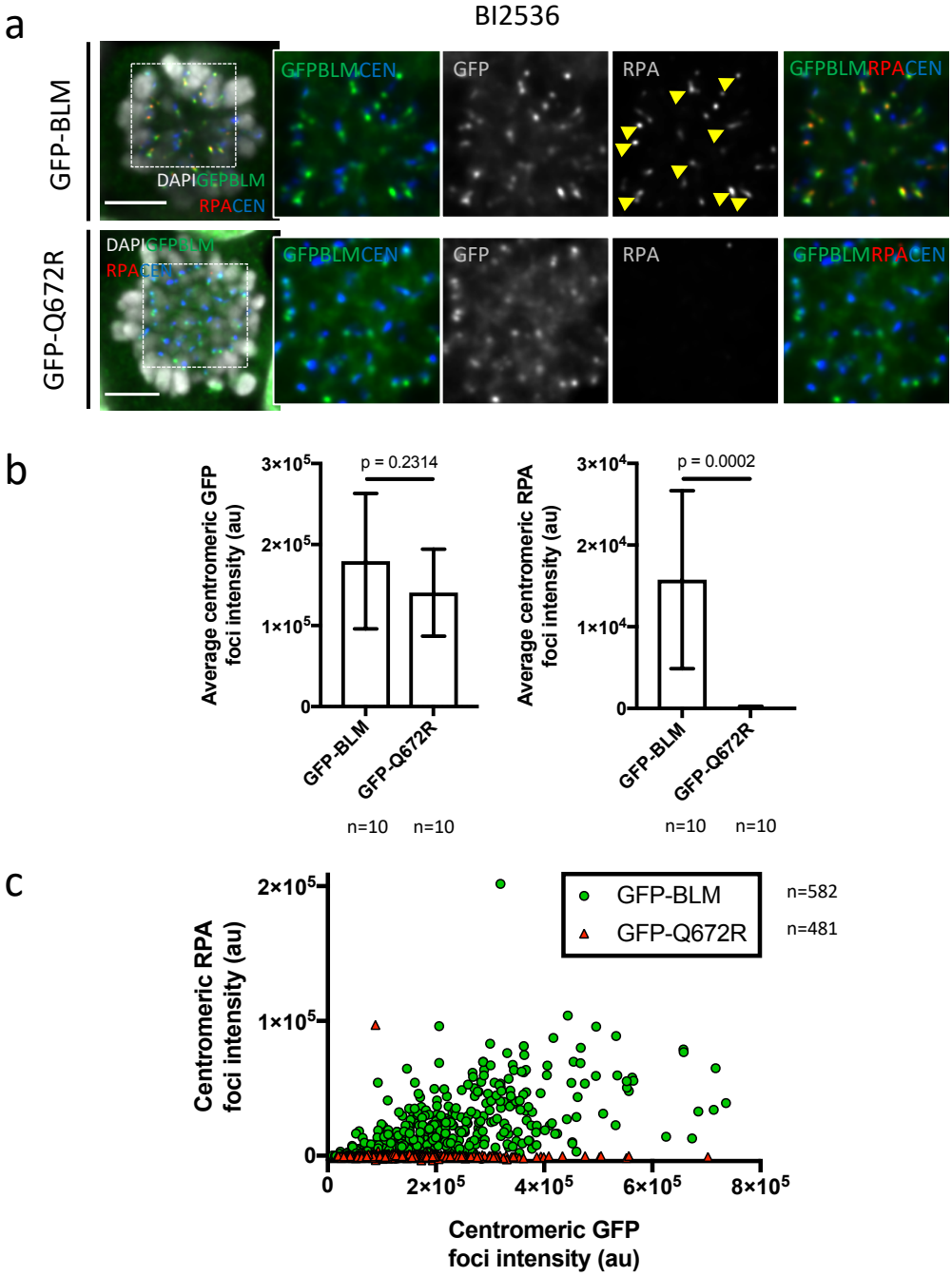

Figure 5.16. BLM helicase actively unwinds centromeric DNA during PLK1 inhibition.
a) Immunofluorescent images of centromeric GFP-tagged BLM detection in GFP-BLM (low expression) and GFP-Q672R (high expression) cells, after BI2536 treatment. Antibody staining for DAPI (Grey), GFP-BLM (Green), RPA (Red) and centromeres (Blue). Centromeric RPA (arrowheads) is only detected in GFP-BLM cells. **b)** Bar charts show the average centromeric GFP foci intensity (left) and the average centromeric RPA foci intensity (right) in GFP-BLM (low expression) and GFP-Q672R (high expression) cells, after BI2536 treatment (mean ±SD is shown from three independent; student t-test was used for p-value calculation; n=number of cells analysed; scale bar 5μm. **c)** Scatter plot of individual centromeric GFP signal, compared against centromeric RPA signal from GFP-BLM (low expression) and GFP-Q672R (high expression) cells, after BI2536 treatment (n=number of centromeric GFP foci counted).

Topoisomerases are known to process DNA, whilst acting to resolve DNA topological states during DNA replication and repair. They achieve this via the catalysis of transient breaks and re-joining of DNA molecules and are categorised depending on their ability to create either a single-strand (type I), or double strand (type II) DNA break (Nitiss 2009). Topoisomerase IIIα (TOP3A) is a type IA topoisomerase, and is consequently understood to be able to functionally catalyse the formation and re-ligation of ssDNA breaks (Wang 2002).

As TOP3A is recognised to form a complex with BLM, it was speculated that during PLK1 inactivation, TOP3A may be required for BLM to actively unwind centromeric DNA. Since BLM and TOP3A work together (Hu 2002; Wu et al. 2000), loss of one may disrupt the others molecular action. However, it has also been reported that TOP3A-RMI1 may have a BLM (Sgs1) independent role, during the resolution of DNA recombination (Kaur et al. 2015). Therefore, the absence of TOP3A, using RNAi, was investigated for its ability to promote centromere deformation during BI2536 treatment.

The depletion of TOP3A was confirmed by western blot and RPE1 cells were then synchronised as before, prior to examining centromere deformation phenotypes (**Fig. 5.17a, b)**. Similar to earlier experiments where BLM or PICH protein had been depleted, the depletion of TOP3A also led to the absence of pre-anaphase DNA thread formation during BI2536 treatment. As expected, control cells remained positive for pre-anaphase DNA thread formation, following the addition of BI2536 **(Fig. 5.17c)**. These results implied that TOP3A may functionally support centromere deformation when PLK1 activity is absent.

Analysis of centromeric TOP3A focal formation, showed that TOP3A was readily detectable at centromeres in control cells treated with BI2536 (siCTRL). In contrast, following TOP3A depletion and BI2536 treatment (siTOP3), TOP3A signals were shown to be significantly reduced **(Fig. 5.18a)**. In addition, centromeric RPA signals were also examined, following TOP3A depletion and BI2536 treatment. As expected, control cells

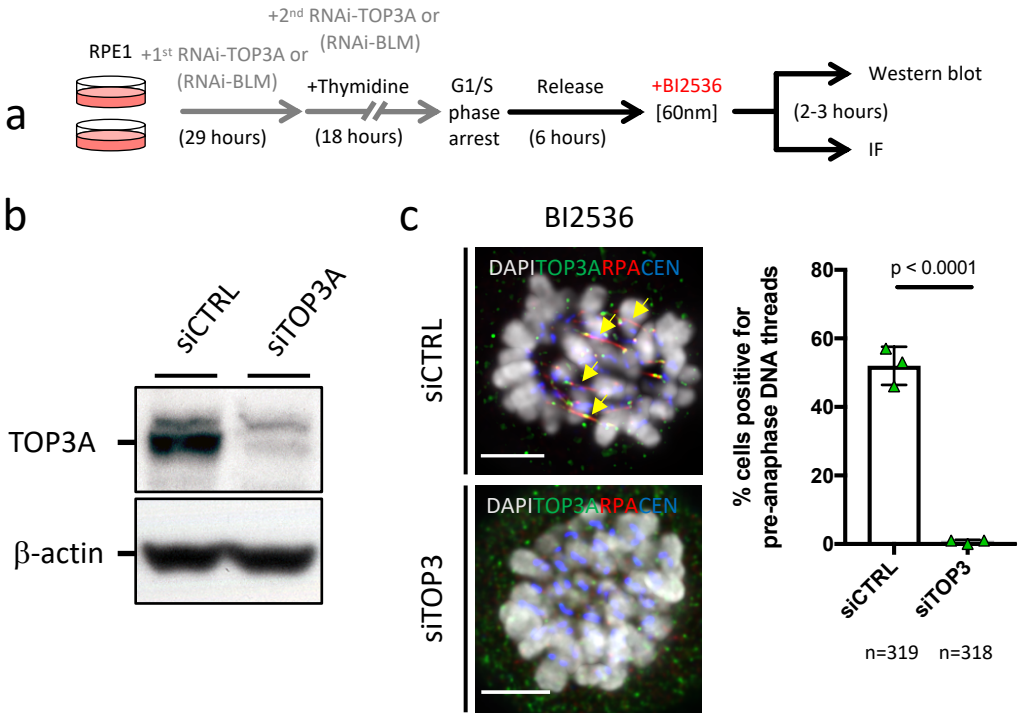

Figure 5.17. TOP3A promotes centromere deformation during PLK1 inhibition.
a) Experimental outline of RNAi during cell-synchronisation, western blot analysis and immunofluorescent staining, using RPE1 cells. **b)** Western blot image using anti-TOP3A antibody shows wild-type TOP3A levels (siCTRL) and depletion (siTOP3A) after RNAi. Anti-beta actin was used as a loading control. **c)** Immunofluorescent images of pre-anaphase DNA threads (arrows) in RPE1 cells after either siCTRL, or siTOP3A during BI2536 treatment. Antibody staining for DAPI (Grey), TOP3A (Green), RPA (Red) and centromeres (Blue). Quantification shows the percentage of cells positive for pre-anaphase DNA threads after RNAi and during PLK1 inhibition using BI2536 (mean ±SD is shown from three independent experiments; student t-test was used for p-value calculation; n=number of cells analysed; scale bar 5μm).

showed an abundance of RPA signals at the centromeres of metaphase cells treated with BI2536, whereas, following TOP3A depletion, this was largely abolished **(Fig. 5.18b)**.

Therefore, the loss of RPA at the centromeres during BI2536 treatment and TOP3A depletion, resembled the effects of earlier BLM or PICH depletion experiments. Thus, it was initially suspected that TOP3A may functionally regulate centromere deformation during PLK1 inactivation. However, following the examination of the recruitment of BLM to centromeres during BI2536 treatment and TOP3A depletion, it then became clear that an absence of TOP3A leads to the loss of BLM recruitment to the centromere **(Fig. 5.18c)**. Therefore, TOP3A depletion most likely indirectly rescues the formation of pre-anaphase DNA threads during PLK1 kinase inhibition. The loss of TOP3A may lead to a destabilising effect on the BTR-complex as a whole. Thus, it is suggested that in the absence of a complete BTR-complex, BLM is no longer capable of recruiting to the centromere, and aberrant DNA unwinding is lost, during the inactivation of PLK1.

The depletion of BLM using RNAi, also led to a significant reduction in detectable TOP3A foci number at centromeres of metaphase cells, during BI2536 treatment **(Fig. 5.18d)**. These results support the suggestion that the BTR complex probably requires the presence of both BLM and TOP3A, in order to correctly function. However, further investigation is required to confirm this idea, as it cannot be ruled out that TOP3A plays a functional role in pre-anaphase DNA thread formation, during PLK1 inactivation. In the future it would be interesting to examine whether a catalytically inactive version of TOP3A, may prevent centromere deformation during PLK1 inactivation.

5.2.8 PICH activity promotes centromere deformation when PLK1 activity is absent

PICH has been shown to interact with BLM (Ke et al. 2011) and this study has also found that PICH is required for BLM to target to centromeres, in particular during PLK1

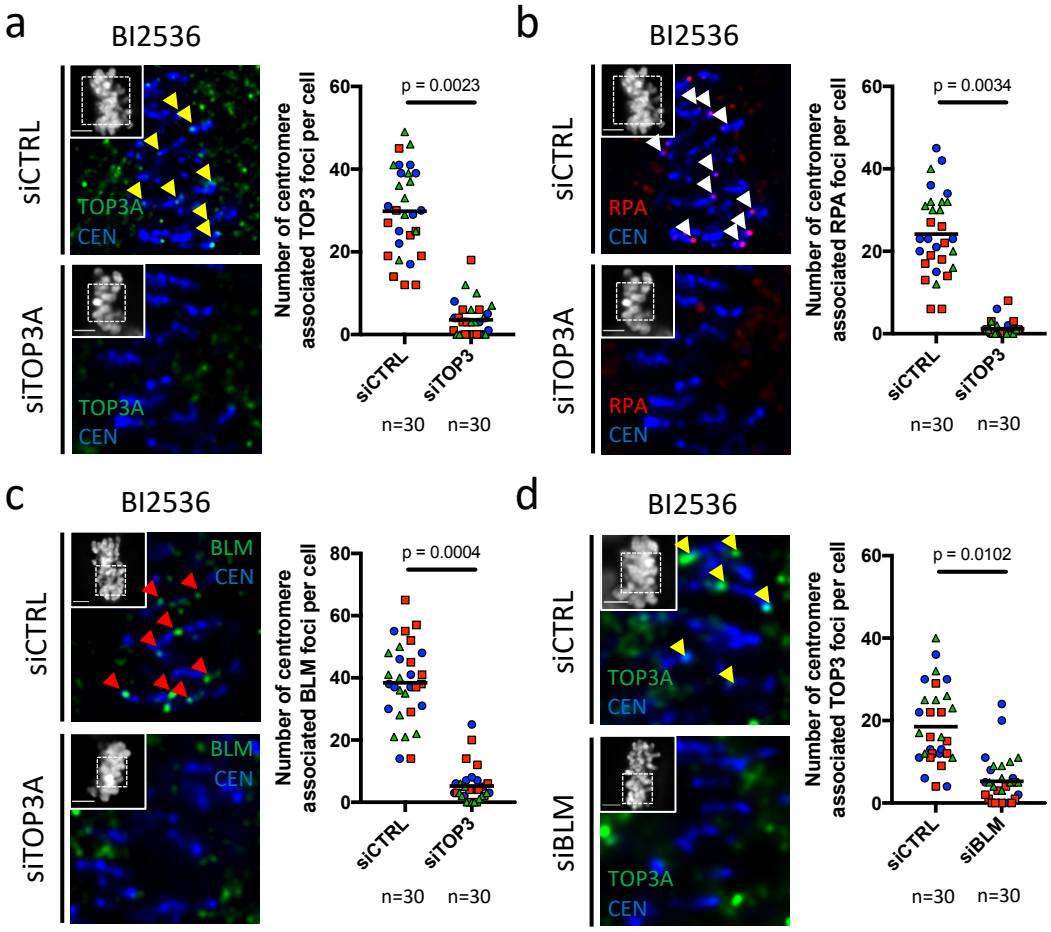

Figure 5.18. BLM requires its partner protein TOP3A for centromere recruitment.
a) Immunofluorescent images of TOP3A foci (yellow arrowheads) at centromeres of metaphase(-like) RPE1 cells after RNAi showing either siCTRL, or siTOP3A during BI2536 treatment. Antibody staining for DAPI (Grey), TOP3A (Green) and centromeres (Blue). Quantification shows the number of TOP3A foci at centromeres after RNAi and during PLK1 inhibition, using BI2536. **b)** Immunofluorescent images of RPA foci (white arrowheads) at centromeres of metaphase(-like) RPE1 cells after RNAi showing either siCTRL, or siTOP3A during BI2536 treatment. Antibody staining for DAPI (Grey), RPA (Red) and centromeres (Blue). Quantification shows the number of RPA foci at centromeres after RNAi and during PLK1 inhibition, using BI2536. **c)** Immunofluorescent images of BLM foci (red arrowheads) at centromeres of metaphase(-like) RPE1 cells after RNAi showing either siCTRL, or siTOP3A during BI2536 treatment. Antibody staining for DAPI (Grey), BLM (Green) and centromeres (Blue). Quantification shows the number of BLM foci at centromeres after RNAi and during PLK1 inhibition, using BI2536. **d)** Immunofluorescent images of TOP3A foci (arrowheads) at centromeres of metaphase(-like) RPE1 cells after RNAi showing either siCTRL, or siBLM during BI2536 treatment. Antibody staining for DAPI (Grey), TOP3A (Green) and centromeres (Blue). Quantification shows the number of TOP3A foci at centromeres after RNAi and during PLK1 inhibition, using BI2536 (overall mean is shown from three independent experiments; student t-test was used for p-value calculation; n=number of cells analysed; scale bar 5μm).

inactivation. However, it remains unclear whether this is through a direct recruitment, or alternatively, if it requires the catalytic activity of PICH. Therefore, PICH translocase mutant cells (K128A) were examined for their ability to promote pre-anaphase DNA threads during BI2536 treatment.

In order to achieve this, two stable cell lines were created which harboured ectopic copies of the PICH gene. The ectopic PICH cDNA was modified so that it assumed resistance to a PICH siRNA oligo, and therefore no longer responded to RNAi **(Fig. 5.19a)**. Individually, each cell line stably expressed either an RNAi resistant copy of a wild-type GFP-PICH gene, or a translocase mutant version of PICH, GFP-K128A. Subsequently, it was possible to deplete endogenous PICH by using a specific PICH siRNA oligo and then examine the cellular effects of PICH translocase activity, during PLK1 inactivation.

To achieve an effective depletion of endogenous PICH, two rounds of RNAi were performed over a period of nearly 72 hours, whilst cells were also arrested and released using thymidine as before **(Fig. 5.19b)**. Western blot analysis showed that the PICH siRNA oligo was able to effectively deplete endogenous PICH levels in each of the HCT116 cell-lines; and most importantly, this included the mutant cell lines. Crucially, both individual clones of GFP-PICH and GFP-K128A were shown to express an extra copy of PICH, which displayed at a higher molecular weight due to GFP-tagging, and most importantly, this extra copy of PICH was largely refractory to the effects of PICH siRNA targeting **(Fig. 5.19c)**. Therefore, these cells were then used to test whether PICH translocase activity was necessary to promote centromere deformation, during PLK1 inhibition using BI2536.

Following cell synchronisation, both wild-type HCT116 cells and the modified GFP-PICH cell lines were released into the presence of BI2536 and fixed in order to analyse the frequency of pre-anaphase DNA thread formation. Two individual clones of each RNAi resistant wild-type (PICH-A1 & -D1) and translocase inactive (K128A-D1 & -I1) cell lines were examined against the parental cells (HCT116), during BI2536 treatment.

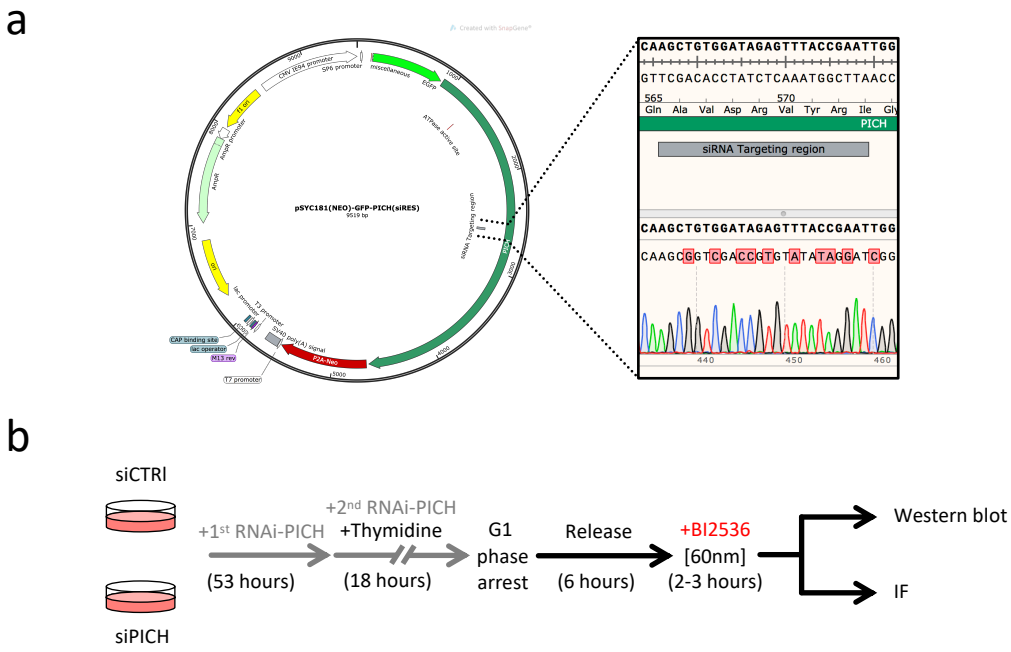

Figure 5.19. Creating PICH-translocase inactive RNAi resistant stable cell lines.
a) A diagram to highlight the specific nucleotide changes to the ectopic PICH expression plasmid, which rendered the stably expressing ectopic PICH resistant to a specific PICH siRNA oligo sequence. Two stable cell lines were created with siRNA resistance in HCT116 cells. First, a wild-type GFP-PICH and secondly, a translocase inactive mutant, GFP-K128A. **b)** Experimental outline of siRNA oligo targeting of endogenous PICH during cell-synchronisation before western blot analysis and immunofluorescent staining, using HCT116 cells. **c)** Western blot image using anti-PICH antibody, showing both endogenous PICH and ectopic PICH expression levels, before and after RNAi. Two clones of each stable cell line are included (GFP-PICH clones – A1 and D1; GFP-K128A – D1 and I1). Anti-KU80 was used as a loading control.

As expected, following BI2536 treatment, control HCT116 cells (siRNA CTRL) displayed the formation of pre-anaphase DNA threads. Importantly however, following the depletion of PICH, HCT116 cells were absent of pre-anaphase DNA thread formation **(Fig. 5.20a, b)**. This demonstrates that PICH depletion in HCT116 cells was sufficient to prevent pre-anaphase DNA thread formation, consistent with previous results in RPE1 hTERT cells.

Cells stably expressing an ectopic GFP-PICH wildtype protein (clones A1 & D1), were also shown to be capable of forming pre-anaphase DNA threads during BI2536 treatment, when subject to either control siRNA oligo transfection or depletion of endogenous PICH **(Fig. 5.20a, b)**. These results demonstrated that the wildtype GFP-tagged PICH protein was active. The HCT116 translocase-dead mutant cells (GFP-K128A) (clones D1 & I1) remained positive for the formation of pre-anaphase DNA threads, during control siRNA conditions and BI2536 treatment **(Fig. 5.20a, b)**. However, following the depletion of endogenous PICH, both the translocase-dead mutant GFP-K128A clones (D1 & I1) failed to induce pre-anaphase DNA threads, during BI2536 treatment **(Fig. 5.20b)**. Therefore, these results imply that in addition to BLM helicase activity, PICH-translocase activity is also required for driving centromere deformation, when PLK1 activity becomes compromised. It remains to be seen whether BLM recruitment to centromeres is affected during the inactivation of PICH translocase activity and BI2536 treatment. However, this would be a subject for future investigation.

It remains unclear exactly how centromeric integrity is affected. PLK1 may directly regulate PICH and/or BLM via protein phosphorylation. In agreement with others, PLK1 was found to contribute to the phosphorylation of both BLM and PICH during a mitotic arrest **(Fig. 5.21a, b)** (Baumann et al. 2007; Dutertre et al. 2000, 2002; Lera et al. 2016). As *in vitro* experiments have shown that PLK1 activity has no influence on the catalytic activity of PICH (Kaulich et al. 2012), BLM was considered a more promising candidate for further investigation.

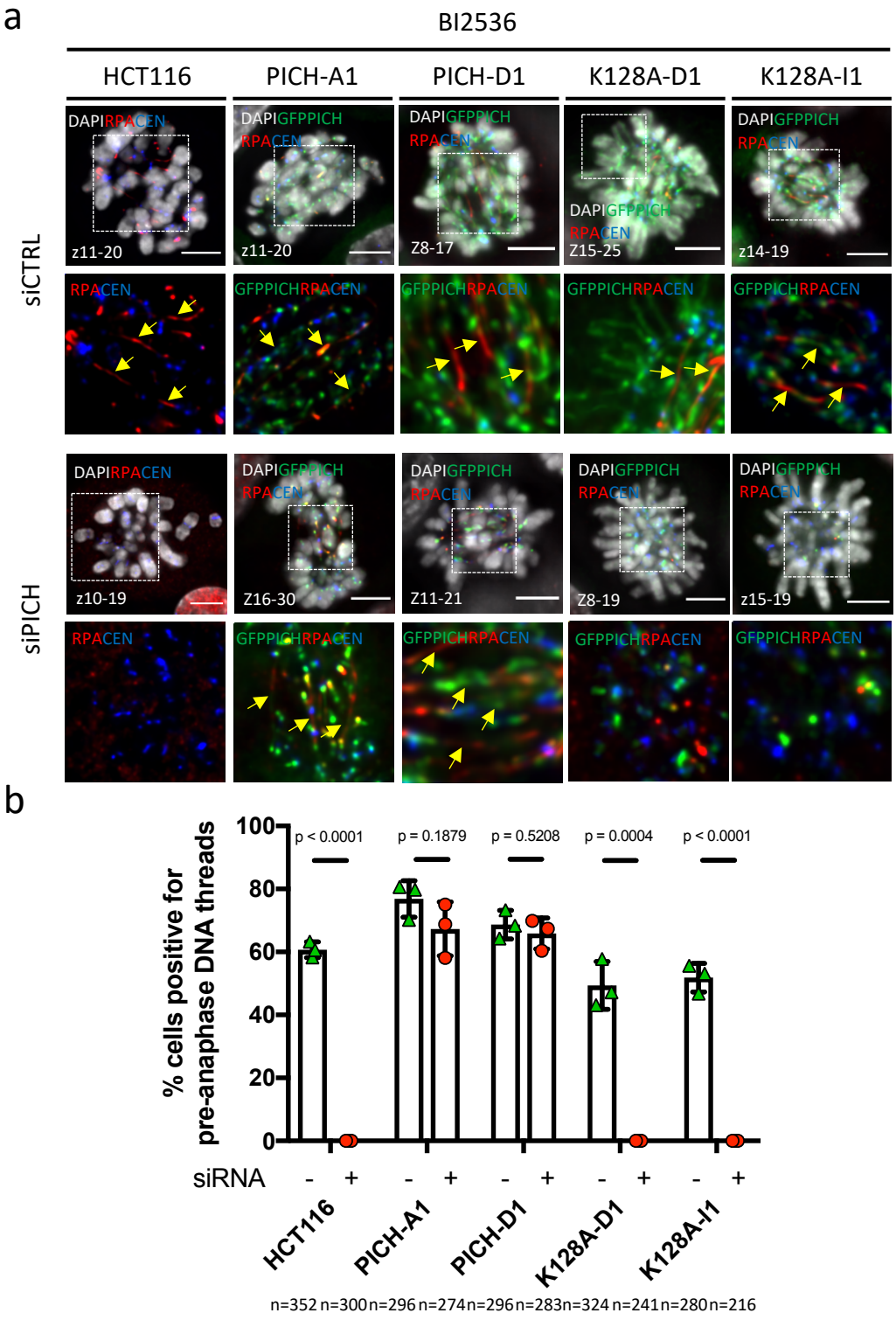

Figure 5.20. PICH translocase activity promotes centromere deformation during PLK1 inhibition.

a) Immunofluorescent images of pre-anaphase DNA threads (arrows) in HCT116, GFP-PICH (clones A1 & D1) and GFP-K128A (clones D1 & I1) cells, after either siCTRL, or siRNA targeting of endogenous PICH during BI2536 treatment. Antibody staining for DAPI (Grey), GFP-PICH (Green), RPA (Red) and centromeres (Blue). **b)** Quantification of the percentage of cells positive for pre-anaphase DNA threads after either siCTRL, or siRNA targeting of endogenous PICH, during BI2536 treatment (mean ±SD is shown from three independent experiments; student t-test was used for p-value calculation; n=number of cells analysed; scale bar 5μm).

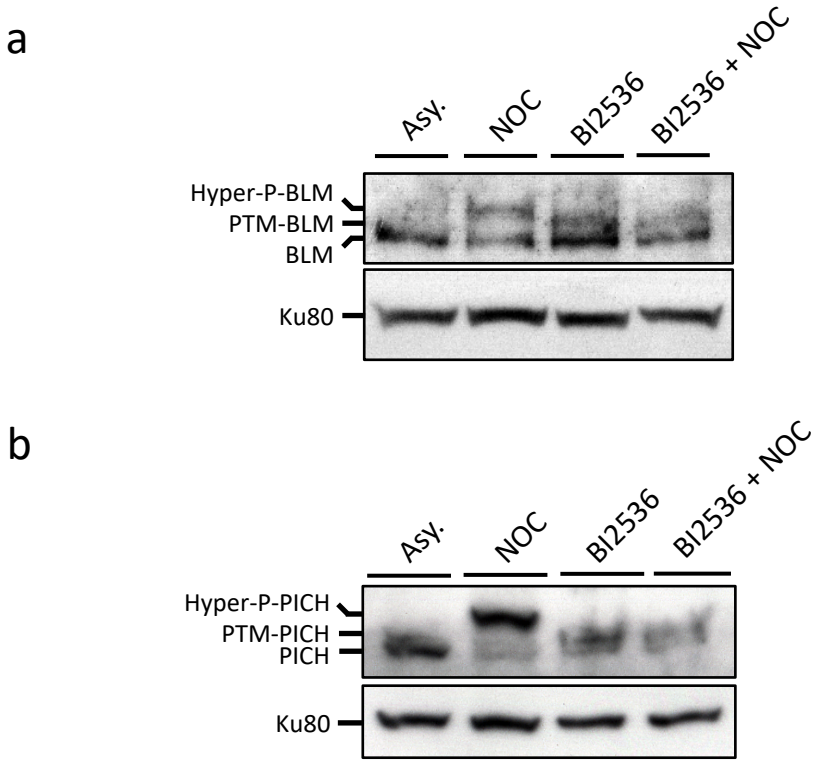

Figure 5.21. Both BLM and PICH are phosphorylation targets of PLK1.
a) Western blot image using anti-BLM antibody, showing the electrophoretic mobility shift of BLM following BI2536 treatment. **b)** Western blot image using anti-PICH antibody, showing the electrophoretic mobility shift of PICH following BI2536 treatment. Anti-KU80 was used as a loading control for both.

BLM has been shown to be detectable at UFB DNA during anaphase (Chan et al. 2007). Therefore, it was speculated that PLK1 activity may prevent the recruitment of BLM to DNA, prior to anaphase onset. PICH, BLM and RPA are readily detectable at anaphase UFBs induced by the addition of the topoisomerase II (TOP2) inhibitor; ICRF-193 **(Fig. 5.22a, b)**. This was compared to the depletion of SGO1 via RNAi, where centromeric cohesin becomes prematurely lost. This occurs prior to anaphase onset and leads to the premature separation of sister-chromatids. Under these conditions premature c-UFBs that are decorated with PICH protein are formed **(Fig. 5.22a)**. However, consistent with previous findings, both BLM and RPA were largely undetectable at these premature forming c-UFBs, despite the existence of PICH **(Fig. 5.22a, c, d)** (Chan et al. 2007). Therefore, mitotic hyperphosphorylation of BLM may prevent BLM chromatin association and/or possibly its activity, prior to anaphase. Hence, PLK1-dependent phosphorylation of BLM may temporarily restrict the recruitment of BLM to chromatin during early mitosis. Loss of PLK1 activity allows BLM to bind to chromatin prematurely during mitosis and subsequently promote centromere deformation.

In agreement to this idea, SGO1 depletion also showed that BLM and RPA associated to premature c-UFBs following a 30-minute treatment with the PLK1 inhibitor, BI2536 **(Fig. 5.22a, c, d)**. This implies that PLK1 activity suppresses BLM recruitment to chromatin prior to anaphase onset and supports the theory that PLK1 regulates the spatiotemporal chromatin association of BLM during mitosis.

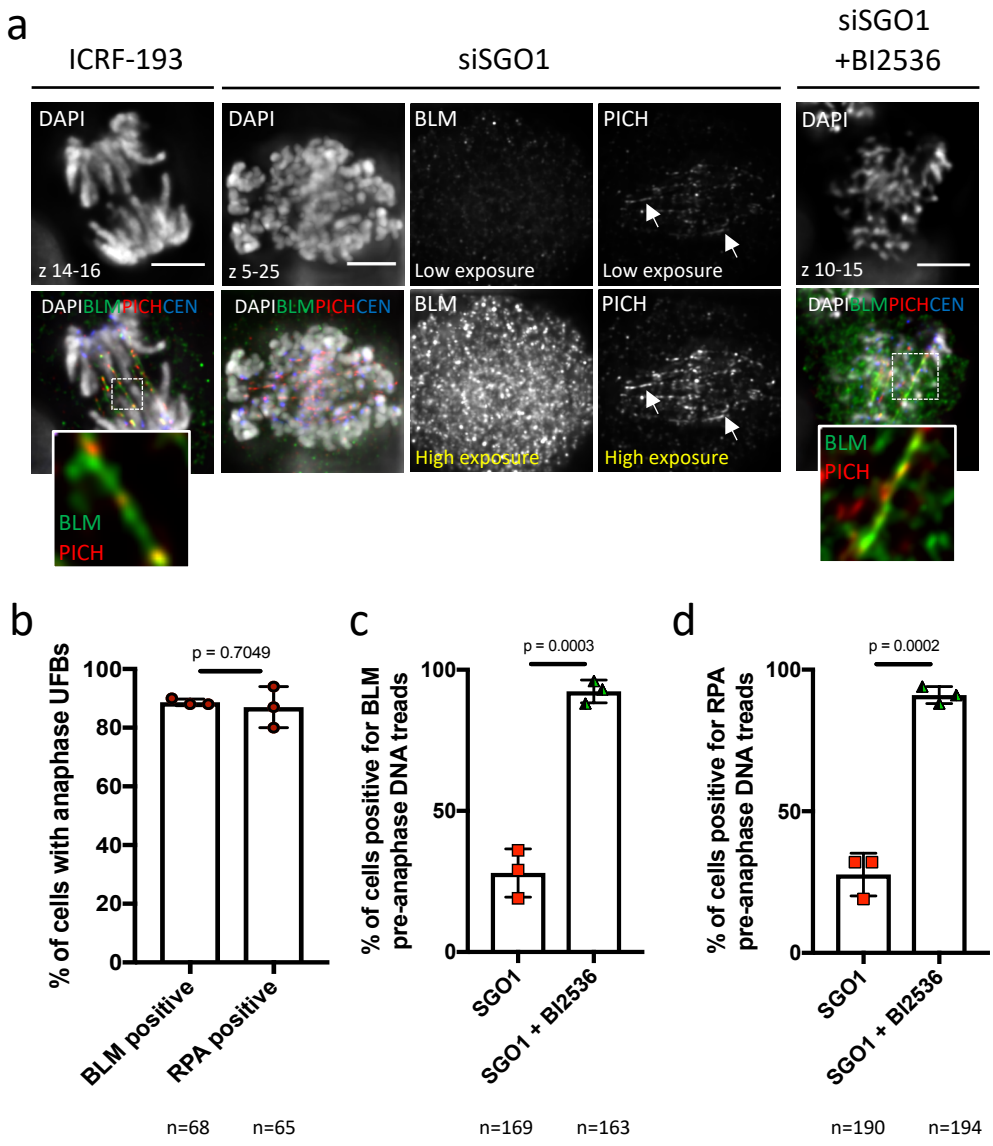

Figure 5.22. BLM recruitment to mitotic chromatin may be regulated by phosphorylation. **a)** Immunofluorescent images of an anaphase cell after ICRF-193 treatment (left), positive for anaphase UFBs. A mitotic cell after SGO1 depletion using RNAi, undergoing premature sister-chromatid separation (middle), positive for PICH-associated UFBs (arrows), but absent of BLM. High exposure image also included (below). Finally, a mitotic cell after both SGO1 depletion and BI2536 treatment (right), showing both PICH and BLM positive UFB association. Antibody staining for DAPI (Grey), BLM (Green), PICH (Red) and centromeres (Blue). **b)** Quantification of the percentage of cells positive for BLM, or RPA UFBs after ICRF-193 treatment in RPE1 hTERT cells. **c)** Quantification of the percentage of cells positive for BLM pre-anaphase DNA threads, due to premature sister separation after SGO1 depletion. **d)** Quantification of the percentage of cells positive for RPA pre-anaphase DNA threads, due to premature sister separation after SGO1 depletion (mean ±SD is shown from three independent experiments; student t-test was used for p-value calculation; n=number of cells analysed; scale bar 5μm).

5.3 Discussion

The experiments described in this chapter support the theory that PLK1 functions to suppress the aberrant recruitment and activity of BLM helicase at the centromere during early mitosis. In the absence of PLK1 kinase activity, BLM helicase promotes the catastrophic deformation of centromeres.

Centromere deformation initially becomes apparent by the uncharacteristic increase in RPA formation at centromeres, in particular during metaphase, when PLK1 activity is compromised. The induction of RPA foci at the centromere coincides with an increase in BLM protein recruitment to the centromeres. This suggests that BLM actively unwinds centromeric DNA, which leads to ssDNA exposure, RPA loading and centromere fragility.

Microtubule spindle pulling forces were shown to exacerbate this centromere fragility. Cells absent of PLK1 activity still undergo chromosome biorientation, and therefore centromeres must encounter MT-spindle tension. However, the MT-spindle tension also helps drive the formation of pre-anaphase DNA threads. Therefore, PLK1 inactivation, the UFB-binding complex and MT-spindle pulling forces promote centromere deformation, which can eventually culminate in severe centromere damage. This centromere specific damage results in the complete separation of chromosome arms, appearing as a chromosome break.

In support of the theory that the UFB-binding complex, and in particular PICH and BLM promote centromere deformation during PLK1 inactivation, cells undergo extended metaphase durations when either BLM or PICH are depleted **(Fig. 5.11b, c)**. Therefore, expression of BLM and PICH jeopardises the integrity of centromeric DNA configuration during chromosome biorientation, when PLK1 activity is absent and this results in centromere deformation.

Additionally, the results also predict that PICH is required for more than BLM recruitment to centromeres during PLK1 inactivation, as the data also suggest a dependency on PICH translocase activity. PICH translocase inactive cells show an absence of pre-anaphase DNA thread formation, after PLK1 kinase inhibition. This highlights the importance of the catalytic activity of both PICH and BLM in generating such centromere destruction when the activity of PLK1 is affected.

PICH and BLM have been shown to be phosphorylated in a PLK1 dependent manner. Therefore, in the future, it would be interesting to test whether PLK1-dependent phospho-mutant versions of BLM and/or PICH, are capable of re-capitulating the phenotypes of centromere deformation, in cells where PLK1 activity remains.

Chapter 6: General discussion and future directions

6.1 Summary of key findings

This thesis has reported that the activity of PLK1 in mitosis is essential for the stability of chromosome biorientation. Following chromosome biorientation, PLK1 functions to protect centromeres against a previously unreported centromere-specific deformation scenario. Cells absent of PLK1 activity can undergo bipolar KT-MT attachment and chromosome alignment during metaphase. However, chromosome alignment becomes compromised due to centromeric DNA unwinding, leading to metaphase collapse. Centromeric DNA unwinding is dependent on the catalytic activity of both BLM and PICH, which illegitimately unwind centromeric DNA and cause centromere deformation. This leads to the formation of pre-anaphase DNA threads, that are also dependent on tension generated by microtubules. Furthermore, an absence of PLK1 activity is also shown to result in centromere-specific breakage, which is believed to be the culmination of pre-anaphase DNA thread breakage. Therefore, PLK1 activity is essential for maintaining centromere architecture and protects against the catalytic activity of BLM and PICH to support chromosome biorientation during microtubule tension.

6.2 General discussion

Overview of centromere deformation caused by the inactivation of PLK1

PLK1 function is critical to cellular progression and survival. In its absence, cells display severe mitotic arrest and alignment defects, which can eventually lead to mitotic catastrophe (Lénárt et al. 2007; Steegmaier et al. 2007). Chromosome alignment defects, during PLK1 inactivation, have been attributed to errors in kinetochore-microtubule (KT-MT) attachment. Cells lacking PLK1 activity arrest due to monopolar spindle attachment. This has been described as the "polo" phenotype (Lénárt et al. 2007). Detailed analysis presented in this thesis has revealed an additional reason for why PLK1 is so critical for chromosome alignment and faithful mitotic progression.

Instead of attributing the phenotype to KT-MT attachment errors, this study reveals that some cells lacking PLK1 activity are able to undergo chromosome congression during metaphase. The majority of cells analysed were able to achieve bipolar spindle attachment and align their chromosomes during metaphase. However, PLK1 inhibited cells do eventually display a metaphase collapse pattern. This collapse pattern can be observed as either the previously described "polo" chromosome morphology (Lénárt et al. 2007); or alternatively, as the currently reported "figure-of-8" shape collapse. Interestingly, cells capable of chromosome alignment, during PLK1 inactivation, generally succumb to the "figure-of-8" shape collapse. These cells are believed to successfully achieve bipolar KT-MT attachment. Therefore, it is speculated that PLK1 activity is required for the long-term stability of KT-MT attachment, rather than its initial establishment (**Fig. 6.1 predicted model, left)**.

Detailed analysis of PLK1 localisation in the figure-of-8 collapsed cells, showed that the PLK1 protein decorated thread-like structures that connected chromatin masses during mitosis. The UFB-binding proteins PICH, BLM, TOP3A and the ssDNA binding protein RPA, were also identified as recruiting to these thread-like structures. The recruitment of RPA strongly suggested that these structures were of DNA in origin. Therefore, as

PLK1 inactivation or depletion prevents cells from progressing into anaphase, these thread-like structures were termed as pre-anaphase DNA threads. This term was not only used to identify them as DNA in composition, but also to help distinguish them from the previously identified anaphase UFBs. Although pre-anaphase DNA threads and UFBs feature ultra-fine DNA structures and therefore their appearance can be considered very similar, they are formed by distinctly different mechanisms. Anaphase UFBs originate between sister chromatids and only become apparent during chromosome segregation. In contrast, pre-anaphase DNA thread formation is a result of centromeric DNA being exposed from intact cohesed chromosomes. Furthermore, pre-anaphase DNA thread formation is specific to centromeres, providing the initial link between metaphase collapse and centromere deformation during PLK1 inactivation.

The absence of PLK1 activity also led to the aberrant recruitment of BLM to centromeres during mitosis. This was linked to BLM-dependent centromeric DNA unwinding and centromere deformation. Centromere deformation was further augmented by MT-pulling forces. This suggests that BLM drives centromere fragility when PLK1 activity is compromised and the combined action of BLM-dependent centromeric DNA unwinding with MT pulling forces, was responsible for centromere fragility during PLK1 inactivation. Centromere fragility was shown to culminate in the complete separation of whole chromosome arms. This was termed as 'centromere dislocation' and highlights a centromere-specific breakage pattern that requires PLK1 activity for its suppression. Therefore, PLK1 activity functions to suppress a previously unreported centromeric DNA deformation pathway and suggests that PLK1 functions as a centromere guardian **(Fig. 6.1 predicted model, right)**.

Pre-anaphase DNA threads

One of the most striking cellular features of PLK1 inactivation, is the formation of protein bound pre-anaphase DNA threads. These show a strong resemblance to the previously identified UFBs, which can arise between sister-chromatids during anaphase (Baumann et al. 2007; Chan et al. 2007). The associated proteins, which include PICH, BLM, TOP3A

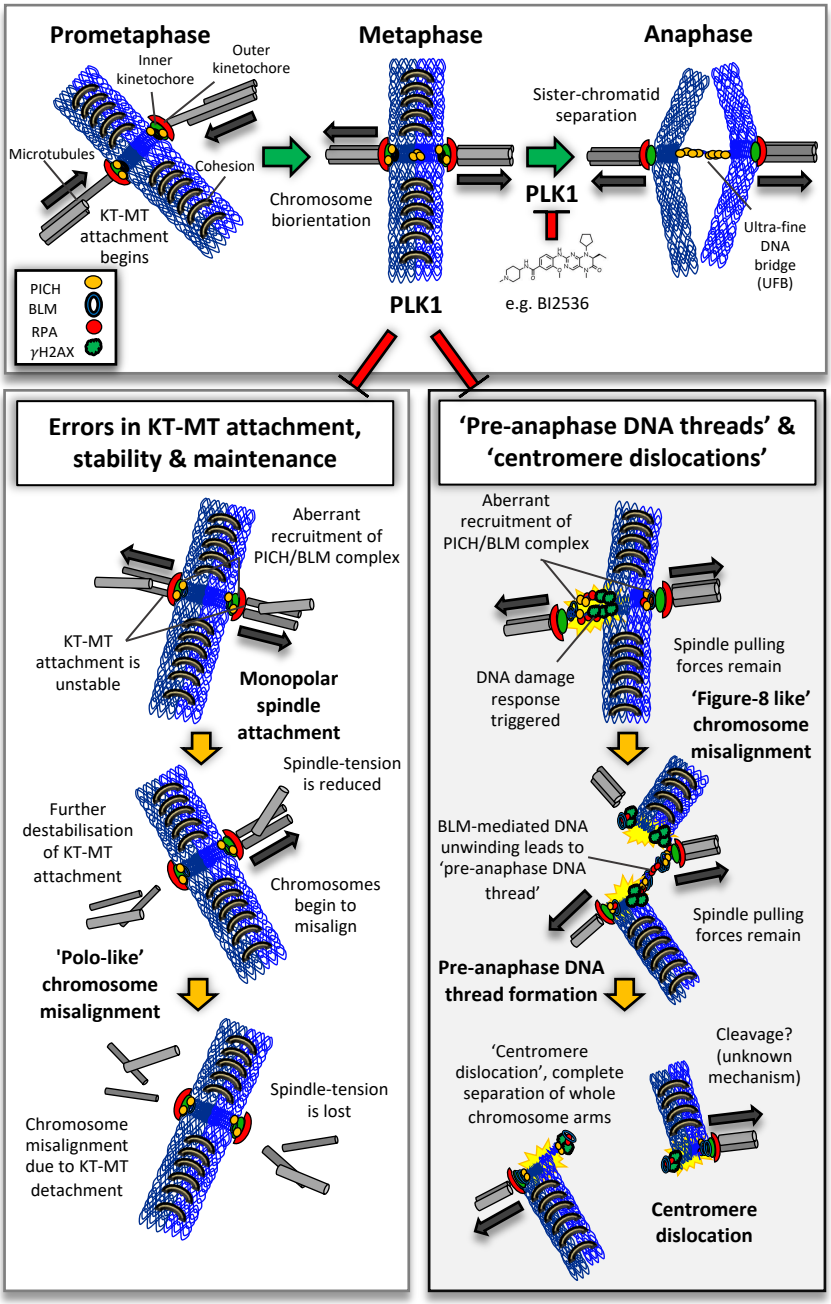

Figure 6.1. A model to demonstrate how PLK1 suppresses PICH/BLM-mediated centromere deformation.

Cells require active PLK1 for mitotic progression. PLK1 functions to promote correct bipolar spindle attachment and also suppress a newly described centromere deformation pathway. An absence of PLK1 activity can lead to two possible mitotic outcomes. **Left:** MT-KT attachment error occurs, which lead to a "polo" like collapse due to monopolar spindle attachment. **Right:** cells that maintain bipolar spindle attachment suffer from an centromere deformation pathway, caused by the aberrant recruitment of BLM to centromeres. This promotes a metaphase collapse pattern that resembles a 'figure-of-8' shape. BLM-helicase actively unwinds the centromeric DNA, resulting in a protein coated 'pre-anaphase DNA thread' bound by various proteins, including PLK1, PICH, BLM, TOP3 and RPA. Eventually, cells undergo 'centromere dislocation', which appears as the complete separation of whole chromosome arms.

and RPA are also similar. This supports the idea that anaphase UFBs and pre-anaphase DNA threads are similar in DNA composition. However, their formation is distinctly different from each other.

The initial formation of pre-anaphase DNA threads during PLK1 inactivation, is believed to be through the co-action of MT-KT attachment and tension, combined with the illegitimate recruitment and catalytic activity of certain UFB binding factors. In particular, centromeric DNA is actively unwound by the activity of BLM helicase, following MT-KT attachment and PLK1 inactivation. This conclusion is based on the observation that strong RPA foci form at centromeres during PLK1 inactivation, but only when catalytically active BLM is present. Furthermore, it is predicted that MT-pulling forces promote the stretching of centromeric DNA, which could explain how pre-anaphase DNA threads form during PLK1 inactivation. However, what PLK1 is doing to prevent such centromere deformation remains unclear. This discussion will explore some of the possible scenarios.

Does PLK1 activity regulate the recruitment of BLM to centromeres?

Following PLK1 inactivation, the catalytic activity of BLM has been shown to promote the recruitment of RPA at centromeres. Therefore, during PLK1 inactivation, the catalytic activity of BLM is responsible for centromere deformation. Interestingly, although BLM has previously been reported to recruit to centromeres of unperturbed cells (Rouzeau et al. 2012), it was not readily detectable during this study. Only after PLK1 activity became compromised did BLM become clearly noticeable at centromeres. Therefore, PLK1 may function to regulate the spatiotemporal recruitment of BLM to centromeres during mitosis, which may explain how PLK1 functions to suppress centromere deformation. Thus, in the absence of PLK1 activity, the temporal regulation of BLM recruitment to centromeres is absent, leading to premature loading of BLM, which promotes centromere deformation.

However, whether BLM is recruited to centromeres prior to mitotic entry remains ambiguous. The previous study showed BLM localises to centromeres of mitotic cells using Bloom's syndrome (BS) patient derived cells ectopically expressing GFP-BLM, or, alternatively, examining endogenous BLM via antibody detection in chromosome spreads of HeLa cells (Rouzeau et al. 2012). It could be argued that the ectopic expression of GFP-BLM in BS cells may lead to a mis-interpretation of BLM detection at centromeres, due to the overexpression of the ectopic construct. Furthermore, antibody detection of BLM on chromosome spreads may not be representative of BLM's spatiotemporal recruitment to centromeres of intact fully condensed mitotic chromosomes. Therefore, it remains unclear whether BLM is a centromere associated protein in unperturbed cellular conditions or whether PLK1 plays a role in regulating the recruitment of BLM to centromeres.

Cells may require a small level of BLM at centromeres in order to deal with recombination structures that may persist into mitosis. BLM is required for processing recombination intermediates that arise during S-phase, and for the dissolution of double-Holliday junctions (dHJ) in DSB repair. Therefore, it is conceivable that the complex DNA composition at centromeres would require processing by factors such as BLM, before chromosome segregation can proceed, as supported by Rouzeau et al. (2012).

If BLM is genuinely a centromere associating protein, it would imply that PLK1 does not prevent BLM recruitment to centromeres. Instead, PLK1 activity may be required to regulate the level of BLM recruitment or retention to centromeres. This is likely via protein phosphorylation. Various lines of research, including within this thesis, have shown that BLM is hyperphosphorylated following a mitotic arrest (Dutertre et al. 2000, 2002; Leng et al. 2006). PLK1 contributes to the hyperphosphorylation status of BLM during a mitotic arrest **(Fig. 5.21a)**, showing that PLK1 contributes to BLM phosphorylation. A quantitative mass spectrometry analysis revealed evidence for a direct PLK1-dependent phosphorylation event on BLM at Ser539 (Grosstessner-Hain et al. 2011). Therefore, PLK1 may directly regulate BLM activity, or its spatiotemporal

localisation through protein phosphorylation. PLK1 has also been shown to directly interact with BLM following an MPS-1 dependent phosphorylation event at BLM-Ser144 and this PLK1-BLM interaction was enhanced following a mitotic arrest using nocodazole (Leng et al. 2006).

The hyperphosphorylated form of BLM is considered to represent the early mitotic status of BLM (Dutertre et al. 2002). The hyperphosphorylated mitotic BLM is found only in a soluble fraction and excluded from the nuclear matrix (Dutertre et al. 2000). Although, it remains unknown whether this BLM is active. Therefore, it could be speculated that BLM is hyperphosphorylated during early mitosis and this prevents BLM from associating with chromatin during this stage. This could explain why BLM was not readily detectable at centromeres of unperturbed pre-anaphase stage mitotic cells during this study. However, it cannot be ruled out that cells require small levels of BLM at the centromere throughout mitosis, in order to deal with sister-chromatid disjunction issues (Rouzeau et al. 2012).

Catalytically active BLM is required during anaphase for UFB processing (Baumann et al. 2007; Chan et al. 2007; Chan et al. 2018). Therefore, it is predicted that early mitotic BLM is hyperphosphorylated and this largely prevents BLM from binding to chromatin. Following anaphase onset, BLM hyperphosphorylation is lost and BLM is then able to recruit to chromatin, in particular centromeres and UFBs.

This potential spatiotemporal coordination of BLM recruitment and activity would require tight regulation. Therefore, it is conceivable that PLK1 dependent phosphorylation of BLM could function to safeguard against the untimely recruitment and activity of mitotic BLM. In support of this idea, BLM has been shown to poorly associate to premature PICH bound c-UFBs, which can be induced by a depletion of the centromeric cohesin protector, shugoshin (SGO1) **(see previous Fig. 5.22)** (Baumann et al. 2007; Chan et al. 2007).

However, it remains unclear whether PLK1-dependent phosphorylation of BLM alters the catalytic potential of BLM. It would be of great interest in the future to examine and identify the exact PLK1-dependent phosphorylation sites of BLM. The creation and experimentation of BLM phospho-mutants may help to reveal greater detail regarding PLK1's potential as a regulator of BLM recruitment and catalytic activity during mitosis.

Does PLK1 regulate the catalytic activity of PICH to promote centromere deformation?

During PLK1 inactivation, PICH alone was insufficient to drive centromere deformation. Instead, the catalytic activity of PICH may be responsible for the initiation of centromere deformation. Exactly how this occurs remains unknown. BLM helicase activity has been identified as being responsible for the DNA unwinding activity at the centromere, during the inactivation of PLK1. However, BLM requires PICH for its subcellular localisation to centromeres. Therefore, it is possible that PICH is responsible for initiating the early events that promote BLM-dependent DNA unwinding, during PLK1 inactivation.

Inactivation of the catalytic activity of PICH suppressed pre-anaphase DNA thread formation, when PLK1 activity was compromised. However, it must be noted that due to time constraints, whether the catalytically inactive PICH mutant protein remains capable of recruiting BLM to centromeres was not determined. Therefore, although catalytically inactive PICH cells no longer display centromere deformation phenotypes (pre-anaphase DNA threads), this could be due to an absence of BLM recruitment to centromeres. Hence, the most immediate future experiment would be to examine whether catalytically inactive PICH mutant cells are able to recruit BLM to centromeres, during PLK1 inhibition.

Both the current study and previous reports have identified that PICH is a substrate of PLK1 **(Fig. 5.21b)** (Baumann et al. 2007; Lera et al. 2016). However, a comprehensive *in vitro* report on the regulation of PICH has shown that the inhibition of PLK1, using the PLK1 inhibitor ZK-Thiazolidinone (TAL), did not have an inhibitory effect to PICH's ATPase

activity (Kaulich et al. 2012). Therefore, it is probable that PLK1 is not responsible for regulating the catalytic activity of PICH.

PICH clearly has an influential role to play in promoting centromere deformation during PLK1 inactivation and in its absence, centromere deformation is abolished. It remains unclear whether PICH just facilitates the recruitment of BLM to centromeres or whether the catalytic activity of PICH directly promotes centromere deformation. If BLM is capable of recruiting to centromeres of catalytically inactive PICH mutants, the catalytic activity of PICH may lead to the creation of a DNA substrate, which BLM can then act upon. Subsequently, this could lead to the initiation of centromere deformation during PLK1 inhibition. In support of this idea, it has been reported that PICH has chromatin remodelling capabilities (Ke et al. 2011). This may help to explain how pre-anaphase DNA threads form.

A surprising feature observed during this study was the apparent disassembly of the centromere, as shown by the loss of CENPA (inner centromere) following a metaphase collapse. CENPA is a centromere specific histone variant and makes up part of centromere located nucleosomes (Earnshaw and Rothfield 1985). CENP-A containing nucleosomes remain present throughout the cell cycle. Therefore, it's apparent absence after PLK1 inactivation is unexpected and suggests that the core centromere was being dismantled. Thus, pre-anaphase DNA threads may be due to a dechromatinisation of centromeric DNA. This could be driven by the activity of PICH, which may also explain the progressive absence of CENPA after metaphase collapse during PLK1 inactivation.

Furthermore, it was also possible, although very rare, to observe centromeres that maintained intact sister-kinetochore complexes (NUF2). One side remained anchored to the core centromere via a short PICH associated DNA thread. This could represent a scenario in which the core centromere is being pulled out from beneath the kinetochore complex and this may be driven by PICH remodelling the chromatin at this site. PICH has previously been implicated in a role that involves histone eviction (Ke et al. 2011), so

PICH may function to remodel centromeric chromatin, which could lead to centromere fragility in the absence of PLK1 activity. However, this remains as speculation, as the catalytic activity of PICH may simply be required for BLM recruitment to centromeres.

Does PLK1 inhibition result in an inappropriate centromeric DNA configuration?

Another possible explanation of how centromere deformation arises is that PLK1 inactivation results in changes to centromeric DNA structure or configuration. PLK1 has a vast number of substrates. In particular, PLK1 targets various centromere and kinetochore associated factors. Therefore, PLK1-dependent phosphorylation of currently unknown factor(s), may enhance centromeric DNA rigidity, thereby protecting centromeres from deformation. Thus, during PLK1 inhibition, centromeres may feature an intrinsic fragility.

It would be interesting to test which PLK-dependent centromere/kinetochore target(s) may affect centromere structure or configuration. However, due to the extensive repertoire of targets PLK1 has, identifying which one is responsible for maintaining correct centromere configuration is not simple. Furthermore, it may be a combination of targets involved. A strong candidate for future investigation would be to examine if PLK1 influences centromeric chromatin organisation, through a direct phosphorylation of histones.

During this study, a very partial rescue of centromere deformation was observed when active PLK1 was directly tethered to chromatin (PLK1-Δ^{C}-H2B). This could imply that PLK1 activity modulates chromatin arrangement. Therefore, the direct phosphorylation of histones may promote chromatin rigidity, particularly at the centromere. However, extensive investigation into PLK1-dependent phosphorylation events of histones are needed to test this idea.

Does an absence of PLK1 activity effect chromosome condensation at centromeres?

An alternative explanation for how centromeric DNA configuration could become incorrectly altered during PLK1 inactivation, may be due to changes in the activity of chromosome condensation. PLK1 inactivation prevents cells from progressing into anaphase. This results in a prolonged mitotic arrest and the appearance of short hyper-condensed chromosomes, due to continual condensation of chromosomes by the action of condensin complexes. Condensation of mitotic chromosomes ensures correct chromosome organisation, beginning at prophase and peaking during metaphase (Hirano 2005). However, during prolonged mitotic arrests, such as during PLK1 inhibition, the continual compaction of chromosomes may negatively affect DNA arrangement and promote unwanted changes to DNA configuration, in particular at centromeres.

Vertebrates require the action of both condensin I and II for correct chromosome assembly during mitosis (Hirano 2005). Depletion of condensin factors results in chromosome morphological changes and errors in segregation (Ono et al. 2004). This highlights the importance of condensin complexes for cellular homeostasis.

Condensin I has been described to compact sister chromatids laterally (i.e. inwards), whilst condensin II supports axial compaction (i.e. shortening of chromosome length) (Hirano 2012). Therefore, it is conceivable that the continual compaction of mitotic chromosomes during PLK1 inactivation, whether lateral or axial, may cause stress build up and tension within the centromeric domain of chromosomes. In particular, excessive axial compaction could generate excessive tension due to compression within the centromeric region of the chromosomes. This idea can be conceptually recreated by twisting a piece of string at each end in opposite directions. Eventually the tension builds at the middle part of the string, representative of the centromere. Therefore, PLK1 inactivation may indirectly promote centromere distortion due to structural changes, driven by excessive chromosome condensation. It could also be speculated that PICH

detects such DNA configuration changes caused by excessive condensation, particularly at centromeres.

The most important experiment to explore this theory would be to examine the effects of condensin depletion. The depletion of condensin complexes may help to limit the hyper-condensation of mitotic chromosomes during PLK1 inhibition, which may then display signs of centromere deformation rescue.

Alternatively, the absence of PLK1 activity may promote inappropriate chromosome compaction at the centromere, possibly caused by a lack of PLK1-dependent regulation of condensin activity. Chromosome condensation is considered to be regulated by protein phosphorylation. CDK1-dependent phosphorylation of condensin II (CAP-D3) promotes the early stages of chromosome condensation, whilst additional mitotic kinases further influence condensin activity (Abe et al. 2011; Bazile et al. 2010). This includes the PLK1-dependent phosphorylation of condensin II, which has been reported to regulate both condensin II abundance and activity (CAP-H2) (Kagami et al. 2017). Therefore, a disruption to the activity of PLK1 could alter the action of condensin complexes.

Additionally, it has also been suggested that condensin II is enriched at the inner kinetochore region (Ono et al. 2004). This highlights a possible requirement for condensin II activity at centromere regions. Centromere specific CENP-A containing nucleosome arrays have been reported to be more condensed than canonical DNA arrays (Panchenko et al. 2011), again highlighting the importance of correct chromosome condensation, specifically at the centromere. Hence, an absence of PLK1 activity could affect the levels of chromosome compaction at the centromeres. This could promote an intrinsic fragility of the centromere/kinetochore region, especially during KT-MT attachment and tension during metaphase.

Depletion of condensin has been shown to promote errors in KT-MT attachment, along with segregation defects (Hirano 2012). Moreover, condensin has been shown to be directly involved in the correct assembly of centromeric DNA (Samoshkin et al. 2009). The same study also revealed phenotypes that resemble the cellular outcomes reported during this study, when PLK1 is inhibited. Following condensin depletion, metaphase alignment becomes disorganised and centromeric regions display signs of stretching, which could be rescued by addition of nocodazole. Additionally, CENP-A detection becomes diminished following condensin depletion (Samoshkin et al. 2009). Each of these observations resemble the findings in the current study, when PLK1 activity has been compromised. Therefore, it is possible that the activity of both PLK1 and condensin complexes are essential for maintaining the correct centromere organisation during mitosis.

The incorrect compaction of centromeric DNA during the depletion of condensin complexes or PLK1 inactivation, may therefore promote centromere deformation. This could become apparent due to the pulling forces of the mitotic spindle, during KT-MT attachment and tension. The incorrect compaction of centromeric DNA could lead to a fragility at the centromere, which results in an inability of centromeres to counteract spindle pulling forces. This could result in the exposure of centromeric DNA via stretching. This stretched DNA may become a target for proteins such as PICH and BLM. This could provide an explanation for the reported centromere deformation pathway during PLK1 inactivation, but extensive investigation is required to confirm this.

It would be interesting to confirm whether condensin depletion resulted in a similar phenotype to the current findings caused by PLK1 inactivation. Additionally, it would also be interesting to determine whether condensin depletion during PLK1 inactivation was able to rescue centromere deformation.

Overall, this study has revealed a previously unreported centromere deformation pathway that is suppressed by the activity of PLK1. Despite identifying the main

contributing factors of centromere deformation, notably the catalytic activity of PICH and BLM, questions remain unanswered. These include whether PLK1 activity regulates the recruitment and/or activity of BLM and/or PICH. Additionally, further research is required to explore how centromere configuration may become disorganised during PLK1 inactivation. Future investigation would aim at trying to address some of these unanswered questions that remain.

Bibliography

Abe, Satoshi et al. 2011. “The Initial Phase of Chromosome Condensation Requires Cdk1-Mediated Phosphorylation of the CAP-D3 Subunit of Condensin II.” *Genes and Development* 25(8): 863–74.

Abrieu, Ariane et al. 2001. “Mps1 Is a Kinetochore-Associated Kinase Essential for the Vertebrate Mitotic Checkpoint.” *Cell* 106(1): 83–93.

Addis Jones, O. et al. 2019. “PLK1 Facilitates Chromosome Biorientation by Suppressing Centromere Disintegration Driven by BLM-Mediated Unwinding and Spindle Pulling.” *Nature Communications* 10(1): 2861.

Ahonen, Leena J. et al. 2005. “Polo-like Kinase 1 Creates the Tension-Sensing 3F3/2 Phosphoepitope and Modulates the Association of Spindle-Checkpoint Proteins at Kinetochores.” *Current Biology* 15(12): 1078–89.

Albers, Eliene et al. 2018. “Loss of PICH Results in Chromosomal Instability, P53 Activation, and Embryonic Lethality.” *Cell Reports* 24(12): 3274–84.

Alexandru, Gabriela et al. 2001. 105 Cell *Phosphorylation of the Cohesin Subunit Scc1 by Polo/Cdc5 Kinase Regulates Sister Chromatid Separation in Yeast*.

Amano, Miho et al. 2009. “The CENP-S Complex Is Essential for the Stable Assembly of Outer Kinetochore Structure.” *Journal of Cell Biology* 186(2): 173–82.

De Antoni, Anna et al. 2005. “The Mad1/Mad2 Complex as a Template for Mad2 Activation in the Spindle Assembly Checkpoint.” *Current Biology* 15: 214–25.

Archambault, Vincent et al. 2008. “Sequestration of Polo Kinase to Microtubules by Phosphopriming-Independent Binding to Map205 Is Relieved by Phosphorylation at a CDK Site in Mitosis.” *Genes and Development* 22(19): 2707–20.

Archambault, Vincent, and David M. Glover. 2009. “Polo-like Kinases: Conservation and Divergence in Their Functions and Regulation.” *Nature Reviews Molecular Cell Biology* 10(4): 265–75.

Arumugam, Prakash et al. 2003. “ATP Hydrolysis Is Required for Cohesin’s Association with Chromosomes.” *Current Biology* 13(22): 1941–53.

Bachrati, Csanád Z., and Ian D. Hickson. 2008. “RecQ Helicases: Guardian Angels of the DNA Replication Fork.” *Chromosoma* 117(3): 219–33.

Barefield, Colleen, and Jan Karlseder. 2012. “The BLM Helicase Contributes to Telomere Maintenance through Processing of Late-Replicating Intermediate Structures.” *Nucleic Acids Research* 40(15): 7358–67.

Barnhart, Meghan C. et al. 2011. “HJURP Is a CENP-A Chromatin Assembly Factor Sufficient to Form a Functional de Novo Kinetochore.” *Journal of Cell Biology* 194(2): 229–43.

Barr, Francis A., Herman H W Silljé, and Erich A. Nigg. 2004. “Polo-like Kinases and the Orchestration of Cell Division.” *Nature Reviews Molecular Cell Biology* 5(6): 429–40.

Barra, Viviana, and Daniele Fachinetti. 2018. “The Dark Side of Centromeres: Types, Causes and Consequences of Structural Abnormalities Implicating Centromeric DNA.” *Nature Communications* 9(1).

Baumann, Christoph, Roman Körner, Kay Hofmann, and Erich A. Nigg. 2007. “PICH, a Centromere-Associated SNF2 Family ATPase, Is Regulated by Plk1 and Required for the Spindle Checkpoint.” *Cell* 128(1): 101–14.

Bazile, Franck, Julie St-Pierre, and Damien D’Amours. 2010. “Three-Step Model for Condensin Activation during Mitotic Chromosome Condensation.” *Cell Cycle* 9(16): 3243–55.

Biebricher, Andreas S. et al. 2013. “PICH: A DNA Translocase Specially Adapted for Processing Anaphase Bridge DNA.” *Molecular Cell* 51(5): 691–701.

Bloom, David. 1954. “Congenital Telangiectatic Erythema Resembling Lupus Erythematosus in Dwarfs. Probably a Syndrome Entity.” *AMA Am J Dis Child* 88(6): 754–58.

Bodnar, Andrea G et al. 1998. “Extension of Life-Span by Introduction of Telomerase into Normal Human Cells Author(S.” *Science* 279(5349): 349–52.

Brosh, Robert M. et al. 2000. “Replication Protein a Physically Interacts with the Bloom’s Syndrome Protein and Stimulates Its Helicase Activity.” *Journal of Biological Chemistry* 275(31): 23500–508.

Bruinsma, Wytse et al. 2013. “Bora and Aurora-A Continue to Activate Plk1 in Mitosis.” *Journal of Cell Science* 127(4): 801–11.

Bruinsma, Wytse, Jonne A. Raaijmakers, and René H. Medema. 2012. “Switching Polo-like Kinase-1 on and off in Time and Space.” *Trends in Biochemical Sciences* 37(12): 534–42.

Burkard, Mark E. et al. 2007. “Chemical Genetics Reveals the Requirement for Polo-like Kinase 1 Activity in Positioning RhoA and Triggering Cytokinesis in Human Cells.” *Proceedings of the National Academy of Sciences* 104(11): 4383–88.

Carbon, John, and Louise Clarke. 1984. “Structural and Functional Analysis of a Yeast Centromere.” *Journal of Cell Science* (Supplement 1): 43–58.

de Cárcer, Guillermo, B. Escobar, et al. 2011. “Plk5, a Polo Box Domain-Only Protein with Specific Roles in Neuron Differentiation and Glioblastoma Suppression.” *Molecular and Cellular Biology* 31(6): 1225–39.

de Cárcer, Guillermo, Gerard Manning, and Marcos Malumbres. 2011. “From Plk1 to Plk5: Functional Evolution of Polo-like Kinases.” *Cell Cycle* 10(14): 2255–62.

Carmena, Mar, Michael Wheelock, Hironori Funabiki, and William C. Earnshaw. 2012. “The Chromosomal Passenger Complex (CPC): From Easy Rider to the Godfather of Mitosis.” *Nature Reviews Molecular Cell Biology* 13: 789–803.

Carroll, Christopher W. et al. 2009. “Centromere Assembly Requires the Direct Recognition of CENP-A Nucleosomes by CENP-N.” *Nature Cell Biology* 11(7): 896–902.

Carroll, Christopher W., Kirstin J. Milks, and Aaron F. Straight. 2010. “Dual Recognition

of CENP-A Nucleosomes Is Required for Centromere Assembly." *Journal of Cell Biology* 189(7): 1143–55.

Casenghi, M., Francis A. Barr, and Erich A. Nigg. 2005. "Phosphorylation of Nlp by Plk1 Negatively Regulates Its Dynein-Dynactin-Dependent Targeting to the Centrosome." *Journal of Cell Science* 118(21): 5101–8.

Chaganti, R. S. K., S. Schonberg, and James German. 1974. "A Manyfold Increase in Sister Chromatid Exchanges in Bloom's Syndrome Lymphocytes." *Proceedings of the National Academy of Sciences* 71(11): 4508–12.

Chan, Kok Lung, and Ian D. Hickson. 2009. "On the Origins of Ultra-Fine Anaphase Bridges." *Cell Cycle* 8(19): 3065–66.

Chan, Kok Lung, Phillip S. North, and Ian D. Hickson. 2007. "BLM Is Required for Faithful Chromosome Segregation and Its Localization Defines a Class of Ultrafine Anaphase Bridges." *EMBO Journal* 26(14): 3397–3409.

Chan, Kok Lung, Timea Palmai-Pallag, Songmin Ying, and Ian D. Hickson. 2009. "Replication Stress Induces Sister-Chromatid Bridging at Fragile Site Loci in Mitosis." *Nature Cell Biology* 11(6): 753–60.

Chan, Ying Wai, Kasper Fugger, and Stephen C. West. 2018. "Unresolved Recombination Intermediates Lead to Ultra-Fine Anaphase Bridges, Chromosome Breaks and Aberrations." *Nature Cell Biology* 20(1): 92–103.

Cheeseman, Iain M. 2014. "The Kinetochore." *Cold Spring Harbor Perspectives in Biology* 94(C): 77–105.

Cheeseman, Iain M., and A. Desai. 2008. "Molecular Architecture of the Kinetochore-Microtubule Interface." *Nature Reviews Molecular Cell Biology* 9(1): 33–46.

Chen, Rey-Huei, Andrej Shevchenko, Matthias Mann, and Andrew W. Murray. 1998. "Spindle Checkpoint Protein Xmad1 Recruits Xmad2 to Unattached Kinetochores." *Journal of Cell Biology* 143(2): 283–95.

Chen, Rey-Huei, Jennifer C. Waters, Edward D. Salmon, and Andrew W. Murray. 1996. "Association of Spindle Assembly Checkpoint Component XMAD2 with Unattached Kinetochores." *Science* 274(5285): 242–46.

Ciccia, Alberto, and Stephen J. Elledge. 2010. "The DNA Damage Response: Making It Safe to Play with Knives." *Molecular Cell* 40(2): 179–204.

Cimini, Daniela, Bonnie J Howell, and Edward D. Salmon. 2015. "Merotelic Kinetochore Orientation Is a Major Mechanism of Aneuploidy in Mitotic Mammalian Tissue Cells." 153(3): 1–11.

Ciosk, Rafal et al. 2000. "Cohesin's Binding to Chromosomes Depends on a Separate Complex Consisting of Scc2 and Scc4 Proteins." *Molecular Cell* 5: 243–54.

Clarke, Louise, and John Carbon. 1980. "Isolation of a Yeast Centromere and Construction of Functional Small Circular Chromosomes." *Nature* 287: 504–9.

Clarke, Louise, and John Carbon. 1983. "Genomic Substitutions of Centromeres in Saccharomyces Cerevisiae."
Nature 305(5929): 23–28.

Conduit, Paul T., Alan Wainman, and Jordan W. Raff. 2015. "Centrosome Function and

Assembly in Animal Cells." *Nature Reviews Molecular Cell Biology* 16(10): 611–24.

Dambacher, Silvia et al. 2012. "CENP-C Facilitates the Recruitment of M18BP1 to Centromeric Chromatin." *Nucleus* 3(1): 101–10.

Darlington, Cyril Dean, and Alfred Daniel Hall. 1936. "The External Mechanics of the Chromosomes I—The Scope of Enquiry." *Proceedings of the Royal Society of London. Series B - Biological Sciences* 121(823): 264–73.

Darzynkiewicz, Zbigniew, H. Dorota Halicka, Hong Zhao, and Monika Podhorecka. 2011. "Cell Synchronization by Inhibitors of DNA Replication Induces Replication Stress and DNA Damage Response: Analysis by Flow Cytometry." *Methods in Molecular Biology* 761: 85–96.

Davies, Sally L., Phillip S. North, and Ian D. Hickson. 2007. "Role for BLM in Replication-Fork Restart and Suppression of Origin Firing after Replicative Stress." *Nature Structural and Molecular Biology* 14(7): 677–79.

DeLuca, Jennifer G., and Andrea Musacchio. 2012. "Structural Organization of the Kinetochore-Microtubule Interface." *Current Opinion in Cell Biology* 24(1): 48–56.

Dreier, Megan R., Michael E. Bekier, and William R. Taylor. 2011. "Regulation of Sororin by Cdk1-Mediated Phosphorylation." *Journal of Cell Science* 124(17): 2976–87.

Drinnenberg, Ines A, Dakota DeYoung, Steven Henikoff, and Harmit Singh Malik. 2014. "Recurrent Loss of CenH3 Is Associated with Independent Transitions to Holocentricity in Insects." *eLife* 3.

Dunleavy, Elaine M. et al. 2009. "HJURP Is a Cell-Cycle-Dependent Maintenance and Deposition Factor of CENP-A at Centromeres." *Cell* 137(3): 485–97.

Dutertre, Stéphanie et al. 2000. "Cell Cycle Regulation of the Endogenous Wild Type Bloom's Syndrome DNA Helicase." *Oncogene* 19(23): 2731–38.

———. 2002. "Dephosphorylation and Subcellular Compartment Change of the Mitotic Bloom's Syndrome DNA Helicase in Response to Ionizing Radiation." *Journal of Biological Chemistry* 277(8): 6280–86.

Earnshaw, William C. et al. 1987. "Molecular Cloning of CDNA for CENP-B, the Major Human Centromere Autoantigen." *Journal of Cell Biology* 104(4): 817–29.

———. 2013. "Esperanto for Histones: CENP-A, Not CenH3, Is the Centromeric Histone H3 Variant." *Chromosome Research* 21(2): 101–6.

Earnshaw, William C., and Naomi Rothfield. 1985. "Identification of a Family of Human Centromere Proteins Using Autoimmune Sera from Patients with Scleroderma." *Chromosoma* 91(3–4): 313–21.

Elia, Andrew, Peter Rellos, et al. 2003. "The Molecular Basis for Phosphodependent Substrate Targeting and Regulation of Plks by the Polo-Box Domain." *Cell* 115(1): 83–95.

Elia, Andrew, Lewis Cantley, and Michael B. Yaffe. 2003. "Proteomic Screen Finds PSer/PThr-Binding Domain Localizing Plk1 to Mitotic Substrates." *Science* 299(5610): 1228–31.

Ellis, Nathan A. et al. 1995. “The Bloom’s Syndrome Gene Product Is Homologous to RecQ Helicases.” *Cell* 83(4): 655–66.

Elowe, Sabine et al. 2007. “Tension-Sensitive Plk1 Phosphorylation on BubR1 Regulates the Stability of Kinetochore-Microtubule Interactions.” *Genes and Development* 21(17): 2205–19.

Fachinetti, Daniele et al. 2013. “A Two-Step Mechanism for Epigenetic Specification of Centromere Identity and Function.” *Nature Cell Biology* 15(9): 1056–66.

———. 2015. “DNA Sequence-Specific Binding of CENP-B Enhances the Fidelity of Human Centromere Function.” *Developmental Cell* 33(3): 314–27.

Fernández-Casañas, María, and Kok Lung Chan. 2018. “The Unresolved Problem of DNA Bridging.” *Genes* 9(12): 623.

Foley, Emily A., and Tarun M. Kapoor. 2013. “Microtubule Attachment and Spindle Assembly Checkpoint Signalling at the Kinetochore.” *Nature Reviews Molecular Cell Biology* 14(1): 25–37.

Foltz, Daniel R. et al. 2006. “The Human CENP-A Centromeric Nucleosome-Associated Complex.” *Nature Cell Biology* 8(5): 458–69.

———. 2009. “Centromere-Specific Assembly of CENP-A Nucleosomes Is Mediated by HJURP.” *Cell* 137(3): 472–84.

Fujita, Risa et al. 2015. “Stable Complex Formation of CENP-B with the CENP-A Nucleosome.” *Nucleic Acids Research* 43(10): 4909–22.

Fujita, Yohta et al. 2007. “Priming of Centromere for CENP-A Recruitment by Human HMis18α, HMis18β, and M18BP1.” *Developmental Cell* 12(1): 17–30.

Funk, Laura C., Lauren M. Zasadil, and Beth A. Weaver. 2016. “Living in CIN: Mitotic Infidelity and Its Consequences for Tumor Promotion and Suppression.” *Developmental Cell* 39(6): 638–52.

Furuya, Kanji, Kohta Takahashi, and Mitsuhiro Yanagida. 1998. “Faithful Anaphase Is Ensured by Mis4, a Sister Chromatid Cohesion Molecule Required in S Phase and Not Destroyed in G1 Phase.” *Genes and Development* 12(21): 3408–18.

Gandhi, Rita, Peter J. Gillespie, and Tatsuya Hirano. 2006. “Human Wapl Is a Cohesin-Binding Protein That Promotes Sister-Chromatid Resolution in Mitotic Prophase.” *Current Biology* 16(24): 2406–17.

Gascoigne, Karen E., and Iain M. Cheeseman. 2013. “CDK-Dependent Phosphorylation and Nuclear Exclusion Coordinately Control Kinetochore Assembly State.” *Journal of Cell Biology* 201(1): 23–32.

Gerlich, Daniel et al. 2006. “Condensin I Stabilizes Chromosomes Mechanically through a Dynamic Interaction in Live Cells.” *Current Biology* 16(4): 333–44.

German, James. 1997. “Bloom’s Syndrome. XX. The First 100 Cancers*.” *Cancer genetics and cytogenetics* 93(1): 100–106.

German, James, Reginald Archibald, and David Bloom. 1965. “Chromosomal Breakage in a Rare and Probably Genetically Determined Syndrome of Man.” *Science* 148(3669): 506–7.

Gibcus, Johan H. et al. 2018. “A Pathway for Mitotic Chromosome Formation.” *Science* 359(6376).

Gillespie, Peter J., and Tatsuya Hirano. 2004. “Scc2 Couples Replication Licensing to Sister Chromatid Cohesion in Xenopus Egg Extracts.” *Current Biology* 14: 1598–1603.

Glover, Thomas W., Thomas E. Wilson, and Martin F. Arlt. 2017. “Fragile Sites in Cancer: More than Meets the Eye.” *Nature Reviews Cancer* 17(8): 489–501. http://dx.doi.org/10.1038/nrc.2017.52.

Golsteyn, R M, K E Mundt, Andrew M Fry, and Erich A. Nigg. 1995. “Cell Cycle Analysis and Chromosomal Localization of Human Plk1, a Putative Homologue of the Protien Kinase Involved in Mitotic Spindle Function.” *J Cell Biol* 129(6): 1617–28.

Goto, Hidemasa et al. 2006. “Complex Formation of Plk1 and INCENP Required for Metaphase-Anaphase Transition.” *Nature Cell Biology* 8(2): 180–87.

Green, L. C. et al. 2012. “Contrasting Roles of Condensin I and Condensin II in Mitotic Chromosome Formation.” *Journal of Cell Science* 125(6): 1591–1604.

Gregan, Juraj et al. 2011. “Merotelic Kinetochore Attachment: Causes and Effects.” *Trends in Cell Biology* 21(6): 374–81.

Grosstessner-Hain, Karin et al. 2011. “Quantitative Phospho-Proteomics to Investigate the Polo-like Kinase 1-Dependent Phospho-Proteome.” *Molecular & Cellular Proteomics* 10(11).

Gruber, Stephan et al. 2006. “Evidence That Loading of Cohesin Onto Chromosomes Involves Opening of Its SMC Hinge.” *Cell* 127(3): 523–37.

Guse, Annika et al. 2011. “In Vitro Centromere and Kinetochore Assembly on Defined Chromatin Templates.” *Nature* 477(7364): 354–58.

Gutiérrez-Caballero, Cristina, Luis R. Cebollero, and Alberto M. Pendás. 2012. “Shugoshins: From Protectors of Cohesion to Versatile Adaptors at the Centromere.” *Trends in Genetics* 28(7): 351–60.

Habedanck, Robert, York Dieter Stierhof, Christopher J. Wilkinson, and Erich A. Nigg. 2005. “The Polo Kinase Plk4 Functions in Centriole Duplication.” *Nature Cell Biology* 7(11): 1140–46.

Haering, Christian H. et al. 2008. “The Cohesin Ring Concatenates Sister DNA Molecules.” *Nature* 454(7202): 297–301.

Haering, Christian H., Jan Löwe, Andreas Hochwagen, and Kim Nasmyth. 2002. “Molecular Architecture of SMC Proteins and the Yeast Cohesin Complex.” *Molecular Cell* 9: 773–88.

Hamanaka, R et al. 1994. “Cloning and Characterization of Human and Murine Homologues of the Drosophila Polo Serine-Threonine Kinase.” *Cell growth & differentiation : the molecular biology journal of the American Association for Cancer Research* 5(3): 249–57.

Hanisch, A. 2006. “Different Plk1 Functions Show Distinct Dependencies on Polo-Box Domain-Mediated Targeting.” *Molecular Biology of the Cell* 17(1): 448–59.

Harrigan, Jeanine A. et al. 2011. “Replication Stress Induces 53BP1-Containing OPT Domains in G1 Cells.” *Journal of Cell Biology* 193(1): 97–108.

Hauf, Silke et al. 2005. “Dissociation of Cohesin from Chromosome Arms and Loss of Arm Cohesion during Early Mitosis Depends on Phosphorylation of SA2.” In *PLoS Biology*, , 0419–32.

Hauf, Silke, C. Waizenegger, Irene, and Jan-Michael Peters. 2001. “Cohesin Cleavage by Seperase Required for Anaphase and Cytokinesis in Human Cells.” *Science* 293: 1320–23.

Heald, Rebecca, and Alexey Khodjakov. 2015. “Thirty Years of Search and Capture: The Complex Simplicity of Mitotic Spindle Assembly.” *Journal of Cell Biology* 211(6): 1103–11.

Hengeveld, Rutger C.C. et al. 2015. “Rif1 Is Required for Resolution of Ultrafine DNA Bridges in Anaphase to Ensure Genomic Stability.” *Developmental Cell* 34(4): 466–74.

———. 2017. “Inner Centromere Localization of the CPC Maintains Centromere Cohesion and Allows Mitotic Checkpoint Silencing.” *Nature Communications* 8.

Heun, Patrick et al. 2006. “Mislocalization of the Drosophila Centromere-Specific Histone CID Promotes Formation of Functional Ectopic Kinetochores.” *Developmental Cell* 10(3): 303–15.

Hinshaw, Stephen M., and Stephen C. Harrison. 2018. “Kinetochore Function from the Bottom Up.” *Trends in Cell Biology* 28(1): 22–33.

Hiraga, Shin Ichiro et al. 2014. “Rif1 Controls DNA Replication by Directing Protein Phosphatase 1 to Reverse Cdc7- Mediated Phosphorylation of the MCM Complex.” *Genes and Development* 28(4): 372–83.

Hirano, Michiko, and Tatsuya Hirano. 2006. “Opening Closed Arms: Long-Distance Activation of SMC ATPase by Hinge-DNA Interactions.” *Molecular Cell* 21(2): 175–86.

Hirano, Tatsuya. 2005. “Condensins: Organizing and Segregating the Genome.” *Current Biology* 15(7).

———. 2012. “Condensins: Universal Organizers of Chromosomes with Diverse Functions.” *Genes and Development* 26(15): 1659–78.

———. 2016. “Condensin-Based Chromosome Organization from Bacteria to Vertebrates.” *Cell* 164(5): 847–57.

Hoffmann, Sebastian et al. 2016. “CENP-A Is Dispensable for Mitotic Centromere Function after Initial Centromere/Kinetochore Assembly.” *Cell Reports* 17(9): 2394–2404.

Holm, Connie. 1994. “Coming Undone: How to Untangle a Chromosome.” *Cell* 77(7): 955–57.

Hori, Tetsuya et al. 2008. “CCAN Makes Multiple Contacts with Centromeric DNA to Provide Distinct Pathways to the Outer Kinetochore.” *Cell* 135(6): 1039–52.

Hori, Tetsuya, and T. Fukagawa. 2012. “Establishment of the Vertebrate Kinetochores.”

Chromosome Research 20(5): 547–61.

Hori, Tetsuya, Masahiro Okada, K. Maenaka, and T. Fukagawa. 2007. "CENP-O Class Proteins Form a Stable Complex and Are Required for Proper Kinetochore Function." *Molecular Biology of the Cell* 19(3): 843–54.

Hori, Tetsuya, Wei Hao Shang, Kozo Takeuchi, and T. Fukagawa. 2013. "The CCAN Recruits CENP-A to the Centromere and Forms the Structural Core for Kinetochore Assembly." *Journal of Cell Biology* 200(1): 45–60.

Hou, Fajian, and Hui Zou. 2005. "Two Human Orthologues of Eco1/Ctf7 Acetyltransferases Are Both Required for Proper Sister-Chromatid Cohesion." *Molecular Biology of the Cell* 16: 3908–18.

Howell, Bonnie J et al. 2000. "Visualization of Mad2 Dynamics at Kinetochores, along Spindle Fibers, and at Spindle Poles in Living Cells." *Journal of Cell Biology* 150(6): 1233–49.

———. 2004. "Spindle Checkpoint Protein Dynamics at Kinetochores in Living Cells." *Current Biology* 14(11): 953–64.

Hoyt, M. Andrew, Laura Totis, and B. Tibor Roberts. 1991. "S. Cerevisiae Genes Required for Cell Cycle Arrest in Response to Loss of Microtubule Function." *Cell* 66(3): 507–17.

Hu, P. 2002. "Evidence for BLM and Topoisomerase IIIalpha Interaction in Genomic Stability." *Human Molecular Genetics* 10(12): 1287–98.

Hübner, Nadja C. et al. 2010. "Re-Examination of SiRNA Specificity Questions Role of PICH and Taol in the Spindle Checkpoint and Identifies Mad2 as a Sensitive Target for Small RNAs." *Chromosoma* 119(2): 149–65.

Hudson, Damien F., Paola Vagnarelli, Reto Gassmann, and William C. Earnshaw. 2003. "Condensin Is Required for Nonhistone Protein Assembly and Structural Integrity of Vertebrate Mitotic Chromosomes." *Developmental Cell* 5(2): 323–36.

Jana, Swadhin Chandra, J. Fernando Bazan, and Mónica Bettencourt Dias. 2012. "Polo Boxes Come out of the Crypt: A New View of PLK Function and Evolution." *Structure* 20(11): 1801–4.

Jansen, Lars E.T., B. E. Black, Daniel R. Foltz, and Don W. Cleveland. 2007. "Propagation of Centromeric Chromatin Requires Exit from Mitosis." *Journal of Cell Biology* 176(6): 795–805.

Kabeche, Lilian, Hai Dang Nguyen, Rémi Buisson, and Lee Zou. 2018. "A Mitosis-Specific and R Loop-Driven ATR Pathway Promotes Faithful Chromosome Segregation." *Science* 359(6371): 108–14.

Kagami, Yuya, Masaya Ono, and Kiyotsugu Yoshida. 2017. "Plk1 Phosphorylation of CAP-H2 Triggers Chromosome Condensation by Condensin II at the Early Phase of Mitosis." *Scientific Reports* 7(1).

Kallio, Marko J., Mark L. McCleland, P. Todd Stukenberg, and Gary J. Gorbsky. 2002. "Inhibition of Aurora B Kinase Blocks Chromosome Segregation, Overrides the Spindle Checkpoint, and Perturbs Microtubule Dynamics in Mitosis." *Current Biology* 12(11): 900–905.

Kang, Young H. et al. 2006. “Self-Regulated Plk1 Recruitment to Kinetochores by the Plk1-PBIP1 Interaction Is Critical for Proper Chromosome Segregation.” *Molecular Cell* 24(3): 409–22.

Karow, Julia K., Ronjon K Chakraverty, and Ian D. Hickson. 1997. “The Bloom’s Syndrome Gene Product Is a 3’-5’ DNA Helicase.” *J. Biol. Chem.* 272(49): 30611–14.

Kaulich, Manuel, Fabien Cubizolles, and Erich A. Nigg. 2012. “On the Regulation, Function, and Localization of the DNA-Dependent ATPase PICH.” *Chromosoma* 121(4): 395–408.

Kaur, Hardeep, Arnaud DeMuyt, and Michael Lichten. 2015. “Top3-Rmi1 DNA Single-Strand Decatenase Is Integral to the Formation and Resolution of Meiotic Recombination Intermediates.” *Molecular Cell* 57(4): 583–94.

Ke, Yuwen et al. 2011. “PICH and BLM Limit Histone Association with Anaphase Centromeric DNA Threads and Promote Their Resolution.” *EMBO Journal* 30(16): 3309–21.

Khodjakov, Alexey, Richard W. Cole, Berl R. Oakley, and Conly L. Rieder. 2000. “Centrosome-Independent Mitotic Spindle Formation in Vertebrates.” *Current Biology* 10(2): 59–67.

Kim, Soonjoung, and Hongtao Yu. 2015. “Multiple Assembly Mechanisms Anchor the KMN Spindle Checkpoint Platform at Human Mitotic Kinetochores.” *Journal of Cell Biology* 208(2): 181–96.

Kimura, Keiji, Michiko Hirano, Ryuji Kobayashi, and Tatsuya Hirano. 1998. “Phosphorylation and Activation of 13S Condensin by Cdc2 in Vitro.” *Science* 282(5388): 487–90.

Kitajima, Tomoya S. et al. 2005. “Human Bub1 Defines the Persistent Cohesion Site along the Mitotic Chromosome by Affecting Shugoshin Localization.” *Current Biology* 15: 353–59.

———. 2006. “Shugoshin Collaborates with Protein Phosphatase 2A to Protect Cohesin.” *Nature* 441(1): 46–52.

Kline, Susan L. et al. 2006. “The Human Mis12 Complex Is Required for Kinetochore Assembly and Proper Chromosome Segregation.” *Journal of Cell Biology* 173(1): 9–17.

Knutsen, Turid et al. 2010. “Definitive Molecular Cytogenetic Characterization of 15 Colorectal Cancer Cell Lines.” *Genes Chromosomes and Cancer* 49(3): 204–23.

Kops, Geert J.P.L., and Jagesh V. Shah. 2012. “Connecting up and Clearing out: How Kinetochore Attachment Silences the Spindle Assembly Checkpoint.” *Chromosoma* 121(5): 509–25.

Krenn, Veronica, and Andrea Musacchio. 2015. “The Aurora B Kinase in Chromosome Bi-Orientation and Spindle Checkpoint Signaling.” *Frontiers in Oncology* 5.

Kruse, T. et al. 2013. “Direct Binding between BubR1 and B56-PP2A Phosphatase Complexes Regulate Mitotic Progression.” *Journal of Cell Science* 126(5): 1086–92.

Kueng, Stephanie et al. 2006. “Wapl Controls the Dynamic Association of Cohesin with Chromatin.” *Cell* 127(5): 955–67.

Lampson, Michael A., and Iain M. Cheeseman. 2011. “Sensing Centromere Tension: Aurora B and the Regulation of Kinetochore Function.” *Trends in Cell Biology* 21(3): 133–40.

Lampson, Michael A., Kishore Renduchitala, Alexey Khodjakov, and Tarun M. Kapoor. 2004. “Correcting Improper Chromosomes-Spindle Attachments during Cell Division.” *Nature Cell Biology* 6(3): 232–37.

Lane, Heidi A., and Erich A. Nigg. 1996. “Antibody Microinjection Reveals an Essential Role for Human Polo-like Kinase 1 (Plk1) in the Functional Maturation of Mitotic Centrosomes.” *The Journal of Cell Biology* 135(6): 1701–13.

Lara-Gonzalez, Pablo, Frederick G. Westhorpe, and Stephen S. Taylor. 2012. “The Spindle Assembly Checkpoint.” *Current Biology* 22(22): R966–80.

Lee, Kyung S., Jung Eun Park, Satoshi Asano, and Chong J. Park. 2005. “Yeast Polo-like Kinases: Functionally Conserved Multitask Mitotic Regulators.” *Oncogene* 24(2): 217–29.

Lénárt, Péter et al. 2007. “The Small-Molecule Inhibitor BI 2536 Reveals Novel Insights into Mitotic Roles of Polo-like Kinase 1.” *Current Biology* 17(4): 304–15.

Leng, Mei et al. 2006. “MPS1-Dependent Mitotic BLM Phosphorylation Is Important for Chromosome Stability.” *Proceedings of the National Academy of Sciences* 103(31): 11485–90.

———. 2008. “Targeting Plk1 to Chromosome Arms and Regulating Chromosome Compaction by the PICH ATPase.” *Cell Cycle* 7(10): 1480–89.

Lera, Robert F. et al. 2016. “Decoding Polo-like Kinase 1 Signaling along the Kinetochore-Centromere Axis.” *Nature Chemical Biology* 12(6): 411–18.

Levine, Michelle S., and Andrew J. Holland. 2018. “The Impact of Mitotic Errors on Cell Proliferation and Tumorigenesis.” *Genes and Development* 32(9–10): 620–38.

Li, Rong, and Andrew W. Murray. 1991. “Feedback Control of Mitosis in Budding Yeast.” *Cell* 66: 519–31.

Lindon, Catherine, and Jonathon Pines. 2004. “Ordered Proteolysis in Anaphase Inactivates Plk1 to Contribute to Proper Mitotic Exit in Human Cells.” *Journal of Cell Biology* 164(2): 233–41.

Lindqvist, Arne, Verónica Rodríguez-Bravo, and René H. Medema. 2009. “The Decision to Enter Mitosis: Feedback and Redundancy in the Mitotic Entry Network.” *Journal of Cell Biology* 185(2): 193–202.

Liu, Dan et al. 2009. “Sensing Chromosome Bi-Orientation by Spatial Separation of Aurora B Kinase from Kinetochore Substrates.” *New Series* 323(5919): 1350–53.

Llamazares, S et al. 1991. “Polo Encodes a Protein Kinase Homolog Required for Mitosis in Drosophila.” *Genes and Development* 5: 2153–65.

Losada, Ana, Michiko Hirano, and Tatsuya Hirano. 2002. “Cohesin Release Is Required for Sister Chromatid Resolution, but Not for Condensin-Mediated Compaction, at

the Onset of Mitosis." *Genes and Development* 16(23): 3004–16.

Losada, Ana, T. Yokochi, Ryuji Kobayashi, and Tatsuya Hirano. 2000. "Identification and Characterization of SA/Scc3p Subunits in the Xenopus and Human Cohesin Complexes." *Journal of Cell Biology* 150(3): 405–16.

Lower, Sarah Sander, Michael P. McGurk, Andrew G. Clark, and Daniel A. Barbash. 2018. "Satellite DNA Evolution: Old Ideas, New Approaches." *Current Opinion in Genetics and Development* 49: 70–78.

Lukas, Claudia et al. 2011. "53BP1 Nuclear Bodies Form around DNA Lesions Generated by Mitotic Transmission of Chromosomes under Replication Stress." *Nature Cell Biology* 13(3): 243–53. http://dx.doi.org/10.1038/ncb2201.

Macůrek, Libor et al. 2008. "Polo-like Kinase-1 Is Activated by Aurora A to Promote Checkpoint Recovery." *Nature* 455(7209): 119–23.

Malvezzi, Francesca et al. 2013. "A Structural Basis for Kinetochore Recruitment of the Ndc80 Complex via Two Distinct Centromere Receptors." *EMBO Journal* 32(3): 409–23.

Mandrioli, Mauro, and Gian Carlo Manicardi. 2012. "Unlocking Holocentric Chromosomes: New Perspectives from Comparative and Functional Genomics?" *Current Genomics* 13(5): 343–49.

Mankouri, Hocine W., and Ian D. Hickson. 2007. "The RecQ Helicase-Topoisomerase III-Rmi1 Complex: A DNA Structure-Specific 'Dissolvasome'?" *Trends in Biochemical Sciences* 32(12): 538–46.

Marshall, Owen J., Anderly C. Chueh, Lee H. Wong, and K.H. Choo. 2008. "Neocentromeres: New Insights into Centromere Structure, Disease Development, and Karyotype Evolution." *American Journal of Human Genetics* 82(2): 261–82.

Martin, Carol Anne et al. 2018. "Mutations in TOP3A Cause a Bloom Syndrome-like Disorder." *American Journal of Human Genetics* 103(2): 221–31.

Masumoto, Hiroshi et al. 1989. "A Human Centromere Antigen (CENP-B) Interacts with a Short Specific Sequence in Alphoid DNA, a Human Centromeric Satellite." *Journal of Cell Biology* 109(5): 1963–73.

Mayer, Thomas U et al. 1999. "Small Molecule Inhibitor of Mitotic Spindle Bipolarity Identified in a Phenotype-Based." *Science* 286(5441): 971–74.

McCleland, Mark L. et al. 2004. "The Vertebrate Ndc80 Complex Contains Spc24 and Spc25 Homologs, Which Are Required to Establish and Maintain Kinetochore-Microtubule Attachment." *Current Biology* 14(2): 131–37.

McGrew, J, B Diehl, and M. Fitzgerald-Hayes. 1986. "Single Base-Pair Mutations in Centromere Element III Cause Aberrant Chromosome Segregation in Saccharomyces Cerevisiae." *Molecular and Cellular Biology* 6(2): 530–38.

McKinley, Kara L., and Iain M. Cheeseman. 2014. "Polo-like Kinase 1 Licenses CENP-a Deposition at Centromeres." *Cell* 158(2): 397–411.

———. 2016. "The Molecular Basis for Centromere Identity and Function." *Nature*

Reviews Molecular Cell Biology 17(1): 16–29.

Meraldi, Patrick, and Peter K. Sorger. 2005. "A Dual Role for Bub1 in the Spindle Checkpoint and Chromosome Congression." *EMBO Journal* 24(8): 1621–33.

Moree, Ben, Corey B. Meyer, Colin J. Fuller, and Aaron F. Straight. 2011. "CENP-C Recruits M18BP1 to Centromeres to Promote CENP-A Chromatin Assembly." *Journal of Cell Biology* 194(6): 855–71.

Morrow, C. J. 2005. "Bub1 and Aurora B Cooperate to Maintain BubR1-Mediated Inhibition of APC/CCdc20." *Journal of Cell Science* 118(16): 3639–52.

Müller, Sebastian et al. 2014. "Phosphorylation and DNA Binding of HJURP Determine Its Centromeric Recruitment and Function in CenH3CENP-A Loading." *Cell Reports* 8(1): 190–203.

Munné, Santiago et al. 2007. "Maternal Age, Morphology, Development and Chromosome Abnormalities in over 6000 Cleavage-Stage Embryos." *Reproductive BioMedicine Online* 14(5): 628–34.

Muro, Yoshinao et al. 1992. "Centromere Protein B Assembles Human Centromeric α-Satellite DNA at the 17-Bp Sequence, CENP-B Box." *Journal of Cell Biology* 116(3): 585–96.

Musacchio, Andrea, and Edward D. Salmon. 2007. "The Spindle-Assembly Checkpoint in Space and Time." *Nature Reviews Molecular Cell Biology* 8(5): 379–93.

Nasmyth, Kim. 2001. "Disseminating the Genome: Joining, Resolving, and Separating Sister Chromatids During Mitosis and Meiosis." *Annual Review of Genetics* 35(1): 673–745.

———. 2011. "Cohesin: A Catenase with Separate Entry and Exit Gates?" *Nature Cell Biology* 13(10): 1170–77.

Nasmyth, Kim, and Christian H. Haering. 2005. "The Structure and Function of SMC and Kleisin Complexes." *Annual Review of Biochemistry* 74(1): 595–648.

Nera, Bernadette, Hui Shun Huang, Thao Lai, and Lifeng Xu. 2015. "Elevated Levels of TRF2 Induce Telomeric Ultrafine Anaphase Bridges and Rapid Telomere Deletions." *Nature Communications* 6.

Nicholson, Joshua M., and Daniela Cimini. 2013. "Cancer Karyotypes: Survival of the Fittest." *Frontiers in Oncology* 3.

Nicklas, R. Bruce, Suzanne C. Ward, and Gary J. Gorbsky. 1995. "Kinetochore Chemistry Is Sensitive to Tension and May Link Mitotic Forces to a Cell Cycle Checkpoint." *Journal of Cell Biology* 130(4): 929–39.

Nielsen, Christian F. et al. 2015. "PICH Promotes Sister Chromatid Disjunction and Co-Operates with Topoisomerase II in Mitosis." *Nature Communications* 6.

Nielsen, Christian F., and Ian D. Hickson. 2016. "PICH Promotes Mitotic Chromosome Segregation: Identification of a Novel Role in RDNA Disjunction." *Cell Cycle* 15(20): 2704–11.

Nishino, Tatsuya et al. 2012. "CENP-T-W-S-X Forms a Unique Centromeric Chromatin Structure with a Histone-like Fold." *Cell* 148(3): 487–501.

———. 2013. “CENP-T Provides a Structural Platform for Outer Kinetochore Assembly.” *EMBO Journal* 32(3): 424–36.

Nishiyama, Tomoko et al. 2010. “Sororin Mediates Sister Chromatid Cohesion by Antagonizing Wapl.” *Cell* 143(5): 737–49.

Nitiss, John L. 2009. “DNA Topoisomerase II and Its Growing Repertoire of Biological Functions.” *Nature Reviews Cancer* 9(5): 327–37.

Normandin, Karine et al. 2016. “Identification of Polo-like Kinase 1 Interaction Inhibitors Using a Novel Cell-Based Assay.” *Scientific Reports* 5.

O’Connor, Aisling et al. 2016. “Requirement for PLK1 Kinase Activity in the Maintenance of a Robust Spindle Assembly Checkpoint.” *Biology Open* 5(1): 11–19.

Obuse, Chikashi et al. 2004. “A Conserved Mis12 Centromere Complex Is Linked to Heterochromatic HP1 and Outer Kinetochore Protein Zwint-1.” *Nature Cell Biology* 6(11): 1135–41.

Okada, Masahiro et al. 2006. “The Cenp-H–I Complex Is Required for the Efficient Incorporation of Newly Synthesized CENP-A into Centromeres.” *Nature Cell Biology* 8(5): 446–57.

Ono, Takao et al. 2003. “Differential Contributions of Condensin I and Condensin II to Mitotic Chromosome Architecture in Vertebrate Cells.” *Cell* 115: 109–21.

Ono, Takao, Yuda Fang, David L Spector, and Tatsuya Hirano. 2004. “Spatial and Temporal Regulation of Condensins I and II in Mitotic Chromosome Assembly in Human Cells.” *Molecular Biology of the Cell* 15: 3296–3308.

Ono, Takao, Daisuke Yamashita, and Tatsuya Hirano. 2013. “Condensin II Initiates Sister Chromatid Resolution during S Phase.” *Journal of Cell Biology* 200(4): 429–41.

Oshimori, Naoki, Miho Ohsugi, and Tadashi Yamamoto. 2006. “The Plk1 Target Kizuna Stabilizes Mitotic Centrosomes to Ensure Spindle Bipolarity.” *Nature Cell Biology* 8(10): 1095–1101.

Ouyang, Karen J., Mary K. Yagle, Michael J. Matunis, and Nathan A. Ellis. 2013. “BLM SUMOylation Regulates SsDNA Accumulation at Stalled Replication Forks.” *Frontiers in Genetics* 4(SEP).

Palmer, D. K. et al. 1987. “A 17-KD Centromere Protein (CENP-A) Copurifies with Nucleosome Core Particles and with Histones.” *Journal of Cell Biology* 104(4): 805–15.

———. 1991. “Purification of the Centromere-Specific Protein CENP-A and Demonstration That It Is a Distinctive Histone.” *Proceedings of the National Academy of Sciences of the United States of America* 88(9): 3734–38.

Palmer, D. K., and R. L. Margolis. 1985. “Kinetochore Components Recognized by Human Autoantibodies Are Present on Mononucleosomes.” *Molecular and Cellular Biology* 5(1): 173–86.

Panchenko, T. et al. 2011. “Replacement of Histone H3 with CENP-A Directs Global

Nucleosome Array Condensation and Loosening of Nucleosome Superhelical Termini." *Proceedings of the National Academy of Sciences* 108(40): 16588–93.

Perez-Castro, Ana V. et al. 1998. "Centromeric Protein B Null Mice Are Viable with No Apparent Abnormalities." *Developmental Biology* 201(2): 135–43.

Peters, Jan-Michael. 2012. "The Many Functions of Cohesin-Different Rings to Rule Them All?" *EMBO Journal* 31(9): 2061–63.

Peters, Jan-Michael, and Tomoko Nishiyama. 2012. "Sister Chromatid Cohesion." *Cold Spring Harbor Perspectives in Biology* 4(11).

Peters, Ulf et al. 2006. "Probing Cell-Division Phenotype Space and Polo-like Kinase Function Using Small Molecules." *Nature Chemical Biology* 2(11): 618–26.

Petrovic, Arsen et al. 2010. "The MIS12 Complex Is a Protein Interaction Hub for Outer Kinetochore Assembly." *Journal of Cell Biology* 190(5): 835–52.

Qi, Wei, Zhanyun Tang, and Hongtao Yu. 2006. "Phosphorylation-and Polo-Box-Dependent Binding of Plk1 to Bub1 Is Required for the Kinetochore Localization of Plk1." *Molecular Biology of the Cell* 17: 3705–16.

Rankin, Susannah, Nagi G. Ayad, and Marc W. Kirschner. 2005. "Sororin, a Substrate of the Anaphase- Promoting Complex, Is Required for Sister Chromatid Cohesion in Vertebrates." *Molecular Cell* 18(2): 185–200.

Raynard, Steven, Wendy Bussen, and Patrick Sung. 2006. "A Double Holliday Junction Dissolvasome Comprising BLM, Topoisomerase IIIα, and BLAP75." *Journal of Biological Chemistry* 281(20): 13861–64.

Regnier, V. et al. 2005. "CENP-A Is Required for Accurate Chromosome Segregation and Sustained Kinetochore Association of BubR1." *Molecular and Cellular Biology* 25(10): 3967–81.

Ribeiro, Susana A. et al. 2009. "Condensin Regulates the Stiffness of Vertebrate Centromeres." *Molecular Biology of the Cell* 20: 2371–80.

Rieder, Conly L., Richard W. Cole, Alexey Khodjakov, and Greenfield Sluder. 1995. "The Checkpoint Delaying Anaphase in Response to Chromosome Monoorientation Is Mediated by an Inhibitory Signal Produced by Unattached Kinetochores." *Journal of Cell Biology* 130(4): 941–48.

Rogakou, Emmy P. et al. 1998. "DNA Double-Stranded Breaks Induce Histone H2AX Phosphorylation on Serine 139." *Journal of Biological Chemistry* 273(10): 5858–68.

Rouzeau, Sébastien et al. 2012. "Bloom's Syndrome and PICH Helicases Cooperate with Topoisomerase IIα in Centromere Disjunction before Anaphase." *PLoS ONE* 7(4).

Sakai, Yuji et al. 2018. "Modeling the Functions of Condensin in Chromosome Shaping and Segregation." *PLoS Computational Biology* 14(6).

Salic, Adrian, Jennifer C. Waters, and Timothy J. Mitchison. 2004. "Vertebrate Shugoshin Links Sister Centromere Cohesion and Kinetochore Microtubule Stability in Mitosis." *Cell* 118: 567–78.

Samoshkin, Alexander et al. 2009. "Human Condensin Function Is Essential for

Centromeric Chromatin Assembly and Proper Sister Kinetochore Orientation." *PLoS ONE* 4(8).

Santamaria, Anna et al. 2007. "Use of the Novel Plk1 Inhibitor ZK-Thiazolidinone to Elucidate Functions of Plk1 in Early and Late Stages of Mitosis." *Molecular Biology of the Cell* 18(10): 4024–36.

Sarangapani, Krishna K., and Charles L. Asbury. 2014. "Catch and Release: How Do Kinetochores Hook the Right Microtubules during Mitosis?" *Trends in Genetics* 30(4): 150–59.

Sarlós, Kata et al. 2018. "Reconstitution of Anaphase DNA Bridge Recognition and Disjunction." *Nature Structural and Molecular Biology* 25(9): 868–76.

Schmucker, Stephane, and Izabela Sumara. 2014. "Molecular Dynamics of PLK1 during Mitosis." *Molecular and Cellular Oncology* 1(2).

Screpanti, Emanuela et al. 2011. "Direct Binding of Cenp-C to the Mis12 Complex Joins the Inner and Outer Kinetochore." *Current Biology* 21(5): 391–98.

Seki, Akiko, Judith A. Coppinger, Chang-Young Jang, et al. 2008. "Bora and the Kinase Aurora a Cooperatively Activate the Kinase Plk1 and Control Mitotic Entry." *Science* 320(5883): 1655–58.

Seki, Akiko, Judith A. Coppinger, Haining Du, et al. 2008. "Plk1- and β-TrCP-Dependent Degradation of Bora Controls Mitotic Progression." *Journal of Cell Biology* 181(1): 65–78.

Seong, Yeon Sun et al. 2002. "A Spindle Checkpoint Arrest and a Cytokinesis Failure by the Dominant-Negative Polo-Box Domain of Plk1 in U-2 OS Cells." *Journal of Biological Chemistry* 277(35): 32282–93.

Ben Shahar, Tom et al. 2008. "Eco1-Dependent Cohesin Acetylation during Establishment of Sister Chromatid Cohesion." *Source: Science, New Series* 321(5888): 563–66.

Shintomi, Keishi, and Tatsuya Hirano. 2011. "The Relative Ratio of Condensing I to II Determines Chromosome Shapes." *Genes and Development* 25(14): 1464–69.

Shintomi, Keishi, Tatsuro S. Takahashi, and Tatsuya Hirano. 2015. "Reconstitution of Mitotic Chromatids with a Minimum Set of Purified Factors." *Nature Cell Biology* 17(8): 1014–23.

Silva, Mariana C.C. et al. 2012. "Cdk Activity Couples Epigenetic Centromere Inheritance to Cell Cycle Progression." *Developmental Cell* 22(1): 52–63.

Simmons, D L et al. 1992. "Identification of an Early-Growth-Response Gene Encoding a Novel Putative Protein Kinase." *Molecular and Cellular Biology* 12(9): 4164–69.

Singh, Thiyam Ramsing et al. 2008. "BLAP18/RMI2, a Novel OB-Fold-Containing Protein, Is an Essential Component of the Bloom Helicase-Double Holliday Junction Dissolvasome." *Genes and Development* 22(20): 2856–68.

Sir, Joo Hee et al. 2013. "Loss of Centrioles Causes Chromosomal Instability in Vertebrate Somatic Cells." *Journal of Cell Biology* 203(5): 747–56.

Skibbens, Robert V., Laura B. Corson, Douglas Koshland, and Philip Hieter. 1999. "Ctf7p

Is Essential for Sister Chromatid Cohesion and Links Mitotic Chromosome Structure to the DNA Replication Machinery." *Genes and Development* 13(3): 307–19.

Song, Bing, X. Shawn Liu, Korbin Davis, and Xiaoqi Liu. 2012. "Plk1 Phosphorylation of Orc2 Promotes DNA Replication under Conditions of Stress." *Cancer Research* 72(8 Supplement): 2050–2050.

Song, Bing, X. Shawn Liu, and Xiaoqi Liu. 2012. "Polo-like Kinase 1 (Plk1): An Unexpected Player in DNA Replication." *Cell Division* 7.

St-Pierre, Julie et al. 2009. "Polo Kinase Regulates Mitotic Chromosome Condensation by Hyperactivation of Condensin DNA Supercoiling Activity." *Molecular Cell* 34(4): 416–26.

Steegmaier, Martin et al. 2007. "BI 2536, a Potent and Selective Inhibitor of Polo-like Kinase 1, Inhibits Tumor Growth In Vivo." *Current Biology* 17(4): 316–22.

Suijkerbuijk, Saskia J E, Mathijs Vleugel, Antoinette Teixeira, and Geert J.P.L. Kops. 2012. "Integration of Kinase and Phosphatase Activities by BUBR1 Ensures Formation of Stable Kinetochore-Microtubule Attachments." *Developmental Cell* 23(4): 745–55.

Sullivan, Kevin F., Mirko Hechenberger, and Khaled Masri. 1994. "Human CENP-A Contains a Histone H3 Related Histone Fold Domain That Is Required for Targeting to the Centromere." *The Journal of Cell Biology* 127(3): 581–92.

Sumara, Izabela et al. 2000. "Characterization of Vertebrate Cohesin Complexes and Their Regulation in Prophase." *Journal of Cell Biology* 151(4): 749–61.

———. 2002. "The Dissociation of Cohesin from Chromosomes in Prophase Is Regulated by Polo-like Kinase." *Molecular Cell* 9(3): 515–25.

———. 2004. "Roles of Polo-like Kinase 1 in the Assembly of Functional Mitotic Spindles." *Current Biology* 14: 1712–22.

Sunkel, Claudio E., and David M. Glover. 1988. "Polo, a Mitotic Mutant of Drosophila Displaying Abnormal Spindle Poles." *Journal of cell science* 89 (Pt 1): 25–38.

Talbert, Paul B. et al. 2012. "A Unified Phylogeny-Based Nomenclature for Histone Variants." *Epigenetics and Chromatin* 5(1).

Tanaka, Tomoyuki U et al. 2002. "Evidence That the Ipl1-Sli15 (Aurora Kinase-INCENP) Complex Promotes Chromosome Bi-Orientation by Altering Kinetochore-Spindle Pole Connections." *Cell* 108: 317–29.

Tang, Zhanyun et al. 2004. "Phosphorylation of Cdc20 by Bub1 Provides a Catalytic Mechanism for APC/C Inhibition by the Spindle Checkpoint." *Molecular Cell* 16(3): 387–97.

Taylor, Stephen S., Maria I.F. Scott, and Andrew J. Holland. 2004. "The Spindle Checkpoint: A Quality Control Mechanism Which Ensures Accurate Chromosome Segregation." *Chromosome Research* 12(6): 599–616.

Tiwari, Ankana, O. Addis Jones, and Kok Lung Chan. 2018. "53BP1 Can Limit Sister-Chromatid Rupture and Rearrangements Driven by a Distinct Ultrafine DNA

Bridging-Breakage Process." *Nature Communications* 9(1).

Tóth, Attila et al. 1999. "Yeast Cohesin Complex Requires a Conserved Protein, Eco1p(Ctf7), to Establish Cohesion between Sister Chromatids during DNA Replication." *Genes and Development* 13(3): 320–33.

Tyler-Smith, Chris et al. 2002. "Transmission of a Fully Functional Human Neocentromere through Three Generations." *The American Journal of Human Genetics* 64(5): 1440–44.

Uhlmann, Frank et al. 2000. "Cleavage of Cohesin by the CD Clan Protease Separin Triggers Anaphase in Yeast." *Cell* 103: 375–86.

Uhlmann, Frank, Friedrich Lottspeich, and Kim Nasmyth. 1999. "Sister-Chromatid Separation at Anaphase Onset Is Promoted by Cleavage of the Cohesin Subunit Scc1." *Nature* 400: 37–42.

Uhlmann, Frank, and Kim Nasmyth. 1998. "Cohesion between Sister Chromatids Must Be Established during DNA Replication." *Current Biology* 8(20): 1095–1102.

Vargas-Rondón, Natalia, Victoria E. Villegas, and Milena Rondón-Lagos. 2018. "The Role of Chromosomal Instability in Cancer and Therapeutic Responses." *Cancers* 10(1): 1–21.

Varma, D., and Edward D. Salmon. 2013. "The KMN Protein Network - Chief Conductors of the Kinetochore Orchestra." *Journal of Cell Science* 125(24): 5927–36.

Vasquez, R. J. et al. 1997. "Nanomolar Concentrations of Nocodazole Alter Microtubule Dynamic Instability in Vivo and in Vitro." *Molecular Biology of the Cell* 8(6): 973–85.

Vigneron, Suzanne et al. 2018. "Cyclin A-Cdk1-Dependent Phosphorylation of Bora Is the Triggering Factor Promoting Mitotic Entry." *Developmental Cell* 45(5): 637-650.e7.

Visnes, T. et al. 2014. "Localisation of the SMC Loading Complex Nipbl/Mau2 during Mammalian Meiotic Prophase I." *Chromosoma* 123(3): 239–52.

Vissel, B., and K.H. Choo. 1987. "Human Alpha Satellite DNA - Consensus Sequence and Conserved Regions." *Nucleic Acids Research* 15(16): 6751–52.

Voullaire, Lucille E, Howard R Slater, Vida Petrovic, and K.H. Choo. 1993. "A Functional Marker Centromere with No Detectable Alpha-Satellite, Satellite Ill, or CENP-B Protein: Activation of a Latent Centromere?" *Am. J. Hum. Genet* 52: 1153–63.

van Vugt, Marcel A.T.M. et al. 2004. "Polo-like Kinase-1 Is Required for Bipolar Spindle Formation but Is Dispensable for Anaphase Promoting Complex/Cdc20 Activation and Initiation of Cytokinesis." *Journal of Biological Chemistry* 279(35): 36841–54.

Waizenegger, Irene, C., Silke Hauf, Andreas Meinke, and Jan-Michael Peters. 2000. "Two Distinct Pathways Remove Mammalian Cohesin from Chromosome Arms in Prophase and from Centromeres in Anaphase." *Cell* 103: 399–410.

Wan, Xiaohu et al. 2009. "Protein Architecture of the Human Kinetochore Microtubule Attachment Site." *Cell* 137(4): 672–84.

Wang, James C. 2002. “Cellular Roles of DNA Topoisomerases: A Molecular Perspective.” *Nature Reviews Molecular Cell Biology* 3(6): 430–40.

Wang, Lily Hui Ching, B. Mayer, Olaf Stemmann, and Erich A. Nigg. 2010. “Centromere DNA Decatenation Depends on Cohesin Removal and Is Required for Mammalian Cell Division.” *Journal of Cell Science* 123(5): 806–13.

Wang, Lily Hui Ching, Thomas Schwarzbraun, Michael R. Speicher, and Erich A. Nigg. 2008. “Persistence of DNA Threads in Human Anaphase Cells Suggests Late Completion of Sister Chromatid Decatenation.” *Chromosoma* 117(2): 123–35.

Warnke, Silke et al. 2004. “Polo-like Kinase-2 Is Required for Centriole Duplication in Mammalian Cells.” *Current Biology* 14: 1200–1207.

Waters, Jennifer C., Rey-Huei Chen, Andrew W. Murray, and Edward D. Salmon. 1998. “Localization of Mad2 to Kinetochores Depends on Microtubule Attachment, Not Tension.” *Journal of Cell Biology* 141(5): 1181–91.

Watrin, Erwan et al. 2006. “Human Scc4 Is Required for Cohesin Binding to Chromatin, Sister-Chromatid Cohesion, and Mitotic Progression.” *Current Biology* 16(9): 863–74.

Waye, John S., and Huntington F. Willard. 1985. “Chromosome-Specific Alpha Satellite DNA: Nucleotide Sequence Analysis of the 2.0 Kilobasepair Repeat from the Human X Chromosome.” *Nucleic Acids Research* 13(8): 2731–43.

Wu, Leonard et al. 2000. “The Bloom’s Syndrome Gene Product Interacts with Topoisomerase III.” *Journal of Biological Chemistry* 275(13): 9636–44.

Wu, Leonard, and Ian D. Hickson. 2003. “The Bloom’s Syndrome Helicase Suppresses Crossing over during Homologous Recombination.” *Nature* 426(6968): 870–74.

Wu, Yuanzhong, Jinping Lu, and Tiebang Kang. 2016. “Human Single-Stranded DNA Binding Proteins: Guardians of Genome Stability.” *Acta Biochimica et Biophysica Sinica* 48(7): 671–77.

Xie, Suqing et al. 2001. “Plk3 Functionally Links DNA Damage to Cell Cycle Arrest and Apoptosis at Least in Part via the P53 Pathway.” *Journal of Biological Chemistry* 276(46): 43305–12.

Xu, Dongyi et al. 2008. “RMI, a New OB-Fold Complex Essential for Bloom Syndrome Protein to Maintain Genome Stability.” *Genes and Development* 22(20): 2843–55.

Xu, Jun, Chen Shen, Tao Wang, and Junmin Quan. 2013. “Structural Basis for the Inhibition of Polo-like Kinase 1.” *Nature Structural and Molecular Biology* 20(9): 1047–53.

Yamashita, Daisuke et al. 2011. “MCPH1 Regulates Chromosome Condensation and Shaping as a Composite Modulator of Condensin II.” *Journal of Cell Biology* 194(6): 841–54.

Yim, H., and R. L. Erikson. 2009. “Polo-Like Kinase 1 Depletion Induces DNA Damage in Early S Prior to Caspase Activation.” *Molecular and Cellular Biology* 29(10): 2609–21.

Zeng, Xing, and Randall W. King. 2012. “An APC/C Inhibitor Stabilizes Cyclin B1 by

Prematurely Terminating Ubiquitination." *Nature Chemical Biology* 8(4): 383–92.

Zhang, Nenggang, Anil K. Panigrahi, Qilong Mao, and Debananda Pati. 2011. "Interaction of Sororin Protein with Polo-like Kinase 1 Mediates Resolution of Chromosomal Arm Cohesion." *Journal of Biological Chemistry* 286(48): 41826–37.

Zitouni, Sihem et al. 2014. "Polo-like Kinases: Structural Variations Lead to Multiple Functions." *Nature Reviews Molecular Cell Biology* 15(7): 433–52.

Appendix: Publications during PhD

Addis Jones, O., Tiwari, A., Olukoga, T., Herbert, A. & Chan, KL. PLK1 facilitates chromosome biorientation by suppressing centromere disintegration driven by BLM-mediated unwinding and spindle pulling. *Nature Communications (2019), 10:2861*

Tiwari, A., Addis Jones, O. & Chan, KL. *53BP1 can limit sister-chromatid rupture and rearrangement driven by a distinct ultrafine DNA bridging-breakage process. Nature Communications (2018), 9(1):677*

nature COMMUNICATIONS

ARTICLE

https://doi.org/10.1038/s41467-019-10938-y OPEN

PLK1 facilitates chromosome biorientation by suppressing centromere disintegration driven by BLM-mediated unwinding and spindle pulling

Owen Addis Jones[1], Ankana Tiwari[1,2], Tomisin Olukoga[1,2], Alex Herbert[1] & Kok-Lung Chan[1]

Centromeres provide a pivotal function for faithful chromosome segregation. They serve as a foundation for the assembly of the kinetochore complex and spindle connection, which is essential for chromosome biorientation. Cells lacking Polo-like kinase 1 (PLK1) activity suffer severe chromosome alignment defects, which is believed primarily due to unstable kinetochore-microtubule attachment. Here, we reveal a previously undescribed mechanism named 'centromere disintegration' that drives chromosome misalignment in PLK1-inactivated cells. We find that PLK1 inhibition does not necessarily compromise metaphase establishment, but instead its maintenance. We demonstrate that this is caused by unlawful unwinding of DNA by BLM helicase at a specific centromere domain underneath kinetochores. Under bipolar spindle pulling, the distorted centromeres are promptly decompacted into DNA threadlike molecules, leading to centromere rupture and whole-chromosome arm splitting. Consequently, chromosome alignment collapses. Our study unveils an unexpected role of PLK1 as a chromosome guardian to maintain centromere integrity for chromosome biorientation.

[1] Genome Damage and Stability Centre, University of Sussex, Brighton BN1 7BG, UK. [2] These authors contributed equally: Ankana Tiwari, Tomisin Olukoga. Correspondence and requests for materials should be addressed to K.-L.C. (email: koklung.chan@sussex.ac.uk)

Chromosome mis-segregation has wide implications in cancer and rare congenital disorders[1]. To achieve faithful chromosome segregation, condensed chromosomes need to be properly aligned prior to disjunction through a mitotic process called chromosome biorientation. This requires a stable connection of spindle microtubules (MTs) emanating from opposite centrosomes to centromeres via the macromolecular complex of kinetochores (KTs)[2]. A single unattached chromosome can activate the spindle assembly checkpoint, inhibiting the anaphase promoting complex/cyclosome (APC/C)[3], and hence blocks anaphase onset[4,5]. This elegant system allows cells to correct possible KT-MT attachment errors and prevent chromosome mis-segregation. During chromosome biorientation, centromeres and KTs are inevitably under constant spindle pulling tension, due to the persistence of sister chromatid cohesion. The centromere architecture is presumably maintained through chromosome condensation, whilst the KT-MT stable attachment requires activity of a key mitotic kinase, Polo-like kinase 1 (PLK1)[6–8]. In early mitosis, PLK1 localises predominantly at KTs and centrosomes. Inactivation of PLK1 has been shown to induce severe chromosome misalignment, which is generally attributed to a failure in building stable KT-MT attachment. However, how PLK1 promotes chromosome biorientation still requires investigation

Once biorientation is achieved on every chromosome, the spindle checkpoint is satisfied. This leads to the activation of APC/C and cleavage of cohesin, allowing the poleward movement of sister chromatids[9]. Interestingly, studies show that despite their separation, sister chromatids can remain intertwined by DNA linkage molecules that manifest as so-called ultrafine DNA bridges (UFBs)[10,11]. Generally, UFBs are thought to be unresolved double-stranded DNA catenanes, especially those that arise at centromeres[12]. However, studies have also shown that incomplete replication intermediates and homologous recombination (HR) structures can give rise to UFB structures[13–16]. Regardless of their origins, UFBs are recognised by a UFB-binding complex comprising of PICH (Plk1-interacting checkpoint helicase) translocase, BLM (Bloom's syndrome) helicase and its interacting factors, including TOP3A and TOP2[10,11,17–19]. However, the precise molecular mechanism of UFB resolution is not yet fully understood

Chromosome biorientation not only plays a critical role to ensure equal chromosome segregation, but also facilitates the regulation of the spindle checkpoint and mitotic progression. Many studies have shown that PLK1 is essential for chromosome biorientation; however, the underlying mechanism(s) is still not fully clear. In the current study, unexpectedly, we find that PLK1 in fact can protect centromere integrity for chromosome biorientation maintenance. We demonstrate that in the absence of PLK1, the UFB-binding complex aberrantly targets and unwinds centromeres, leading to their rupture in concerted action with bipolar spindle pulling. As a consequence, cells lose centromere integrity and fail to maintain metaphase alignment. Therefore, our study provides an alternative mechanism of chromosome misalignment in PLK1-defective cells. Importantly, it also reveals a previously undescribed pathway of centromere protection during mitosis

Results

PLK1 inactivation leads to collapse of metaphase alignment. It is well-documented that cells cannot achieve proper chromosome alignment without PLK1 activity[6]. Consistent with this, inhibition of PLK1 using a well-characterised small molecule inhibitor, BI2536 ($IC_{50} = 0.83$ nM)[20], induced severe chromosome misalignment in hTERT-immortalised human RPE1 cells. The BI2536-induced mitotic arrest manifested in a way similar to treatments of the spindle poison (nocodazole) and kinesin inhibitor (Monastrol) (Supplementary Fig. 1a). However, live-cell time-lapse microscopy on pre-synchronised RPE1 cells revealed that, unlike nocodazole and monastrol treatments, BI2536 did not fully prevent chromosome congression (Fig. 1a and Supplementary Fig. 1b). Nearly 80% of BI2536-treated RPE1 cells managed to align their chromosomes in the metaphase plane, but shortly after, succumbed to a loss of maintenance; namely chromosomes drifting away from the equator and scattering into a 'Fig-8' or 'polo'[21]-like pattern (Fig. 1a–c, Supplementary Fig. 1c and Supplementary Movie 1). We referred to this phenomenon as 'metaphase collapse'. In contrast, cells treated with the APC/C inhibitor, ProTAME, remained arrested at metaphase for extended periods (Fig. 1c)

Formation of centromeric DNA linkages between chromosomes. Strikingly, in the metaphase-collapse cell population, we observed a threadlike structure that was decorated by the PLK1 protein (Fig. 2a; arrows). It was not present in DMSO-treated pre-anaphase cells (i.e., prometaphase and metaphase) (Fig. 2a). As the threadlike structure was reminiscent of anaphase UFBs[10,11], we investigated whether they were DNA molecules; or a mis-localisation of PLK1 to cytoskeleton structures. Immunofluorescence co-staining showed that PICH translocase, a well-known UFB marker, was present along the PLK1-coated threads induced by BI2536 (Fig. 2b and Supplementary Fig. 1d). Furthermore, other known UFB-associated factors including BLM helicase and replication protein A (RPA) were also present (Fig. 2c). It is worth noting that RPA decorates the threads without necessarily following the PICH/BLM signals, and it can also be found on regions where no or weak PICH/BLM signals were detected (Fig. 2c; arrows). Similar results were obtained by using different antibodies against BLM and different subunits of RPA (Fig. 2d). This localisation pattern is similar to recent reports showing the binding of RPA to stretched DNA molecules, or DNA bridges, is not always coupled with the PICH/BLM complex[12,22]. Therefore, the RPA association likely represents the presence of single-stranded DNA. To validate the immunofluorescence staining results, we examined Bloom's syndrome fibroblast cells stably expressing a GFP-tagged BLM, and RPE1 cells expressing a GFP-tagged PLK1. We found both GFP-tagged proteins were also present along the thread molecules induced by BI2536 (Supplementary Fig. 1e, f; arrows). In addition to this, we also found that PLK1 indeed associated with UFBs in anaphase cells (Supplementary Fig. 1g; arrows). Together, these data suggest that the BI2536-induced thread molecules are highly likely a form of DNA structure; and possibly composed of both single-stranded and double-stranded DNA. As predicted, the threadlike structures did not co-localise with mitotic MTs (Supplementary Fig. 1h)

Next, we investigated the origin of the DNA threads. We found that all of the DNA threads analysed linked to centromeric regions, either through one or both of their termini (Fig. 2e). In some optical sections, it was apparent that two separating centromeres were inter-connected by a DNA thread (Fig. 2e; arrows). Since PLK1 inhibition prevents anaphase onset, these DNA threads cannot be explained as the centromeric UFBs coming from disjoined sister chromatids. However, another possibility is that PLK1 inhibition might induce precocious sister chromatids separation; an effect similar to Shugosin 1 (SGO1) depletion[23,24] (Supplementary Fig. 2a), which exposes UFBs before anaphase[11] (Supplementary Fig. 2b; arrows). This proposal, however, is very unlikely because PLK1 has been shown to be required for the release of arm cohesin; its

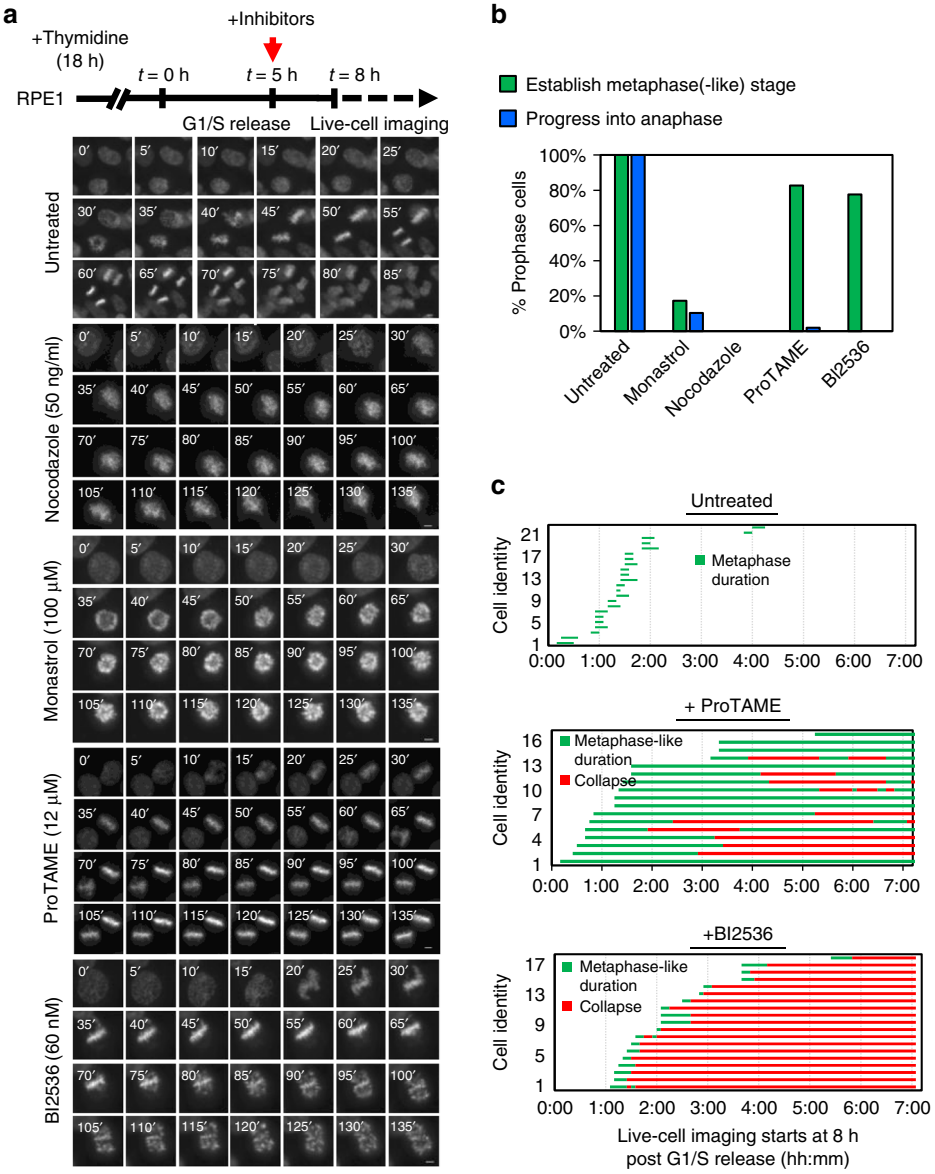

Fig. 1 PLK1 inactivation causes metaphase collapse. **a** Experimental outline and time-lapse imaging examples showing the mitotic progression of RPE1 cells under the indicated drug treatment. RPE1 cells were arrested in G1/S by a single thymidine block. Five hour post-G1/S-release, the indicated inhibitors were added for another 3 h, followed by live-cell microscopy (started at $t = 8$ h post-G1/S release). Time-lapse imaging was carried out with a 5-min interval. **b** Percentages of prophase cells establishing metaphase(-like) alignment and progressing into anaphase under the indicated treatment. A total of 41, 29, 21, 52 and 58 prophase cells were analysed in untreated, monastrol, nocodazole, ProTAME- and BI2536-treated conditions. **c** The durations of metaphase (-like) and collapse stages (h:min) of RPE1 cells under the indicated treatment. Note: only cells that established a metaphase(-like) stage were measured. 23, 17 and 19 cells were analysed in untreated, ProTAME- and BI2536-treated conditions. DNA was stained by SiR-DNA. Scale bars = 5 µm

inactivation in fact blocks premature loss of cohesion[25–27]. Consistent with these studies, we confirmed that BI2536 did not induce premature separation of sister chromatids in RPE1 cells (Supplementary Fig. 2c). More importantly, by co-staining with topoisomerase 2alpha (TOP2A), a chromatid-axis marker, we visualised that cohesed chromosomes were linked by the DNA threads, induced by PLK1 inhibition (Fig. 2f; arrows). Therefore, the absence of PLK1 activity leads to the formation of a DNA linkage structure that strikingly connects centromeres between cohesed chromosomes. Because of the concomitant occurrence of metaphase collapse and centromere DNA linkages, we speculate that the failure of chromosome alignment in PLK1-inactivated cells may not be merely attributed to unstable KT-MT attachments as previously thought.

Mitotic loss of PLK1 causes centromeric DNA linkages. The DNA linkages induced by BI2536 arise predominantly at centromeres—a genomic region composed of highly repetitive sequences. We sought to test if they might be caused by potential disturbance of DNA replication (or HR) during the course of BI2536 treatment. We used EdU labelling to distinguish between cells that were in an ongoing, or post DNA replication stage, whilst under BI2536 treatment (Supplementary Fig. 3a). If centromere DNA threads are a by-product of abnormal DNA replication, we expected to observe their formation only in the EdU-positive, but not negative, mitotic population. Contrary to this hypothesis, we found that the majority of EdU-negative mitotic cells (69 ± 4%), which were presumably in G2/M while BI2536 was applied, remained positive for DNA thread formation (Supplementary

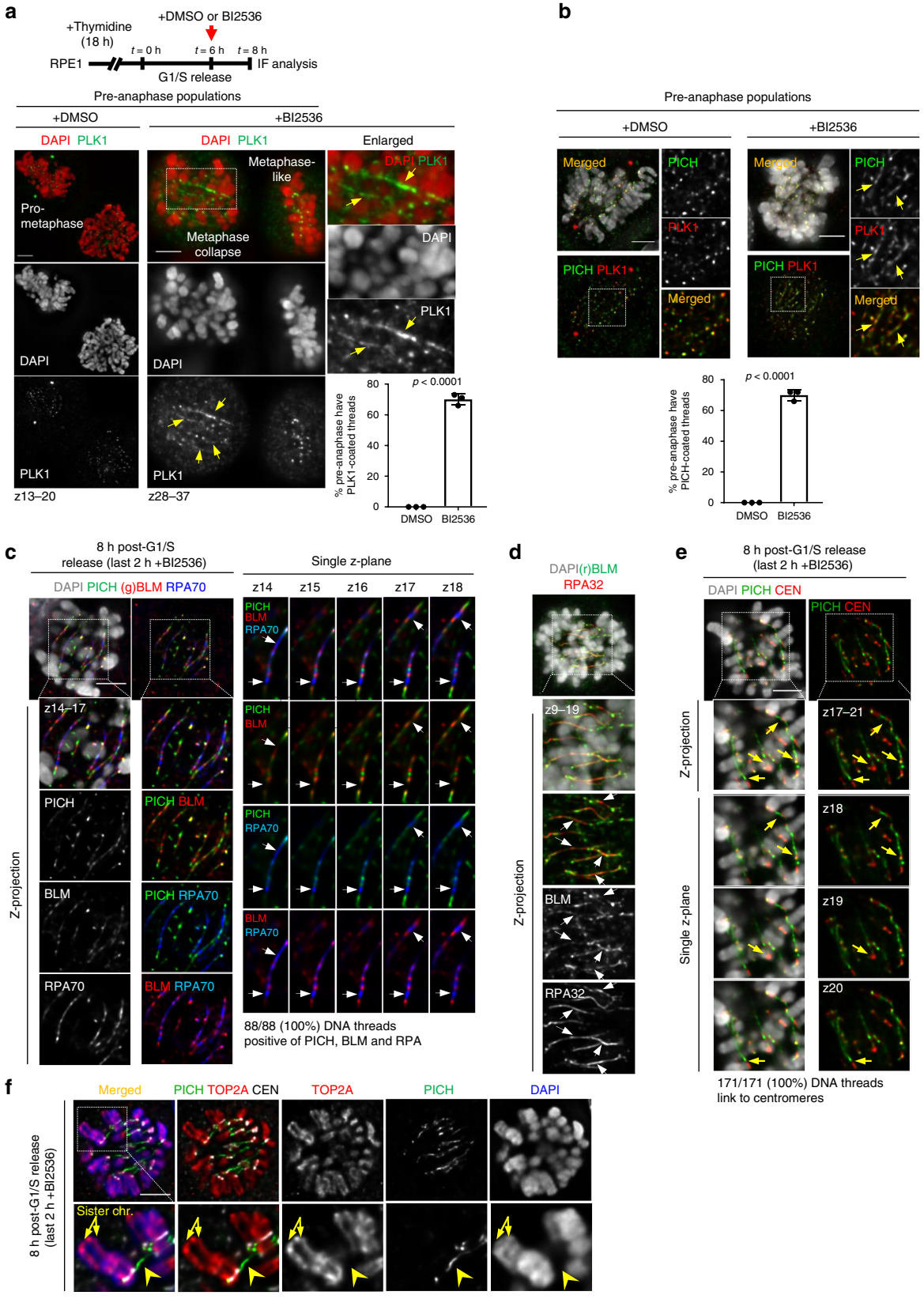

Fig. 3b). Moreover, inhibition of PLK1 in early mitotic RPE1 cells obtained through a release from RO3306-induced G2 arrest also induced centromere DNA threads (Supplementary Fig. 3c). In addition, treating asynchronous RPE1 cells with BI2536 for 1 h also caused centromere DNA thread formation, albeit with a lower frequency (Supplementary Fig. 3d). These data indicate that the formation of centromere DNA linkages likely results from a loss of M-phase specific function of PLK1. However, thymidine pre-treatment and/or synchronistic mitotic entry may enhance the phenotype appearance

Fig. 2 Formation of centromere DNA linkages after PLK1 inactivation. **a** Experimental outline (top) and representative images showing the immunofluorescent staining of PLK1 in DMSO- and BI2536-treated RPE1 pre-anaphase cells (prometaphase and metaphase). BI2536 induced the formation of a PLK1-decorated threadlike structure (arrows) in the 'metaphase collapse' cell. Enlarged region is shown at right. Quantification (bottom) showing the percentage of cells positive for PLK1-coated threads (mean ± S.D. is shown; $n = 3$ independent experiments analysing 75 and 224 pre-anaphase cells in DMSO- and BI2536-treated conditions, respectively). **b** The experimental setup is same as in (**a**). PICH co-localises with PLK1 on the threadlike structures induced by BI2536. Quantification (below) showing the percentage of cells positive for PICH-coated threads (mean ± S.D. is shown; $n = 3$ independent experiments analysing 120 and 308 pre-anaphase cells in DMSO and BI2356 treated conditions, respectively). **c** Representative images showing the association of the UFB-binding complex (PICH, BLM and RPA70) along the threadlike molecules induced by BI2536. Enlarged regions of both z-projected (below) and single z-planes (right) are shown. Eighty-eight thread structures were examined and all were positive for PICH, BLM and RPA70 staining. Arrows showing regions where the RPA70 staining is strong but with no or weak PICH/BLM signals. Note: BLM was stained by a goat antibody (C-18). **d** RPA32 localises on the thread regions where BLM signal is weak (arrows). Note: BLM was stained by a rabbit antibody (ab2179). **e** DNA threads link between centromeres (arrows). Enlarged regions of z-projection and single z-planes are shown below. Note: all DNA threads examined (171/171 in 10 cells; 100%) are positive for centromere linkages at either one or both of their termini. **f** Representative images showing cohesed sister chromatids as labelled by TOP2A (arrows) are linked by DNA threads at their centromeres (arrowhead). The enlarged region is shown below. DNA was stained by DAPI. Scale bars = 5 μm

Using the same treatment protocol, we also found that BI2536 induced centromere DNA threads in all other examined cell types, though with different frequencies (Supplementary Fig. 4a). They included 1BR3 primary fibroblasts (31%), 82-6 hTERT-immortal fibroblasts (24%), HCT116 colon (69%) and HeLa cervical cancer cells (21%). Since the DNA thread formation occurs following metaphase collapse, the different frequencies between cell lines, (e.g., RPE1 vs. HeLa), may relate to their ability to establish metaphase. In agreement with this, time-lapse microscopy revealed that, as compared to RPE1, HeLa cells poorly progressed into a metaphase(-like) stage under BI2536 treatment (Supplementary Fig. 4b). These data are consistent with other studies[27,28], and may indicate that the formation of bipolar spindle attachment in HeLa cells is more sensitive to the loss of PLK1 activity

PLK1 inactivation induces whole-chromosome arm splitting. As shown above, centromere DNA threads cannot be described as originating from the DNA entanglements between sister chromatids/centromeres. We thus investigated other possible cause(s). PICH translocase binds with a high affinity to DNA molecules under tension[29]. This could indicate that the DNA threads may be a form of abnormally stretched centromeric chromatin. Interestingly, we detected activation of DNA damage responses at (peri)centromeric regions, as labelled by γH2AX staining, following BI2536 treatment (Supplementary Fig. 5a). The damage response was mainly observed in metaphase collapse populations rather than in early mitotic cells (e.g., prophase/early prometaphase) (Supplementary Fig. 5a). As expected, γH2AX was mostly not detected at (peri)centromeric regions in DMSO-treated mitotic cells (Supplementary Fig. 5b).

To determine if this was caused by chromatin damage, we examined mitotic chromosome spreads (Supplementary Fig. 6a). In control RPE1 cells (DMSO- and nocodazole-treated), their chromosomes displayed normal configurations and their average numbers were very close to 46 (diploid) (Supplementary Fig. 6b, c). In contrast, chromosomes of BI2536-treated cells exhibited a shorter and more compact structure, but strikingly, their chromosome numbers increased to an average of 59 (Supplementary Fig. 6b, c). This increment cannot be explained by chromosome mis-segregation, because PLK1 inactivation blocks anaphase onset. Thus, a plausible explanation is chromosome fragmentation. Moreover, we found that the increase in chromosome numbers in BI2536-treated cells was suppressed by co-treatment with nocodazole (Supplementary Fig. 6b, c), implying a spindle (or tension)-dependent process. Furthermore, centromere-telomere fluorescence in situ hybridisation (ctFISH) analysis confirmed that the mitotic chromosomes in BI2536-treated cells were indeed broken (Fig. 3a and Supplementary Fig. 7). Notably, the broken chromatin largely resembled telocentric chromosomes; namely the centromere residing at one end of the chromatin, but lacking the telomere signals (Fig. 3a, middle panels—asterisks and Supplementary Fig. 7a, middle panels). This pattern suggests that the breakage occurs either at, or very close to the centromere. Supporting this, we also observed partial centromere splitting (Fig. 3a, middle panels—arrowheads and Supplementary Fig. 7a), and occasionally, saw a CEN DNA thread linking two separating broken chromosome arms (Fig. 3a, middle panels—connecting arrow and Supplementary Fig. 7a). Nocodazole treatment again suppressed chromosome arm breakages, but seemed to have a lesser effect on the partial splitting of centromeres (Fig. 3b). Together, these results demonstrate that the loss of PLK1 activity induces centromere rupture in a spindle-dependent manner. In agreement to this, we found that nearly all the broken chromatin (99.6%) retained centromere sequences (Fig. 3c and Supplementary Fig. 7b), indicating that most, if not all of the breakages, occur within the core centromere.

Our results from both cytological and cytogenetic analyses suggest that the centromere DNA threads induced by PLK1 inhibition are highly likely caused by abnormal stretching of the core centromere chromatin by the spindle pulling forces. As predicted, nocodazole suppressed both centromere splitting and DNA thread formation (Fig. 3b and Supplementary Fig. 8). Given that centromeric DNA threads arise mostly after metaphase establishment, we postulated that rather than by spindle-dependent chromosome movement, they are likely mediated by the tension exerting across the centromeres due to 'bipolar' spindle attachment. We thus used Monastrol, the Eg5 inhibitor, to prevent bipolar spindle establishment while keeping MT attachment[30]. As predicted, 'monopolar' spindle attachment is not sufficient to induce centromere DNA threads (Supplementary Fig. 8). Therefore, centromere splitting requires bipolar spindle pulling forces.

To our knowledge, this striking phenomenon of spindle-mediated centromere rupture has never been described; we thus termed this 'centromere dislocation'. Using multi-colour FISH (mFISH) analysis, we further validated that PLK1 inactivation can cause whole-chromosome arm separation (Fig. 3d). In some cases, the separated whole-arms were located in close vicinity (Fig. 3d; e.g., chromosomes 7p–7q, 12p–12q and 17p–17q), which may imply a residual physical connection, presumably through the ultrafine centromeric DNA threads. In addition, centromere dislocation tended to occur more frequently on longer chromosomes (Fig. 3d, inset). Collectively, our data show that, in the absence of PLK1 activity, centromere chromatin fails to withstand

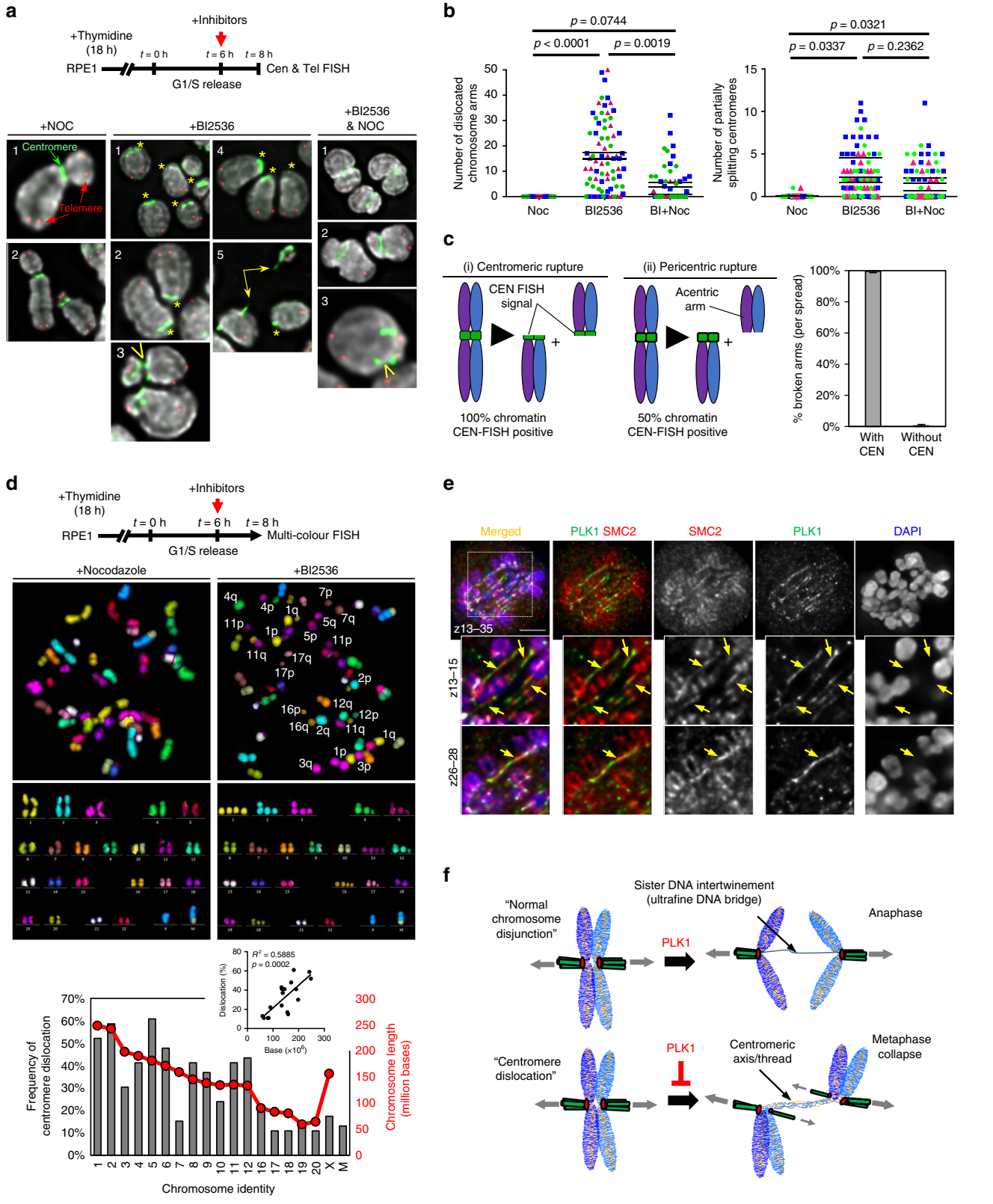

bipolar spindle tensions and the core axis is transformed into an ultrafine DNA threadlike structure. Indeed, we were able to detect condensin, a chromosome axial element, associating along the stretched DNA threads (Fig. 3e; arrows). The disintegration of centromeres therefore causes whole-chromosome arm splitting and explains why cells simultaneously lose their metaphase alignment (Fig. 3f).

PLK1 kinase activity suppresses centromere disintegration. Thus far, most of the experiments were carried out using the PLK1 inhibitor, BI2536. To rule out potential off-target effects, such as inhibition to other PLK members[20], we employed an engineered RPE1 cell line in which the endogenous wild-type (WT) PLK1 has been replaced with an analogue-sensitive allele, PLK1as. The catalytic cavity of the PLK1as protein has been

Fig. 3 PLK1 inactivation induces spindle-dependent centromere dislocation. **a** Experimental outline (top) and representative deconvolved images showing chromosomes isolated from RPE1 cells under the indicated treatment. Chromosomes were hybridised with FISH DNA probes against centromeres (green) and telomeres (red). Left panels: examples of normal chromosome configuration (+nocodazole). Middle panels: examples of BI2536-induced 'centromere dislocations' (asterisks; 1–5), 'partial centromere splitting' (arrowhead; 3), and a centromere DNA thread linking two separate chromosome arms (connecting arrow; 5). Right panels: chromosomes with 'partial centromere splitting' (arrowhead) after BI2536 and nocodazole co-treatment. Note: also see Supplementary Fig. 7 for the whole-chromosome spread images. **b** Quantification of 'chromosome arm dislocations' (left) and 'partially centromere splitting' (right) under the indicated inhibitor treatment ($n = 3$ independent experiments analysing 75 spreads in each condition; the means of each experiment are shown). **c** A diagram depicting the outcomes of chromosome breakage within or outside centromeres. (i) Breakage at centromeres generates both broken arms (100%) positive for CEN FISH signal; (ii) breakage at pericentric or arm regions generates one of the broken arms (50%) positive for a CEN FISH signal. Quantification (right) of the examined broken chromosome arms with or without centromere FISH signal at their termini (524 broken chromosome arms were scored from 11 separate chromosome spreads showing the highest centromere dislocation frequency). **d** Experimental outline (top) and mFISH karyotyping of RPE1 cells. BI2536 induced chromosome 'p'- and 'q'-arm separation. Note: there is a marker 'M' chromosome with a translocation of chromosome X and 10 in RPE1 cells. Bar graph (bottom) showing the frequency of 'centromere dislocations' among individual chromosomes. Inset graph showing the positive correlation between chromosome length and 'centromere dislocation' frequency (23 spreads were analysed). Note: acrocentric chromosomes were not determined and the length of the 'marker' chromosome is unknown. **e** Condensin (SMC2) is detected on some PLK1-associated DNA threads (arrows). Scale bars = 5 μm. **f** A model of centromere dislocation induced by PLK1 inactivation in a spindle-dependent manner. Spindle-mediated tension causes decompaction of centromere axis, the formation of centromere DNA threads and whole-chromosome arm separation

modified such that it no longer binds to BI2536; instead only to the unrelated ATP-analogue, 3-MB-PP1[31] (Supplementary Fig. 9a). As predicted, BI2536 failed to induce metaphase collapse and centromere DNA thread formation in the engineered PLK1as cells. Importantly, these mitotic defects were recapitulated by using 3-MB-PP1 analogue (Supplementary Fig. 9a–d). In addition, depletion of the PLK1 protein in RPE1 cells by RNA interference (RNAi) also induced centromere DNA threads and dislocations (Supplementary Fig. 9e, f), which further rules out the potential dominant effect as a result of trapping an inactive form of PLK1 onto chromatin by the small molecule inhibitors. Therefore, PLK1 kinase activity per se is essential to suppress centromere disintegration.

Aberrant association of UFB-binding factors to KTs. The failure of centromeres to withstand bipolar spindle pulling in the absence of PLK1 function might indicate that centromere chromatin structure is impaired. We thus analysed the centromeres in the BI2536-treated RPE1 cells before metaphase collapse occurs. We found that there was a progressive formation of RPA foci at or near KTs; from early prometaphase to metaphase(-like) stages (Fig. 4a). This was also sensitive to nocodazole treatment (Fig. 4a). In control, we rarely detected RPA foci at centromeres in normal metaphase cells (Fig. 4b). More interestingly, we also found increased accumulations of BLM and PICH foci at or near the KTs in the metaphase(-like) cells, again only after BI2536 treatments (Fig. 4c and Supplementary Fig. 10a). Occasionally, PICH was found at the inner centromeres of untreated cells (Supplementary Fig. 10a; yellow arrows), perhaps reflecting the unresolved DNA entanglements between sister centromeres as proposed previously[10,11,13,18,32]. Earlier studies have reported that (phospho)-RPA and BLM foci are observed at centromeres of cytospun chromosomes[33,34]. However, under our experimental conditions, both RPA and BLM foci were rarely detected at centromeres in normal intact mitotic cells (Fig. 4b, c). In contrast, PICH foci were consistently visualised at KTs in normal mitotic cells[10] (Supplementary Fig. 10a). To confirm that PLK1 inactivation also enhances PICH loading, we performed quantitative imaging analysis on co-cultured RPE1 cells, using a mixture of cells expressing either a WT PLK1 or GFP-tagged PLK1as protein. This allowed us to directly compare the relative amount of PICH at KTs. Under BI2536 treatment, there was a marked increase in both intensity and number of PICH foci at KTs in WT PLK1, but not in the GFP-PLK1as cells (Supplementary Fig. 10b–d). Conversely, 3-MB-PP1 induced PICH accumulation at KTs in the GFP-PLK1as cells (Supplementary Fig. 10b–d). As expected, PICH, BLM and RPA foci were mostly co-localised at KTs (Supplementary Fig. 10e; arrows). Therefore, the UFB-binding complex is aberrantly recruited to KT regions when PLK1 function is compromised. Since BLM and PICH possess activities of DNA unwinding and of DNA displacement, respectively[29,35], this led us to speculate that the increase in centromeric RPA foci formation may be due to illegitimate DNA unwinding.

Centromere distortion underneath KTs. The localisation of PICH to KTs is independent of PLK1[18,28] (Supplementary Fig. 9e). Our data show that inactivating PLK1 even increases the binding of PICH, BLM and RPA to KTs. Whether the complex actually targets the centromere chromatin, or is aberrantly enriched at KTs is unclear. To address this, we employed high-resolution microscopy to precisely locate the complex within the territory of centromeres (Supplementary Fig. 11a). We found that PICH localised in centromeres at a position ~160 nm away from the outer KT component, as marked by NUF2 (Supplementary Fig. 11b, d). In a control measurement, the inner KT component, CENPA, was mapped ~100 nm inwards from NUF2 in metaphase cells (Supplementary Fig. 11c, d). The CENPA-NUF2 distance was reduced (~80 nm) in anaphase cells (Supplementary Fig. 11c, d), probably due to a reduction of intra-KT tension following sister chromatids cohesion loss[36,37]. This inward position of PICH suggests that it likely locates at centromere chromatin. Further co-staining of PICH and CENPA confirmed that PICH resides at a centromeric domain ~100 nm beneath CENPA (Fig. 4d and Supplementary Fig. 11d). Likewise, both BLM and RPA foci, were mapped underneath CENPA, with distances of ~120 and ~150 nm, respectively (Fig. 4d and Supplementary Fig. 11d). All of these proteins displayed mirror localisation patterns, reflecting a typical symmetry of sister centromere-KT organisation. We referred to this specific centromere site as 'kinetochore-chromatin' or 'K-chromatin' (Fig. 4e).

The K-chromatin localisation finding is consistent with our notion that centromeric chromatin is probably targeted by the UFB-binding complex after PLK1 inhibition. If the increased formation of RPA foci at K-chromatin reflects aberrant DNA unwinding, this may weaken centromere rigidity to counteract spindle pulling forces. Notably, we observed detachments of KT complex in a small population of centromeres (<4%) in metaphase(-like) cells prior to collapse. Intriguingly, some of the KTs remained connected by a short thread, as labelled by

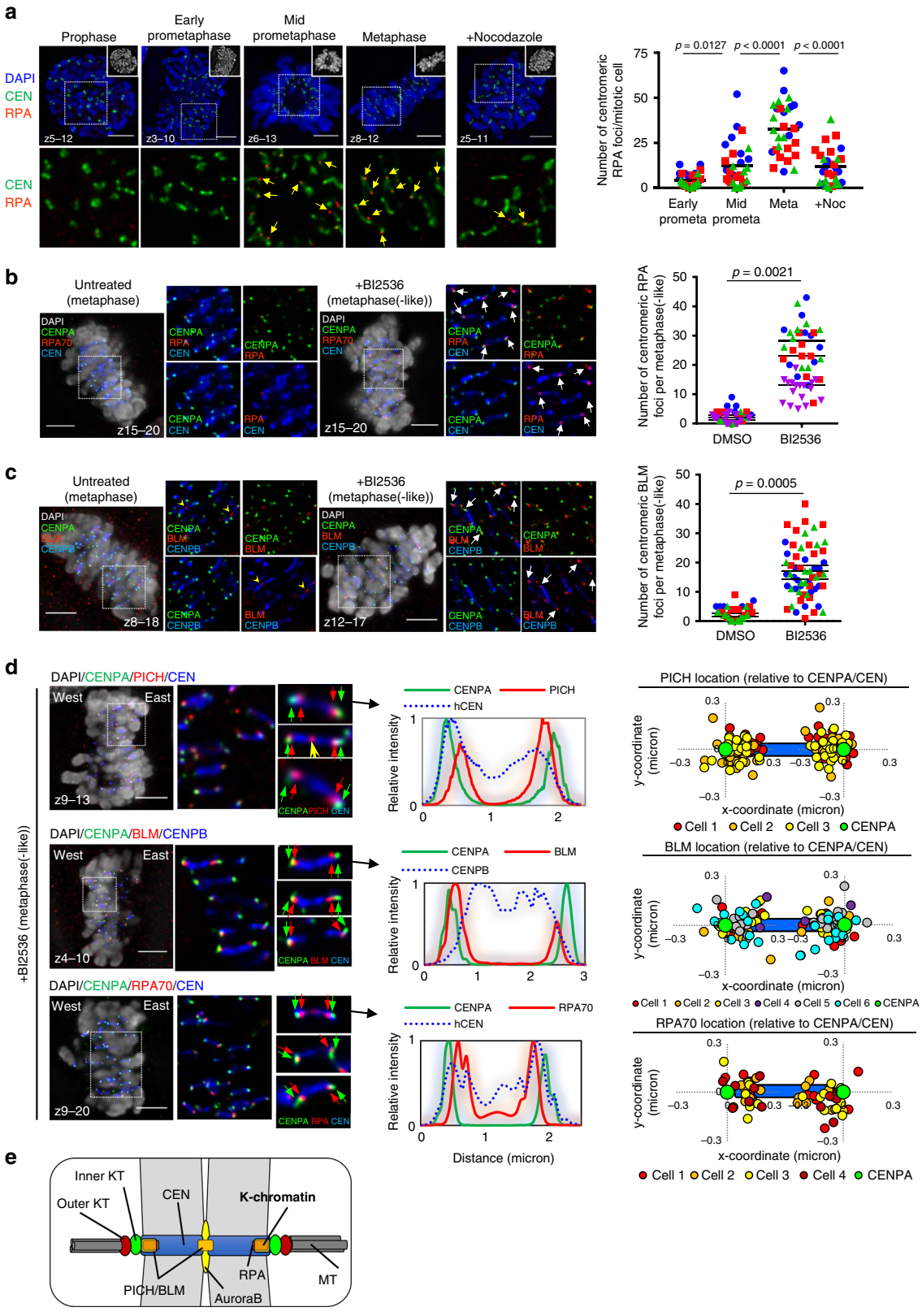

PICH or RPA staining (Fig. 5a, b; arrows). Centromere staining was sometimes evident along the short thread (Fig. 5a; arrows), implying a protrusion of centromeric DNA. We postulated that this might be the early sign of centromere disintegration. Further analysis of the centromere-KT integrity revealed that there was a large percentage of centromeres losing one of the two sister KTs after metaphase collapse (Fig. 5b–d). The side of the centromere where a KT was missing was concomitant with the formation of DNA thread linkages (Fig. 5c; connecting arrows). Therefore, there are apparent alterations on the centromere-KT configuration prior to and during centromere disintegration.

Fig. 4 PLK1 inactivation increases PICH, BLM and RPA foci at K-chromatin. **a** Increased RPA foci formation at centromeres during mitotic progression after PLK1 inhibition (from prophase to metaphase-like stage). Right: Quantification of the numbers of RPA foci at centromeres in the indicated mitotic stages and treatments ($n = 3$ independent experiments analysing a total of 30 cells in each stage of early, mid prometaphase and metaphase; and of 29 cells in the nocodazole-treated condition; average mean is shown). **b** BI2536 increased the formation of centromeric RPA foci in precollapsed metaphase-like cells. Representative images comparing RPA foci at centromeres in DMSO- (left) and BI2536-treated (right) metaphase-like cells. Enlarged images of the selected regions are shown at right. Arrows indicate centromeric RPA foci. Quantification of RPA foci number at centromeres of metaphase (DMSO), and metaphase(-like) (BI2536) cells ($n = 3$ independent experiments analysing 47 cells per condition). **c** Same as (**b**), but stained with BLM ($n = 3$ independent experiments analysing 59 and 60 cells in DMSO- and BI2536-treated conditions; means of each experiment are shown). **d** Mapping the locations of PICH/BLM/RPA complex at centromeres. Representative images showing the relative locations of PICH (top), BLM (middle) and RPA (bottom) at the centromeres, comparing to the inner kinetochore marker, CENPA. Profile plots of signal intensity accompanies each example. Right: graphs showing the relative position of each protein at both sides of the centromere. **e** A model depicts the localisation of the PICH/BLM/RPA complex at a specific domain of centromeres, named kinetochore-chromatin/K-chromatin. Note: all RPE1 cells analysed were pre-synchronised at G1/S by a single thymidine block. Drugs were added at 6 h post-release. After 2 h treatment, cells were subject to immunofluorescence staining. Scale bars = 5 μm

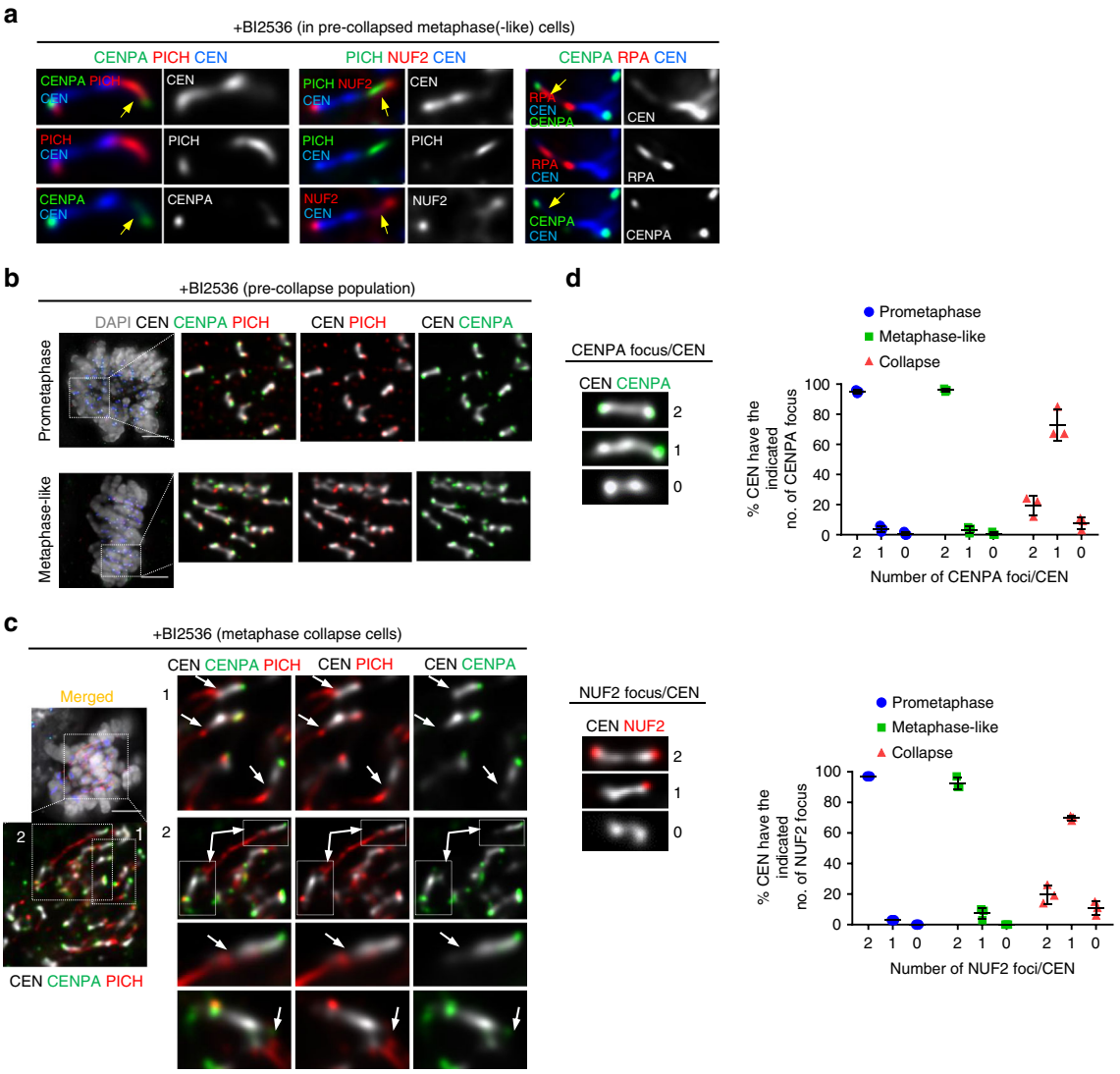

Fig. 5 Loss of kinetochore attachment at centromeres after dislocation. **a** Representative images showing the kinetochore complex detaches from the core centromere, whilst remaining connected by PICH- or RPA-coated DNA threads (arrows) in BI2536-treated metaphase-like RPE1 cells. Inner and outer kinetochores were labelled by CENPA and NUF2, respectively. **b** Examples showing the majority of centromeres retain two kinetochores in pre-collapsed mitotic populations (prometaphase and metaphase-like cells) after BI2536 treatment. **c** Representative image showing the metaphase-collapse cells losing kinetochore complex at one side of the centromere. Note: the side without the kinetochore is concomitant with the formation of PICH-associated DNA linkages (arrows). Enlarged images (1 and 2) highlight the loss of CENPA signal at regions of where PICH-decorated DNA linkages form (arrows). **d** Quantification of the numbers of CENPA- and NUF2-labelled kinetochores at centromeres in prometaphase, metaphase-like and collapse stages after BI2536 treatment ($n = 3$ independent experiments analysing a total of 3020 CENPA-labelled centromeres and 3625 NUF2-labelled centromeres; mean ± S. D. is shown). Note: all RPE1 cells analysed were pre-synchronised at G1/S by single thymidine block. Drugs were added at 6 h post-release. After 2 h treatment, cells were subject to immunofluorescence staining. Scale bars = 5 μm

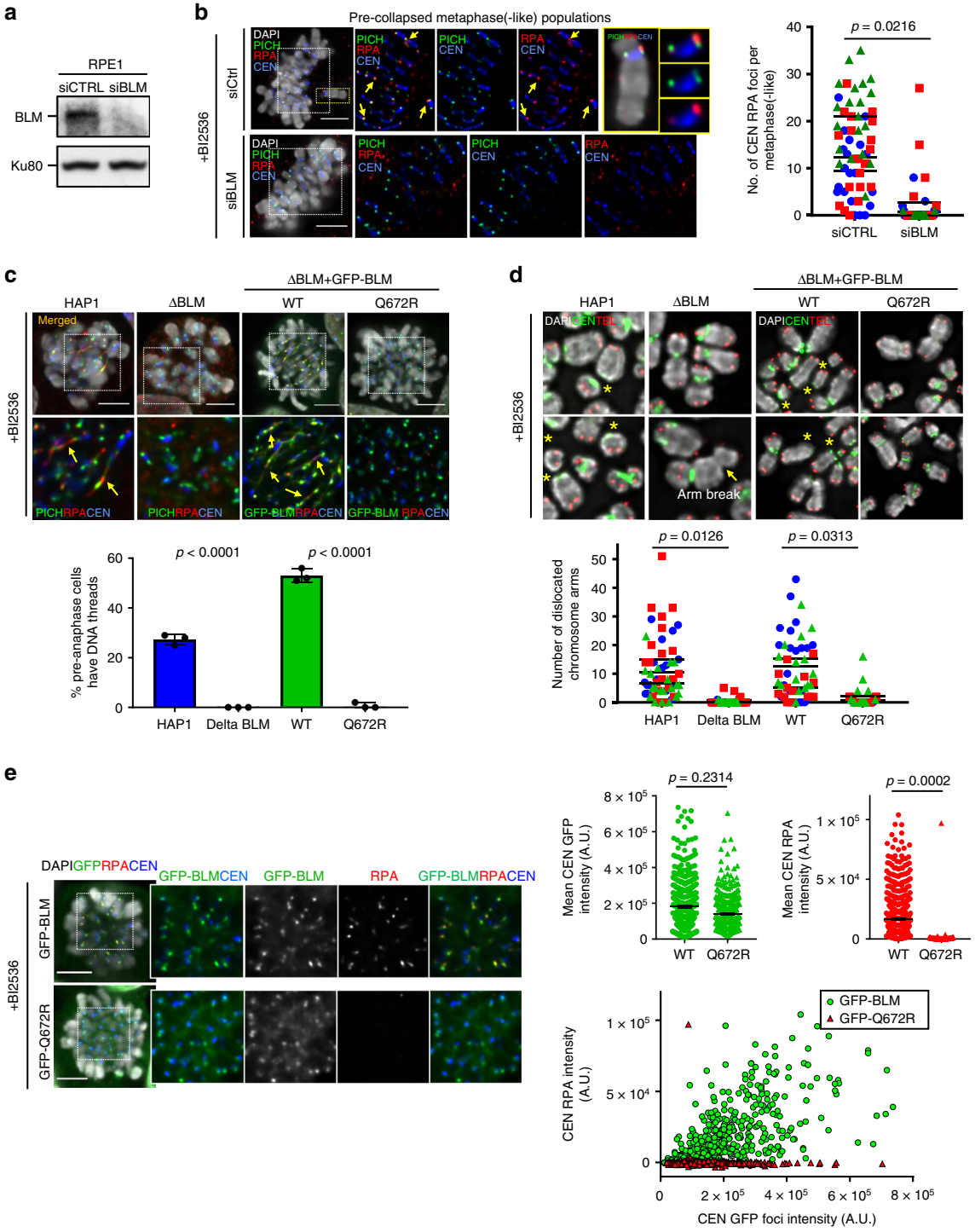

BLM helicase activity mediates centromere disintegration. Next, we examined whether centromere disintegration is mediated by BLM and PICH. We knocked down BLM by RNAi before BI2536 treatment (Fig. 6a). Silencing BLM for longer than 48 h in RPE1 cells reduced the efficiency of thymidine release, therefore we treated cells with siBLM oligos for only 24 h prior to G1/S release (Supplementary Fig. 12a). Despite partial depletion (Supplementary Fig. 12b–d), we found that first, BLM knockdown significantly reduced the formation of RPA foci at K-chromatin induced by BI2536 (Fig. 6b); second, it also diminished both centromere DNA thread formation and centromere dislocation (Supplementary Fig. 12e, f). BLM depletion did not impair PICH centromeric localisation (Supplementary Fig. 12g), suggesting that, without BLM, PICH alone is not sufficient to drive centromere disintegration. To confirm the specificity of BLM knockdown, we performed our analyses on HAP1 cells in which the endogenous BLM was knocked out by CRISPR genome editing[38] (Supplementary Fig. 13a, b). Consistently, BLM knockout abolished centromere DNA thread formation and centromere dislocations (Fig. 6c, d). Though, occasionally, chromatid breaks were observed in ΔBLM HAP1 cells, the breakpoint was not at the centromere (Fig. 6d, arrow). Therefore, in addition to the bipolar spindle pulling forces, BLM is a key driver of centromere disintegration after the loss of PLK1 activity.

Centromere disintegration might be initiated through unlawful DNA unwinding by BLM. Thus, we determined if BLM's helicase

Fig. 6 BLM helicase activity triggers centromere disintegration. **a** Western blot showing BLM depletion after RNAi treatment in RPE1 cells. Ku80 is used as a loading control. **b** BLM depletion reduced centromeric RPA foci formation induced by BI2536 in pre-collapsed metaphase(-like) cells. Representative images showing the loss of RPA, but not PICH foci, at centromeres in siBLM cells. Right: quantification of centromeric RPA foci in metaphase(-like) cells ($n = 3$ independent experiments analysing 60 cells per condition; mean ± S.D. is shown). **c** Representative images and quantification of DNA thread formation in wild-type (HAP1) cells, BLM knockout cells (ΔBLM), and ΔBLM HAP1 cells complemented with a wild-type GFP-BLM (WT) and a BLM-helicase mutant (Q672R) protein under BI2536 treatment ($n = 3$ independent experiments analysing a total of 291, 218, 204 and 184 cells in HAP1, ΔBLM, WT and Q672R cell lines; mean ± S.D. is shown). **d** Representative chromosome images of 'centromere dislocations' (yellow asterisks) in the indicated HAP1 cells shown in (**c**). Note: occasional arm breaks (arrow) were observed in ΔBLM cells. Quantification of centromere dislocation is shown below ($n = 3$ independent experiments analysing a total of 60, 60, 51 and 51 spreads in HAP1, ΔBLM, WT and Q672R cell lines; means of each experiment are shown). **e** Centromeric RPA foci formation in ΔBLM HAP1 cells expressing wild-type GFP-BLM (WT) and a BLM helicase-dead mutant (GFP-Q672R) following BI2536 treatment. Representative images showing the lack of RPA foci at centromeres in the GFP-Q672R cells. Right: bar graphs showing the average fluorescence intensities of centromere GFP and RPA foci, respectively, in GFP-BLM and GFP-Q672R cells (mean + S.E.M. is shown). A scatter plot of RPA foci intensity by GFP foci intensity at centromeres (total numbers of centromere foci analysed: GFP-BLM, $n = 582$; and GFP-Q672, $n = 481$). All RPE1 and HAP1 cells, including their derivatives, were pre-synchronised at G1/S by single thymidine block. Drugs were added at 6 h post-release. After 2 h treatment, cells were subject to immunofluorescence staining. RNAi treatment of RPE1 cells was performed for 23 h before G1/S release. Scale bars = 5 μm

activity is required. We generated polyclonal cell lines from the ΔBLM HAP1 cells, which stably express either a GFP-tagged WT or a helicase-dead (Q672R) BLM protein. The expression of the GFP-Q672R protein was similar to the endogenous BLM level in HAP1 cells; whereas, the GFP-WT was over-expressed (Supplementary Fig. 13b). In agreement with our notion, the helicase-dead (Q672R) BLM failed to induce centromere DNA threads and dislocations caused by BI2536 treatments (Fig. 6c, d). However, as the expression level of the GFP-Q672R mutant was lower than the WT control; to perform a better comparison, we re-sorted the WT GFP-BLM cells to obtain a cell population with a lower BLM expression (Supplementary Fig. 13c). Despite a much lower abundance, the WT GFP-BLM protein was still capable of driving centromere DNA thread formation (Supplementary Fig. 13d). More importantly, the GFP-Q672R mutant protein no longer induced RPA foci formation, despite its aberrant enrichment at centromeres following PLK1 inhibition (Fig. 6e). Therefore, we conclude that centromere disintegration is mediated by BLM-dependent DNA unwinding at centromeres.

Next, we investigated the role of PICH. Knockdown of PICH, like BLM, also suppressed BI2536-induced centromere DNA thread formation and centromere dislocations (Fig. 7a–c). However, it also abolished BLM localisation and RPA formation at K-chromatin. (Fig. 7d). Therefore, PICH acts upstream to facilitate the recruitment of BLM to centromeres after PLK1 inactivation. Taken together, our data suggest that PLK1 has an important function to protect centromeres from unlawful DNA unwinding, mediated by the PICH/BLM complex. The structural change probably impairs centromere rigidity and causes the failure to withstand bipolar spindle pulling forces. Consequently, centromeres are torn apart, leading to whole-chromosome arm splitting and chromosome biorientation failure.

Centromeric tethering of BLM does not induce metaphase collapse. Both PICH and BLM interact with PLK1 and are hyperphosphorylated during mitosis[10,39–41]. Hyperphosphorylation of PICH and BLM is partially dependent on PLK1[42] (Supplementary Fig. 14). It has been proposed that hyperphosphorylation of BLM can prevent its association with mitotic chromosomes[41,43]. Thus, we sought to test whether the abnormal loading of BLM to centromeres, presumably due to the loss of PLK1-mediated phosphorylation, might cause centromeric DNA unwinding and dislocation. We tethered BLM to centromeres in HeLa cells by fusing a truncated CENPB (1–158) to a GFP-tagged BLM. Transient expression of the WT GFP-BLM and the CENPB-GFP-BLM fusion proteins showed that the WT GFP-BLM exhibited diffused localisation pattern and was mostly excluded from mitotic chromosomes after nuclear envelope breakdown. In contrast, the CENPB-GFP-BLM fusion protein was enriched at core centromeres throughout mitosis (Supplementary Fig. 15a). However, we did not find that tethering BLM to centromeres induced obvious mitotic defects such as mitotic arrest, as observed by PLK1 inhibition. Time-lapse live-cell imaging showed that the CENPB-GFP-BLM transfected cells, like the WT GFP-BLM, progressed successfully into anaphase, without metaphase collapse (Supplementary Fig. 15b). Moreover, RPA (ssDNA) formation was not detected at centromeres where the CENPB-GFP-BLM protein was enriched (Supplementary Fig. 15c). Therefore, artificially over-loading BLM at centromeres seems not sufficient to trigger DNA unwinding and centromere disintegration when PLK1 remains active. Though speculative, the triggering of centromere dislocation in PLK1-inactivated cells might be caused by mis-regulation of BLM (and PICH) activity; and/or because of improper formation of centromere structures that mis-activates the PICH/BLM complex prior to chromosome disjunction.

Constitutive PLK1 activity for centromere integrity maintenance. To test if centromere disintegration might be caused by centromere malformation during early mitosis, we inhibited PLK1 only after mitotic cells had fully formed their chromosomes and progressed into metaphase, whilst in the presence of active PLK1. RPE1 cells stably expressing a GFP-tagged PLK1 were first blocked at metaphase using the APC/C inhibitor, ProTAME. Time-lapse live-cell imaging recorded that upon the addition of BI2536, the fully bioriented chromosomes started losing their alignment. Most importantly, this was accompanied by the formation of DNA threads (Fig. 8a and Supplementary Movies 2 and 3), indicating the occurrence of centromere dislocation. Furthermore, we found that centromere dislocation can happen rapidly, as within 30 min of BI2536 addition, more than 60% of the metaphase-arrested cells generated centromere DNA threads (Fig. 8b). As centromere dislocation depends on bipolar spindle pulling, this would imply that the KT-MT attachment is not instantly destroyed, at least in those centromeres with DNA threads. Therefore, rather than due to an initial malformation, centromere disintegration is likely triggered because of a defect in centromere structure maintenance.

Depletion of PICH and BLM prolongs metaphase alignment. Thus far, our data indicates that apart from the proposed model of KT-MT destabilisation, a failure in centromere integrity maintenance is another cause of chromosome misalignment. To further test this, we examined if suppression of centromere dislocation, by PICH and BLM depletion, might rescue the

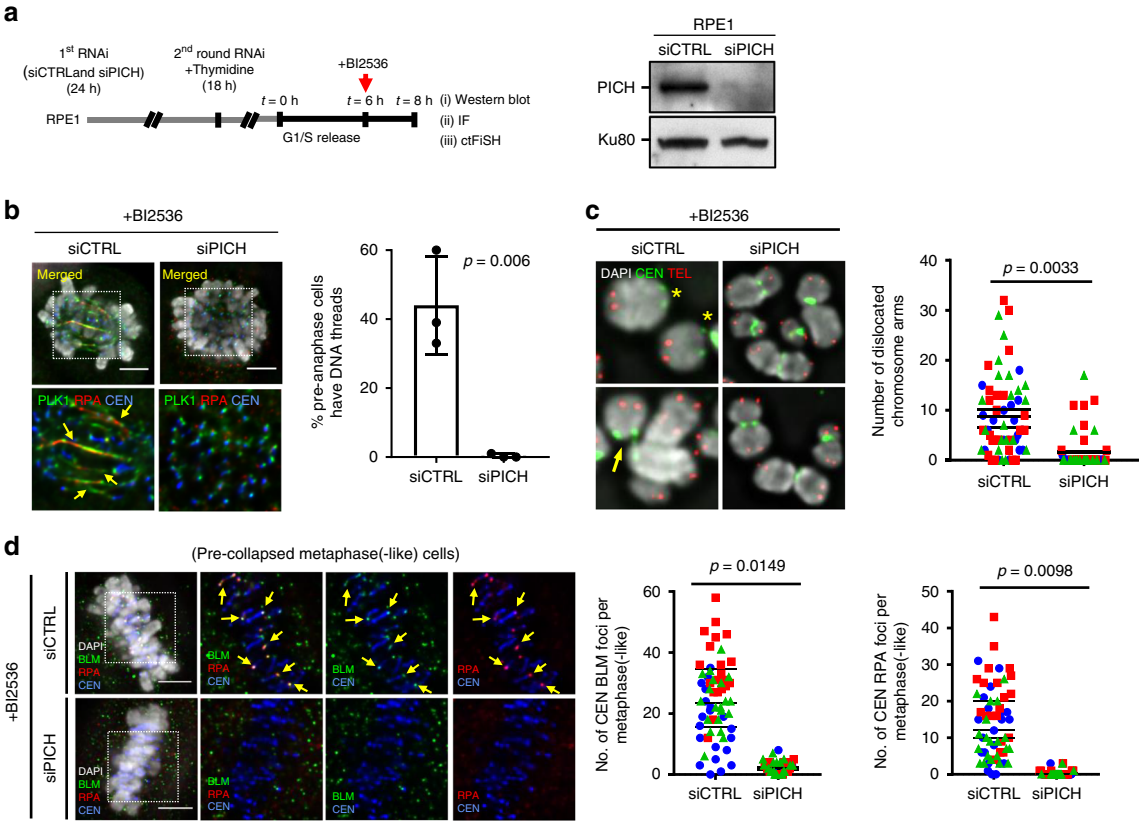

Fig. 7 PICH acts upstream of BLM in centromere disintegration. **a** Experimental outline of RNAi depletion, in combination with thymidine synchronisation and drug treatment. Right: western blot showing PICH protein level in siCTRL and siPICH treatment. Ku80 is used as a loading control. **b** Centromeric DNA thread formation in siCTRL and siPICH cells under BI2536 treatment. Quantification of DNA thread formation in RPE1 cells after siCTRL and siPICH treatment ($n = 3$ independent experiments analysing 315 and 314 cells in siCTRL and siPICH conditions, respectively; mean ± S.D. is shown). **c** Representative images of mitotic spread chromosomes from cells prepared in (**a**) showing centromere dislocations (asterisks) and partial centromere splitting (arrow). Quantification of centromere dislocation is shown at right ($n = 3$ independent experiments analysing 64 and 61 dislocated chromosome arms in siCTRL and siPICH conditions, respectively; means of each experiment are shown). **d** Reductions of BLM and RPA foci formation at centromeres in siPICH cells after BI2536 treatment. Representative images (left) and quantifications (right) are shown ($n = 3$ independent experiments analysing a total of 60 cells in each treatment; means of each experiment are shown, Scale bars = 5 μm)

metaphase alignment defect in PLK1-inhibited cells. Knocking down PICH or BLM had no adverse effect on metaphase establishment in RPE1 cells under BI2536 treatments. However, it significantly prolonged the metaphase(-like) stage as compared to control cells (Fig. 8c and Supplementary Movies 4–6). Although the metaphase chromosomes inevitably misaligned after long delays in the PICH/BLM-depleted cells, they dispersed more like a 'polo' pattern, rather than the 'Fig-8' collapsed shape. As we showed that PICH/BLM depletion abolished centromere dislocations, we believe that the ultimate alignment failure is likely caused by KT-MT destabilisation. Nevertheless, it seems that even in the absence of PLK1 activity, the centromeres and KTs remain competent to support chromosome biorientation, at least in RPE1 cells, as long as the PICH/BLM complex is inactivated. Moreover, our data also implies that KT-MT destabilisation, if it occurs, seems to do so at a relatively slow rate as compared to centromere disintegration.

In summary, we report an unexpected role of PLK1 during chromosome biorientation, which prevents centromeres from destruction, mediated by the co-action of DNA unwinding by BLM helicase and bipolar spindle pulling (Fig. 9).

Discussion

One of the key mitotic functions of PLK1 is to promote stable attachments between spindle MTs and KTs[6]. In the current study, we reveal a hitherto undescribed role of PLK1 as a centromere guardian for chromosome alignment. We show that the lack of PLK1 activity leads to the failure of centromeres to withstand bipolar spindle pulling tension. As a consequence, centromere chromatin is stretched into a threadlike structure, resulting in centromere splitting, whole-chromosome arm separation and loss of metaphase alignment. Further experiments demonstrate that the disintegration of centromeres is not a passive process, but is actively driven through illegitimately unwinding of centromeric DNA by the PICH/BLM complex. Our results highlight a PLK1-dependent pathway for centromere maintenance during mitosis.

BLM is the key molecular driver of centromere disintegration, but it remains unclear how PLK1 counteracts its mediated destruction. Given that both BLM and PICH proteins are substrates of PLK1, a reasonable speculation is that PLK1 can regulate the activity of PICH/BLM complexes during mitosis. Previous studies have shown that before anaphase onset, BLM poorly associates with mitotic chromosomes[41,43] and on UFBs generated from prematurely disjoined sister chromatids[11]. The chromatin exclusion of BLM, presumably by hyperphosphorylation, could limit its DNA transaction activity. However, artificially tethering BLM to centromeres is not sufficient to induce DNA unwinding and centromere dislocation, which may suggest that either the BLM protein remains inactive, or additional factors such as PICH activation and/or chromatin

remodelling are required. Alternatively, PLK1 may protect centromeres through facilitating normal condensation of centromeres, a process if compromised might create a DNA substrate that mis-activates the PICH/BLM complex. However, impairing chromosome condensation by condensin depletion, which leads to abnormal stretching of sister centromeres[44,45], does not trigger similar phenotypes of centromere rupture and chromosome misalignment as induced by PLK1 inhibition. In addition, the fact that centromere disintegration can be induced in 'mature' mitotic cells; namely those cells that have fully formed normal metaphase, would suggest that rather than due to an initial chromatin malformation, it is probably caused by centromere maintenance

Fig. 8 Constitutive PLK1 activity suppresses centromere disintegration. **a** Experimental outline and time-lapse live-cell images of GFP-tagged PLK1 RPE1 cells treated with BI2536 after metaphase establishment. Cells were arrested at metaphase by ProTAME after G1/S release. High-resolution movies were recorded immediately after the addition of BI2536. The formation of DNA threads is revealed by GFP-PLK1 protein (arrows). **b** Experimental outline and quantification of DNA thread formation in metaphase-arrested RPE1 cells. BI2536 was added in ProTAME-arrested metaphase cells for 30 min. Centromeric DNA threads were labelled by PICH, BLM and RPA staining. BLM thread counting ($n = 3$ independent experiments analysing a total of 188 and 189 cells in ProTAME and ProTAME + BI2536 conditions, respectively. RPA thread counting ($n = 3$ independent experiments of a total of 174 and 187 cells in each condition; mean ± S.D. is shown). **c** Depletion of PICH or BLM, prolongs the metaphase-(like) stage of RPE1 cells under PLK1 inactivation. Time-lapse microscopy images showing the mitotic progression of RPE1 cells treated with the indicated siRNA oligos, and BI2536. Red bars indicate the metaphase(-like) stage; yellow bars indicate 'metaphase collapse'. Quantification (right) of the overall duration of metaphase(-like) stage in control, PICH- and BLM-depleted cells, following BI2536 treatment ($n = 3$ independent experiments analysing 50, 60 and 57 cells in siCTRL, siPICH and siBLM conditions; means of each experiment are shown). Scale bars = 5 μm

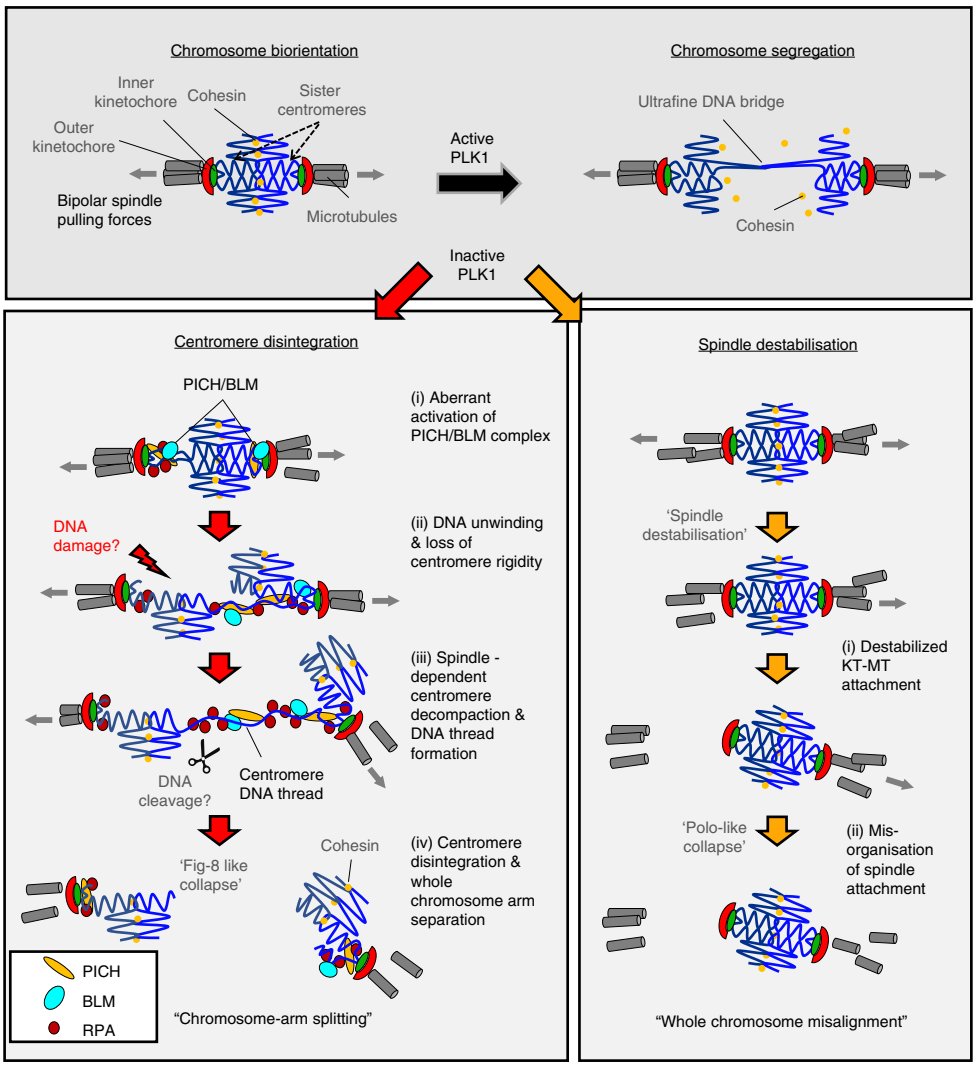

Fig. 9 A model of centromere disintegration in chromosome misalignment. Active PLK1 is required to stabilise chromosome biorientation for chromosome segregation. In addition to the existing role for spindle stabilisation, our current study demonstrates that PLK1 also functions to maintain centromere integrity for chromosome alignment. In the absence of PLK1 activity, centromeres are aberrantly targeted by BLM helicase in a PICH-dependent manner. It leads to unlawful, excessive formation of ssDNA, which impairs centromere configuration and weakens it ability to withhold kinetochore complexes. Forces exerted by the bipolar spindle attachment pull out the centromere chromatin, which might trigger further DNA unwinding by the PICH/BLM complex. As a consequence, it decompacts the centromere axis, leading to the formation of centromere DNA threads and whole-chromosome arm separation. Cells therefore fail to maintain chromosome biorientation and result in metaphase collapse with a 'Fig-8' like misalignment pattern. Alternatively, if the spindle attachment is destabilised first, it prevents centromere dislocation but this will lead to whole-chromosome misalignment, which probably manifests as more like a 'Polo' pattern. Therefore, we propose that PLK1 plays a multifactorial role in establishing and maintaining chromosome biorientation by both protection of centromere integration and stabilisation of KT-MT attachment

impairment. Nevertheless, no matter if there is a structural defect, loss of PLK1 does not seem to greatly compromise chromosome biorientation, at least in RPE1 cells, as long as the PICH/BLM complex is inactivated. We postulate that PLK1 may protect centromeres through both chromatin structure maintenance and the regulation of the PICH/BLM complex activity. Further experiments will need to dissect the underlying mechanism(s).

Another very intriguing finding is that when acting in concert with bipolar spindle tension, the PICH/BLM complex can promote decompaction of the centromere axis. This converts the centromeric chromatin into an ultrafine DNA structure, reminiscent of anaphase UFBs[10,11], leading to whole-chromosome arm separation. Conceivably, if such decompaction activity is applied at a chromosomal region where sister DNA intertwinements persist, it may be able to relieve the entangling constraints and facilitate the poleward separation of sister chromatids during anaphase. Though this is speculative, this finding could provide an alternative clue to understand how the UFB-binding complex may function during chromosome disjunction, and potentially also explain why a long region of UFBs is always coated by the PICH/BLM complex. In principle, such powerful action would need to be under a tight control before anaphase onset, otherwise it could lead to pathological damage at chromatin sites where tension is exerted; namely the centromere. Finally, the identification of a centromere-specific breakage pathway, independent of chromosome mis-segregation[46,47], also offers an alternative direction in understanding the origin of complex chromosome rearrangements, such as whole-chromosome arm rearrangements, which are observed in many human tumours and rare genetic disorders[48–51].

In conclusion, our study unveils an unexpected participation of PLK1 and the UFB-binding complex in the safeguard of centromere integrity during mitosis, which is critical for faithful chromosome segregation and chromosome stability.

Methods

Cell culture. RPE1-hTERT, 82-6-hTERT normal diploid cell lines, 1BR3 primary fibroblasts, HCT116 colon and HeLa cancer cells were obtained from the Genome Damage and Stability Centre (GDSC) Cell Bank. All cell lines were authenticated by STR genotyping from European Collection of Cell Cultures. RPE1-hTERT derivative cells were generated and supplied by Mark Burkard (University of Wisconsin). Bloom's syndrome fibroblasts (GM08505) were obtained from Phillip North (University of Oxford). HAP1 cells and HAP1 ΔBLM cells were obtained from Marcel van Vugt (University of Groningen). All cell lines passed mycoplasma tests (Lonza MycoAlert kit). RPE1-hTERT and its derivative cells were grown in DMEM/F-12 medium (Sigma) containing 15% foetal calf serum (FCS) and Pen/Strep antibiotics (P/S). 82-6 Fibroblast cells were grown in DMEM/F-12 medium containing 15% FCS and P/S. HAP1 cells were grown in IMDM (Gibco) containing 10% FCS and P/S. 1BR3 primary cells were grown in MEM (Gibco) containing 2mM L-glutamine, 15% FCS and P/S. HCT116 cells were grown in McCoy's 5A (Gibco) containing 15% FCS and P/S. Bloom's syndrome fibroblasts (GM08505) were transfected with a pEGFP-hBLM construct and selected by 700μg/ml G418 for 14 days. A single clone was isolated and maintained in MEM (Gibco) containing 2 mM L-glutamine, 10% FCS, P/S and G418. Cell cultures were maintained at 37 °C in a humidified atmosphere containing 5% CO_2. GFP-BLM(WT) and GFP-BLM(Q672R) HAP1 cells were generated by stable transfection with the corresponding constructs in HAP1 ΔBLM cells by using FuGene HD (Promega) according to the manufacturer's guidelines. The DNA constructs were created by sub-cloning EGFP-hBLM (WT) or Q672R (helicase dead mutant) fragments into a pSYC-181-(NEO) vector. Following a 1.2 mg/ml of G418 selection for 14 days, GFP-positive populations were sorted and isolated using a FACS cell sorter (BD FACSMelody).

Cell synchronisation and drug treatments for mitotic cell analysis. Cells were treated with 2 mM of thymidine for 18 h to enrich cells at the G1/S boundary. Cells were then released into S-phase by washing three times with pre-warmed culturing medium, or pre-warmed 1× PBS and released into fresh medium. Totally, 5–6 h post-G1/S release, indicated inhibitors were added. At approximately 8–9 h post the G1/S release, mitotic cells were fixed or enriched for analyses.

RNA interference. Cells were transfected with siRNA oligonucleotides using Lipofectamine RNAiMAX transfection reagent (Thermo Fisher Scientific) following the manufacturer's guidelines. Cells underwent 1 or 2 rounds of siRNA transfection as necessary.

Non-targeting siRNA pool (Dharmacon ON-TARGET plus Non-targeting Pool—D-001810-10-05. UGGUUUACAUGUCGACUAA; UGGUUUACAUGUUG UGUGA; UGGUUUACAUGUUUUCUGA; UGGUUUACAUGUUUUCCUA)

PLK1 siRNA sequence (Dharmacon ON-TARGET plus SMARTpool—L-003290-00-0005. GCACAUACCGCCUGAGUCU; CCACCAAGGUUUUC GAUUG; GCUCUUCAAUGACUCAACA; UCUCAAGGCCUCCUAAUAG)

Sgo1 siRNA sequence (Dharmacon ON-TARGET plus SMARTpool—L-015475-00-0005. CAGCCAGCGUGAACUAUAA; GUUACUAUCUCACAU GUCA; AAACGCAGGUCUUUUAUAG; GUGAAGGAUUUACCGCAAA)

BLM siRNA sequence (Dharmacon ON-TARGET plus Individual—J-007287-08-0005. GGAUGACUCAGAAUGGUUA)

PICH siRNA sequence (Invitrogen—AAUUCGGUAAACUCUAUCCAC AGCU)

Fluorescence immunostaining. For immunostaining analyses, cells were seeded onto No. 1.5 or No. 1.5H cover glass and fixed with Triton X-100-PFA buffer (250 mM HEPES, 1× PBS, pH7.4, 0.1% Triton X-100, 4% methanol-free paraformaldehyde) at 4 °C for 20 min, or with PBS–PFA buffer (1× PBS, 4% methanol-free paraformaldehyde) at room temperature for 10 min. Pre-extraction was carried out in indicated experiments before fixation by incubation of the cover glass in pre-extraction buffer (20 mM HEPES pH7.4, 0.5% Triton X-100, 50 mM NaCl, 3 mM $MgCl_2$, 300 mM sucrose) for 10–15 s. Cells were incubated in permeabilisation buffer (0.5% Triton X-100, 1XPBS) for 20 min on ice followed by blocking with foetal calf serum for 15 mins at room temperature. Cells were incubated with primary antibody at 37 °C for 90 min followed by secondary antibody incubation at room temperature for 30 min. Slides were washed with 1× PBS for 5 times at room temperature after antibody incubation. Cells were mounted using DAPI-containing Vectashield mounting medium.

Primary antibodies used: anti-PICH (Abnova; H00054821-B01P, 1:100), anti-PICH (Abnova; H00054821-D01P, 1:100), anti-BLM (Santa Cruz; sc-7790, 1:50), anti-BLM (Abcam; ab2179, 1:200), anti-γH2AX (Upstate; JBW-301, 1:400), anti-TOP2A (Santa Cruz; sc-5348, 1:100), anti-SMC2 (Bethyl Lab; A300-058A, 1:200), anti-RPA70 (Abcam; ab79398, 1:200), anti-RPA32 (Abcam; ab2175, 1:200), anti-CENPA (Abcam; ab13939, 1:100), anti-CENPB (Abcam; ab25734, 1:800), anti-NUF2 (Abcam; ab122962, 1:200), anti-PLK1 (Santa Cruz; sc-55504, 1:100), anti-pericentrin (Abcam; ab4448, 1:400), anti-centromere (ImmunoVision; HCT-0100, 1:400) and GFP booster (ChromoTek; gba-488, 1:200). Secondary antibodies used: donkey anti-mouse Alexa Fluor 488, 555 and 647; donkey anti-rabbit Alexa Fluor 488, 555 and 647; donkey anti-goat Alexa Fluor 488 and 555; goat anti-human DyLight 550 and 650 (All secondary antibodies are purchased from ThermoFisher and used at 1:500 dilution).

High-resolution deconvolution microscopy. Images were acquired under a Zeiss AxioObserver Z1 epifluorescence microscopy system with 40×/1.3 oil Plan-Apochromat, 63×/1.4 oil Plan-Aprochromat and 100×/1.4 oil Plan-Aprochromat objectives and a Hamamatsu ORCA-Flash4.0 LT Plus camera. The system is calibrated and aligned by using 200 nm-diameter TetraSpeck microspheres (T7280, ThermoFisher). Ten to fifty z-stacking images were acquired at 200 nm intervals covering a range from 2 to 10 μm by using ZEN Blue software.

Deconvolution was carried out using Huygens Professional deconvolution software (SVI) with a measured point-spread-function generated by 200 nm diameter TetraSpeck microspheres. Classical maximum likelihood estimation method with iterations of 40–60 and signal-to-noise of 20–60 was applied.

Time-lapse Live-cell microscopy. Cells were seeded on 2-well or 4-well tissue culture chambers coverglass II (Sarstedt). SiR-DNA (Spirochrome) was added for at least 5 h prior to live-cell imaging. Images were acquired under a Zeiss AxioObserver Z1 epifluorescence microscopy system equipped with a heating and CO_2 chamber (Digital Pixel) by using 40×/0.6 Plan-Neofluar or 40×/1.3 oil Plan-Apochromat objectives and a Hamamatsu ORCA-Flash4.0 LT Plus camera. For mitotic progression analysis, 5–10 z-stacking images with 2 μm intervals were taken with the indicated time intervals by using ZEN Blue software. Images were processed using ImageJ software and in-focus z-plane images were manually extracted to make image montages. For imaging of DNA thread formation in live cells, 40×/1.3 oil Plan-Apochromat objective was used to capture eight z-stack images with 800 nm intervals and in-focus z-plane images were extracted using ImageJ software.

Chromosome spread preparation. Following synchronisation using thymidine, cells were treated with pre-warmed hypertonic solution for 5–10 min at 37 °C (0.075M KCL). The swollen cells were then fixed and washed twice with methanol: acetic (3:1 ratio), before finally being re-suspended in fresh methanol:acetic solution. Chromosome spreads were dropped onto glass slides and either counter-stained with Vectashield plus DAPI, or stored at room temperature for

forthcoming FISH hybridisation. Colcemid was omitted in all mitotic spread preparations.

Centromere and telomere peptide nucleic acid (PNA) FISH. Centromere (CENPB-FAM; PNABio) & Telomere (Tel-Cy3 PNA FISH kit; DAKO, Agilent) PNA probes were hybridised according to the manufacturer's instructions. Briefly, chromosome spreads were rehydrated in 1× TBS prior to fixation in 3.7% PFA solution. Slides were then washed and pre-treated before dehydration using a gradient ice-cold ethanol wash (70, 90 and 100%). Slides were air dried and PNA probes were added. Slides were then co-denatured at 80 °C for 1 min and incubated for 2 h at room temperature. Slides were then washed in FISH Wash solution (Tel-Cy3 PNA FISH kit; DAKO, Agilent) for 5 min at 65 °C following by dehydration using a series of ethanol wash before counterstaining using DAPI Vectashield.

Multi-colour FISH. mFISH was performed by using 24XCyte Human Multicolour FISH probe (MetaSystems) according to the manufacturer's instructions. Images were acquired by MetaSystems using a Zeiss AxioObserver Z1 epifluorescence microscopy system with a CoolCube CCD camera and 100×/1.4 oil Plan-Aprochromat objective. Multi-colour FISH (mFISH) karyotyping was carried out by using ISIS Imaging software.

Immunoblotting. Cells were trypsinized and lysed on ice for 15–20 min with lysis buffer (50 mM Tris pH 7.5, 300 mM NaCl, 5 mM EDTA, 1% Triton X-100, 1.25 mM DTT, 1 mM PMSF and cOmplete^{TM} protease inhibitor cocktail). Protein concentration was quantified using a Bradford assay (Bio-Rad). Immunoblotting (IB) was performed following standard procedures. Primary antibodies used for IB in this study: anti-BLM (Abcam, ab2179, 1:2000), anti-PICH (Abnova; H00054821-B01P, 1:300), anti-GFP (Abcam, ab290, 1:1000) and anti-Ku80 (Abcam, ab80592, 1:10000). All uncropped blot scans are available in the Supplementary excel data file.

Flow cytometry. Cells were trypsinised, washed with PBS and fixed with 70% ice-cold ethanol. For cell cycle analysis, cells were washed with PBS and re-suspended in propidium iodide/RNaseA staining buffer. FACS profiles were then determined and analysed using BD Accuri C6 sampler.

KT/centromere foci measurement. Samples were subjected to pre-extraction in pre-extraction buffer (20 mM HEPES pH7.4, 0.5% Triton X-100, 50 mM NaCl, 3 mM $MgCl_2$, 300 mM sucrose) for 10–15 s followed by fixation and immuno-fluorescent staining as described above. Thirty to fifty z-stacking images with 200 nm intervals were acquired and deconvolved using Huygens Professional deconvolution software (SVI). KT foci on each single z-plane were marked and measured using the ImageJ Plugins detailed below.

ImageJ measurement of KT foci coordinates, distances and intensities. Spot Pair Distance Tool: Measures the distance between spots in two channels of an image. The tool searches within a focus/box radius, typically± 5px, for a local maxima in the two pre-selected analysis channels. The centre-of-mass around each maxima, typically± 2px, is computed as the centre of intensity for each channel. Dragging from the clicked point creates a reference direction. The Euclidean distance between the centres is reported, optionally with the signed XY distance and angle relative to the reference direction. Visual guides are overlaid on the image to assist in spot selection and direction orientation. Available in the latest GDSC ImageJ plugins.

Spot Fit Tool: Fits a 2D Gaussian to a spot in an image. The tool searches within a box radius, typically± 3px, for a local maxima in the pre-selected analysis channel. A 3 × 3 smoothing filter is applied before identification of the maxima. A 2D Gaussian function is then fitted to the data using non-linear least-squares fitting and poor fits rejected using a signal-to-noise ratio. The parameters for the fit are reported including the total intensity under the Gaussian function and the local background value. Visual guides are overlaid on the image to show the fitted location. Available in the pre-release GDSC SMLM ImageJ plugins.

Statistics. Statistical analysis was performed using GraphPad Prism 7 software by two-tailed unpaired Student's *t* test and two-way ANOVA as per the experimental requirement.

Recombinant DNA and transfections. CENPB (1–158aa) cDNA fragment was PCR amplified from a PLK1 plasmid in which the C-terminal PBD domain was replaced with the first 158 amino acids of CENPB (pQCXIN-Flag-Plk1deltaC-CENPB(1–158)) (a gift from Mark Burkard) and cloned into full length pEGFP-hBLM and pEGFP-hBLM(Q672) plasmids at AgeI site to generate N-terminally tagged CENPB (1–158aa) fusion proteins. Transfections of DNA plasmids were performed using FuGene HD (Promega) according to the manufacturer's guidelines. All plasmids and their sequences are available upon request. Forward primer: (CENPB-For1) 5′-TAAGCAACCGGTATGGGCCCCAAGAGGCGACAG-3′; Reverse primer: (CENPB-linker-Rev1)5′-TAAGCAACCGGTCTAGCACTT GCGCCCCCAGCACTTGCTCCACCGGCCGGACTG GCAGGCGCCGC-3′

Reporting summary. Further information on research design is available in the Nature Research Reporting Summary linked to this article.

Data availability

The authors declare that the data supporting the findings of this study are available within the paper and its Supplementary information files. Raw imaging data are available from the corresponding author upon reasonable request.

Received: 22 November 2018 Accepted: 7 June 2019
Published online: 28 June 2019

References

1. Potapova, T. & Gorbsky, G. J. The consequences of chromosome segregation errors in mitosis and meiosis. *Biology* **6**, E12 (2017).
2. Cleveland, D. W., Mao, Y. & Sullivan, K. F. Centromeres and kinetochores: from epigenetics to mitotic checkpoint signaling. *Cell* **112**, 407–421 (2003).
3. Shirayama, M., Toth, A., Galova, M. & Nasmyth, K. APC(Cdc20) promotes exit from mitosis by destroying the anaphase inhibitor Pds1 and cyclin Clb5. *Nature* **402**, 203–207 (1999).
4. Musacchio, A. & Salmon, E. D. The spindle-assembly checkpoint in space and time. *Nat. Rev. Mol. Cell Biol.* **8**, 379–393 (2007).
5. Khodjakov, A. & Pines, J. Centromere tension: a divisive issue. *Nat. Cell Biol.* **12**, 919–923 (2010).
6. Barr, F. A., Sillje, H. H. & Nigg, E. A. Polo-like kinases and the orchestration of cell division. *Nat. Rev. Mol. Cell Biol.* **5**, 429–440 (2004).
7. Llamazares, S. et al. polo encodes a protein kinase homolog required for mitosis in Drosophila. *Genes Dev.* **5**, 2153–2165 (1991).
8. Sunkel, C. E. & Glover, D. M. polo, a mitotic mutant of Drosophila displaying abnormal spindle poles. *J. Cell Sci.* **89**(Pt 1), 25–38 (1988).
9. Uhlmann, F., Lottspeich, F. & Nasmyth, K. Sister-chromatid separation at anaphase onset is promoted by cleavage of the cohesin subunit Scc1. *Nature* **400**, 37–42 (1999).
10. Baumann, C., Korner, R., Hofmann, K. & Nigg, E. A. PICH, a centromere-associated SNF2 family ATPase, is regulated by Plk1 and required for the spindle checkpoint. *Cell* **128**, 101–114 (2007).
11. Chan, K. L., North, P. S. & Hickson, I. D. BLM is required for faithful chromosome segregation and its localization defines a class of ultrafine anaphase bridges. *EMBO J.* **26**, 3397–3409 (2007).
12. Fernandez-Casanas, M. & Chan, K. L. The unresolved problem of DNA bridging. *Genes* **9**, E623 (2018).
13. Chan, K. L., Palmai-Pallag, T., Ying, S. & Hickson, I. D. Replication stress induces sister-chromatid bridging at fragile site loci in mitosis. *Nat. Cell Biol.* **11**, 753–760 (2009).
14. Naim, V. & Rosselli, F. The FANC pathway and BLM collaborate during mitosis to prevent micro-nucleation and chromosome abnormalities. *Nat. Cell Biol.* **11**, 761–768 (2009).
15. Chan, Y. W., Fugger, K. & West, S. C. Unresolved recombination intermediates lead to ultra-fine anaphase bridges, chromosome breaks and aberrations. *Nat. Cell Biol.* **20**, 92–103 (2018).
16. Tiwari, A., Addis Jones, O. & Chan, K. L. 53BP1 can limit sister-chromatid rupture and rearrangements driven by a distinct ultrafine DNA bridging-breakage process. *Nat. Commun.* **9**, 677 (2018).
17. Ke, Y. et al. PICH and BLM limit histone association with anaphase centromeric DNA threads and promote their resolution. *EMBO J.* **30**, 3309–3321 (2011).
18. Broderick, R., Nieminuszczy, J., Blackford, A. N., Winczura, A. & Niedzwiedz, W. TOPBP1 recruits TOP2A to ultra-fine anaphase bridges to aid in their resolution. *Nat. Commun.* **6**, 6572 (2015).
19. Nielsen, C. F. et al. PICH promotes sister chromatid disjunction and co-operates with topoisomerase II in mitosis. *Nat. Commun.* **6**, 8962 (2015).
20. Steegmaier, M. et al. BI 2536, a potent and selective inhibitor of polo-like kinase 1, inhibits tumor growth in vivo. *Curr. Biol.* **17**, 316–322 (2007).
21. Sumara, I. et al. Roles of polo-like kinase 1 in the assembly of functional mitotic spindles. *Curr. Biol.* **14**, 1712–1722 (2004).
22. Sarlos, K. et al. Reconstitution of anaphase DNA bridge recognition and disjunction. *Nat. Struct. Mol. Biol.* **25**, 868–876 (2018).
23. Marston, A. L., Tham, W. H., Shah, H. & Amon, A. A genome-wide screen identifies genes required for centromeric cohesion. *Science* **303**, 1367–1370 (2004).

24. McGuinness, B. E., Hirota, T., Kudo, N. R., Peters, J. M. & Nasmyth, K. Shugoshin prevents dissociation of cohesin from centromeres during mitosis in vertebrate cells. *PLoS Biol.* **3**, e86 (2005).
25. Sumara, I. et al. The dissociation of cohesin from chromosomes in prophase is regulated by Polo-like kinase. *Mol. Cell* **9**, 515–525 (2002).
26. Gimenez-Abian, J. F. et al. Regulation of sister chromatid cohesion between chromosome arms. *Curr. Biol.* **14**, 1187–1193 (2004).
27. Lenart, P. et al. The small-molecule inhibitor BI 2536 reveals novel insights into mitotic roles of polo-like kinase 1. *Curr. Biol.* **17**, 304–315 (2007).
28. Santamaria, A. et al. Use of the novel Plk1 inhibitor ZK-thiazolidinone to elucidate functions of Plk1 in early and late stages of mitosis. *Mol. Biol. Cell* **18**, 4024–4036 (2007).
29. Biebricher, A. et al. PICH: a DNA translocase specially adapted for processing anaphase bridge DNA. *Mol. Cell* **51**, 691–701 (2013).
30. Kapoor, T. M., Mayer, T. U., Coughlin, M. L. & Mitchison, T. J. Probing spindle assembly mechanisms with monastrol, a small molecule inhibitor of the mitotic kinesin, Eg5. *J. Cell Biol.* **150**, 975–988 (2000).
31. Burkard, M. E. et al. Chemical genetics reveals the requirement for Polo-like kinase 1 activity in positioning RhoA and triggering cytokinesis in human cells. *Proc. Natl Acad. Sci. USA* **104**, 4383–4388 (2007).
32. Chan, K. L. & Hickson, I. D. On the origins of ultra-fine anaphase bridges. *Cell Cycle* **8**, 3065–3066 (2009).
33. Kabeche, L., Nguyen, H. D., Buisson, R. & Zou, L. A mitosis-specific and R loop-driven ATR pathway promotes faithful chromosome segregation. *Science* **359**, 108–114 (2018).
34. Rouzeau, S. et al. Bloom's syndrome and PICH helicases cooperate with topoisomerase IIalpha in centromere disjunction before anaphase. *PLoS One* **7**, e33905 (2012).
35. Karow, J. K., Chakraverty, R. K. & Hickson, I. D. The Bloom's syndrome gene product is a 3'-5' DNA helicase. *J. Biol. Chem.* **272**, 30611–30614 (1997).
36. Maresca, T. J. & Salmon, E. D. Intrakinetochore stretch is associated with changes in kinetochore phosphorylation and spindle assembly checkpoint activity. *J. Cell Biol.* **184**, 373–381 (2009).
37. Uchida, K. S. et al. Kinetochore stretching inactivates the spindle assembly checkpoint. *J. Cell Biol.* **184**, 383–390 (2009).
38. Hengeveld, R. C. et al. Rif1 is required for resolution of ultrafine DNA bridges in anaphase to ensure genomic stability. *Dev. Cell* **34**, 466–474 (2015).
39. Leng, M. et al. MPS1-dependent mitotic BLM phosphorylation is important for chromosome stability. *Proc. Natl Acad. Sci. USA* **103**, 11485–11490 (2006).
40. Bayart, E. et al. The Bloom syndrome helicase is a substrate of the mitotic Cdc2 kinase. *Cell Cycle* **5**, 1681–1686 (2006).
41. Dutertre, S. et al. Cell cycle regulation of the endogenous wild type Bloom's syndrome DNA helicase. *Oncogene* **19**, 2731–2738 (2000).
42. Kaulich, M., Cubizolles, F. & Nigg, E. A. On the regulation, function, and localization of the DNA-dependent ATPase PICH. *Chromosoma* **121**, 395–408 (2012).
43. Dutertre, S. et al. Dephosphorylation and subcellular compartment change of the mitotic Bloom's syndrome DNA helicase in response to ionizing radiation. *J. Biol. Chem.* **277**, 6280–6286 (2002).
44. Gerlich, D., Hirota, T., Koch, B., Peters, J. M. & Ellenberg, J. Condensin I stabilizes chromosomes mechanically through a dynamic interaction in live cells. *Curr. Biol.* **16**, 333–344 (2006).
45. Ribeiro, S. A. et al. Condensin regulates the stiffness of vertebrate centromeres. *Mol. Biol. Cell* **20**, 2371–2380 (2009).
46. Janssen, A., van der Burg, M., Szuhai, K., Kops, G. J. & Medema, R. H. Chromosome segregation errors as a cause of DNA damage and structural chromosome aberrations. *Science* **333**, 1895–1898 (2011).
47. Ly, P. et al. Selective Y centromere inactivation triggers chromosome shattering in micronuclei and repair by non-homologous end joining. *Nat. Cell Biol.* **19**, 68–75 (2017).
48. Caspersson, T., Hulten, M., Lindsten, J., Therkelsen, A. J. & Zech, L. Identification of different Robertsonian translocations in man by quinacrine mustard fluorescence analysis. *Hereditas* **67**, 213–220 (1971).
49. Beroukhim, R. et al. The landscape of somatic copy-number alteration across human cancers. *Nature* **463**, 899–905 (2010).
50. Davoli, T. et al. Cumulative haploinsufficiency and triplosensitivity drive aneuploidy patterns and shape the cancer genome. *Cell* **155**, 948–962 (2013).
51. Barra, V. & Fachinetti, D. The dark side of centromeres: types, causes and consequences of structural abnormalities implicating centromeric DNA. *Nat. Commun.* **9**, 4340 (2018).

Acknowledgements

We would like to thank the people in the Genome Centre for their great support. We thank Robert Lera and Mark Burkard for providing the RPE1 derivative cells and the CENPB cDNA, Marcel van Vugt for HAP1 and HAP1 BLM-knockout cells, and Phillip North for GM08505 Bloom Syndrome fibroblasts. We thank Jessica Hudson for BLM siRNA oligos. We also thank Kim Nasmyth, Jon Baxter and Mark Burkard for helpful comments on the study. This work is supported by Sir Henry Dale Fellowship (Ref. 104178/Z/14/Z) from Wellcome Trust and the Royal Society, and by the Genome Damage and Stability Centre. K.L.C. is the recipient of Sir Henry Dale Fellowship. Funding for open access charge: Charity Open Access Fund (COAF).

Author contributions

O.A.J. and K.L.C designed and performed the experiments with help from A.T., T.O. and A.H. O.A.J, A.T., T.O. and K.L.C. analysed the data. K.L.C. wrote the paper with inputs from all authors.

Additional information

Supplementary Information accompanies this paper at https://doi.org/10.1038/s41467-019-10938-y.

Competing interests: The authors declare no competing interests.

Reprints and permission information is available online at http://npg.nature.com/reprintsandpermissions/

Peer review information: *Nature Communications* would like to thank anonymous reviewers for their contribution to the peer review of this work. Peer review reports are available.

Publisher's note: Springer Nature remains neutral with regard to jurisdictional claims in published maps and institutional affiliations.

nature COMMUNICATIONS

ARTICLE

DOI: 10.1038/s41467-018-03098-y OPEN

53BP1 can limit sister-chromatid rupture and rearrangements driven by a distinct ultrafine DNA bridging-breakage process

Ankana Tiwari[1], Owen Addis Jones[1] & Kok-Lung Chan[1]

Chromosome missegregation acts as one of the driving forces for chromosome instability and cancer development. Here, we find that in human cancer cells, HeLa and U2OS, depletion of 53BP1 (p53-binding protein 1) exacerbates chromosome non-disjunction resulting from a new type of sister-chromatid intertwinement, which is distinct from FANCD2-associated ultrafine DNA bridges (UFBs) induced by replication stress. Importantly, the sister DNA intertwinements trigger gross chromosomal rearrangements through a distinct process, named sister-chromatid rupture and bridging. In contrast to conventional anaphase bridge-breakage models, we demonstrate that chromatid axes of the intertwined sister-chromatids rupture prior to the breakage of the DNA bridges. Consequently, the ruptured sister arms remain tethered and cause signature chromosome rearrangements, including whole-arm (Robertsonian-like) translocation/deletion and isochromosome formation. Therefore, our study reveals a hitherto unreported chromatid damage phenomenon mediated by sister DNA intertwinements that may help to explain the development of complex karyotypes in tumour cells.

[1] Chromosome Dynamics and Stability Group, Genome Damage and Stability Centre, University of Sussex, Brighton BN1 9RQ, UK. Correspondence and requests for materials should be addressed to K.-L.C. (email: koklung.chan@sussex.ac.uk)

Gross chromosome rearrangements, as a result of chromosomal instability (CIN) is a hallmark of most, if not all, tumour cells; however, the underlying mechanism is not fully understood. It is generally accepted that CIN contributes to the initiation of tumorigenesis, metastasis progression and multidrug resistance[1,2]. One of the major causes of CIN can be attributed to defects in mitosis such as chromosome misalignments and chromatid non-disjunction, which manifest in the form of lagging chromosomes and anaphase bridges. Generally, lagging chromosomes are generated because of kinetochore-microtubule attachment errors, which not only leads to imbalanced chromosome transmission[3], but also to structural chromosome rearrangements in both a cytokinesis-dependent and cytokinesis-independent manner[4,5]. Additionally, anaphase bridges are generated by abnormal configurations of chromosomes, such as fusions of chromosomes/sister-chromatid arms, or via dysfunctional telomeres[6]. It has been proposed by McClintock that anaphase bridges drive chromosomal rearrangements through a so-called breakage-fusion-bridge (BFB) cycle, where multiple rounds of the joined chromatid bridges break apart during telophase (or cytokinesis) and re-fusing occurs[7,8]. Recently, an elegant study has shown that the breakage of chromatin bridges can be triggered by a cytoplasmic nuclease, TREX1, at telophase-G1 transition and leads to chromothripsis[9].

Previously, we and others have shown that replication of stress-induced DNA entanglements, which are associated with the FANCD2/I dimer, can be carried into mitosis, manifesting as so-called ultrafine DNA bridges (UFBs) in human anaphase cells[10–15]. The resolution of which also leads to DNA damage in the daughter offspring cells[16–18]. It is speculated that this is a result of the separation of DNA intertwining structures at under-replicated regions between sister chromatids[19]. Therefore, the accumulation of DNA entanglements arising during DNA replication and/or homologous recombination (HR) should be limited; otherwise, this could pose substantial threats to chromosome segregation and genome integrity. It is conceivable that this could be more problematic to cancerous cells that bear high intrinsic DNA replication/recombination activities. In fact, a recent study has shown the association of replication stress and CIN[20]. Nevertheless, it remains enigmatic how ultrafine DNA bridging structures may affect faithful chromosome segregation and genome stability.

Here, we have determined that human cancer cells (HeLa and U2OS) rely heavily on a non-homologous end-joining (NHEJ) factor 53BP1[21,22], for chromosome segregation, by limiting the formation of a new type of sister DNA intertwining structure that is not associated with FANCD2, but is dependent of RAD51. Intriguingly, we demonstrate that these sister DNA entanglements drive a novel chromatid damage phenomenon, which induces a rupture of the sister-chromatid axes prior to the breakage of the intertwining DNA bridges. As a result, the ruptured sister chromatids remain tethered by the ultrafine DNA molecules and failed to fully disjoin. Depending on the rupture-bridging positions, this process drives typical and signature chromosome rearrangements, including whole-arm (Robertsonian-like) translocations and isochromosome formation, which are commonly observed in tumour cells. The chromatid rupture-bridging phenomenon is also observed in several unmodified cancer cell lines, suggesting that this alternative mitotic damage action may contribute to the evolution of their karyotypes. In this study, we reveal a new ultrafine DNA bridge-breakage process that drives gross chromosomal rearrangements in cultured human cancer cells, which is regulated by 53BP1.

Results

53BP1 co-localises adjacently to FANCD2 in normal S phase. The Fanconi anaemia (FA) pathway is activated during S-phase progression[23]. Previously, we showed that, under replication stress, foci of the FANCD2/I heterodimer persist into mitosis, and subsequently associates with a subclass of UFBs in anaphase cells[10]. Furthermore, the defects in the FA pathway increase chromosome missegregation[11], implying their roles in the formation of DNA intertwining structures. Unresolved DNA entanglements can interfere with faithful chromosome segregation and genome stability. Therefore, to gain insight into how cells prevent DNA entanglements arising during replication, we searched for proteins that co-localise with FANCD2 during unperturbed S phase. We found that 53BP1 forms spontaneous nuclear foci during DNA replication in both normal diploid and cancer cells (Supplementary Fig. 1a, b), where more than half of them surround the FANCD2 foci (Supplementary Fig. 1c, d). This observation suggests that 53BP1 may also participate in the process of DNA replication and/or HR.

Generation of 53BP1Δ and 53BP1^{hypo} cancer and normal cells. To explore the role of 53BP1, we generated 53BP1 knockouts in HeLa cervical carcinoma cells, U2OS osteosarcoma cells and hTERT-immortalised RPE1 diploid cells by CRISPR-cas9 genome editing technology. Two guide-RNAs targeting exon 2 and exon 14 of 53BP1 were used. Targeting exon 2 failed to eliminate 53BP1 expression completely in HeLa and RPE1 cells, where residual full-length like protein, and/or small 53BP1 foci were still detectable (Supplementary Fig. 2a–d). However, exon 2 targeting successfully eliminated 53BP1 in U2OS cells (Supplementary Fig. 2e, f). In contrast, targeting exon 14 efficiently eliminated 53BP1 expression in the above three cell lines (Supplementary Fig. 2c, e–h). DNA sequence analysis on the 53BP1 hypomorphic (53BP1^{hypo}) HeLa cells detected no wild-type exon 2 sequence, but three new mutations; all leading to premature translation termination (Supplementary Fig. 3a–c). We thus speculated that the 53BP1 hypomorphic expression in HeLa and RPE1 cells might be due to a leaky expression through a downstream alternative translation site (Supplementary Fig. 3d). Collectively, the 53BP1Δ and 53BP1^{hypo} in both cancer and normal cell lines provide us with useful tools to dissect the functions of 53BP1 during DNA replication.

53BP1 depletion in HeLa and U2OS cells compromises chromosome segregation and cell growth. In the absence of any exogenous DNA assaults, we found that knocking out 53BP1 (53BP1Δ) caused pronounced chromosome missegregation phenotypes, including anaphase bridge and lagging chromatin formation in both U2OS and HeLa cancer cells (Fig. 1a, b). These mitotic defects were also observed in the HeLa cells expressing hypomorphic 53BP1 protein (Fig. 1b). In addition, all 53BP1-depleted U2OS and HeLa cancer cells, including the 53BP1^{hypo} cells, displayed apparent proliferation retardation (Supplementary Fig. 4a, b). Notably, 53BP1^{hypo} HeLa cells grew slightly better than the complete 53BP1Δ cells (Supplementary Fig. 4c), suggesting that a residual activity of 53BP1^{hypo} protein may remain. The mitotic and growth defect phenotypes, however, were either not or only moderately detected in 53BP1^{hypo} and 53BP1Δ RPE1 cells (Fig. 1c & Supplementary Fig. 4d), indicating that HeLa and U2OS cells exhibit a higher reliance on 53BP1 for optimal cell division. Stable overexpression of an EGFP-tagged 53BP1 in 53BP1^{hypo} HeLa cells largely rescued the phenotypes of slow growth and anaphase bridges, but unexpectedly, not lagging chromatin formation (Supplementary Fig. 5 & see explanation in Fig. 5f–h below).

53BP1 has been shown to facilitate DNA double-stranded break (DSB) repair mediated by the NHEJ pathway. We, therefore, investigated whether the missegregation phenotypes

observed might relate to the incompetency of NHEJ. In agreement to other reports[22], we found that 53BP1Δ HeLa (D4 & D10) and U2OS (B4, B18, D29 and D30) displayed increased sensitivities to ionisation radiation (IR) treatments (Supplementary Fig. 6a, b). Similarly, moderately increased IR sensitivities were also detected in RPE1 53BP1Δ cells (D6 and D24) (Supplementary Fig. 6c), although they did not show severe mitotic and growth defects. Intriguingly, we found that HeLa 53BP1^{hypo} cells, which exhibited elevated chromosome missegregation, were not sensitive to IR treatments (Fig. 1d). As predicted, we observed colocalisation of γH2AX and hypomorphic 53BP1 protein at damage foci, but of a much smaller size (Fig. 1e). In addition, the recruitment of 53BP1 to its binding partner, hRIF1[24–26], was still evident in these cells

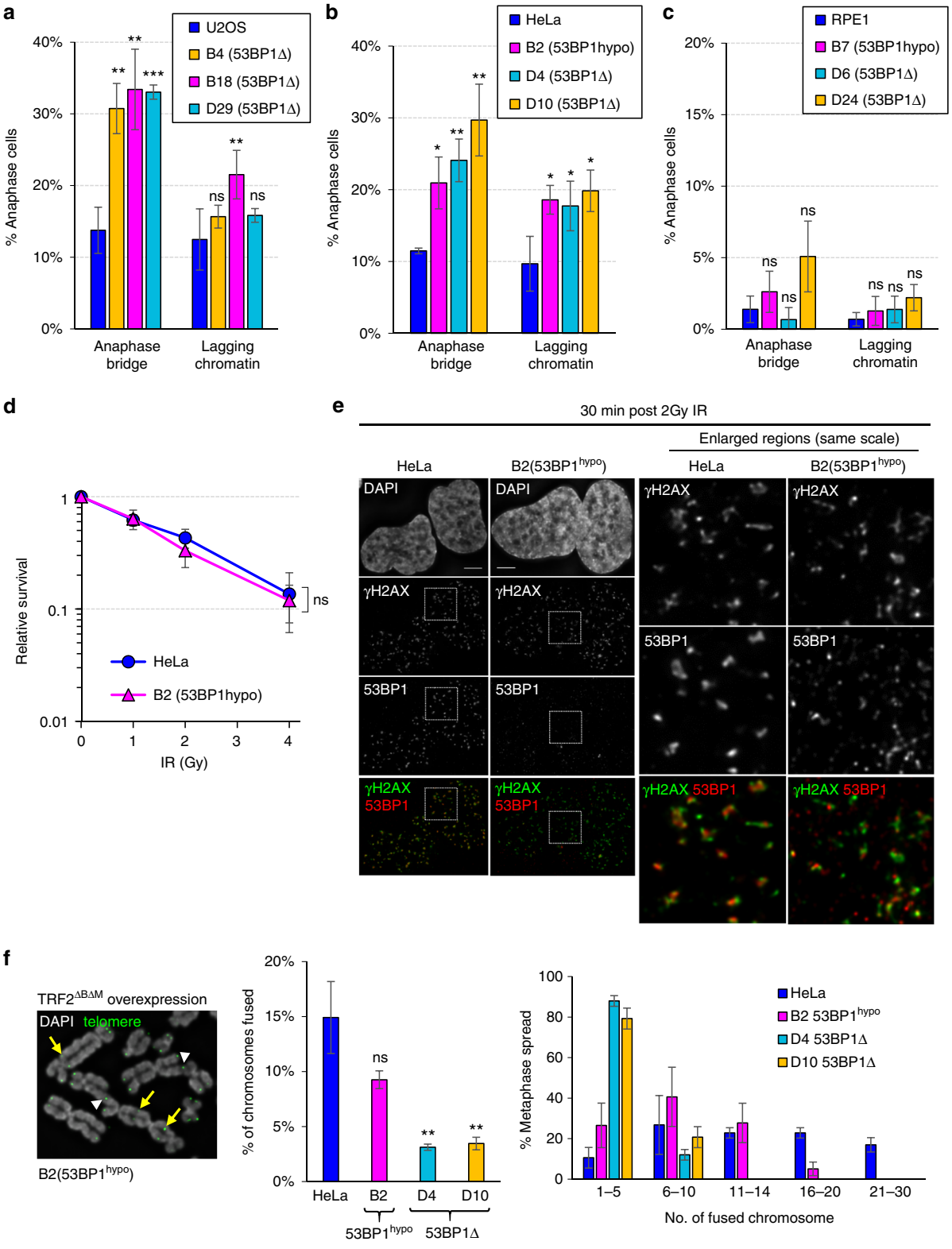

(Supplementary Fig. 6d). Consistently, RPE1 53BP1^{hypo} cells also maintained IR resistance despite having very-low 53BP1 expression (Supplementary Fig. 6e). Telomere-end fusion assays revealed that HeLa 53BP1^{hypo} cells still exhibited a higher activity of end-joining compared with 53BP1Δ cells, but slightly lower than the parental HeLa cells (Fig. 1f).[27,28]. These results indicate that the hypomorphic 53BP1 protein remains competent, at least partially, in NHEJ repair of exogenously induced DSBs. Therefore, we conclude that the increased susceptibilities to the mitotic defects in HeLa and U2OS cancer cells after 53BP1 depletion cannot be merely attributed to NHEJ incompetency. The high reliance of 53BP1 activities in these cancer cell lines, is likely not only because of its necessity for NHEJ repair, but also for a function in facilitating chromosome segregation under physiological growth conditions.

53BP1 suppresses sister DNA intertwining in cultured cancer cells. We noticed that there were distinct chromatid non-disjunction features in 53BP1-depleted cancer cells, namely a delay of chromosome separation, manifesting as bridge-like structures (Fig. 2a; arrows) and the formation of multiple lagging chromatin, notably existing as a symmetric pair (Fig. 2a, b; arrowheads). These non-disjunction patterns indicated that they might be caused by ultrafine DNA intertwinements that we and the others previously identified[12,13]. Immunofluorescence staining of UFB-binding proteins, such as PICH and hRIF1[12,29], revealed that the characteristic anaphase bridge(-like) structures and lagging chromatin pairs were indeed tethered by UFBs (Fig. 2c, d). As predicted, the frequency and number of UFBs were significantly increased in both 53BP1Δ and 53BP1^{hypo} cancer cells (Fig. 2e, f), suggesting that 53BP1 is required for the suppression of UFB formation.

Chromatin bridges in anaphase can be caused by inter-chromosomal linkage formed in dicentric or radial chromosomes, or via sister-chromatid intertwining. To distinguish these, we developed a protocol using EdU to differentially label one of the two sister chromatids in mitotic cells (Fig. 3a, b). To avoid complications arising from NHEJ malfunction, we performed most of our investigation using HeLa 53BP1^{hypo} cells, which, as demonstrated above, largely maintain the NHEJ pathway. Remarkably, almost all anaphase bridges (98%) in the HeLa 53BP1^{hypo} cells displayed a symmetric (but opposite) staining pattern (Fig. 3c), showing either EdU labelling on one-half of the DNA bridge (Fig. 3d), or resembling sister-chromatid exchange (SCE) patterns (Fig. 3e). Similarly, the lagging chromatin pairs also displayed the symmetric labelling patterns (Fig. 3f), highly suggesting that the non-disjoined chromatin structures are composed of sister chromatids. Therefore, we conclude that 53BP1 acts to suppress DNA intertwinements, arising mainly between sister chromatids. In agreement with this conclusion, dicentric or radial chromosomes were rarely observed in metaphase spreads of both 53BP1^{hypo} and 53BP1Δ HeLa cells (Fig. 3g). We henceforth name this phenomenon as "sister-chromatid bridging" to distinguish it from the general terminology of anaphase bridges.

The FANCD2 non-associated sister UFB is RAD51-dependent. DNA catenation, (sister-)telomere fusion or replication stress can lead to UFB formation[19,30–32]. The fact that 53BP1 accumulates adjacently to FANCD2 foci during S phase led us to speculate that its deficiency might exacerbate replication stress particularly in these cancer cells, mimicking the effect of DNA polymerase inhibition induced by aphidicolin treatments, which causes the accumulation of late replication intermediates (LRIs) and the formation of UFBs positive for FANCD2 foci[10,11] (Supplementary Fig. 7a). Contrary to our hypothesis, we found that 53BP1 depletion in HeLa and U2OS cells significantly increased anaphase populations having FANCD2-negative UFBs (Fig. 4a). In contrast to aphidicolin-induced replication stress, it mainly increased anaphase cells with FANCD2-positive, but not the FANCD2-negative UFBs (Supplementary Fig. 7a). Consistently, most of the UFBs (56–86%) detected in the 53BP1-depleted cells are FANCD2 negative, except when the 53BP1^{hypo} cells were pre-treated with aphidicolin, which increased the proportion of UFBs positive for FANCD2 foci from 14 to 55% (Fig. 4b & Supplementary Fig. 7b). These results suggest that a new subclass of sister DNA bridge arises in these cancer cells when 53BP1 activities become limiting. Moreover, this also indicates that the FA pathway is not compromised in 53BP1^{hypo} cells, which is further supported by the fact that, like the parental HeLa, aphidicolin treatment readily elevated mitotic FANCD2 foci in the 53BP1^{hypo} cells (Supplementary Fig. 7c, d). The lack of increased replication stress phenotypes, including spontaneously elevated FANCD2 mitotic foci, abnormal S phase accumulation and increased common fragile site (CFS) expression (Supplementary Fig. 7c–f), highly suggests that the induction of FANCD2-negative UFB formation in the 53BP1-depleted cells is unlikely caused by the same mechanism of replication stress, induced by DNA polymerase inhibition.

A very characteristic feature of the anaphase bridge observed in the 53BP1^{hypo} cells is that the sister-chromatid arms are tethered by UFBs. We found that nearly 75% of the associated chromosomes were positive for γH2AX signal (Fig. 4d, e), implicating a DNA damage response acting in this phenomenon. The fact that most of the UFB-tethered chromatin bridges arise originally from sister chromatids and negative of FANCD2 binding infers that their formation may associate with HR activity. To test this, we knocked down RAD51, a key initiation factor of HR[33] in HeLa 53BP1^{hypo} cells (Fig. 4f). As shown previously, RAD51 depletion led to increased replication stress[10], and hence elevated the anaphase population having FANCD2-postive UFBs (Fig. 4g, h). Crucially, the RAD51 knockdown

Fig. 1 53BP1 depletion leads to increased chromosome non-disjunction in human cancer cells. Quantitation of anaphase bridge and lagging chromatin in 53BP1Δ and 53BP1^{hypo} cells **a** U2OS, **b** HeLa and **c** RPE1. Numbers of cell counted: U2OS = 529, B4 = 327, B18 = 344, D29 = 372; HeLa = 540, B2 = 351, D4 = 426, D10 = 317; RPE1 = 435, B7 = 449, D6 = 382, D24 = 458 from 3–4 separate preparations. **d** IR sensitivity assay on HeLa and B2 (53BP1^{hypo}) cells (*N* = three independent experiments). Statistical significance was determined by two-way ANOVA. **e** The formation of IR-induced DNA damage foci in HeLa and B2 (53BP1^{hypo}) cells. Thirty minutes post 2 Gy IR, the cells were immunostained with anti-53BP1 and anti-γH2AX antibodies. Enlarged regions demonstrating the recruitment of 53BP1 (red) at the IR-induced DNA breaks, marked by γH2AX (green). **f** Representative image of telomere fusions on metaphase chromosomes of B2 (53BP1^{hypo}) cells overexpressing TRF2^{ΔBΔM}. An example of fusions on single (arrowheads) and both (arrows) sister telomeres indicated (left). Middle: percentage of chromosome fusion events in HeLa, B2 (53BP1^{hypo}), D4 and D10 (53BP1Δ) cells, >75 metaphases of each cell line were analysed from three independent experiments. Right: histogram showing telomere fusion events in HeLa, B2 (53BP1^{hypo}), D4 and D10 (53BP1Δ). Total number of chromosomes analysed in HeLa = 3890, B2 = 3792, D4 = 4720 and D10 = 4790 from >60 metaphase spreads. Statistical significance was determined by *T*-test (* $p < 0.0$, ** $p < 0.01$, *** $p < 0.001$, ns nonsignificant). Error bars represent s.d. of three independent experiments. Scale bars, 5 μm

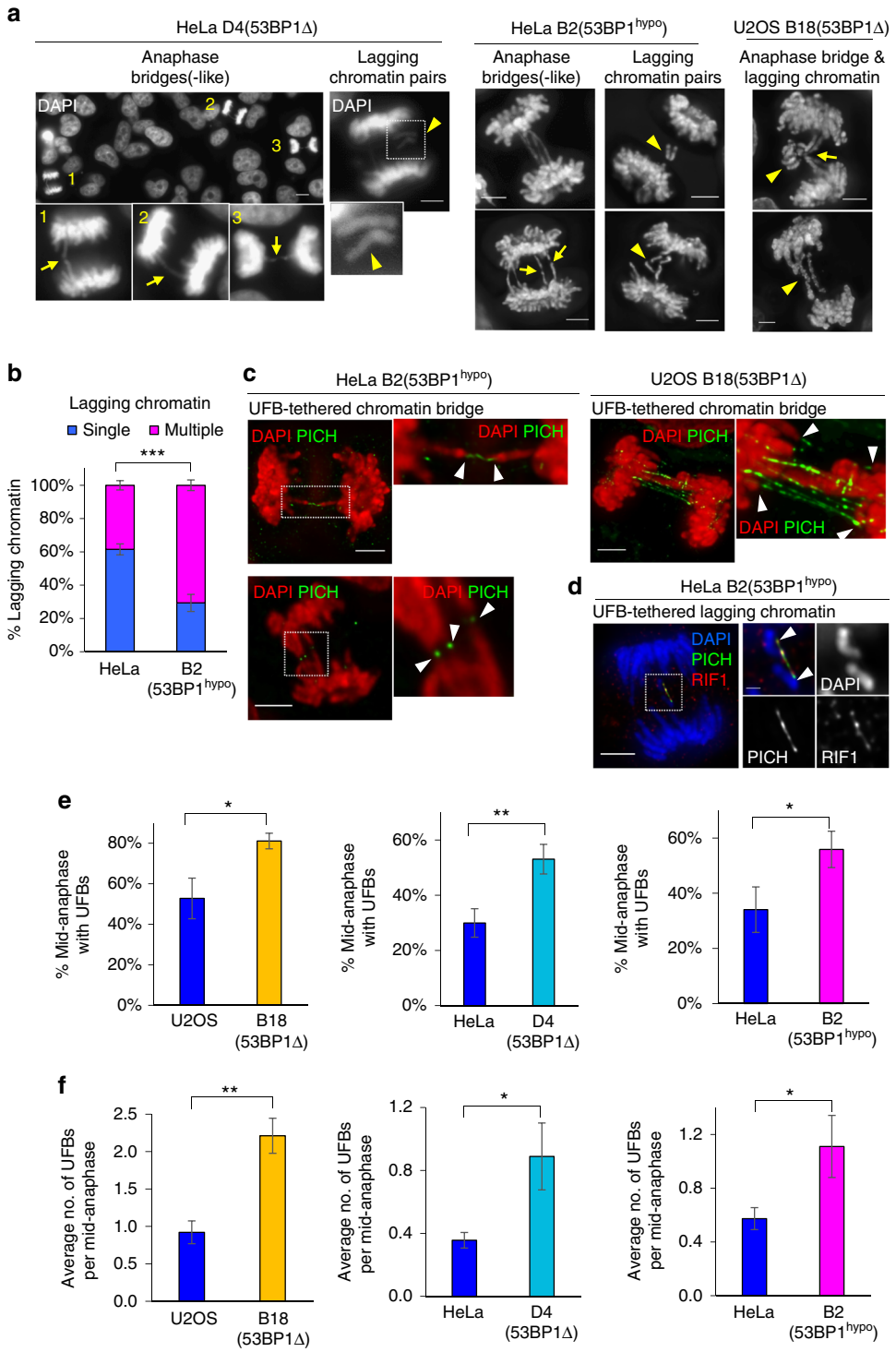

Fig. 2 Chromosome non-disjunction in 53BP1-depleted cancer cells is mediated by ultrafine DNA bridges. **a** Representative images of DAPI-stained HeLa D4 (53BP1Δ), HeLa B2 (53BP1^{hypo}) and U2OS B18 (53BP1Δ) cells showing anaphase bridges, bridge-like structures and lagging chromatin pairs (arrowheads). Insets show enlarged view of the numbered cells exhibiting bridge-like (arrows; 1 & 3), bridge structures (arrow; 2). **b** Increased formation of multi-lagging chromosomes in HeLa B2 (53BP1^{hypo}) cells as compared to HeLa. Quantification of single or multiple lagging chromatin in HeLa and B2 (53BP1^{hypo}) cells. more than 100 cells with lagging chromatin were counted from three separate preparations. **c** Deconvolved high-resolution images showing the two separating chromatin arms (red) connected by PICH-UFBs (green) in HeLa B2 (53BP1^{hypo}, Left) and in U2OS B18 (53BP1Δ, Right). Insets shows enlarged views of the selected region. **d** Deconvolved image showing hRIF1 (red) localises at a PICH-coated UFB (green), intertwining a pair of lagging chromatin in HeLa B2 (53BP1^{hypo}). Inset shows enlarged view of selected region. **e** Percentage of mid-anaphase cells with PICH-UFBs in U2OS B18 (53BP1Δ), HeLa D4 (53BP1Δ) and HeLa B2 (53BP1^{hypo}). Numbers of anaphase counted: U2OS = 91, B18 = 90; HeLa = 123, D4 = 105; HeLa = 138, B2 = 139 from three separate preparations. **f** Average number of PICH-UFB per mid-anaphase cell in U2OS B18 (53BP1Δ), HeLa D4 (53BP1Δ) and HeLa B2 (53BP1^{hypo}). Error bars represent s.d. of three independent experiments. Statistical significance was determined by *T*-test (* $p < 0.05$, ** $p < 0.01$, *** $p < 0.001$). Scale bars, 5 μm

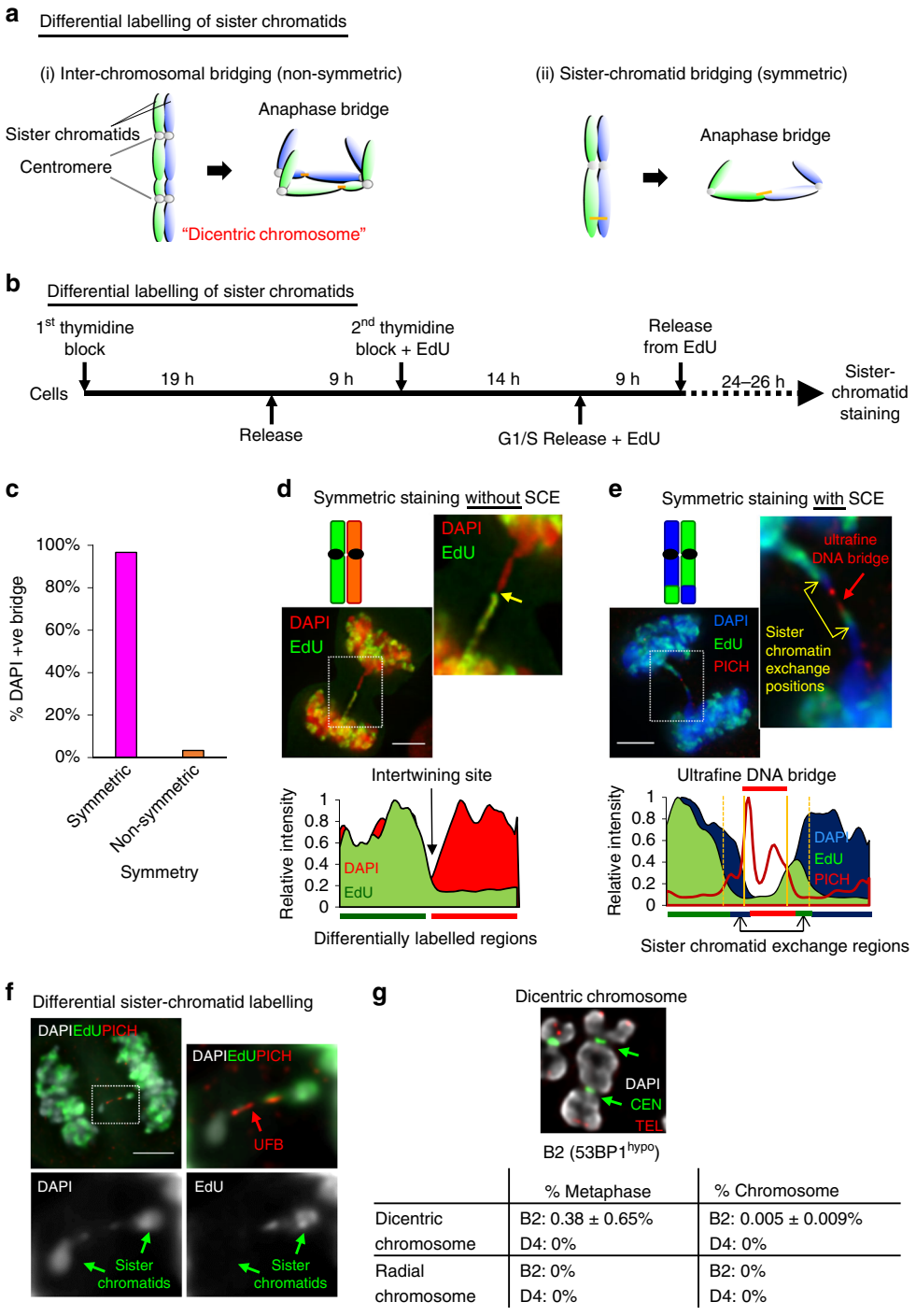

	% Metaphase	% Chromosome
Dicentric chromosome	B2: 0.38 ± 0.65% D4: 0%	B2: 0.005 ± 0.009% D4: 0%
Radial chromosome	B2: 0% D4: 0%	B2: 0% D4: 0%

Fig. 3 DNA entanglements between sister chromatids are the major cause of chromosome non-disjunction in 53BP1^{hypo} cells. **a** Diagram depicts differential sister-chromatid labelling (green; EdU) to distinguish between anaphase bridges caused by (i) inter-chromosomal fusion, shown as non-symmetric or by (ii) DNA intertwining between sister chromatids, shown as symmetric. **b** Experimental setup of differentially labelling sister chromatids. **c** Quantitation of anaphase DAPI bridges with symmetrical and non-symmetrical staining patterns in HeLa B2 (53BP1^{hypo}) cells. Over 65 anaphase cells with chromatin bridges were counted from two independent experiments. Total numbers of DNA bridge ($n = 74$) were counted. **d** Representative image of a HeLa B2 (53BP1^{hypo}) cell showing a symmetrical (but opposite) staining pattern along a DAPI anaphase bridge (Top). Yellow arrow in the inset shows EdU (green) staining was present on only one-half of the bridge. Area chart displaying the relative intensity along the differentially labelled sister chromatids (Bottom). **e** Representative example of a chromatin bridge, linked by a PICH-UFB (red), displaying a staining pattern resembling sister-chromatid exchange (SCE) (Top). Yellow arrows in the inset indicates the sister-chromatid exchange positions. Area chart displaying the relative intensity of differentially labelled sister chromatids with sister-chromatid exchange regions (Bottom). **f** A pair of lagging chromosomes showing differential staining (green arrow) were inter-linked by a PICH-UFB (red arrow) in HeLa B2 (53BP1^{hypo}) cells. **g** Quantitation of dicentric and radial chromosomes in HeLa B2 (53BP1^{hypo}) and HeLa D4 (53BP1Δ) metaphase cells. Top: an example of a dicentric chromosome in B2 (53BP1^{hypo}) cells (arrows indicate centromeres). Over 6000 chromosomes in 88 metaphase spreads from three independent experiments were examined. Chromosomes were hybridised with telomere and centromere PNA FISH probes. DNA was stained with DAPI. Scale bars, 5 μm

significantly diminished the percentage of the 53BP1^{hypo} anaphase cells having the FANCD2-negative UFBs (Fig. 4i). These results indicate that the increased formation of FANCD2-negative sister DNA bridges in 53BP1^{hypo} cells is dependent on the HR activity. It is plausible that (partial) loss of 53BP1 function may increase a distinct type of replication difficulty, which is converted into the sister DNA intertwinements by HR reaction. Alternatively, 53BP1 may prevent the formation of, or facilitate resolution of, HR intermediates (Fig. 4j). In fact, we detected increases in SCEs in the 53BP1^{hypo} HeLa cells (Supplementary

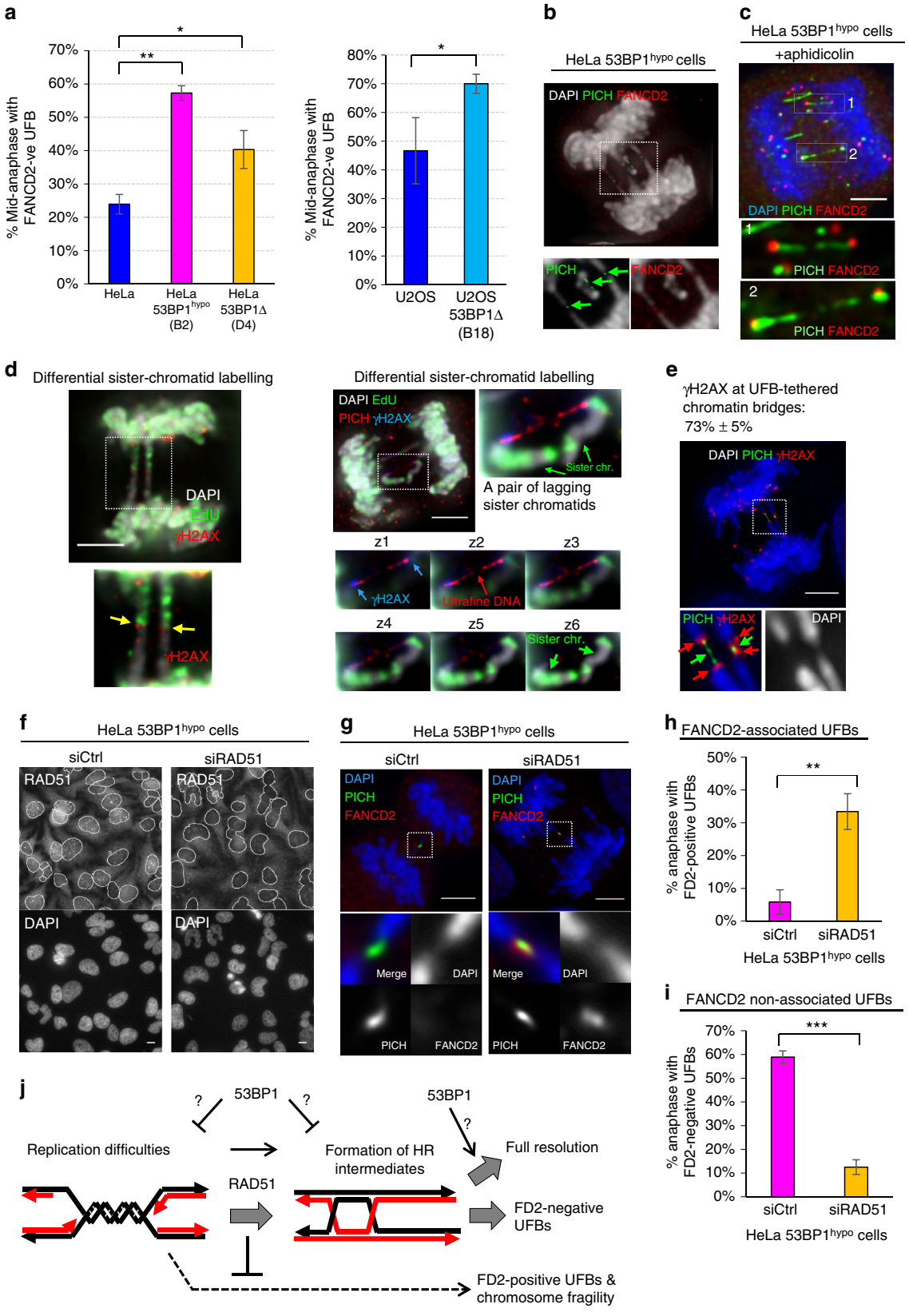

Fig. 8a). However, we cannot rule out that this may be also be due to impairments of non-crossing over resolution activity.

Contrary to our speculation, a recent report suggested that 53BP1 is required for high fidelity of HR repair on double-ended DSBs, probably through the prevention of exacerbated DNA end resection that channels excessive single-stranded annealing (SSA) reaction[34]. However, we did not detect significant changes in the ssDNA formation (as measured by chromatin-bound RPA) in unperturbed 53BP1^{hypo} S-phase cells (Supplementary Fig. 8b). It is possible that 53BP1 may influence HR fidelity differently on double-ended and single-ended DSBs, where the latter (associated with replication forks) is not an ideal substrate for SSA even if excessive DNA end resection occurs. On the other hand, loss of 53BP1, as shown previously to rescue HR in *brca1−/−* cells[35], may further relieve the constraints of HR at damaged forks. Nevertheless, our data demonstrate that the HR pathway participates to a certain extent on the formation/accumulation of the FANCD2-negative sister-chromatid bridges in the 53BP1^{hypo} cells.

DNA intertwinements lead to sister-chromatid rupture. We next characterised this subclass of sister-chromatid bridges and their effects on chromosome integrity. A very striking feature of the FANCD2-negative UFBs is that they were frequently found to emerge at the terminal regions of the separating or lagging sister chromatids, which could represent telomeres[32]. Alternatively, this may be explained as a result of two sister arms being tethered by UFBs, leading to their termini pointing towards each other during segregation (Fig. 5a). According to these hypotheses, telomeres are expected to be always present on anaphase/DNA bridges as shown as an example in Fig. 5b. Surprisingly, telomeres were rarely found on the DNA bridges and, indeed, they were missing at the UFB-tethered sister chromatids (Fig. 5c, d). In contrast, inter-chromosomal fusion generated by overexpression of TRF2$^{\Delta B \Delta M}$, as expected, led to the majority of anaphase bridges linking via their telomeres (Fig. 5d, e; arrows), validating our ability to detect such events when they arise. In parallel, we observed the loss of telomeric regions on the lagging chromatid pairs, specifically at the chromosomal termini where the UFBs emerged (Fig. 5f; asterisks). A simple interpretation of these results is that the UFB-tethered sister chromatids (whether they exist as anaphase bridges or lagging chromatin) are broken chromosomes. Most notably, the breakage of the sister-chromatid axes occurred at the sites where the ultrafine DNA linkage emerged and persisted.

53BP1 localises to kinetochores in early mitosis[36]. A previous study has reported that 53BP1 knockdown can cause kinetochore-microtubule attachment errors and the subsequent formation of lagging chromosomes[37]. However, our extensive chromosome analyses in anaphase cells have led us to reveal an alternative explanation for the missegregation phenotype. The facts that genuine intact lagging chromosomes were not detected and the presence of UFB stretching between the lagging chromatin pairs highly indicate that the missegregation is caused by persistent DNA intertwinements rather than kinetochore-microtubule mis-attachment[38]. Because of the unexpected finding of chromatid breakage, we re-examined the failure of an EGFP-53BP1 wild-type protein to suppress lagging chromatin in HeLa 53BP1^{hypo} cells (as shown in Supplementary Fig. 5d). We found that the ectopic overexpression of 53BP1 successfully reduced the formation of the broken lagging chromatin pairs (Fig. 5g; single telomere end). However, it also generated extra intact lagging chromosomes (Fig. 5g, h). Thus, the overall anaphase population with lagging chromatin remained unchanged. These data indicate that overexpression, but not depletion, of 53BP1 probably interferes with proper kinetochore-microtubule attachment.

More importantly, we found that the sister DNA bridges not only caused distinct chromatid non-disjunction, but also led to the identification of a new mitotic damage phenomenon, we termed sister-chromatid rupture and bridging. Contrary to conventional anaphase bridge-breakage models, our data clearly show that the occurrence of DNA damage on the intertwined sister chromatids is not coupled to the breakage of the DNA bridges and is independent of cytokinesis.

Sister-chromatid rupture occurs strictly upon anaphase onset. One plausible explanation for the appearance of the ruptured (but remaining intertwined) sister chromatids during anaphase is that they have already broken during DNA replication. If this is correct, we should expect to see chromosomes with broken arms or sister-chromatid arm fusion[7] in (pro)metaphase cells (Supplementary Fig. 9a). Of the thousands of metaphase chromosomes analysed on both 53BP1Δ and 53BP1^{hypo} HeLa cells, we found that almost all (>99.9%) were in a normal intact configuration (both termini were present). Only <3% of metaphases showed evidence of a chromosome with a sister-arm fusion (Supplementary Fig. 9b), which cannot explain the high fraction (>30%) of anaphase cells harbouring ruptured sister-chromatid bridges or lagging chromatin. Thus, the chromatid breakage is inferred to occur after anaphase onset. Next, we tested if the microtubule pulling on the intertwined chromatids causes the rupture. We triggered premature sister-chromatid separation by knocking down Sgo1 in 53BP1^{hypo} (pro)metaphase cells.

Fig. 4 The formation of sister DNA entanglements in 53BP1-depleted HeLa cells is dependent on RAD51. **a** Quantitation of 53BP1-depleted HeLa (left) and U2OS (right) anaphase cells forming FANCD2-negative UFBs. Numbers of anaphase counted: HeLa = 135, B2 = 112, D4 = 105; U2OS = 91, B18 = 90 from three independent experiments. **b** Maximum z-projection high-resolution image showing multiple short FANCD2-negative PICH-coated UFBs (arrows), linking the separating chromatin and lagging chromosomes in B2 (53BP1^{hypo}) cells. Inset shows that PICH stained UFBs (green) are not associated with FANCD2 foci (red). **c** Maximum z-projection high-resolution image showing the association of FANCD2 foci (red) on PICH-UFBs (green) in aphidicolin-treated HeLa B2 (53BP1^{hypo}) cells. Inset shows enlarged view of PICH-coated UFBs are positive of FANCD2 foci at their termini. **d** Representative images showing γH2AX present on chromatin bridges and lagging chromatin pairs in HeLa 53BP1^{hypo} cells. Left: maximum z-projection image showing γH2AX (red) at the junction (arrows) of the differentially labelled sister-chromatid bridges (EdU; green). Right: a pair of lagging sister chromatin intertwined by a PICH-UFB (red) and positive of γH2AX (blue) at their termini. Bottom Right: panels showing single-plane images of the intertwining lagging sister chromatin. Blue arrows indicate γH2AX present at the tips of the chromatin. **e** HeLa B2 (53BP1^{hypo}) cell showing the presence of γH2AX signals (red) at the termini of chromatin that were tethered by PICH-coated UFBs (green). **f** HeLa B2 (53BP1^{hypo}) cells were transfected with control or Rad51 siRNA oligos, followed by IF analysis using anti-Rad51. Nuclei are outlined (grey). **g** RAD51 knockdown caused the formation of FANCD2-assoicated (red) PICH-UFBs (green) in HeLa B2 (53BP1^{hypo}) cells. **h** Quantitation of HeLa B2 (53BP1^{hypo}) anaphase cells with FANCD2-positive UFBs following RAD51 knockdown. **i** Quantitation of HeLa B2 (53BP1^{hypo}) anaphase cells with FANCD2-negative UFBs following RAD51 knockdown. Numbers of anaphase cells scored: B2 + control siRNA = 350, B2 + RAD51 siRNA = 220 from three independent experiments. **j** A model showing the potential roles of 53BP1 and RAD51 in the formation of FANCD2-negative sister DNA bridges in the 53BP1-depleted cells. Error bars represent s.d of three independent experiments. Statistical significance was determined by *T*-test (* $p < 0.05$, ** $p < 0.01$, *** $p < 0.001$). Scale bars, 5 μm

Although we detected increase in chromatin breakage on single chromatids (Supplementary Fig. 9c; 10% in HeLa and 15% in B2 53BP1^{hypo} cells), the frequency was still lower than the observed one in anaphase (>30%). Collectively, these data strongly indicate that the rupture of the sister-chromatid axes occurs strictly after anaphase onset, which may infer their damage is mediated by factors requiring APC/C activation rather than merely spindle pulling.

Sister-chromatid rupture exacerbates chromosomal rearrangements. A prediction arising from the above findings is that it will lead to chromosomal damage and CIN in the offspring cells. In agreement with this, we observed increased numbers of G1 53BP1 nuclear bodies in HeLa 53BP1^{hypo} daughter cells (Supplementary Fig. 9d). Additionally, we observed an increase in numerical chromosome alterations. Interestingly, chromosome loss, over gain, seemed to be dominant in all 53BP1^{hypo} clones (Supplementary Fig. 10a). Next, we examined the structural chromosome alterations. Although, the HeLa cancer genome is considered unstable, we found that their karyotypes are relatively stable, as reported previously[39]. Whole chromosome painting and fluorescence in situ hybridisation (FISH) analyses revealed that all HeLa cells maintained four copies of chromosome7 plus one derivative, whereas the majority of them (94%) maintaining three

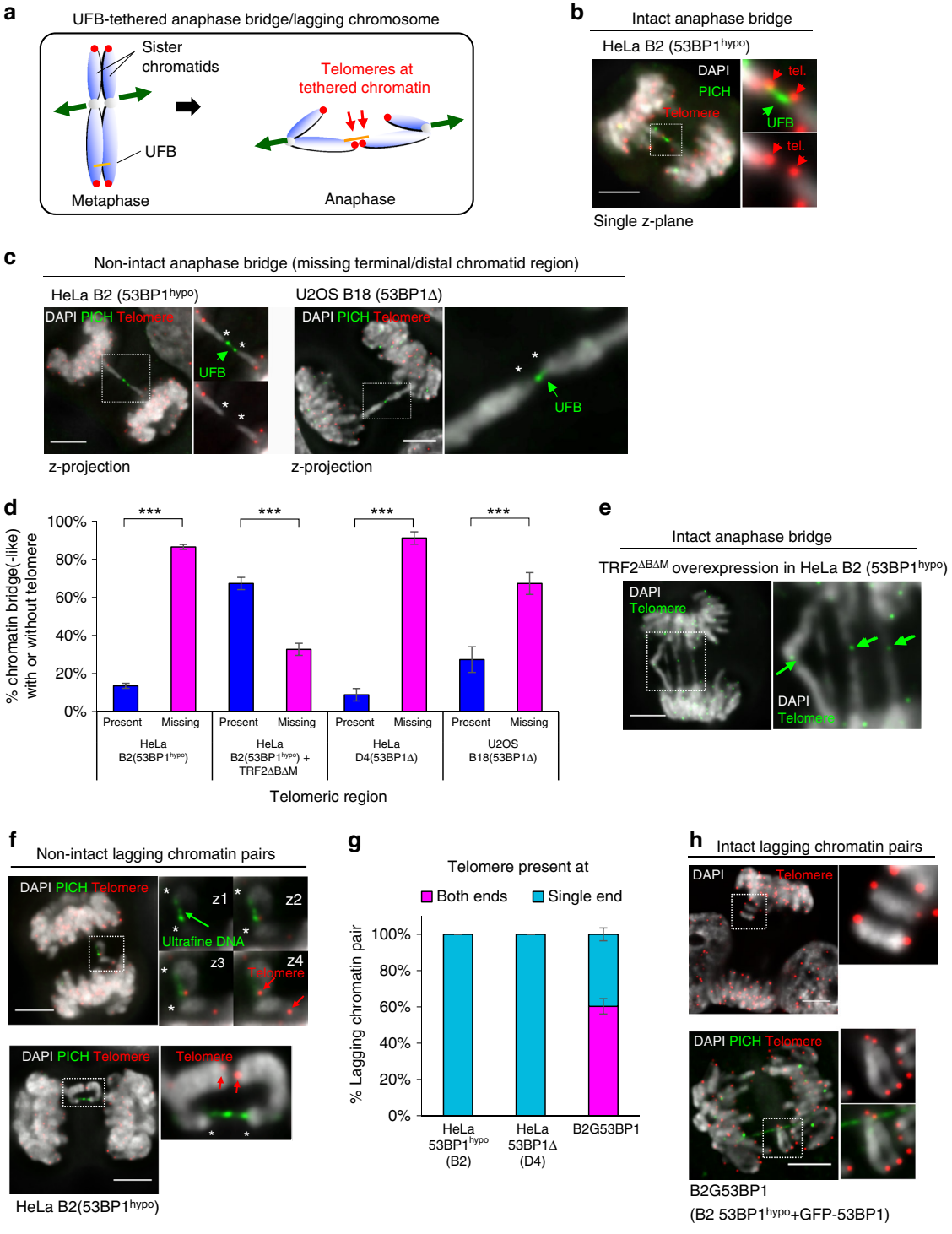

copies of chromosome16 and a 16p derivative, (6% with two chr16 + one derivative) (Supplementary Fig. 10b, c). However, in the 53BP1-depleted (53BP1^{hypo} and 53BP1Δ) HeLa cells, we found a variety of structural rearrangements on these chromosomes. They included deletions and translocations on the distal arm of 16q, chr7 and 16 whole-arm deletion, chr7 and 16 whole-arm (Robertsonian-like) translocations and 16p/16q isochromosome formation (Fig. 6a–e). Crucially, such rearrangements were never observed in the parental HeLa cells (Fig. 6f). A common breakpoint was assigned at a site just upstream of a common fragile site (CFS), FRA16D, in the WWOX locus, while interestingly another one was mapped to, or very close to, centromeres. Together, these results suggest that the sister-chromatid rupture in anaphase can lead to gross chromosome rearrangements.

Chromosome rearrangements link to sister-chromatid bridging. To provide further evidence that the observed rearrangements are directly related to the sister-chromatid rupture/bridging, we carefully examined the existence of DNA entanglements at these regions. By extending our FISH probes along the FRA16D/WWOX locus (Fig. 7a), we revealed a hitherto unidentified DNA thread structure linking the sister chromatids in 53BP1^{hypo} HeLa metaphase spreads (but not in the parental HeLa cells), which presumably is a precursor of the sister DNA bridging structures in anaphase. It was mapped at the promoter (91O9), or the gene body (264L1), of the WWOX locus (Fig. 7b–d; arrows and Supplementary Fig. 10d). To our knowledge, this is the first time that a genuine DNA intertwining molecule on cohesed sister chromatids has been visualised and mapped. Importantly, CFS fragility was not observed in the intertwined FRA16D locus, which supports our above data that the intertwining molecule is unlikely originating from an incomplete replication intermediate. By measuring inter-sister locus distances, we determined that the promoter region (91O9) of one WWOX allele displayed the highest frequency of DNA thread formation, something that was absent in a region 2.7 Mb upstream (352J17) (Fig. 7d). Correlatively, this new form of DNA thread structure was found in 53BP1^{hypo} clones (B2 and b9), each of which also harboured the corresponding rearrangements at 16q distal regions in the new derivative chromosome. By contrast, the 53BP1^{hypo} clone (b15) did not show either of these features. These observations demonstrate a high correlation between region-specific rearrangements and sister DNA bridging.

We next investigated whether centromeres, another hotspot of rearrangements, also have high incidence of rupture/bridging. Because centromeres remain cohesed in early mitosis, we examined the chromatin bridges and lagging chromatin structures in anaphase cells. We did not observe centromeres on the UFB-tethered chromatin bridges. Instead, centromeres were detected at the point at which the vast majority of lagging chromatin was intertwined (Fig. 7e, f). Importantly, the centromeres were located at the chromatid ends where the telomeric regions (or the distal arms) were missing, but remained tethered (Fig. 7g). Live-cell imaging of 53BP1^{hypo} (B2) cells stably expressing mCherry-H2B revealed that the lagging chromatin pairs failed to disjoin and co-segregated into the same daughter cell (Supplementary Fig. 10e). This is presumably due to the persistent DNA tethering at their sister centromeres counteracting the spindle-separation force. The co-segregation of ruptured sister whole-arms, thus provides an ideal precursor for isochromosome formation that was found in these cells. Taken together, our study reveals that the illegitimate sister DNA entanglements can drive gross chromosomal rearrangements via a distinct sister-chromatid rupture-bridging action that has never been reported before.

Sister-chromatid rupture occurs in cultured cancer cells. We next addressed if this phenomenon is limited in the 53BP1-depleted cancer cells, or occurs generally in other unmodified human cancer cells. We carefully characterised the mis-segregating chromatin in anaphases of a variety of human cancer cell lines, including HeLa, U2OS, Saos-2 and HCT116, in the absence of exogenous perturbation. As expected, we observed spontaneous chromosome missegregeation in these cells, but most importantly, we detected a subset of non-disjunction following a similar pattern of sister-chromatid rupture and bridging (Fig. 7h; HeLa (10%), U2OS (7%), Saos-2 (8%) and HCT116 (13%). Thus, our results highly suggest that in addition to the conventional anaphase bridge-breakage mechanism, sister DNA intertwining structures may contribute to influence the complex karyotypes during cancer evolution. Indeed, we have determined that the HeLa genome harbours several Robertsonian(-like) translocations or deletions, they involved chromosomes 1, 3, 7, 9, 15 and 16 (Supplementary Fig. 11), and more reported previously[39]. Thus, our study of sister-chromatid rupture and bridging may provide an alternative explanation for their formation.

In summary, we have revealed a distinct sister-chromatid rupture and bridging phenomenon for how ultrafine sister DNA entanglements may drive excessive gross chromosome rearrangements that can be suppressed by 53BP1 in cultured cancer cells (Fig. 8). Our study may provide an alternative explanation of how complex karyotypes arise during cancer developments in the context of illegitimate formation and resolution of sister DNA intertwinements.

Fig. 5 Sister-chromatid rupture is associated with HR-mediated DNA intertwining. **a** Diagram depicting the formation of telomere-positive DNA bridges, resulting from DNA entanglements between sister chromatids. **b** A single-plane high-resolution image showing the presence of telomeres (red) at the termini of chromatin tethered by an UFB (PICH; green) in a HeLa B2 (53BP1^{hypo}) anaphase cell. **c** Maximum z-projection image of an UFB-tethered chromatin bridge missing telomeric regions (asterisks) at their terminal ends in HeLa B2 (53BP1^{hypo}) (left) and in U2OS B18 (53BP1Δ) cells (right). Insets show enlarged images of the DNA/chromatin bridges. **d** Quantitation of DAPI bridges with and without telomeres in HeLa, HeLa 53BP1^{hypo}, U2OS 53BP1Δ and in HeLa 53BP1^{hypo} cells overexpressing TRF2^{ΔBΔM}. Note: Majority of DNA bridges are negative for telomere signals in 53BP1-depleted cells, except after TRF2^{ΔBΔM} overexpression. Total numbers of DAPI bridge analysed were B2 = 85, B2 + TRF2^{ΔBΔM} = 60, D4 = 45 and B18 = 55 from three independent experiments. Statistical significance was determined by *T*-test (***, $p < 0.001$). **e** A representative image showing telomeres were detected on chromatin bridges induced by telomere end-joining. Inset indicates the presence of telomere signals (green) at chromatin bridges (arrows). **f** Representative images of HeLa B2 (53BP1^{hypo}) cells showing UFBs tethering a pair of lagging chromatin at their termini, at where telomere (red) signals are absent (asterisks), but remained connected by PICH-UFBs. Insets showing consecutive single z-plane images of the lagging chromatin. **g** Quantitation of telomeres present at one or both ends of lagging chromatin pairs. Note that all lagging chromatin pairs lack one telomere end in HeLa B2 (53BP1^{hypo}) and D4 (53BP1Δ) cells. In contrast, HeLa 53BP1^{hypo} cells stably overexpressing GFP-tagged 53BP1 (B2G53BP1) cells contain lagging chromatin having telomere signals at both, or single ends. Total numbers of lagging chromatin pair analysed were B2 = 35, D4 = 41 and B2G53BP1 = 44, from three independent experiments. **h** Representative images of B2G53BP1 cells showing intact lagging chromosome with telomere signals (red) at both termini. Insets showing enlarged view of the lagging chromatin with telomere signals present at both their termini. Error bars represent s.d of three independent experiments. Scale bars, 5 μm

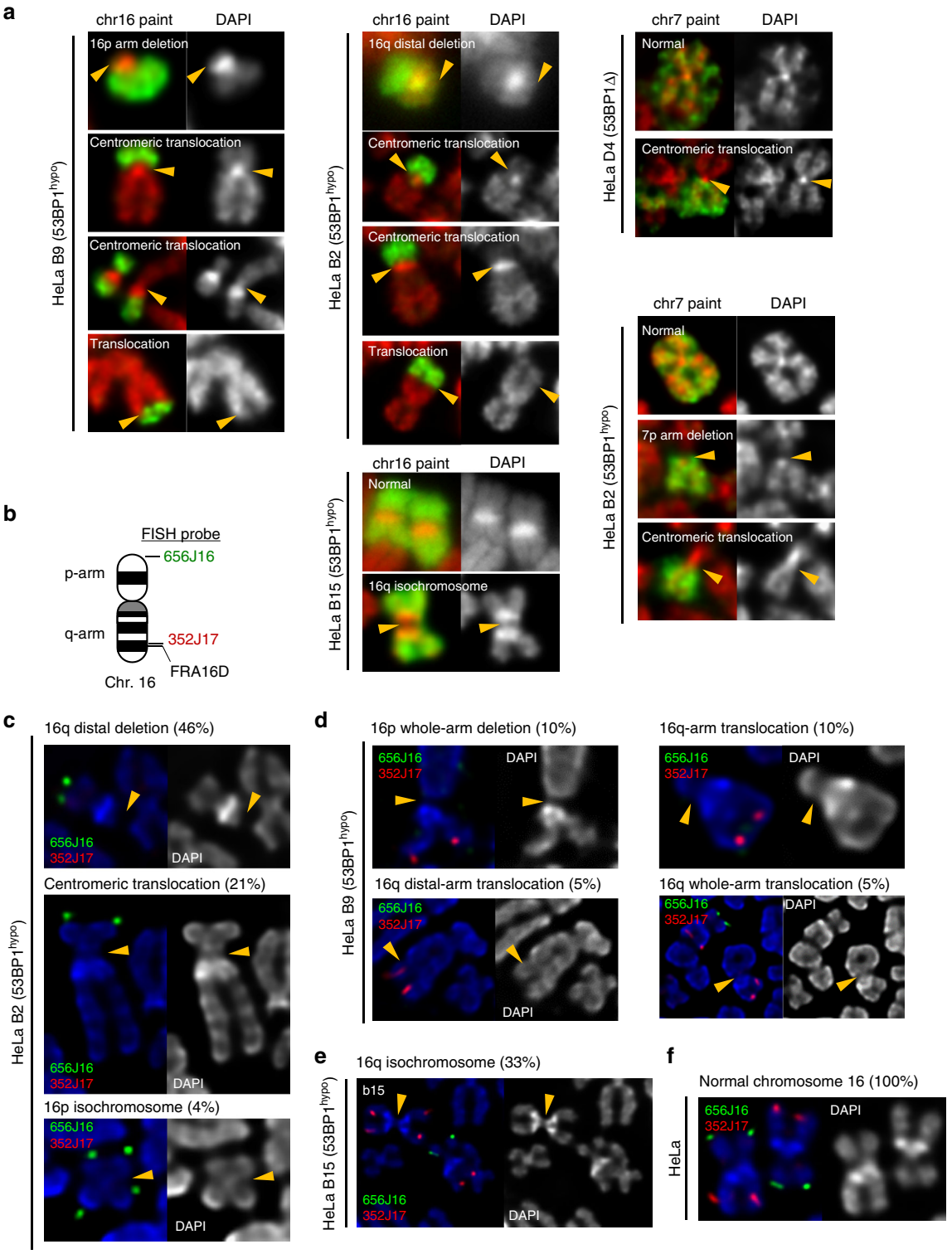

Fig. 6 Gross chromosomal hyper-rearrangements mediated by sister-chromatid bridging in 53BP1-depleted cancer cells. **a** Formation of new chromosome 16 and 7 derivatives in HeLa 53BP1^{hypo} and 53BP1Δ clones. Left panels: whole chromosome 16 painting revealing 16p arm deletion and arm/centromeric translocations in HeLa b9 (53BP1^{hypo}) cells. Middle panels: 16q deletions and arm/centromeric translocations in HeLa B2 (53BP1^{hypo}) cells; Isochromosome 16q formation in HeLa b15 (53BP1^{hypo}) cells. Right panels: whole chromosome 7 painting revealing centromeric translocation in HeLa D4 (53BP1Δ) cells and arm deletion and centromeric translocation in HeLa B2 (53BP1^{hypo}) cells. **b** Ideogram of human chromosome 16, marking the positions of FISH probes used in Fig. 6c–f. **c** 16q distal arm deletion, centromeric translocation and 16p isochromosome formation was identified in HeLa B2 (53BP1^{hypo}) populations with the indicated percentages. **d** 16p whole-arm deletion, 16q whole-arm translocation and 16q distal-arm translocation were detected in HeLa b9 (53BP1^{hypo}) populations with the indicated percentages. **e** 16q isochromosome formation was detected in HeLa b15 (53BP1^{hypo}) populations with the indicated percentages. **f** Normal chromosome 16 showing both p-arm and q-arm is maintained in all HeLa cells

Discussion

Extensive studies report that 53BP1 facilitates repair of double-ended DSBs via the NHEJ pathway in G1, by protecting DNA ends from resection[24–26,35], a key initiation step for HR. During S phase, this activity is neutralised by BRCA1-CtIP, which channels it to an error-free HR repair pathway[40]. In the current study, we have identified that a new role of 53BP1, shown in HeLa and U2OS human cancer cells, is to limit the formation of illegitimate sister DNA entanglements, which otherwise interferes with proper chromosome segregation. The cultured cancer cells,

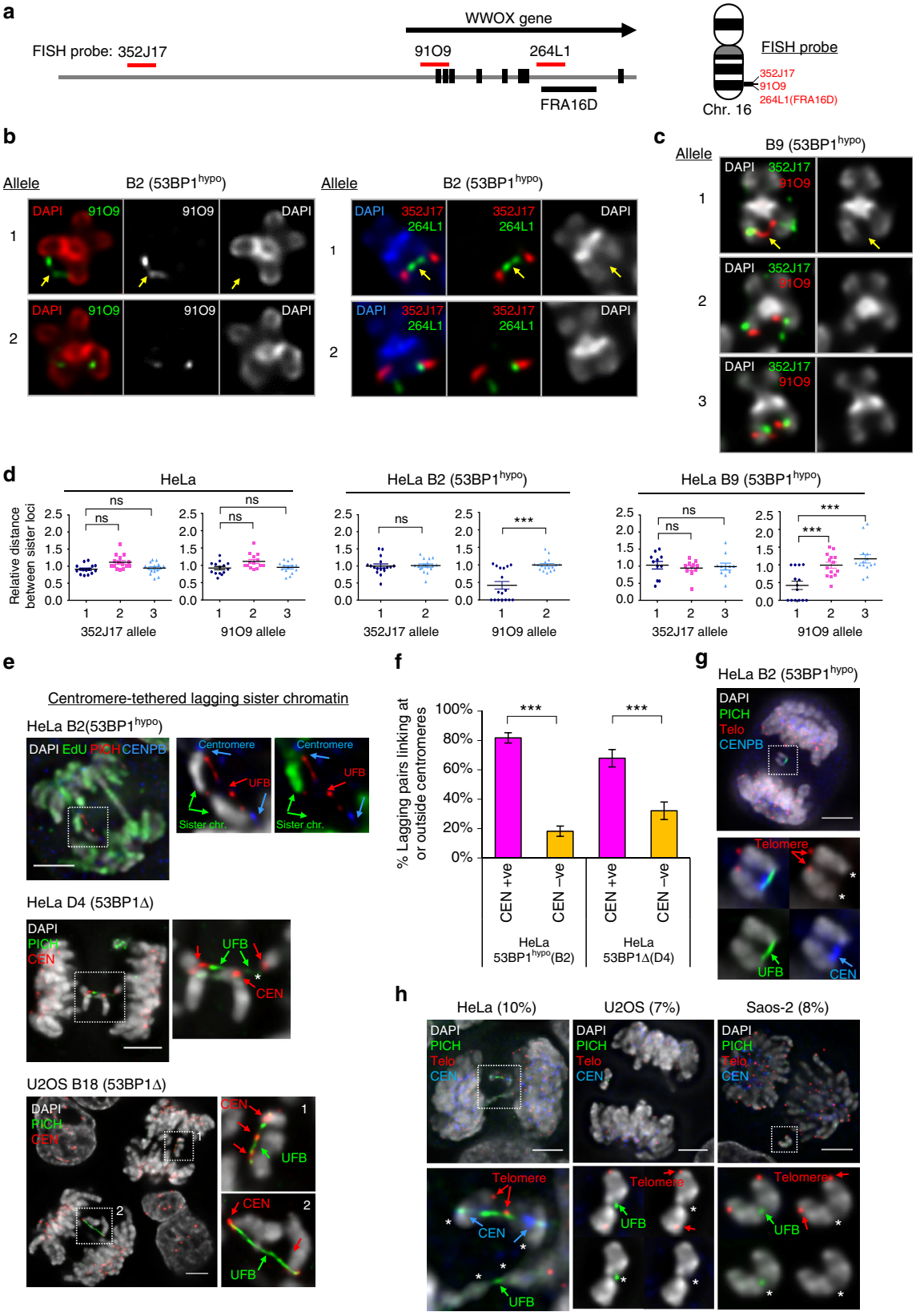

however, not normal diploid cells, are more susceptible to the loss of 53BP1 activities, even when NHEJ function is not fully compromised. This may reflect that 53BP1 has a cell-type specific function. Alternatively, cancerous cell lines may bear high genome instability, DNA replication demands and/or recombination activities, which predispose the formation or accumulation of sister DNA intertwining molecules when 53BP1 activity is limited. Indeed, transformed cells—including HeLa—are reported to display >3-fold increase in HR activity[41]. A striking consequence of 53BP1 depletion in these cancer cells is the elevation of UFB formation that is not associated with the FANCD2 protein (a marker of replication stress or DNA crosslinking). Interestingly, the DNA intertwinements are still found at a common fragile site, but this is not coupled to chromosomal fragility (the latter being a feature of replication stress induced by DNA polymerase inhibition or DNA repair deficiency[42–46]). The lack of fragility at these sites suggest that the new form of UFB caused by 53BP1-deficiency in the cancer cells, may be fundamentally different from those originating from LRIs. The fact that depleting RAD51 can significantly diminish the FANCD2-negative UFBs makes us believe that they are likely a by-product of a HR reaction. However, we cannot rule out that there is a distinct form of replication intermediate structure that does not trigger the FA pathway and chromosomal fragility, and then again retains the intertwining of sister chromatids.

It remains unclear how 53BP1 prevents illegitimate formation of sister-chromatid bridging in the examined cancer cells. It is plausible that (partial) loss of 53BP1 function may lead to the formation of a distinct type of replication intermediate that is subsequently converted by RAD51 into FANCD2-negative DNA intertwining molecules, to prevent fork stalling or incomplete replication. Alternatively, 53BP1 may act to suppress HR initiation and/or promote resolution of HR-mediated joint molecules during DNA replication (Supplementary Fig. 12). Extensive studies have shown that 53BP1 exerts DNA end-blocking, but is counteracted by BRAC1-CtIP during S phase[24–26,40]. It is conceivable that the (partial) loss of 53BP1 activity may relieve the constraints of HR initiation at damaged replication forks. On the other hand, loss of 53BP1 may weaken the anti-recombinogenic and/or dHJ dissolution activities exerted via interaction of the BLM complex[47–49]. Therefore, defects in one or all of these potential activities may result in excessive formation of sister-chromatid bridges.

Another striking finding in the current study is that the new type of sister DNA intertwinement can drive signature chromosome rearrangements, notably, via a distinct chromatid damage process. We termed this as "sister-chromatid rupture-bridging". Models such as BFB cycle have been proposed to explain the development of gross chromosomal rearrangements via single or multiple rounds of DNA damage introduced, mostly on chromatid arms concomitant with the breakage of anaphase bridges during or after cytokinesis. Subsequent fusion of the broken arms leads to re-generation of anaphase bridges and further breakages in the next cell cycle[7,8]. Contrary to this mechanism, we found that the sister DNA intertwinements induce chromatid rupture upon anaphase onset, and unexpectedly it happens prior to the breakage of the DNA bridges. Consequently, the ruptured sister arms remained tethered and gave rise to the characteristic non-disjunction chromatid products. When occurring at centromeres, it can drive co-segregation of the ruptured whole-arm chromatin and the formation of signature chromosomal rearrangements, including whole-arm (Robertsonian-like) deletions/translocations and isochromosome formation that are as-yet-unexplained alterations observed in tumour cells[50]. Our findings thus provide an alternative explanation for how distinct whole-arm rearrangements may arise from illegitimate sister DNA bridging. It is conceivable that if the rupture-bridging phenomenon occurs on rDNA-bearing chromosomes in germ cells, this could lead to Robertsonian translocations that are present in a subset of Patau and Down syndrome patients[51].

Lagging chromosomes are frequently observed in tumour cells. Based on our in-depth cytogenetic analyses, we speculate that some of the reported lagging chromosome formation may not be due to kinetochore-microtubule attachment errors, but due to the persistence of sister-chromatid bridges presented here. Further examinations will need to revisit the origin(s) of chromosome missegregation in cancers.

CIN is generally thought to be beneficial for tumour progression[1,2]. A recent study has shown that whole-arm deletions are positively correlated with loss of tumour suppressor islands that may confer growth advantages[52]. Undoubtedly, 53BP1 serves as a genome stability guardian and suppresses tumourigenesis as shown in mouse studies[53,54]. However, our study also indicates that in the examined cancer cells, 53BP1 is required to prevent excessive chromosome missegregation and probably genome hyper-instability, and also for optimal growth. Thus, we believe that chromosomal (hyper-)instability may need to be restrained in cancers, (e.g. by 53BP1-mediated pathway) otherwise the adverse effects such as chromatid intertwining and unwanted rearrangements may hinder tumour survival fitness. Thus, targeting the 53BP1 pathway may be, on the other hand, a promising therapeutic remedy in cancer treatments.

In conclusion, we show a distinct mitotic chromatid rupture-bridging process mediated by ultrafine sister DNA

Fig. 7 Sister-chromatid rupture-bridging is strongly linked to distinct chromosomal rearrangements. **a** Positions of FISH probes at WWOX gene locus on chromosome 16. **b** Representative FISH images showing DNA thread structures linking the promoter region (left) and at CFS-FRA16D site (right) of WWOX sister alleles on HeLa B2 (53BP1^{hypo}) metaphase chromosomes. **c** DNA thread structures (91O9 probe; red) were also detected in HeLa b9 (53BP1^{hypo}) cells. Arrows indicate DNA threads linking the well-separated chromatid arms. Probe 352J17 was used as a control. **d** Relative distance between sister signals of FISH probes, 352J17 and 91O9, in HeLa and 53BP1^{hypo} cells. FISH signals showing a line or connected dot is considered as zero distance—DNA thread formation. Eighteen metaphase spreads were counted. Note: HeLa B2 (53BP1^{hypo}) cells retain only two intact WWOX alleles. **e** Examples of centromere-tethered lagging sister chromatin in 53BP1-depleted HeLa and U2OS cells. A pair of lagging sister chromatin as differentially labelled by EdU (green), intertwined by a PICH-UFB (red) at their centromeres (CENB, blue) in HeLa B2 (53BP1^{hypo}) anaphase cell (Top). Pairs of broken lagging chromatin tethered at centromeres (red) by PICH-UFBs (green) in HeLa D4 (53BP1Δ) (Middle) and U2OS B18 (53BP1Δ) cells (Bottom). **f** Frequencies of lagging-chromatin pairs with UFBs linking at centromeres in HeLa 53BP1^{hypo} and 53BP1Δ cells. Numbers of lagging chromatin pairs analysed, B2 = 49 and D4 = 44 from three independent experiments. **g** Immuno-FISH analysis revealed loss of whole chromatid arms on lagging chromatid pairs tethered by UFBs at centromeres. A representative image of HeLa 53BP1^{hypo} cell showing a PICH-UFB (green) intertwines the sister centromeres (blue) of a pair of lagging chromatin, at where the telomeres (red) are missing (asterisks). **h** Frequencies of sister-chromatid rupture-bridging phenomenon in unperturbed HeLa (4/40; 10%), U2OS (3/43; 7%) and Saos-2 (2/25; 8%) cells. Representative images showing ruptured chromatin tethered by PICH-UFBs (green), sometimes at centromeres (blue). Asterisks mark the ruptured positions at where the rest of chromatids is lost, as determined by telomere FISH (red). Scale bars, 5 μm. Error bars represent s.d. of three independent experiments. Statistical significance was determined by *T*-test (***, $p < 0.001$; ns, nonsignificant)

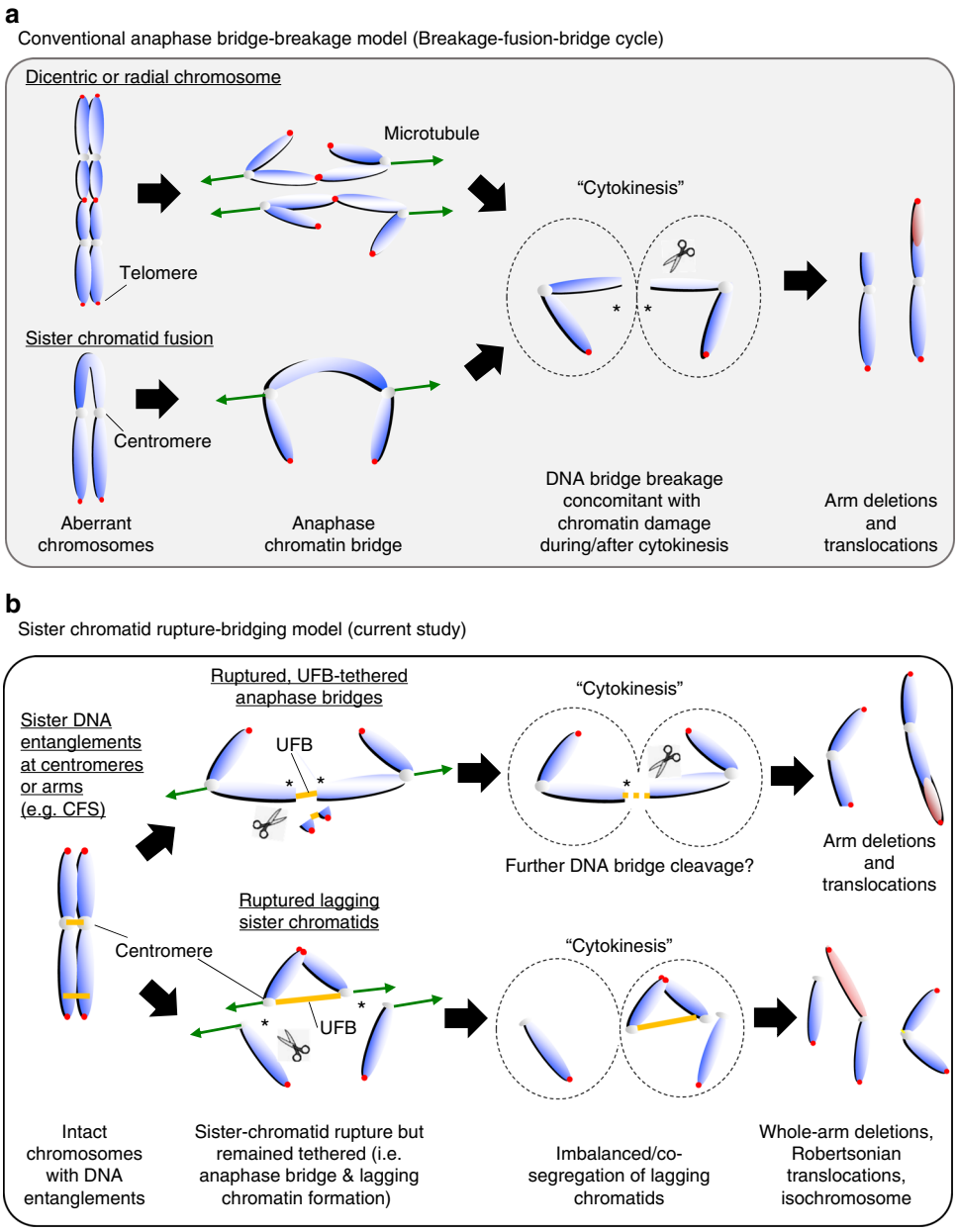

Fig. 8 Models of gross chromosomal rearrangements driven by conventional anaphase bridge-breakage and sister-chromatid rupture-bridging pathways. **a** Conventional anaphase bridge-breakage (also known as breakage-fusion-bridge cycle) model driven gross chromosomal rearrangements (GCRs). Aberrant chromatids or chromosomes, such as dicentric/radial chromosomes and sister-arm fusion lead to chromatin bridge formation in anaphase. The breakage of anaphase bridges during or after cytokinesis results in chromosome damage, which subsequently can lead to deletions, translocations and/or the re-formation of dicentric chromosomes and sister-arm fusion. Cells enter another anaphase bridge-breakage cycle in the next mitosis that accumulate further chromosome alterations. **b** Sister-chromatid rupture-bridging model driven GCRs (in the current study). Illegitimate formation/accumulation of ultrafine sister DNA intertwinements lead to a symmetrical rupture of sister-chromatid axes (asterisks). The resulting sister arms remain tethered by UFB structures resulting in anaphase bridges or lagging chromatin pairs formation (when the rupture occurs at centromeres). Further breakage may occur on the UFB-tethered anaphase bridges in late mitosis (e.g. during abscission in cytokinesis), which lead to arm deletions or translocations. On the other hand, the centromere-tethered lagging chromatin pairs, which lose the entire opposite arms, may escape abscission and co-segregate into one of the daughter cells. Hence, this provides an ideal precursor for isochromosome formation, or causes whole-arm translocations in the next cell cycle. Our current model, therefore, provides an alternative explanation on the formation of whole-arm rearrangements that may arise in cancer karyotypes

intertwinements that promotes characteristic chromosomal rearrangements in 53BP1-depleted human cancer cells.

Methods

Cell culture, treatment and transfection. All cell lines were obtained from Cell Bank of Genome Damage and Stability Centre and were originally purchased from ATCC. All cell lines were authenticated by STR genotyping from European Collection of Cell Cultures and passed mycoplasma tests (Lonza Mycoplasma testing kit). HeLa, U2OS and SAOS-2 cells were grown in DMEM containing 10% foetal bovine serum (Gibco), L-glutamine and Pen/Strep antibiotics. RPE1-hTERT cells were grown in DMEM/F-12 containing 10% foetal bovine serum (Gibco) and Pen/Strep antibiotics. HCT116 cells were grown in McCoy's 5 A containing 10% foetal bovine serum (Gibco), L-glutamine and Pen/Strep antibiotics. HeLa B2G53BP1 cells were maintained with 0.4 mg/ml G418. Cell cultures were maintained at 37 °C in a humidified atmosphere containing 5% CO_2. As indicated, the

cells were treated with the DNA polymerase inhibitor aphidicolin (Sigma, A0781; 0.3 μM).

53BP1-knockout HeLa and RPE1 cells were generated using the CRISPR-Cas9 m, with the following guide-RNAs targeting *exon 2* (CAGGTTCTAGAGGATGATTCTGG) for 53BP1^{hypo} and *exon 10* (TTTATC GTTCCTAGCAGTCC) for *53BP1Δ knockout*.

Briefly, gene-specific gRNAs were cloned in pSpCas9(BB)-2A-Puro (Addgene) containing a puromycin resistance cassette. HeLa cells were transfected (Fugene HD, Promega) and RPE1 cells were electroporated (Neon Transfection System, ThermoFisher) with pSpCas9(BB)-2A-Puro-53BP1gRNA. Transfected HeLa, U2OS and RPE1 cells were selected by 0.25 μg/ml and 2 μg/ml of puromycin, respectively, for 72 h. B2 (HeLa-53BP1^{hypo}) cells were generated by cotransfecting pMACSK^{K}II and pSpCas9(BB)-2A-Puro-53BP1gRNA-b in HeLa cells. Forty-eight hours later, the cells were labelled by MACSselectK^{K}II microbeads and enriched by MACSselect K^{K}II column without any antibiotic selection.

Individually isolated clones were isolated and screened by immunoblotting and immunofluorescence. The presence of mutations in knockout cells were identified by Sanger sequencing following TA-cloning (35 clones) using primers (Fwd: CAGGATTGGACACAACATCCTAG; Rev: CTCTCAGCAAGATACTCCTTG CC). Primers used for 53BP1 wild-type allele-specific PCR (Fwd; AAGCCAGGT TCTAGAGGATG; Rev: CTCTCAGCAAGATACTCCTTGCC).

To generate B2G53BP1 cells, full-length pEGFP-C3-53BP1 (isoform1) construct was transfected in B2 (53BP1^{hypo}) cells and were selected by G418 (0.8 mg/ml) for 2 weeks. Individual clones were screened and cultured.

HeLa or B2 cells were transfected with siRNAs using Lipofectamine RNAiMAX (Invitrogen) following the manufacturer's instruction. The sequences of stealth siRNAs (ThermoFisher) are as follows:

RAD51 (CCACCAGACCCAGCUCCUUUAUCAA),

Non-targeting pool (UGGUUUACAUGUCGACUAA,UGGUUUACAUGU UGUGUGA, UGGUUUACAUGUUUUCUGA and UGGUUUACAUGUUU UCCUA).

Fluorescence immunostaining. For immunostaining analyses, the cells were seeded onto No:1.5 H cover glass and fixed with PFA buffer (250 mM HEPES, 1x PBS, pH7.4, 0.1% Triton X-100, 4% methanol-free paraformaldehyde) for 20 min at 4 °C or with room temperature PFA buffer (1x PBS, 4% methanol-free paraformaldehyde) for 10 min. Pre-extraction was carried out in indicated experiments before fixation by incubation of the cover glass into pre-extraction buffer (20 mM HEPES, pH 7.4, 0.5% Triton X-100, 50 mM NaCl, 3 mM $MgCl_2$, 300 mM sucrose) for 15 sec.

Primary antibodies used: anti-FANCD2 (Novusbio NB100-82; 1:600), anti-53BP1 (Abcam ab36823; 1:800), anti-53BP1 (Bethyl Lab A300-272A; 1:1000), anti-53BP1 (Millipore MAB3802; 1:800), anti-53BP1 (Santa Cruz H-300; 1:400), anti-RIF1 (Bethyl Lab A300-568A-3; 1:200), anti-PICH (Abnova H00054821-B01P; 1:150), anti-PICH (Abnova; H00054821-D01P; 1:100), anti-γH2AX (Upstate JBW-301; 1:400), anti-RAD51 (Abcam ab63801; 1:200), anti-RPA70 (Abcam ab79398; 1:200), anti-CENPB (Abcam ab25734; 1:600) and anti-centromere (ImmunoVision HCT-0100; 1:800). All secondary antibodies were used in a dilution of 1:500 and purchased from ThermoFisher Scientific, unless stated otherwise. Secondary antibodies used: donkey anti-mouse Alexa Fluor 488 (A-21202), 555 (A-31570) and 647 (A-31571); donkey anti-rabbit Alexa Fluor 488 (A-21206), 555 (A-31572) and 647 (A-31573); donkey anti-goat Alexa Fluor 555 (A-21432); goat anti-rabbit Abberior STAR 635 P (Abberior 2-0012-007-2) and goat anti-human DyLight 550 (Abcam ab96908) and 650 (Abcam ab96910). Immunofluorescence staining was performed according to previously described protocols[13]. In brief, the samples were incubated with primary antibodies at 37 °C for 90 minutes and rinsed with 1 × PBS followed by incubation of secondary antibodies in room temperature for 25 minutes. The cells were mounted using Vectasheild containing DAPI.

High-resolution deconvolution microscopy. Image acquisition was carried out under a Zeiss AxioObserver Z1 epifluorescence microscopy system with 40 × /1.3 oil Plan-Apochromat, 63 × /1.4 oil Plan-Aprochromat and 100 × /1.4 oil Plan-Aprochromat objectives and a Hamamatsu ORCA-Flash4.0 LT camera. The system is calibrated and aligned by using 200 nm-diameter TetraSpeck microspheres (ThermoFisher). Z-stack images were acquired at 0.2 μm intervals covering a range from 3–8 μm by using ZEN blue software.

Deconvolution was carried out using Huygens Professional deconvolution software (SVI) with a measured point-spread-function generated by 200 nm-diameter TetraSpeck microspheres. Classical maximum likelihood estimation method with iterations of 40–60 and signal-to-noise of 20–40 was applied.

Anaphase bridges and lagging chromosomes counting. Cells were grown on coverslips for 18 h and fixed with 4% paraformaldehyde in 1x PBS at room temperature for 10 min. The cells were then stained with Hoechst 33342 and slides were mounted in Vectashield mounting medium. Anaphase cells with chromatin bridges and lagging chromatin were scored under Zeiss Axio Observer Z1 microscope. The counting was completed by three different assessors between experiments. The cells were counted from random microscopic fields.

Differential sister-chromatid labelling on mitotic cells. Differential labelling of sister chromatids was performed by modifying the cell synchronisation method of a double thymidine arrest. Briefly, the cells were incubated with EdU during the second thymidine arrest period. EdU was then maintained following the release and washed away after 9 h of incubation. After 24–26 h, the samples were collected for metaphase spread preparation or anaphase cell fixation as mentioned before and subjected to immunofluorescence staining and microscopy analysis.

EdU was detected using Click-iT Plus EdU labelling kits (Alexa Fluor 488, 555 or 647). For EDU pulse labelling, the cells were treated with EdU (10 μM) 10–15 min prior to fixation. EdU staining was performed according to the manufacturer's instruction.

Immunoblotting. Cells were trypsinized and lysed on ice for 20 min with lysis buffer (50 mM Tris, pH 7.5, 300 mM Nacl, 5 mM EDTA, 1% Triton X-100, 1.25 mM DTT, 1 mM PMSF and cOmplete^{TM} protease inhibitor cocktail). Protein concentration was quantified using Bradford assay (Bio-Rad). Immunoblotting (IB) was performed following standard procedures. Primary antibodies used for IB in this study: anti-53BP1 (Abcam, ab36823; 1:7000), anti-53BP1 (Santa Cruz, H-300; 1:800), anti-Ku80 (Abcam, ab80592; 1:10000) and anti-β-actin (Sigma, A5316; 1:5000).

Secondary antibodies used: goat anti-rabbit HRP (Amersham NA9340V; 1:25000) and goat anti-mouse HRP (Abcam ab6789; 1:10000).

MTT proliferation assay. Cell proliferation was assessed using MTT (3-(4,5-dimethylthiazol-2-yl)-2,5-diphenyltetrazolium bromide). Briefly, the cells were seeded in triplicate on a 24-well plate and 50 μl of 0.5 g/L MTT was added at indicated times. After incubation at 37 °C for 2 h, the MTT medium was aspirated and 250 μl of DMSO was added to each well. The absorbance was measured using CLARIOstar plate reader (BMG Labtech) at 595 nm.

Clonogenic cell survival and Micro-colony formation assay. For clonogenic cell survival assay, HeLa, U2OS and its derived 53BP1 knockout cells or RPE1 and its derived 53BP1 knockout cells were plated in 10-cm tissue culture petri dishes. Five hours later, the cells were treated with different doses of irradiation using an X-ray machine. The treated cells were allowed to grow for 15 days to form colonies. The colonies were fixed with 70% ethanol and stained with 1 mg/ml bromophenol blue for 2 h.

For micro-colony formation assay, ~50 single cells were seeded onto a coverslip (24 × 24 mm) to form colonies. After 7 days, the cells were stained with CellMask™ Deep Red (ThermoFisher Scientific) and fixed with PFA. The cells were mounted in DAPI Vectasheild and captured under a 40 × objective using 3 × 3 tiling to image the whole colony size in an area of 900 × 900 μm^2.

Metaphase spread preparation. Cells were collected for metaphase spread preparation after 1 h of colcemid (Gibco, 0.5 μg/ml) treatment and were swelled with pre-warmed KCl (0.075 M) hypotonic solution at 37 °C for 5 min. The cells were washed twice and fixed with 3:1 methanol:acetic acid. The cells were dropped onto glass slides. For chromosome number frequency the metaphase spreads from random microscopic fields were counted.

Telomere end-to-end fusion assay. For telomere fusion assay pLPC-NMYC TRF2$^{\Delta B\Delta M}$ construct (Addgene) was transiently transfected in HeLa or B2 (53BP1^{hypo}) for 36 h using Fugene HD. Following transfection, the cells were harvested for metaphase spread preparation and quantitation after FISH staining (described below).

Fluorescence in situ hybridisation (FISH). Bacterial artificial chromosome (BAC) clones were purchased from BACPAC resources centre, C.H.O.R.I. BAC DNA was isolated using QIAGEN® Plasmid Purification MaxiPrep kit. A volume of 1 μg of BAC clone DNA was labelled by nick translation for 90 min at 15 °C with digoxigenin-11-dUTP (Roche) using a nick translation kit (Roche) or ATTO labelling kit (Jena Bioscience). Labelled probe together with cot-1 DNA (Roche) was dehydrated. The denatured probe was re-suspended in hybridisation buffer and placed on a metaphase slide (prepared as described earlier), which had been dehydrated in a graded ethanol series (70%, 85% and 100%). The slide was sealed, denatured (82.5 °C for 2 min) and incubated O/N at 37 °C. The slide was washed at 65 °C in 0.1 × SSC. DIG-labelled probe was detected with FITC-conjugated anti-digoxigenin for 30 min at RT. Chromosomes were counterstained with DAPI Vectasheild.

Peptide nucleic acid (PNA) fluorescent in situ hybridisation. PNA probes were hybridised according to the manufacturer's instructions telomere-CY3 (DAKO, Agilent technologies) or FAM488-CENPB (PNAbio). Briefly, metaphase slides were washed in TBS buffer, fixed in 3.7% PFA and dehydrated in a graded ethanol series (70%, 85% and 100%). The slides were air dried and hybridised with PNA probe and co-denatured (80 °C for 2 min) and incubated for 2 h at room temperature. Chromosomes were counterstained with DAPI Vectasheild.

Immuno-FISH. Immuno-FISH was performed after standard IF-staining procedures. Briefly, the cells were subjected to immunofluorescence as described above and re-fixed with 8% paraformaldehyde at room temperature for 10 min. The samples were co-denatured with 10 µl of Cy-3-labelled telomere specific PNA probe (80 °C for 5 mins) and hybridised for 2 h at room temperature in the dark. The cells were then washed and mounted with DAPI Vectasheild.

Flow cytometry. The cells were trypsinised, washed with PBS and fixed with 70% ice-cold ethanol. For cell cycle analysis, the cells were washed with PBS and re-suspended in PI/RNase staining buffer. FACS profile were then determined and analysed using BD accuri C6 sampler.

Statistics. Statistical analysis was performed using GraphPad Prism software by two-tailed unpaired Student's *t*-test or two-way Anova as per the experimental requirement. Data were presented as the mean + s.d. unless specified. Probability value '$p \leq 0.05$' was considered to be significant.

Data availability. All the data and materials supporting this work are available upon reasonable request to the corresponding author.

Received: 28 September 2017 Accepted: 18 January 2018
Published online: 14 February 2018

References

1. Lengauer, C., Kinzler, K. W. & Vogelstein, B. Genetic instabilities in human cancers. *Nature* **396**, 643–649 (1998).
2. Funk, L. C., Zasadil, L. M. & Weaver, B. A. Living in CIN: mitotic infidelity and its consequences for tumor promotion and suppression. *Dev. Cell.* **39**, 638–652 (2016).
3. Weaver, B. A., Silk, A. D. & Cleveland, D. W. Cell biology: nondisjunction, aneuploidy and tetraploidy. *Nature* **442**, E9–E10 (2006). discussion E10.
4. Janssen, A., van der Burg, M., Szuhai, K., Kops, G. J. & Medema, R. H. Chromosome segregation errors as a cause of DNA damage and structural chromosome aberrations. *Science* **333**, 1895–1898 (2011).
5. Crasta, K. et al. DNA breaks and chromosome pulverization from errors in mitosis. *Nature* **482**, 53–58 (2012).
6. Maciejowski, J. & de Lange, T. Telomeres in cancer: tumour suppression and genome instability. *Nat. Rev. Mol. Cell. Biol.* **18**, 175–186 (2017).
7. McClintock, B. The fusion of broken ends of chromosomes following nuclear fusion. *Proc. Natl Acad. Sci. USA* **28**, 458–463 (1942).
8. Coquelle, A., Pipiras, E., Toledo, F., Buttin, G. & Debatisse, M. Expression of fragile sites triggers intrachromosomal mammalian gene amplification and sets boundaries to early amplicons. *Cell* **89**, 215–225 (1997).
9. Maciejowski, J., Li, Y., Bosco, N., Campbell, P. J. & de Lange, T. Chromothripsis and kataegis induced by telomere crisis. *Cell* **163**, 1641–1654 (2015).
10. Chan, K. L., Palmai-Pallag, T., Ying, S. & Hickson, I. D. Replication stress induces sister-chromatid bridging at fragile site loci in mitosis. *Nat. Cell Biol.* **11**, 753–760 (2009).
11. Naim, V. & Rosselli, F. The FANC pathway and BLM collaborate during mitosis to prevent micro-nucleation and chromosome abnormalities. *Nat. Cell Biol.* **11**, 761–768 (2009).
12. Baumann, C., Korner, R., Hofmann, K. & Nigg, E. A. PICH, a centromere-associated SNF2 family ATPase, is regulated by Plk1 and required for the spindle checkpoint. *Cell* **128**, 101–114 (2007).
13. Chan, K. L., North, P. S. & Hickson, I. D. BLM is required for faithful chromosome segregation and its localization defines a class of ultrafine anaphase bridges. *EMBO J.* **26**, 3397–3409 (2007).
14. Ying, S. et al. MUS81 promotes common fragile site expression. *Nat. Cell. Biol.* **15**, 1001–1007 (2013).
15. Naim, V., Wilhelm, T., Debatisse, M. & Rosselli, F. ERCC1 and MUS81-EME1 promote sister chromatid separation by processing late replication intermediates at common fragile sites during mitosis. *Nat. Cell Biol.* **15**, 1008–1015 (2013).
16. Lukas, C. et al. 53BP1 nuclear bodies form around DNA lesions generated by mitotic transmission of chromosomes under replication stress. *Nat. Cell Biol.* **13**, 243–253 (2011).
17. Harrigan, J. A. et al. Replication stress induces 53BP1-containing OPT domains in G1 cells. *J. Cell Biol.* **193**, 97–108 (2011).
18. Moreno, A. et al. Unreplicated DNA remaining from unperturbed S phases passes through mitosis for resolution in daughter cells. *Proc. Natl Acad. Sci. USA* **113**, E5757–E5764 (2016).
19. Chan, K. L. & Hickson, I. D. New insights into the formation and resolution of ultra-fine anaphase bridges. *Semin. Cell Dev. Biol.* **22**, 906–912 (2011).
20. Burrell, R. A. et al. Replication stress links structural and numerical cancer chromosomal instability. *Nature* **494**, 492–496 (2013).
21. Xie, A. et al. Distinct roles of chromatin-associated proteins MDC1 and 53BP1 in mammalian double-strand break repair. *Mol. Cell* **28**, 1045–1057 (2007).
22. Wang, B., Matsuoka, S., Carpenter, P. B. & Elledge, S. J. 53BP1, a mediator of the DNA damage checkpoint. *Science* **298**, 1435–1438 (2002).
23. Taniguchi, T. et al. S-phase-specific interaction of the Fanconi anemia protein, FANCD2, with BRCA1 and RAD51. *Blood* **100**, 2414–2420 (2002).
24. Chapman, J. R. et al. RIF1 is essential for 53BP1-dependent nonhomologous end joining and suppression of DNA double-strand break resection. *Mol. Cell* **49**, 858–871 (2013).
25. Di Virgilio, M. et al. Rif1 prevents resection of DNA breaks and promotes immunoglobulin class switching. *Science* **339**, 711–715 (2013).
26. Zimmermann, M., Lottersberger, F., Buonomo, S. B., Sfeir, A. & de Lange, T. 53BP1 regulates DSB repair using Rif1 to control 5' end resection. *Science* **339**, 700–704 (2013).
27. Karlseder, J., Smogorzewska, A. & de Lange, T. Senescence induced by altered telomere state, not telomere loss. *Science* **295**, 2446–2449 (2002).
28. Dimitrova, N., Chen, Y. C., Spector, D. L. & de Lange, T. 53BP1 promotes non-homologous end joining of telomeres by increasing chromatin mobility. *Nature* **456**, 524–528 (2008).
29. Hengeveld, R. C. et al. Rif1 is required for resolution of ultrafine DNA bridges in anaphase to ensure genomic stability. *Dev. Cell* **34**, 466–474 (2015).
30. Chan, K. L. & Hickson, I. D. On the origins of ultra-fine anaphase bridges. *Cell Cycle* **8**, 3065–3066 (2009).
31. Spence, J. M. et al. Depletion of topoisomerase IIalpha leads to shortening of the metaphase interkinetochore distance and abnormal persistence of PICH-coated anaphase threads. *J. Cell. Sci.* **120**, 3952–3964 (2007).
32. Nera, B., Huang, H. S., Lai, T. & Xu, L. Elevated levels of TRF2 induce telomeric ultrafine anaphase bridges and rapid telomere deletions. *Nat. Commun.* **6**, 10132 (2015).
33. Baumann, P., Benson, F. E. & West, S. C. Human Rad51 protein promotes ATP-dependent homologous pairing and strand transfer reactions in vitro. *Cell* **87**, 757–766 (1996).
34. Ochs, F. et al. 53BP1 fosters fidelity of homology-directed DNA repair. *Nat. Struct. Mol. Biol.* **23**, 714–721 (2016).
35. Bunting, S. F. et al. 53BP1 inhibits homologous recombination in Brca1-deficient cells by blocking resection of DNA breaks. *Cell* **141**, 243–254 (2010).
36. Jullien, D., Vagnarelli, P., Earnshaw, W. C. & Adachi, Y. Kinetochore localisation of the DNA damage response component 53BP1 during mitosis. *J. Cell Sci.* **115**, 71–79 (2002).
37. Wang, H. et al. Aurora kinase B dependent phosphorylation of 53BP1 is required for resolving merotelic kinetochore-microtubule attachment errors during mitosis. *Oncotarget* **8**, 48671–48687 (2017).
38. Biebricher, A. et al. PICH: a DNA translocase specially adapted for processing anaphase bridge DNA. *Mol. Cell* **51**, 691–701 (2013).
39. Macville, M. et al. Comprehensive and definitive molecular cytogenetic characterization of HeLa cells by spectral karyotyping. *Cancer Res.* **59**, 141–150 (1999).
40. Escribano-Diaz, C. et al. A cell cycle-dependent regulatory circuit composed of 53BP1-RIF1 and BRCA1-CtIP controls DNA repair pathway choice. *Mol. Cell* **49**, 872–883 (2013).
41. Xia, S. J., Shammas, M. A. & Shmookler Reis, R. J. Elevated recombination in immortal human cells is mediated by HsRAD51 recombinase. *Mol. Cell. Biol.* **17**, 7151–7158 (1997).
42. Glover, T. W., Berger, C., Coyle, J. & Echo, B. DNA polymerase alpha inhibition by aphidicolin induces gaps and breaks at common fragile sites in human chromosomes. *Hum. Genet.* **67**, 136–142 (1984).
43. Turner, B. C. et al. The fragile histidine triad/common chromosome fragile site 3B locus and repair-deficient cancers. *Cancer Res.* **62**, 4054–4060 (2002).
44. Arlt, M. F. et al. BRCA1 is required for common-fragile-site stability via its G2/M checkpoint function. *Mol. Cell. Biol.* **24**, 6701–6709 (2004).
45. Casper, A. M., Nghiem, P., Arlt, M. F. & Glover, T. W. ATR regulates fragile site stability. *Cell* **111**, 779–789 (2002).
46. Schwartz, M. et al. Homologous recombination and nonhomologous end-joining repair pathways regulate fragile site stability. *Genes Dev.* **19**, 2715–2726 (2005).
47. Tripathi, V., Kaur, S. & Sengupta, S. Phosphorylation-dependent interactions of BLM and 53BP1 are required for their anti-recombinogenic roles during homologous recombination. *Carcinogenesis* **29**, 52–61 (2008).
48. Sengupta, S. et al. Functional interaction between BLM helicase and 53BP1 in a Chk1-mediated pathway during S-phase arrest. *J. Cell Biol.* **166**, 801–813 (2004).
49. Tripathi, V., Nagarjuna, T. & Sengupta, S. BLM helicase-dependent and -independent roles of 53BP1 during replication stress-mediated homologous recombination. *J. Cell Biol.* **178**, 9–14 (2007).
50. Beroukhim, R. et al. The landscape of somatic copy-number alteration across human cancers. *Nature* **463**, 899–905 (2010).

51. Caspersson, T., Hulten, M., Lindsten, J., Therkelsen, A. J. & Zech, L. Identification of different Robertsonian translocations in man by quinacrine mustard fluorescence analysis. *Hereditas* **67**, 213–220 (1971).
52. Davoli, T. et al. Cumulative haploinsufficiency and triplosensitivity drive aneuploidy patterns and shape the cancer genome. *Cell* **155**, 948–962 (2013).
53. Ward, I. M. et al. 53BP1 cooperates with p53 and functions as a haploinsufficient tumor suppressor in mice. *Mol. Cell. Biol.* **25**, 10079–10086 (2005).
54. Ward, I. M., Minn, K., van Deursen, J. & Chen, J. p53 Binding protein 53BP1 is required for DNA damage responses and tumor suppression in mice. *Mol. Cell. Biol.* **23**, 2556–2563 (2003).

Acknowledgements

We thank people in the Genome Centre for their great support and help. We would also like to thank Nadia Hegarat for puromycin-sensitive RPE1-hTERT cells and Matthew Neale, Aidan Doherty and Anthony Carr for helpful comments on the manuscript. We also thank Stephen West for sharing unpublished research information. This work is supported by Sir Henry Dale Fellowship (Ref: 104178/Z/14/Z) from Wellcome Trust and the Royal Society, and by the Genome Damage and Stability Centre. K-L.C. is the recipient of Sir Henry Dale Fellowship. Funding for open access charge: Charity Open Access Fund (COAF).

Author contributions

A.T. and K.-L.C. designed and performed the experiments with help from O.A.J. A.T. O.A.J. and K.-L.C. wrote the manuscript.

Additional information

Supplementary Information accompanies this paper at https://doi.org/10.1038/s41467-018-03098-y.

Competing interests: The authors declare no competing financial interests.

Reprints and permission information is available online at http://npg.nature.com/reprintsandpermissions/

Publisher's note: Springer Nature remains neutral with regard to jurisdictional claims in published maps and institutional affiliations.